APPLICATION OF CHITOSAN-CARBON NANOTUBE HYDROGEL BEADS COMPOSITE IN THE REMOVAL OF ANTIBIOTIC COMPOUNDS AND PERFLUOROALKYL SUBSTANCES FROM AQUEOUS SOLUTIONS

Doctoral Thesis

by

Siphesihle Mangena Khumalo

This thesis is submitted to the Department of Chemical Engineering in the Faculty of Engineering and the Built Environment at the Durban University of Technology, KwaZulu-Natal, South Africa, in fulfilment of academic requirements for the degree of Doctor of Engineering majoring in Chemical Engineering.

Supervisor: Prof. Sudesh Rathilal

Co-Supervisor: Prof. Babatunde Femi Bakare

September 2024

DECLARATION 1 – PLAGIARISM

I, Siphesihle Mangena Khumalo hereby declare that;

i. The research reported in this thesis, except where otherwise indicated, is my own original work.
ii. This thesis has not been submitted for any degree or examination at any other university.
iii. This thesis does not contain data, pictures, graphs or other information belonging to other people, unless specifically acknowledged as being sourced from other persons.
iv. This thesis does not contain the writing of others, unless specifically acknowledged as being sourced from other researchers. Where other sources have been quoted then;
    a) Their words have been re-written, but the general information attributed to them has been referenced,
    b) Where their exact words have been used, their writing has been inside quotations marks, and referenced.
v. This thesis does not contain text, graphics or tables copied and pasted from the internet, unless specifically acknowledged, and the source being detailed in the thesis and in the References sections.

Signed…… ……..

Siphesihle Mangena Khumalo

As the candidate's supervisors we agree to the submission of this thesis

Signed… Signed…… …….

Prof. Sudesh Rathilal Prof. Babatunde Femi Bakare

DECLARATION 2 – PUBLICATIONS

DETAILS OF CONTRIBUTIONS TO PUBLICATIONS

Paper I: Khumalo, S.M., Makhathini, T.P., Bwapwa, J.K., Bakare, B.F. and Rathilal, S., 2023. The Occurrence and Fate of Antibiotics and Nonsteroidal Anti-Inflammatory Drugs in Water Treatment Processes: A Review. *Journal of Hazardous Materials Advances,* p. 100330 (https://doi.org/10.1016/j.hazadv.2023.100330).

Contribution: I designed the layout of the manuscript with suggestions from Dr. Makhathini and Dr. Bwapwa. I wrote the manuscript with suggestions and corrections from Dr. Makhathini, Dr. Bwapwa, Prof. Bakare and Prof. Rathilal.

Paper II: Khumalo, S.M., Bakare, B.F. and Rathilal, S., 2022. The occurrence and bioremediation of emerging polyfluorinated compounds in water bodies: a mini review. *Applied Sciences*, *12*(23), p.12196 (https://doi.org/10.3390/app122312196).

Contribution: I designed the layout of the manuscript and wrote the first draft. Prof. Bakare and Prof. Rathilal proofread the manuscript with recommendations.

Paper III: Khumalo, S.M., Bakare, B.F. and Rathilal, S., 2024. Single and Multicomponent Adsorption of Amoxicillin, Ciprofloxacin, and Sulfamethoxazole on Chitosan-Carbon Nanotubes Hydrogel Beads from Aqueous Solutions: Kinetics, Isotherms, and Thermodynamic Parameters. *Journal of Hazardous Materials Advances*, p.100404 (https://doi.org/10.1016/j.hazadv.2024.100404).

Contribution: I designed the study with suggestions from Prof. Bakare and Prof. Rathilal. I performed the calculations and wrote the manuscript with recommendations from Prof. Bakare and Prof. Rathilal.

Paper IV: Khumalo, S.M., Bakare, B.F. and Rathilal, S., 2024, April. The Effect of Competing Ions on the Sorption of Amoxicillin, Ciprofloxacin, and Sulfamethoxazole on Chitosan-Carbon Nanotube Hydrogel Beads. In *Proceedings of the 9th World Congress on Civil, Structural, and Environmental Engineering (CSEE 2024),* April 14 – 16, London, United Kingdom (The Effect of Competing Ions on the Sorption of Amoxicillin, Ciprofloxacin, and Sulfamethoxazole on Chitosan-Carbon Nanotube Hydrogel Beads (avestia.com)).

Contribution: I wrote the manuscript with suggestions from Prof. Bakare and Prof. Rathilal. I did the paper presentation at the Imperial College in London, United Kingdom.

Paper V: Khumalo, S.M., Bakare, B.F. and Rathilal, S., 2024. Single and Binary Adsorption of Perfluorooctanoic Acid and Perfluorooctane Sulfonic Acid on Chitosan-Carbon Nanotubes Hydrogel Beads: Optimization, Kinetics, Isotherms, Thermodynamic Parameters and Effect of Competing ions. *(Under review).*

Contribution: I designed the study with suggestions from Prof. Bakare and Prof. Rathilal. I performed the calculations and wrote the manuscript with recommendations from Prof. Bakare and Prof. Rathilal.

Paper VI: Khumalo, S.M., Bakare, B.F. and Rathilal, S., 2024. Sorption of antibiotics and perfluoroalkyl acids on chitosan-carbon nanotube hydrogel beads in a fixed-bed column: Effect of Operating Conditions on Breakthrough Curves. *(Under review).*
Contribution: I designed the study with suggestions from Prof. Bakare and Prof. Rathilal. I performed the calculations and wrote the manuscript with recommendations from Prof. Bakare and Prof. Rathilal.

Paper VII: Khumalo, S.M., Lasich, M., Bakare, B.F. and Rathilal, S., 2022. Sorption of perfluorinated and pharmaceutical compounds in plastics: a molecular simulation study. *Water*, *14*(12), p.1951 (https://doi.org/10.3390/w14121951).
Contribution: I designed the study with the help of Dr. Lasich. I wrote the manuscript with suggestions from Dr. Lasich. Prof. Bakare and Prof. Rathilal, proofread the manuscript and made critical recommendations.

Paper VIII: Khumalo, S.M., Babatunde, F.B. and Rathilal, S., 2023. Optimization of Ciprofloxacin Sorption on Chitosan-Nanotube Composite Using Response Surface Methodology: Process Variables and Affinity Evaluation. *International Journal of Design & Nature and Ecodynamics* (https://doi.org/10.18280/ijdne.180610).
Contribution: I designed the study and performed data analysis. I wrote the manuscript, Prof. Bakare and Prof. Rathilal made recommendations on the final draft.

Paper IX: Khumalo, S.M., Bakare, B.F. and Sudesh, Rathilal., 2023, November. Simultaneous Sorption of Ciprofloxacin and Amoxicillin on Chitosan Composites from Aqueous Solutions: Kinetics and Isotherms. In *Proceedings of the 39th JOHANNESBURG International Conference on "Chemical, Biological and Environmental Engineering" (JCBEE-23),* Johannesburg 16 - 17, South Africa (https://doi.org/10.17758/IICBE5.C1123026).
Contribution: I wrote the manuscript with suggestions from Prof. Bakare and Prof. Rathilal. I did the paper presentation.

…
Mr. Siphesihle Mangena Khumalo

…
Prof. Sudesh Rathilal

…
Prof. Babatunde Femi Bakare

DEDICATION

I dedicate this thesis to,

My loving and caring mother, Ntombikayise Dlamini, even though words will never do enough in thanking you for the great contribution you made in my life, I want you to know I am deeply grateful for you. You have supported me and encouraged me through my entire life. You are the best among the rest, all I am or hope to be, I truly owe to you.

In memory of my father, Krasmus Khumalo, if I could write a story, it would be the greatest ever told of a kind and loving father who had a heart of gold.

To my family, you all taught me being a family means you are a part of something very wonderful. It means you will love and be loved for the rest of your life.

And

To Phumelele Mkhize, if I were to judge you by the cover, I wouldn't have you anywhere around me, but when you came close, I realised it's the hard shell covering a lot of kindness, caring and sweetness inside. We know each other so well and make a great team. I will forever be grateful for your courageous words.

ACKNOWLEDGEMENTS

"*No man is an island, entire of himself*" John Donne (1572 – 1631). I would like to express my heartfelt gratitude to the following persons and organisations for their endless help and support they furnished me during the period I was conducting this research work. Without their passionate participation and input, this doctorate would not have been possible.

i. My supervisors, **Prof. Sudesh Rathilal** and **Prof. Babatunde Femi Bakare**, the diverse knowledge in this research field, constructive critics, and valuable insight has added significant value to this doctoral thesis.
ii. The Environmental Pollution and Remediation Research Group at the Mangosuthu University of Technology and the Durban University of Technology for funding this project.
iii. **Dr. Madison Matt Lasich** for her valuable contribution with the use of material studio.
iv. **Dr. Thobeka Makhathini** and **Dr. Joseph Bwapwa** for their valuable contributions in the design of the literature review layout and writing.
v. The **Department of Chemical Engineering** staff members at the Mangosuthu University of Technology and **Green Engineering Research Group** postgraduate students at the Durban University of Technology for their unceasing moral support and valuable insight towards this project.
vi. **Mrs. Maureen Msimango** for her valuable contribution in performing samples analysis.

ABSTRACT

The environmental occurrence of antibiotics and perfluoroalkyl acids (PFAAs), particularly in portable water sources, is very evident that current wastewater treatment plants cannot completely eradicate these emerging contaminants of environmental concern. On the other hand, long term exposure to these contaminants poses serious health risks to human and aquatic life. Available literature suggests that antibiotics and PFAAs can be eradicated by solid-liquid adsorption. Therefore, there is an urgent need to develop environmentally green and cost-effective adsorbents for the remediation of antibiotics and PFAAs.

As such, the present study focuses on investigating the treatment efficiency of chitosan-carbon nanotube (CCNT) hydrogel beads for the removal of antibiotics viz. amoxicillin (AMX), ciprofloxacin (CIP), and sulfamethoxazole (SMX) as well as PFAAs i.e., perfluorooctanoic acid (PFOA) and perfluorooctane sulfonic acid (PFOS) from synthetic aqueous solutions. The scope of the present work includes elucidating the adsorption kinetics, isotherms, thermodynamic parameters as well as breakthrough curves for the uptake of AMX, CIP, SMX, PFOS and PFOS on CCNT hydrogel beads. Moreover, Monte Carlo simulations were performed to elucidate the interaction of PFOA, PFOS and sulfamethazine (SMT) with polyethylene (PE) and polypropylene (PP) relative to water.

Herein, CCNT hydrogel beads were synthesised using a two-step precipitation approach and analysed using Fourier transformation infrared (FTIR) technology. From the FTIR results it was evident that the synthesised model adsorbent was characterised with strong peaks of carboxylic and hydroxyl functional groups which were essential for the uptake of the model adsorbates i.e., AMX, CIP, SMX, PFOA and PFOS. Post the adsorption process, band stretches were observed cementing the uptake of the model adsorbates on CCNT hydrogel beads. Single adsorption kinetics experimental data for the uptake of AMX, CIP, SMX, PFOA and PFOS were well fitted by the nonlinear pseudo-first order (PFO) kinetic model recording R^2 values of more than 0.9 for all model adsorbates. It is worth noting that the competing PFO and pseudo-second order (PSO) kinetic models were validated by applying the Bayesian Information Criterion (BIC) as a statistical analysis parameter. Furthermore, the findings of the present study from the Weber-Morris kinetic model suggest that multiple processes were limiting the overall adsorption rate of AMX, CIP, SMX, PFOA and PFOS on CCNT hydrogel beads.

Adsorption isotherm studies were conducted for a temperature range of 283 K, 293 K and 303 K for a contact time of 24 hours for AMX, CIP, and SMX, and 168 hours for PFOA and PFOS. The findings of the present study suggest that AMX, CIP, SMX, PFOA and PFOS single adsorption experimental data were well fitted by the nonlinear Freundlich isotherm model suggesting the heterogeneity of the surface as well as the exponential distribution of the active sites of the model adsorbent. On the other hand, the binary and ternary AMX, CIP, and SMX adsorption experimental data were well fitted by the nonlinear

competitive extended Sips adsorption isotherm model. Furthermore, results for the binary and ternary adsorption systems explicitly demonstrated that the multicomponent adsorption systems exhibited both antagonistic and synergistic effects on the uptake of AMX, CIP and SMX. Interestingly, binary adsorption experimental data for PFOA and PFOS were well fitted by the extended-Langmuir isotherm model (R^2=0.996 for PFOA and R^2=0.995 for PFOS) and extended-Sips isotherm model (R^2=0.996 for PFOA and R^2=0.997 for PFOS), with the system strictly exhibiting antagonistic effects for the uptake of one adsorbate in the presence of another adsorbate. From thermodynamic studies, it is evident that the uptake of AMX, CIP, SMX, PFOA and PFOS is an endothermic process, and it cannot be explicitly classified as a chemical nor physical adsorption process but as a physicochemical adsorption process.

The presence of sodium chloride (NaCl) and humic acid (HA) demonstrated antagonistic effects on the uptake of AMX, CIP and SMX by CCNT hydrogel beads due to formation of aggregates with an increase in ionic strength. Single factor analysis of variance results recorded p-values of less than 0.05 for the uptake of AMX, CIP and SMX indicating that there was a statistical difference between the means of the independent and depended variables, thus cementing the negative effect of increasing ionic strength on the uptake of the mode adsorbates. However, NaCl ions exhibited minimal competitive effects with adsorbate molecules for active adsorption sites on CCNT hydrogel beads compared to HA. On the other hand, the presence of NaCl as a competing ion exhibited synergistic effects in the uptake of PFOA and PFOS from aqueous solutions.

Furthermore, for the present work, breakthrough curves from the experimental data were well fitted by the Thomas model recording R^2 and adjusted-R^2 values of greater than 0.9 for all adsorbates investigated indicating that the breakthrough curves for the present work can be described by a symmetrical function. Additionally, the breakthrough points time predicted by the Thomas model was aligned with the experimentally determined breakthrough points time cementing its practical utility and superiority over the log-Gompertz and Bohart-Adams models. On the other hand, from the Monte Carlo simulation results, it is evident that, in an aqueous environment, both PFOA and PFOS may be taken up preferentially by PP and PE, although less strongly by PE. The degree of polymerisation of PE and PP did not significantly influence the observed behaviour. In terms of sorption affinity, the observed affinity was PFOA>PFOS>SMT which was consistent for both PE and PP.

Based on the results obtained, it was concluded that CCNT hydrogel beads composites have the potential to be applied as adsorbents for the removal of antibiotics and PFAAs from aqueous solutions. Furthermore, the simulation results obtained suggest that Monte Carlo simulations in Material Studio can be used as an effective tool in elucidating the interaction between antibiotics and PFAAs with microplastics relative to water as co-existing contaminants. Therefore, the findings of the present work have successfully addressed the research questions for the current study.

TABLE OF CONTENT

LIST OF FIGURES

LIST OF TABLES

CHAPTER ONE: INTRODUCTION

1.1. Background Information

1.1.1. Antibiotics

Antibiotics can be defined as chemotherapeutic agents that inhibit or eliminate the growth of microorganisms, such as bacteria, fungi, and/or protozoa (de Ilurdoz, Sadhwani and Reboso 2022). As such, they are widely used for the treatment of common infectious diseases making them crucial drugs for humans and veterinary medicine (Darvishi *et al.* 2023). However, the misuse and/or long-term exposure to antibiotics has resulted in the rapid rise of antimicrobial resistance with some infections now effectively untreated (Hutchings, Truman and Wilkinson 2019). Sadly, in South Africa, different classes of antibiotics have been detected in wastewater treatment plant (WWTP) effluent streams, surface water, seawater as well as in drinking water at trace concentrations ranging from ng/L to µg/L posing a serious health risk to human and aquatic organisms (Madikizela, Tavengwa and Chimuka 2017; Madikizela, Ncube and Chimuka 2020; Madikizela *et al.* 2020). The occurrence of antibiotics in aquatic environments is ascribed to their excretion through urine or faeces in their original forms or their metabolites, improper disposal of antibiotics, as well as the use of animal manure (Madikizela *et al.* 2020; Khumalo *et al.* 2023). Madikizela *et al.* (2020) reported that, due to high water solubility and presence of polar functional groups in the chemical structures of antibiotics, their native compounds and metabolites are discharged into surface water as part of WWTP effluent streams thus increasing their exposure to humans and aquatic organisms making them susceptible to antimicrobial resistance.

Figure 1.1 presents, through the human food chain, the connection between the use of antibiotics and human health which has become an issue of global concern. It is apparent from Figure 1.1 that it begins with the normal intake of antibiotics by human and animals. These antibiotics are subsequently excreted by humans and animals which eventually enter WWTPs which generate biosolids and effluent discharges that causes soil and aquatic environment pollution. The polluted environment subsequently result in food and drinking water contamination leading to infections by drug resistant bacteria which have become even more difficult to treat, as elucidated by de Ilurdoz, Sadhwani and Reboso (2022). The current problem faced by South Africa and other countries in the African region, is that WWTPs are not designed to eliminate these types of emerging contaminants. As such, there is an urgent need of new wastewater treatment technologies for the removal of antibiotics from various water bodies.

1.1.2. Perfluoroalkyl Acids

Perfluoroalkyl acids (PFAAs), also known as “perfluorinated compounds (PFCs),” are synthetic organic surfactants that contain one or more carbon atoms on which all the hydrogen substituents have been

replaced by fluorine atoms such that they contain the perfluoroalkyl moiety attached to a hydrophilic functional group (i.e., C_nF_{2n+1}-R) (Buck *et al.* 2011; Xiao 2017; Lenka, Kah and Padhye 2021). Due to the carbon-fluorine bond, the perfluoroalkyl moiety is characterised with chemical and thermal stability in addition to its hydrophobic and lipophobic nature (Lee *et al.* 2020).

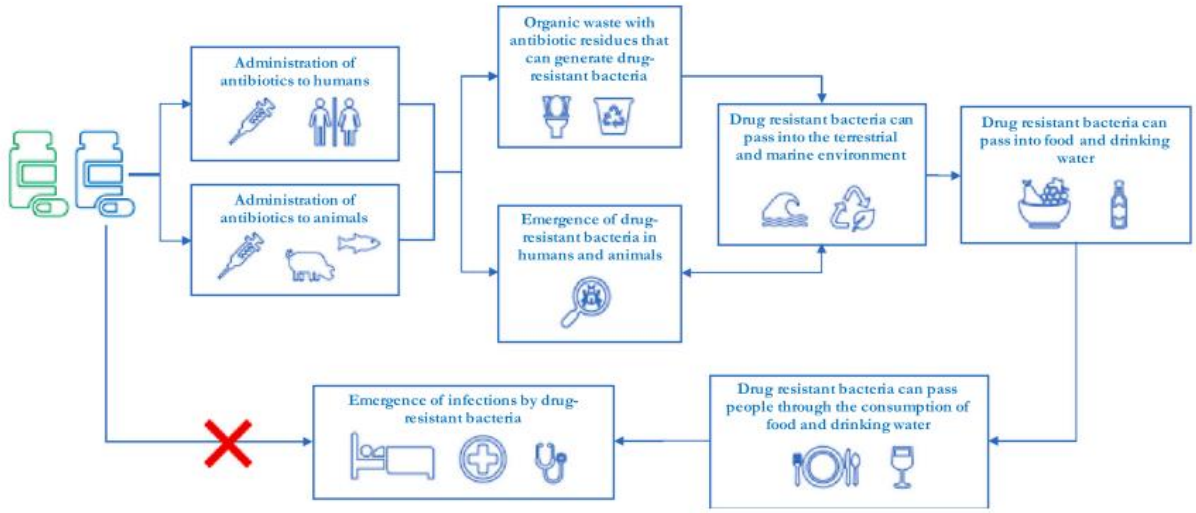

Figure 1.1: Connection between the use of antibiotics and human health. Adapted from de Ilurdoz, Sadhwani and Reboso (2022).

Owing to these properties, PFAAs are widely used in diverse industrial applications and consumer products such as firefighting foams, surfactants, surface protectors, erosion inhibitors in aircraft hydraulic fluid, coating-ingredient for clothing fabrics, leather and carpets, electronic etching bath surfactants, photographic emulsifiers, paints and adhesives, as elucidated by Lee *et al.* (2020); Zhang *et al.* (2021) and Lenka, Kah and Padhye (2021) in their latest reviews. As such, PFAAs are released into the aquatic environment through surface runoff, product degradation and/or industrial wastewater effluent. Consequently, PFAAs have been detected in aquatic environments, drinking water, WWTP effluent streams as well as in wild life and human serum (Lenka, Kah and Padhye 2021).

Human and animal exposure to PFAAs can cause a wide range of adverse health effects such as reproductive toxicity, oxidative stress, metabolism disturbance, immune toxicity, developmental toxicity, genotoxicity, neurotoxicity, disrupting thyroid functions as well as carcinogenicity (Lee *et al.* 2020; Ojo, Peng and Ng 2021; Zhang *et al.* 2021). The exposure sources to PFAAs can be via. direct source i.e., dietary intake, water intake as well as skin contact and indirect source i.e., metabolic transformation of PFAA precursors into more toxic PFAAs such as perfluorooctanoic acid (PFOA) and perfluorooctane sulfonic acid (PFOS) enriching them in the aquatic environment. As such, PFOA and PFOS are the most detected and used classes of PFAAs drawing the attention of national and

international environmental authorities due to their hazardous and toxic effects on human and ecological environments. It is apparent that the removal of PFAAs particularly in WWTP influent streams has become an utmost need and a demand for the protection of the environment.

1.2. Motivation

Despite the advancement in the development of water and wastewater treatment technologies, such as the use of carbon-based adsorbents, contaminants of emerging environmental concern (i.e., antibiotics and PFAAs) are still being detected in WWTP effluent streams. Carbon based adsorbents such as carbon nanotubes have demonstrated the ability to minimise contaminants of emerging concern from aqueous environments. However, the topic on carbon-based adsorbents, carbon nanotubes in particular, is not yet exhausted since there are some challenges that are associated with this technology such as adsorbent (CNTs) regeneration, high processing costs and the occupation of adsorption sites by non-targeted pollutants. Furthermore, literature on multicomponent adsorption studies, thermodynamic parameters, breakthrough curves modelling as well as elucidating the environmental interaction of antibiotics and PFAAs with other coexisting emerging contaminants of environmental concern such as microplastics is scanty. On the other hand, the environmental occurrence of antibiotics and PFAAs is posing a serious health risk to humans as well as fauna and flora. As such, there is a need to develop low-cost adsorbents from natural material such as chitosan composites for the removal of antibiotics and PFAAs from aqueous solutions.

Therefore, the present study provides a holistic understanding on the environmental occurrence and fate of antibiotics and PFAAs in wastewater treatment processes. The study contributes to elucidating the uptake mechanisms of antibiotics and PFAAs on chitosan-carbon nanotube composites through the study of adsorption kinetics, isotherms, and thermodynamic parameters for an effective system design. Moreover, the study contributes to the investigation of the effect of operating parameters for a continuous process through the modelling of breakthrough curves which provides understanding on the process behaviour and its dynamics. Lastly, the study contributes to the understanding of the interactions between antibiotics and PFAAs with microplastics relative to water, thus elucidating to their health effects to humans and aquatic organisms.

1.3. Research hypotheses and questions

The following are the conceptual theories upon which this study is based on, consequently, there are various questions that need to be addressed.

i. It is hypothesised that chitosan and carbon nanotubes will form stable hydrogel beads for possible application in water treatment processes for the uptake of antibiotics and PFAAs.

ii. It is hypothesised that chitosan-carbon nanotube hydrogel beads will exhibit functional groups that will promote the uptake of antibiotics and PFAAs.
iii. It is hypothesised that the uptake of one adsorbate in the presence of another adsorbate will exhibit antagonistic effects due to competition of active sites for adsorption.
iv. It is hypothesised that antibiotics and PFAAs can be adsorbed into microplastics in aquatic environments as a transport vector.

The present study therefore ought to answer the following questions:

i. Would chitosan-carbon nanotube composites, therefore, feasibly be used as an adsorbent for the removal of antibiotics and PFAAs?
ii. Can artificial intelligence through the application of Material Studio as a simulation tool be effectively used in studying the interaction between antibiotics and PFAAs with microplastics relative to water as co-existing contaminants?

1.4. Aim and Objectives

The primary aim of the present study is to investigate the treatment efficiency of chitosan-carbon nanotube hydrogel beads for the removal of antibiotics (i.e., amoxicillin, ciprofloxacin and sulfamethoxazole) and PFAAs (i.e., PFOA and PFOS) from aqueous solutions. In achieving the aim of the present study, the following objectives were investigated:

i. Evaluate the performance of synthesised chitosan-carbon nanotube hydrogel beads on the removal of amoxicillin, ciprofloxacin, sulfamethoxazole, PFOA and PFOS from aqueous solutions through batch studies.
ii. Evaluate adsorption kinetics, isotherms, thermodynamic parameters as well as the effect of solution pH, adsorbent dose, contact time and initial adsorbate concentration on the removal of the model antibiotics and PFAAs.
iii. Perform fixed-bed adsorption column studies to investigate the effect of operating parameters such as volumetric flow rate, initial adsorbate concentration and fixed-bed height on the adsorption breakthrough curves.
iv. Investigate the sorption of antibiotics and PFAAs relative to water on micro-plastics as a carrier in water bodies by employing the extended Flory-Huggin's approach in Material Studio.

1.5. Thesis organisation

Chapter One:

This chapter presents a brief discussion on the impact on human and animal health as a result of the occurrence of antibiotics and PFAAs in aquatic environments. The motivation, primary aim as well as objectives of the study are described in this chapter. Moreover, the chapter presents the layout of the thesis and a brief discussion of the content presented in the subsequent chapters.

Chapter Two:

The environmental occurrence and fate of pharmaceutical compounds, precisely antibiotics and nonsteroidal anti-inflammatory drugs, were systematically examined and presented in this chapter. The scope of the work presented in this chapter is in the order of a brief introduction on environmentally threatening pharmaceutical compounds, a section discussing the occurrence of pharmaceutical compounds from different point sources, a discussion on environmental impact and regulations, a comprehensive discussion on the treatment technologies of pharmaceutical compounds i.e., biological processes, advanced oxidation processes as well as chitosan-based adsorption processes. The chapter concludes by addressing the current gap through a discussion on future perspectives as far as chitosan-based adsorption processes are concerned. It is worth noting that this chapter is published as **paper I** (https://doi.org/10.1016/j.hazadv.2023.100330).

Scientific contribution/novelty: This chapter provides an overview of the findings reported in literature on the detection frequency and quantity of selected pharmaceutical compounds in wastewater treatment plants influent and effluent streams. The chapter identifies knowledge gaps of the emerging water treatment technologies with future perspectives.

Chapter Three:

This chapter which is published as **paper II** (https://doi.org/10.3390/app122312196) presents a systematic review on the occurrence of PFOA and PFOS in water bodies and emerging research on their biodegradation as they are known to be xenobiotic compounds. The chapter begins with an introduction on the chemistry of PFOA and PFOS as well as their industrial applications. Moreover, the occurrence of PFOA and PFOS in water bodies was examined in this chapter together with emerging bioremediation techniques of PFOA and PFOS from aquatic environments. The chapter concludes with a discussion on future perspectives.

Scientific contribution/novelty: This chapter provides an overview on the occurrence of PFAAs precisely PFOA and PFOS in water bodies as well as the latest development in PFAAs remediation subsequently contributing to the design of sustainable green PFAAs remedial processes.

Chapter Four:

This chapter endeavours to answer the questions raised in objectives i and ii of the current study precisely on the sorptive studies of amoxicillin, ciprofloxacin and sulfamethoxazole on chitosan-carbon nanotube hydrogel beads. The chapter begins with a brief introduction explicitly addressing the research gap that is being addressed by the findings of the present study. The experimental procedure that was adopted as well as model evaluation is explicitly presented under the material and methods section. The discussion of results is presented into four main subsections i.e., 1) a succinct discussion on the synthesised adsorbent, 2) a discussion on the effect of operating parameters such as solution pH, initial adsorbate concentration, and adsorbent dose on the removal of the model antibiotics as adsorbates. Moreover, the results section presents a discussion on single adsorption kinetics, isotherms and thermodynamic studies examining the uptake mechanism of the model adsorbates on chitosan-carbon nanotube hydrogel beads. Binary and ternary adsorption isotherms for the uptake of the model antibiotics on chitosan-carbon nanotube hydrogel beads are also presented in this chapter. The chapter concludes with a discussion on future perspectives on single and multicomponent adsorption of antibiotics on chitosan-carbon nanotube hydrogel beads. This chapter is published as **paper III** (https://doi.org/10.1016/j.hazadv.2024.100404).

Scientific contribution/novelty: Available literature suggest that no studies have been conducted on multicomponent adsorption for the removal of AMX, CIP and SMX from solution using chitosan-CNT hydrogel beads. Furthermore, available literature suggests that, the application of nonlinear adsorption kinetics and isotherms empirical models are scanty. As such, the novelty of this chapter entails the study of adsorption kinetics by utilising nonlinear empirical models, the study of adsorption isotherms for single, binary and ternary adsorption systems to elucidate the synergistic and/or antagonistic effects of the sorption of one antibiotic in the presence of other antibiotics, and the evaluation of thermodynamic adsorption parameters.

Chapter Five:

This chapter presents the findings of the present study on the effect of competing ions in the form of humic acid and sodium chloride on the uptake of amoxicillin, ciprofloxacin and sulfamethoxazole on chitosan-carbon nanotube hydrogel beads from aqueous solutions. The chapter endeavours to answer the questions raised in objective i. It begins with a brief introduction on the status of antibiotics consumption rate and their occurrence in aquatic environments, which is then followed by a subsection on the methodological approach that was adopted in executing the investigation. Thereafter, the chapter presents a discussion of results on the effect of varying humic acid and sodium chloride on the uptake of the model antibiotics adsorbates on chitosan-carbon nanotube hydrogel beads alongside a discussion on the analysis of variance. This chapter ends with concluding remarks. It is worth noting that this chapter is published as **paper IV**, which is part of a peer reviewed conference proceedings (The Effect

of Competing Ions on the Sorption of Amoxicillin, Ciprofloxacin, and Sulfamethoxazole on Chitosan-Carbon Nanotube Hydrogel Beads (avestia.com)).

Scientific contribution/novelty: Due to the lack of studies focusing on the uptake of antibiotics from solution in the presence of competing ions, herein chitosan-carbon nanotube (chitosan-CNT) hydrogel beads were synthesised via precipitation in an alkaline solution. As such, the novelty of this chapter is evaluating the adsorption efficacy of chitosan-CNT hydrogel beads for the uptake of AMX, CIP and SMX in the presence of sodium chloride and humic acid as competing ions.

Chapter Six:

This chapter presents the findings of the study on single and binary adsorption of PFOA and PFOS on chitosan-carbon nanotube hydrogel beads. The chapter endeavours to answer the questions raised in objectives i and ii of the present study. This chapter begins with an introduction describing the environmental status of PFOA and PFOS, drawbacks that are associated with remedial technologies reported in literature, a brief discussion on the properties of chitosan as well as the scientific contribution of the present study. The methodological approach adopted in executing the study is explicitly described under the materials and methods subsection alongside with the adsorption kinetics and isotherms empirical models and parametric optimisation modelling technique that was utilised. The subsection on results and discussion begins with a discussion on the adsorbent functional groups before and after adsorption of PFOA and PFOS, which is then followed by a discussion on parametric optimisation using response surface methodology. Moreover, this chapter also presents a comprehensive discussion on the adsorption kinetics, isotherms, and thermodynamic parameters for the uptake of PFOA and PFOS on chitosan-carbon nanotubes. The chapter ends with a discussion of results on the effect of sodium chloride on the uptake of PFOA and PFOS on the model adsorbent. It is worth noting that, this chapter is presented as **paper V** which is currently under review.

Scientific contribution/novelty: The scientific contribution or novelty of this chapter is the evaluation of the adsorption efficacy of chitosan-CNT hydrogel beads for single and binary adsorption of PFOA and PFOS from aqueous solutions as well as the effect of competing ions on the sorption of PFOA and PFOS.

Chapter Seven:

This chapter is presented as **paper VI** which is currently under review, and it endeavours to answer the question raised in objective iii. This chapter presents the findings of the present study on the effect of operating parameters i.e., volumetric flow rate, initial adsorbate concentration and fixed bed height on the breakthrough curves for the uptake of amoxicillin, ciprofloxacin, sulfamethoxazole, PFOA and PFOS. Moreover, the chapter presents a discussion of results on adsorption column breakthrough curves modelling aimed at investigating the dynamic behaviour of the fixed-bed adsorption system report for the present study.

Scientific contribution/novelty: Most studies in solid-liquid adsorption reported in literature are based on batch adsorption suggesting that studies in continuous systems (i.e., fixed-bed column) are scanty. Therefore, the scientific contribution of this chapter is investigating the effect of operating parameters on the breakthrough curves for the sorptive removal of AMX, CIP, SMX, PFOA and PFOS on chitosan-CNT hydrogel beads in a fixed-bed column as the first case.

Chapter Eight:

The question raised in objective iv of the present study is addressed in this chapter which is published as **paper VII** (https://doi.org/10.3390/w14121951). The chapter begins with an introduction discussing the status as well as human and aquatic life health effects as a result of the occurrence of microplastics, antibiotics (i.e., sulfamethazine), PFOA and PFOS in aquatic environment. The scientific contribution of the present study is described in the introduction subsection of this chapter. The chapter also consists of a materials and methods subsection which presents a comprehensive discussion of the simulation approach that was adopted for the present work. Furthermore, the chapter presents a comprehensive discussion of the results obtained and it ends with concluding remarks as well as future perspectives.

Scientific contribution/novelty: The scientific contribution of this chapter is the study of adsorption mechanisms of antibiotics and PFAAs by investigating the thermodynamic interaction of PFOA, PFOS and sulfamethazine in polyethylene (PE) and polypropylene (PP) through phase equilibrium and mixing using the extended Flory-Huggins approach in Material Studio as the first case. It is worth noting that, there are no reported studies on investigating the effect of temperature and polymerization on the thermodynamic interaction of the aforementioned compounds with PE and PP using the extended Flory-Huggins approach

Chapter Nine:

This chapter provides conclusions and recommendations based on the findings presented in the previous chapters. Recommendations for future research on antibiotics and PFAAs removal from aquatic environments are also presented in this chapter.

References

Buck, R. C., Franklin, J., Berger, U., Conder, J. M., Cousins, I. T., De Voogt, P., Jensen, A. A., Kannan, K., Mabury, S. A. and van Leeuwen, S. P. 2011. Perfluoroalkyl and polyfluoroalkyl substances in the environment: terminology, classification, and origins. *Integrated environmental assessment and management*, 7 (4): 513-541.

Darvishi, P., Mousavi, S. A., Mahmoudi, A. and Nayeri, D. 2023. A comprehensive review on the removal of antibiotics from water and wastewater using carbon nanotubes: synthesis, performance, and future challenges. *Environmental Science: Water Research & Technology*, 9 (1): 11-37.

de Ilurdoz, M. S., Sadhwani, J. J. and Reboso, J. V. 2022. Antibiotic removal processes from water & wastewater for the protection of the aquatic environment - a review. *Journal of Water Process Engineering*, 45: 102474.

Hutchings, M. I., Truman, A. W. and Wilkinson, B. 2019. Antibiotics: past, present and future. *Current opinion in microbiology*, 51: 72-80.

Khumalo, S. M., Makhathini, T. P., Bwapwa, J. K., Bakare, B. F. and Rathilal, S. 2023. The Occurrence and Fate of Antibiotics and Nonsteroidal Anti-Inflammatory Drugs in Water Treatment Processes: A Review. *Journal of Hazardous Materials Advances*: 100330.

Lee, J. W., Choi, K., Park, K., Seong, C., Yu, S. D. and Kim, P. 2020. Adverse effects of perfluoroalkyl acids on fish and other aquatic organisms: A review. *Science of The Total Environment*, 707: 135334.

Lenka, S. P., Kah, M. and Padhye, L. P. 2021. A review of the occurrence, transformation, and removal of poly- and perfluoroalkyl substances (PFAS) in wastewater treatment plants. *Water Research*, 199: 117187.

Madikizela, L. M., Ncube, S. and Chimuka, L. 2020. Analysis, occurrence and removal of pharmaceuticals in African water resources: A current status. *Journal of environmental management*, 253: 109741.

Madikizela, L. M., Ncube, S., Tutu, H., Richards, H., Newman, B., Ndungu, K. and Chimuka, L. 2020. Pharmaceuticals and their metabolites in the marine environment: sources, analytical methods and occurrence. *Trends in Environmental Analytical Chemistry*, 28: e00104.

Madikizela, L. M., Tavengwa, N. T. and Chimuka, L. 2017. Status of pharmaceuticals in African water bodies: Occurrence, removal and analytical methods. *Journal of environmental management*, 193: 211-220.

Ojo, A. F., Peng, C. and Ng, J. C. 2021. Assessing the human health risks of per- and polyfluoroalkyl substances: A need for greater focus on their interactions as mixtures. *Journal of Hazardous Materials*, 407: 124863.

Xiao, F. 2017. Emerging poly- and perfluoroalkyl substances in the aquatic environment: A review of current literature. *Water Research*, 124: 482-495.

Zhang, W., Pang, S., Lin, Z., Mishra, S., Bhatt, P. and Chen, S. 2021. Biotransformation of perfluoroalkyl acid precursors from various environmental systems: advances and perspectives. *Environmental Pollution*, 272: 115908.

CHAPTER TWO: LITERATURE REVIEW – PART I

THE OCCURRENCE AND FATE OF ANTIBIOTICS AND NONSTEROIDAL ANTI-INFLAMMATORY DRUGS IN WATER TREATMENT PROCESSES

2.1. Abstract

The recent surfacing of novelty viruses such as the coronavirus (COVID-19) and other conventional viruses have resulted in a significant increase in the use of pharmaceuticals, particularly antibiotics and nonsteroidal anti-inflammatory drugs (NSAIDs). This is attributed to their design to modulate the endocrine and immune system of the body. Subsequently, these contaminants of emerging concern are introduced into water-receiving bodies through animal and human excretion, unregulated disposal, and anthropogenic activities, resulting in their occurrence in trace amounts. Despite their occurrence in trace amounts, these classes of emerging contaminants can be persistent or only partially degraded during water treatment processes; hence they have eluded conventional wastewater treatment plant (WWTP) technologies. Moreover, long-term exposure to pharmaceutical compounds poses serious health risks to human and aquatic flora and fauna due to their bioaccumulation. Hence, the current study provides a holistic review on the occurrence of selected antibiotics and NSAIDs in surface water and their fate in wastewater treatment processes. This chapter provides an overview of the findings reported in the literature on the detection frequency and quantity of selected pharmaceuticals in WWTP influent and effluent streams. Furthermore, the review highlights the findings reported in the literature on the potential application of bioremediation processes, advanced oxidation processes, and chitosan-based adsorbents on pharmaceutical remediation. Finally, the chapter concludes by identifying knowledge gaps in the reported technologies with future perspectives.

2.2. Introduction

Pharmaceuticals are characterised as drugs containing active pharmaceutical ingredients designed to treat various ailments in animals and humans (Kanakaraju, Glass and Oelgemöller 2018). Although pharmaceuticals are utilised for human and animal health improvement, their environmental occurrence has become a health hazard owing to their persistence, Deoxyribonucleic Acid (DNA) damage, microbial resistance, toxic effects, ecotoxicity, bioaccumulation, and non-bioremediation by conventional wastewater treatment plants (WWTPs) (Felis *et al.* 2020; Khan *et al.* 2020). Recently, there has been a growing interest in studies focusing on the occurrence and fate of pharmaceutical compounds in the environment (Liu and Wong 2013; Matongo *et al.* 2015b, 2015a; Liu *et al.* 2016; Madikizela and Chimuka 2016; Balakrishna *et al.* 2017; Lyu *et al.* 2020; O'Flynn *et al.* 2021; Jurado *et*

al. 2022; Khumalo *et al.* 2022; Silori and Tauseef 2022; Arvaniti *et al.* 2023). As such, these compounds have been characterised as contaminants of emerging concern to raise awareness in the scientific community about the need to develop methods for their detection, fate, biochemistry, treatment, and toxicity in water bodies.

The detection of pharmaceuticals in surface water is attributed to their continuous release into the ecosystem from various point sources such as households, hospitals, and pharmaceutical industries (Almomani *et al.* 2016). Environmentally threatening groups of pharmaceuticals include antibiotics, nonsteroidal anti-inflammatory drugs (NSAIDs), beta-blockers, X-ray contrast media, antidepressants, and hormones (Kanakaraju, Glass and Oelgemöller 2018). These compounds end up in WWTPs; as such, their occurrence in water bodies (Madikizela and Chimuka 2016, 2017; Folarin *et al.* 2019; Patel *et al.* 2019; Kovalakova *et al.* 2020) is evident that they elude conventional biological and chemical wastewater treatment processes. Hence, WWTPs have been characterised as the main point source for pharmaceutical compounds, which is attributed to the fact that untreated effluents from veterinaries, hospitals, and industries are combined with domestic wastewater and transferred to WWTPs (Khan *et al.* 2020; Kovalakova *et al.* 2020).

Different treatment processes, including biological processes (Larcher and Yargeau 2011; Amorim *et al.* 2014; Mueller 2016; Bessa *et al.* 2017; Pan *et al.* 2017; Pan *et al.* 2018), advanced oxidation processes (Ying *et al.* 2015; Patel *et al.* 2019), nanofiltration (Cristóvão *et al.* 2019; Wei *et al.* 2021), reverse osmosis (Lopera, Ruiz and Alonso 2019), as well as the application of chitosan-based adsorbents (Yaqubi *et al.* 2021) have been reported as effective treatment options for the removal of pharmaceutical compounds from wastewater. This chapter provides a holistic review on the occurrence and environmental impact of pharmaceutical compounds in water bodies, followed by an overview of the antibiotics and NSAIDs remediation processes reported in literature. The chapter focuses on the degradation mechanism of pharmaceutical compounds by novel bacterial strains and advanced oxidation processes reported in literature. Lastly, the chapter gives special attention to the work reported on the potential application of chitosan-based processes on the removal of pharmaceuticals from wastewater streams.

2.3. Occurrence of pharmaceutical compounds (PCs) in surface water

2.3.1. Through human consumption

The environmental and health risks associated with the occurrence of pharmaceuticals in aquatic streams have been widely researched (Agunbiade and Moodley 2016; Madikizela and Chimuka 2016; Ali *et al.* 2017; Madikizela and Chimuka 2017). One of the most prevalent pharmaceuticals in the aquatic system are antibiotics (Wang, Wang and Yang 2018; Hou *et al.* 2019; Martin-Laurent *et al.* 2019), as well as NSAIDs (Thalla and Vannarath 2020). Antibiotics are commonly used by humans and

animals as the primary treatment of acute illnesses. As a result, these pharmaceuticals are abundant in the environment because millions of people use them daily, thus resulting in their occurrence in surface water (see Table 2.1). Most countries have been showing an upward trend in antibiotic consumption; for instance, China was identified as the largest consumer after India, then followed by the US (Van Boeckel *et al.* 2014). Also, countries in developing economies like South Africa, Russia, and Brazil were highlighted (Gelband *et al.* 2015).

Noticeably, most well-developed economies like Finland, Sweden, Italy, Netherlands, Norway, Luxembourg, and United Kingdom have not recorded an upward trend in antibiotics consumption (CDDEP 2015). Sadly, it is predicted that antibiotics consumption in developing countries will continue to increase until 2030, as their population increases, and presumably, no policy changes imposed (Van Boeckel *et al.* 2014). Ideally, the consumption of antibiotics should decrease to reduce their occurrence in the environment.

Generally, the consumption of antibiotics happens in households, not necessarily in hospitals (Tiseo *et al.* 2020). The frequent prescription of antibiotics by medical practitioners, even for conditions that may not need such treatment, like colds, contributes to environmental stress. As such, these antibiotics end up in the environment owing to human secretion through urine and faeces, sometimes as original compounds (Tran, Reinhard and Gin 2018), as its metabolites (Ghirardini, Grillini and Verlicchi 2020), or as conjugates glucuronic and sulfuric acid (Milić *et al.* 2013). According to Patel *et al.* (2019) pharmaceuticals may metabolize by <10% or >90% before human excretion. Nonetheless, in cases of high antibiotic consumption, there will be high metabolisation, but the original compound will still exist, which contaminates the water stream immensely (Patel *et al.* 2019). This is supported by Dinh *et al.* (2017), who found that sewage systems contained between 70% and 80% of antibiotics in their original compounds. Noticeably, the source for pharmaceuticals existence in water bodies is difficult to identify since they may enter through many sources (Figure 2.1), like, hospital wastewater, household effluent or even manufacturing sites with poor disposal management systems (Hendriksen *et al.* 2019).

Additionally, poorly managed medical waste disposal sites may experience the leaching of antibiotics to contaminate groundwater (Liu and Wong 2013). Also, leaching is possible in cases where latrines or pit toilets are used, leading to groundwater pollution. Moreover, pharmaceuticals can interact with co-existing emerging contaminants such as microplastics and prolong their fate in the aquatic environment while posing even higher health risks to aquatic life and humans.

Table 2.1: Average concentrations of pharmaceutical compounds detected in surface water.

Compound	Structure*	Water solubility (mg/mL)*	Use*	Detection levels	Reference
Amoxicillin	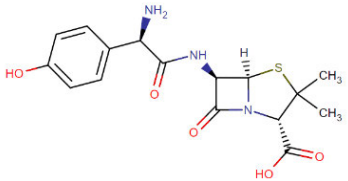	0.958	Treatment of infections caused by gram-positive bacteria.	0 - 88 µg/L	(Patel *et al.* 2019)
				0.008 µg/L	(Folarin *et al.* 2019)
				1.67 µg/L	(Kovalakova *et al.* 2020)
Tetracycline	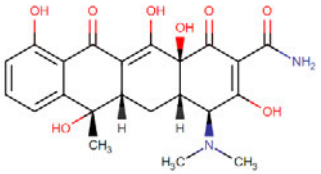	1.33	Treats a wide variety of susceptible infections.	0.08 µg/L	(Patel *et al.* 2019)
				10 ng/g	(Hu *et al.* 2018)
				15.3 ng/L	(Scaria, Anupama and Nidheesh 2021)
Erythromycin	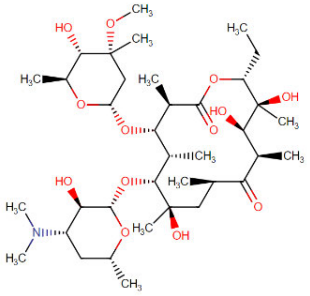	0.002	Is a macrolide antibiotic used to treat and prevent a variety of bacterial infections.	65.8 ng/L	(Lyu *et al.* 2020)
				428 ng/L	(Jurado *et al.* 2022)
				0.03 – 0.26 µg/L	(Madikizela, Tavengwa and Chimuka 2017)
				0.06 – 1.00 µg/L	
Norfloxacin	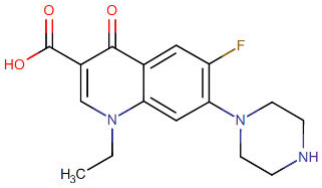	1.01	Treatment of gram-positive and gram-negative bacteria	1.15 µg/L	(Patel *et al.* 2019)
				0.55 ng/g	(Hu *et al.* 2018)
				103 µg/kg	(Lyu *et al.* 2020)

Table 2.1: Continues

Compound	Structure*	Water solubility (mg/mL)*	Use*	Detection levels	Reference
Ciprofloxacin	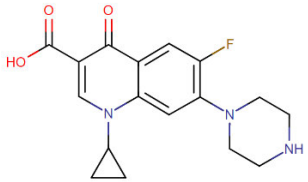	1.35	Treats various susceptible bacterial infections	45.4 µg/L	(Patel *et al.* 2019)
				0.87 ng/g	(Hu *et al.* 2018)
				42.6 ng/L	(Lyu *et al.* 2020)
Sulfamethoxazole	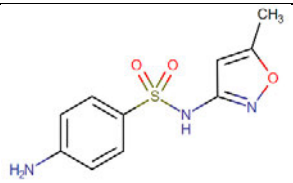	0.459	Treat a variety of infections of the urinary tract, respiratory system, and gastrointestinal tract	0 - 304 µg/L	(Patel *et al.* 2019)
				4.5 ng/g	(Hu *et al.* 2018)
				67.8 µg/kg	(Lyu *et al.* 2020)
Ibuprofen	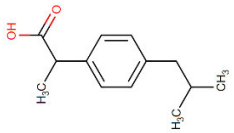	0.0684	Treats mild-moderate pain, fever, and inflammation	17.4 µg/L	(K'oreje *et al.* 2016)
				85 µg/L	(Matongo *et al.* 2015b)
				32.9 µg/L	(Hlengwa and Mahlambi 2020)
				62 µg/L	(Matongo *et al.* 2015a)
Diclofenac	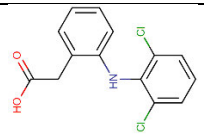	0.00447	Treats the signs and symptoms of osteoarthritis and rheumatoid arthritis	1.2 µg/L	(Amos Sibeko *et al.* 2019)
				2.58 µg/L	(Mhuka, Dube and Nindi 2020)
				0.73 µg/L	(K'oreje *et al.* 2016)
				12.4 µg/L	(Agunbiade and Moodley 2016)

*****Compound structures and solubility data was obtained from https://go.drugbank.com/drugs assessed on 12 December 2022.

Khumalo *et al.* (2022), in a molecular simulation study, investigated the sorption of sulfamethazine relative to water on polyethylene (PE) and polypropylene (PP), and high sorption affinity of sulfamethazine on both PE and PP was reported. The findings suggest that sulfamethazine can be absorbed into microplastics under an aqueous environment. For the most part, wastewater treatment facilities cannot completely remove pharmaceuticals simply because they were not designed with such capabilities (Makhathini, Mulopo and Bakare 2020).

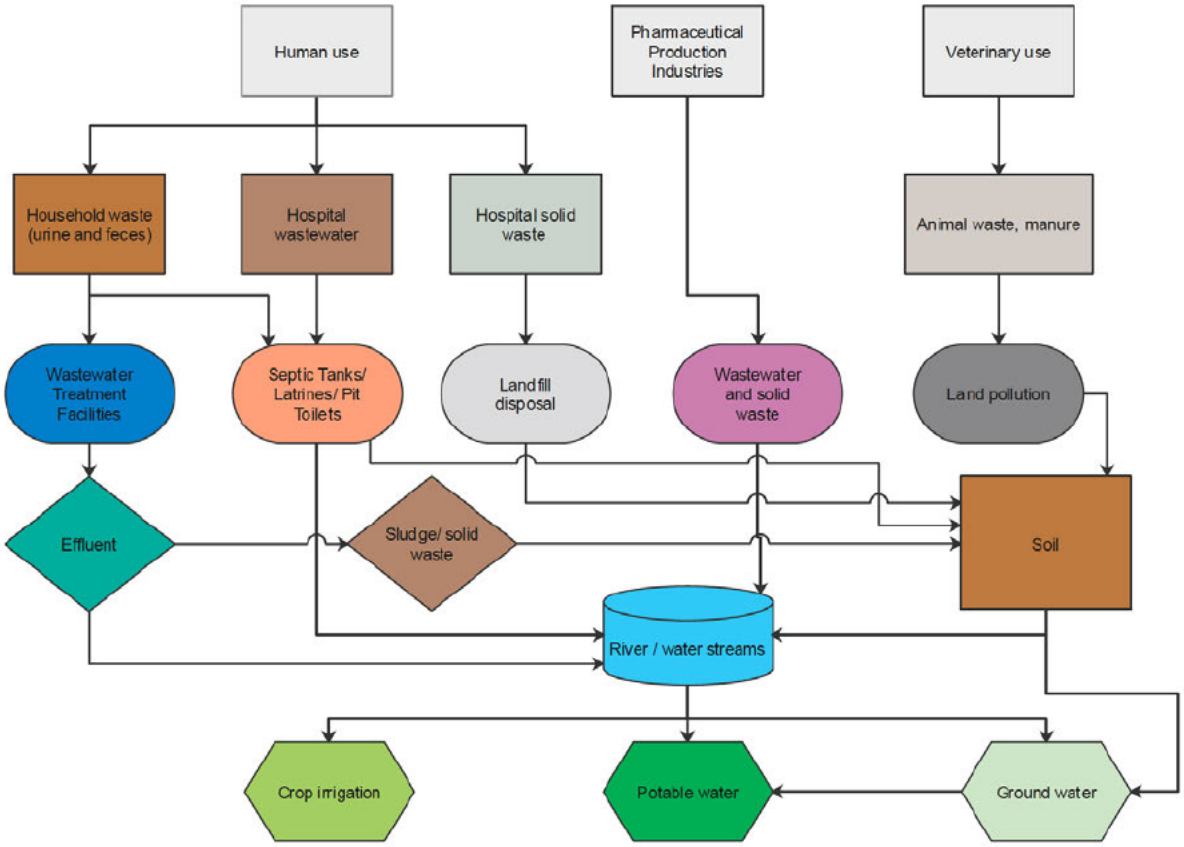

Figure 2.2: Pathway for antibiotics through human use, pharmaceuticals manufacturing industry, and animal use.

2.3.2. Through animal use

Many researchers report that the main source of veterinary pharmaceuticals, including antibiotics to the aquatic environment is due to livestock and farming activities (Kaczala and Blum 2015). The demand for animal protein has increased exponentially around the globe over the last decade; as such, the consumption of antibiotics by food-producing animals has rapidly grown (Van Boeckel *et al.* 2014). Animal antibiotics are commonly present in supplements for fast growth support. These are then excreted as feaces or urine in livestock farms, thus, adversely affecting the aquatic ecosystem (Bilal *et al.* 2020). Some of the antibiotics found in animal medicine are summarised in Table 2.2, with their

potential side effects if ingested by humans. Most importantly, veterinary antibiotics are not absorbed in animal organisms because they are bioactive, seem efficient at low doses, and are excreted after a short period (Tasho and Cho 2016). As such, these antibiotics can convert back into their primary compound after excretion (Tasho and Cho 2016). For instance, some antibiotics become ineffective and analytically undetectable after converting into conjugates like acetylated metabolites. Yet, for manure to be activated, there should be a separation of the acetyl group (Liu *et al.* 2020). It has been a common practice in farming to use some of the excreted organic by-products like faeces as an option for fertiliser (Park *et al.* 2019), then recycle it as manure to lessen the environmental impact of the waste. Moreover, manure is a valuable fertiliser, as it has critical nutrients for plant growth like potassium, phosphorus, organic carbon, and nitrogen (He *et al.* 2015). Regrettably, this practice will likely cause veterinary antibiotics to end up in the environment and ultimately surface and groundwater systems through runoff and percolation, respectively (Yao *et al.* 2017).

Additionally, there is another way through which veterinary antibiotics may enter the environment: ventilation systems containing antibiotics dust from animal stables (Tasho and Cho 2016). The released antibiotics pathway may be in a dissolved state or adsorbed to colloids and soil particles into the surface and/or groundwater (Xing *et al.* 2020). As a result, it is crucial to research and assess how antibiotics are used in farming, from administration to excretion, waste collection, input of land, and potential soil-water transmission.

Table 2.2: Some of the common veterinary antibiotics

Class	Compounds	Group of animals	Potential side effects	Reference
Aminoglycosides	Neomycin	All animals	Nephrotoxic	(Krause *et al.* 2016)
	Specinomycin	Chickens, cattle, pigs	Ototoxic	(Becker and Cooper 2013)
	Kanamycin	cattle, horses, dogs, pigs	Nephrotoxic	
β-Lactum	Oxacillin	Cattle	Allergic reactions	(Miguel, Orlando and Simionato 2013)
	Dicloxacilin	Cattle		(Prescott 2013)
	Cloxacilin	Cattle		(Liu *et al.* 2016)
	Benzylpenicillin	All animals		
	Ampicillin, amoxicillin	All animals		
Fenicoles	Chloramphenicole	Cats, dogs	Anemia	(Hanekamp and Bast 2015)
Cephalosporines	Cefalexin	Dogs	Allergic reactions	(Liu *et al.* 2016)
	Ceftiofur, cefquinom	Pigs, Cattle		
Sulphonamides	Sulphadimethoxine	cats, chickens, pigs	Nephrotoxic	(Liu *et al.* 2016)
	Sulphadimidine	cats, chickens, pigs		
	Sulphapyridine	Pigs		
Lincosamides	Clindamycin	Dogs	Gastro-intestinal challenges	(Lappin *et al.* 2017)
	Lincomycin	Pigs, dogs, cats, cattle		
Tetracyclines	Chlortetracycline	Cattle, pigs	Hepatotoxic	(Chung *et al.* 2017)
	Doxycycline	cats, dogs		
	Oxytetracycline	cattle, sheep, pigs		
	Tetracycline	horse, sheep, pigs		

2.3.3. Through Landfill Leachate

There is less literature on the occurrence of veterinary antibiotics through the leaching of traditional disposal systems, and there is an opportunity for studies to address the impact on public health that this might cause. For example, the environmental footprint of leaching veterinary pharmaceuticals from livestock mortalities and the burial of animals in farms or urban areas is still poorly understood. Yuan, Snow and Bartelt-Hunt (2013) emphasise that the consequences of animal carcass burial on water quality are essential to investigate. Moreso, because the burial pits are constructed with no liners, thus allowing leachate to infiltrate into the ground (Kwon *et al.* 2017). As such, these veterinary antibiotics may be taken up by plants which could lead to secondary exposure to humans as food consumption (Bártíková, Podlipná and Skálová 2016). A study by Rajapaksha *et al.* (2014) observed veterinary antibiotics in plant tissue grown in soil mixed with sulfamethazine. Even though the concentration of these antibiotics is low with a typical range of 0.1 ppm to 1.2 ppm, which may be consumed through ingestion of food but it is still considered unsafe due to chronic toxicity (Bártíková, Podlipná and Skálová 2016). Therefore, if animal burial pits or abandoned dead animals in sites used for cultivation without proper management, they could be a source of antibiotics that pose a danger of transmission to public health.

2.4. Environmental Impact and Regulations

Pharmaceutical compounds, particularly antibiotics, are critical for human and animal health and well-being. The active agents and metabolites excreted from pharmaceutical use can have various environmental effects. Antibiotics may be present in various water resource streams, sewage sludges, manure, and sediments (Balakrishna *et al.* 2017; Harrower *et al.* 2021; Chang *et al.* 2023). Antibiotics' main sources are healthcare wastewater, household wastewater, sludge, and landfill leaks (Almomani *et al.* 2016; Harrower *et al.* 2021). The predominance of antibiotics in municipal wastewater and surface waters can develop antibiotic-resistant bacteria due to long-term exposure to low concentrations of antibiotics in the ng/L to g/L range. Leachates from landfills may contain antibiotics as well as antibiotic-resistant microorganisms (Borquaye *et al.* 2019; Song *et al.* 2022). Some antibiotics used in humans and animals are excreted in faeces and urine (Tran, Reinhard and Gin 2018); therefore, it is evident that wastes from toilets can be an important source of antibiotics.

Antibiotics are classified as "persistent or pseudo-persistent substances because their entry rate into the environment exceeds their elimination rate" which implies that more antibiotics are retained by the treatment systems rather than being removed. Also, they are composed of heterogeneous compounds with various functional groups that can account for various physicochemical properties and behaviours in the ecosystem (Coman 2016). Furthermore, the presence of antibiotic residues in the environment is determined by the antibiotic's pharmacokinetic profile (Coman 2016).

There are several mechanisms for antibiotics degradation in the environment; some can be biotic (biodegradation by bacteria and fungi) and others non-biotic (hydrolysis, photolysis, oxidation, and reduction) based on the physicochemical properties and environmental conditions (temperature, light, pH) (Jechalke *et al.* 2014; Chang *et al.* 2015; Wohde *et al.* 2016).

The conventional wastewater treatment processes cannot effectively remove these contaminants related to modern pharmaceuticals and drugs (Makhathini, Mulopo and Bakare 2020). It is also a fact that their metabolites cannot allow the biodegradation of antibiotic-resistant microorganisms. Therefore, these compounds end up in the final effluent and/or are absorbed in the sludge (Song *et al.* 2022). Antibiotics can also cause inhibition of a microbial-led process, such as the activated sludge process, in the biological treatment of wastewater. This will have an impact on the quality of the produced effluent. The indirect effects of antibiotics in water resources or ecosystems are still not well-known; however, their long-term effects could be important (Grenni, Ancona and Caracciolo 2018).

According to Mackuľak *et al.* (2019), there is still a lack of understanding about the amounts of pharmaceuticals entering the environment, the origin of pharmaceutical active agents, metabolism and transformation pathways, the effects of active substances, metabolites, and transformation products on aquatic organisms, and their persistence or degradability in the environment. Following sludge disposal, several antibiotics in sludge are discharged into the environment, causing serious environmental issues, including contamination, as mentioned earlier. Because the primary use of disposed sludge can be agriculture or landfills, antibiotics in sludge may contaminate the soil, food chain, and water supply (Mackuľak *et al.* 2019; Harrower *et al.* 2021). Their presence in sewage sludge can be a serious environmental issue, as millions of tonnes of dry sludge are produced yearly (Chen *et al.* 2020). Antibiotics can generally range from several µg per kg to mg per kg in sewage sludge, depending on the sampling point and the properties of the sludge (Harrower *et al.* 2021). Antibiotics have been prioritised among all pharmaceuticals studied due to antibiotic-resistance genes discovered in bacteria. Several countries' most common antibiotic classes in sewage sludge samples are tetracyclines, fluoroquinolones, sulfonamides, and macrolides (Harrower *et al.* 2021).

In terms of impacts, there are many impacts on human health, the soil, and freshwater resources, including rivers, lakes, and groundwater. Weather conditions, such as acid rain, may promote the retention of antibiotics on the surface soil, creating risks to plants through soil uptake or soil microorganisms (Solliec *et al.* 2016; Pan and Chu 2017). Fluoroquinolones are known to have cumulative effects on the environmental risk assessment. They may interfere with photosynthetic paths, cause abnormalities related to the morphology of plants, and significantly inhibit net assimilation due to reduced somatic conductivity (Janusch *et al.* 2014; Wang *et al.* 2015). Tetracyclines have the reputation of being phytotoxic, causing anomalies at the chromosome level and inhibiting the growth of plants by lowering the content of photosynthetic chlorophyll and carotenoid pigments in plants

(Vasquez *et al.* 2014). Oxytetracycline is concentrated in some aquatic plants grown for human consumption and previously fertilised with pig manure (Vasquez *et al.* 2014).

Current policies or regulations are focused on monitoring, but the magnitude of the crisis necessitates more forward-thinking policies. Understanding antibiotic pollution and resistance as part of a "One Holistic Approach" may help develop more social interaction and, eventually, more efficient policies. Such policies must assess the problem posed by specific contaminated environments while also accounting for the complex patterns of inter-environmental transmissions that may exist. Because antibiotic resistance and pollution are global issues. There is a need to identify the policy gap regarding water contamination by antibiotics. This can be achieved by regulating the causes of antibiotic occurrence in the environment (such as antibiotic consumption) and ending with regulating antibiotic discharge and risk assessment; environmental antibiotic contamination should be reduced. The detection and quantification of antibiotics and the characterisation of their behaviour in the environment are important intermediate steps that could support future regulatory decisions.

Legislation, regulations, or policies play an important role in defining roles and responsibilities among stakeholders in the fight against antibiotic discharges into the environment. Nevertheless, it is important to be realistic when it comes to implementation. Environmental regulations, policies, and laws are important for protecting ecosystems and humans, but their implementation can be difficult depending on regions and countries. A recently done study (Rogers Van Katwyk *et al.* 2019) identified 17 policy strategies for reducing human antibiotic use, with most of the policies having never been evaluated in terms of their impact on antibiotic use. A high level of specific regulations has been found to be significantly correlated with lower antibiotic consumption in 20 countries across the European Region (Mueller 2016).

2.5. Treatment Technologies of Pharmaceutical Compounds

Conventional wastewater treatment plants were not designed to eradicate contaminants of emerging concern, such as pharmaceutical compounds, from entering the environment (Krzeminski *et al.* 2019). Recently, there have been noticeable high loads of pharmaceutical compounds entering WWTPs, and they are still detectable in WWTP effluent streams (Matongo *et al.* 2015b; Agunbiade and Moodley 2016; Madikizela and Chimuka 2016; Madikizela, Tavengwa and Chimuka 2017; Mlunguza *et al.* 2019). The occurrence of pharmaceutical compounds in WWTP effluent streams is evidence that most of the current WWTP designs fail to completely eradicate emerging contaminants from entering the environment. In the context of an African country's wastewater treatment infrastructure, conventional WWTPs consist of three treatment stages (Figure 2.2), i.e., primary, secondary, and sometimes tertiary, depending on the WWTP design. The preliminary stage, in most cases, is a mechanical and/or chemical (coagulant addition) process where solid matter is significantly reduced by filtration and/or

sedimentation. The secondary treatment stage takes advantage of biological processes, such as using activated sludge to reduce organic matter and biological nutrients from the wastewater stream under different operating conditions (i.e., aerobic or anaerobic) depending on the WWTP design. It is worth mentioning that the application of membrane bioreactors, fixed bed bioreactors, or sequencing batch reactors is not commonly used at an industrial scale. Ultimately, depending on the WWTP design, the tertiary stage is the disinfection stage, typically by chlorination or filters to remove solid particles.

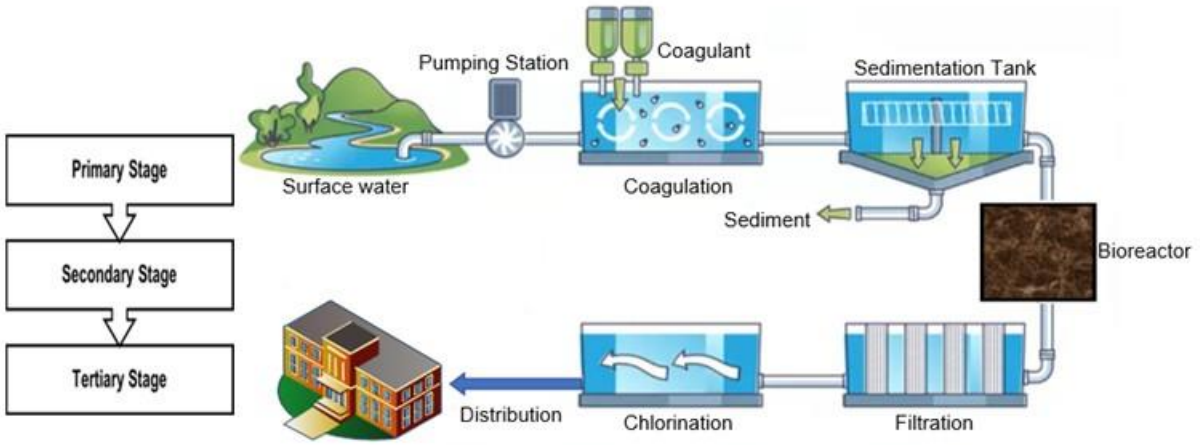

Figure 3.2: Wastewater treatment process.

The subsequent subsection of the current study summarises the fate of pharmaceuticals in WWTPs and reported technologies on pharmaceutical remediation from the aquatic environment.

2.5.1. Biological treatment of pharmaceutical compounds in wastewater streams

The remediation of pharmaceutical compounds, antibiotics, and NSAIDs, in biological treatment processes, is attributed to biotic and abiotic processes [84] that occur during the treatment process. Biotic remediation of pollutants is mainly attributed to biodegradation by bacteria and fungi (Mulla *et al.* 2021). On the other hand, abiotic remediation is attributed to the sorption of contaminants on sludge and possibly by hydrolysis and photolysis (Mulla *et al.* 2021). The removal of antibiotics and NSAIDs from aqueous streams is attributed to their biodegradation by bacteria and sorption on sludge (Michael *et al.* 2013). It is worth noting that non-polar antibiotics and NSAIDs are highly likely to be removed at the primary stage of the treatment process by sedimentation. However, Pilli *et al.* (2020) reported that hydrophobic compounds are retained in the sludge for better microbial degradation. Whereas hydrophilic compounds are characterised by high affinity to biosolids (sludge), they concentrate in organic-rich sludge (Michael *et al.* 2013). It is worth noting that some hydrophilic micropollutants

escape the biodegradation process and leave the plant as permeate (Pilli *et al.* 2020). Photolysis might not be favourable for most WWTPs due to the minimal exposure of wastewater streams during treatment.

The affinity of pharmaceuticals and NSAIDs on sludge is primarily measured by the sludge sorption constants (K_d). Generally, organic compounds characterised by high K_d values have a high affinity for sludge. Apart from K_d values, recently done studies (Khairy, Noonan and Lohmann 2019) suggest that the octanol-water partition coefficient (K_{OW}) can be used to predict the tendency of organic compounds to accumulate in sludge. Michael *et al.* (2013) reported on K_{OW} values for selected polar antibiotics (Table 2.3) that the sludge sorption prediction of antibiotics can only be done for polar compounds with minimal error margin.

Table 2.3: Octanol-water partition coefficients for selected types of antibiotics, adapted from (Michael *et al.* 2013).

Type of antibiotic	**log*K*$_{OW}$**	**Sludge sorption potential**
Tetracyclines, sulfonamides, aminoglycopeptides	< 2.5	Low
β-lactams, macrolides	2.5 < logK_{OW} < 4.0	Medium
Glycopeptides	> 4.0	High

For most WWTPs, biodegradation is the main mechanism for pollutant removal, which depends on the chemical nature of the compound, redox potential, pH, biochemical oxygen demand, suspended solids loading, hydraulic retention time, sludge retention time, food-microorganism ratio, mixed liquor suspended solids, temperature and the microbial consortium (Michael *et al.* 2013). The aforementioned variables are not explicitly accounted for in this current study. Pilli *et al.* (2020) reported that the decomposition kinetics of organic pollutants at minute concentration is given by the first-order reaction (2.1):

$$R_d = K_d \times C_{SS} \times C_p \qquad (2.1)$$

where R_d is the degradation rate, K_d is the degradation constant, C_{SS} is the concentration of suspended solids, and C_p is the concentration of pollutant to be degraded.

It is worth noting that the two dominant mechanisms in the bioremediation of organic pollutants, particularly emerging contaminants, are co-metabolism and single substrate degradation. Pilli *et al.* (2020) reported the biodegradation of selected pharmaceutical compounds i.e., ibuprofen, bezafibrate, and naproxen, to be co-metabolism while ketoprofen was degraded as a sole substrate. Generally, the bioremediation of organic pollutants by microbial species is highly dependent on the metabolic capacity of microorganisms to degrade pollutants by means of natural detoxification processes. Therefore, to

optimise the bioremediation of organic pollutants, there is a need to select and isolate naturally degrading microbial species to populate microbial inocula that is able to degrade targeted contaminants (Fernandes *et al.* 2021). Hitherto, the bioremediation of organic pollutants has cemented its application due to microbial species' ability to adapt to many conditions (Bessa *et al.* 2017; Pan *et al.* 2017; Pan *et al.* 2018). The bioremediation process of organic pollutants can take place by: (1) bio-stimulation – this is the stimulation of a microbial community by the addition of an inorganic nutrient mainly containing nitrogen or phosphorus to avoid metabolic inhabitation; (2) bio-augmentation – this process involves microbial inoculation of pollutant degrading microbial species to enhance biodegradation of targeted pollutants; and (3) the combination of both bio-stimulation and bio-augmentation process (Haripriyan *et al.* 2022).

Furthermore, studies (Larcher and Yargeau 2011; Amorim *et al.* 2014; Reis *et al.* 2014; Bessa *et al.* 2017; Pan *et al.* 2017; Mulla *et al.* 2018; Pan *et al.* 2018) have indicated that the bioremediation of pharmaceutical compounds can be achieved by a single bacterial strain and/or by bacterial consortia. Table 2.4 presents selected bacterial strains reported in the literature that can biodegrade pharmaceutical compounds. Larcher and Yargeau (2011) investigated the ability of pure cultures of individual and mixed consortia of bacteria i.e., *Baceillus subtilis, Pseudomonas aeruginosa, Pseudomonas putida, Rhodococcus equi, Rhodococcus erythropolis, Rhodococcus rhodocrous*, and *Rhodococcus zopfii* to biodegrade sulfamethoxazole. It was reported that *Rhodococcus equi* solely was able to biodegrade sulfamethoxazole as a model pharmaceutical compound in wastewater streams using glucose as a secondary carbon source supplement. In an attempt of using a mixed culture of *Rhodococcus equi* with other microorganisms, Larcher and Yargeau (2011) did not observe any significant removal of the model contaminant.

Table 2.4: Reported literature pharmaceutical compounds biodegrading bacterial strains.

Bacterial Strain	**Pharmaceutical compound**	**Reference**
Brevibacterium sp. D4	Diclofenac	(Bessa *et al.* 2017)
Starkeya sp. C11	Carbanazepine	
Rhizobium sp. C12	Carbanazepine	
Geobacillus sp. S-07	Sulfamethazine	(Pan *et al.* 2017)
Geobacillus thermoleovorans	Sulfamethazine	
Thermus thermophilus sp. C419	Ciprofloxacin	(Pan *et al.* 2018)
Labrys portucalensis F11	Oflaxacin, ciprofloxacin, norfloxacin	(Amorim *et al.* 2014)
Ochrobactrum sp. SA1 *Labrys* sp. SC11 *Gordonia* sp. SCD14	Sulfamethoxazole	(Mulla *et al.* 2018)

Table 2.4. (continues)

Achromobacter denitrificans PR1	Sulfamethoxazole	(Reis *et al.* 2014)
Rhodococcus equi	Sulfamethoxazole	(Larcher and Yargeau 2011)

Mulla *et al.* (2018) conducted a study for the biodegradation of sulfamethoxazole at an initial concentration of 5 mg/L on three isolated pure bacterial cultures i.e., *Ochrobactrum* sp. SA1, *Labrys* sp. SC11 and *Gordoni* asp. SCD14. The findings of their study explicitly showed that all three strains investigated can degrade sulfamethoxazole. Sulfamethoxazole degradation of up to 45.2%, 62.2%, and 51.4% was recorded for strain SA1, strain SC11, and SCD14, respectively. Reis *et al.* (2014) reported a sulfamethoxazole removal rate of 73.6 $\mu mol/g_{cell}.h$ using *Achromobacter denitrificans* PR1 as a bacterial strain and the model contaminant as a sole carbon source. It is worth noting that the sulfamethoxazole removal rate reported by Reis and co-workers (Reis *et al.* 2014) was doubled when a supplement of amino acids was added. The findings suggest that the reported supplement as a carbon source significantly improved microbial activities for the reported system under investigation. Furthermore, Reis *et al.* (2014) reported no sulfamethoxazole degradation by other *Achromobacter* strains but by strain PR1.

Bessa *et al.* (2017) harvested bacterial strains capable of degrading carbamazepine and diclofenac from activated sludge of a municipal wastewater treatment plant. The strains were identified by 16S rRNA gene sequencing. Bessa and co-workers (Bessa *et al.* 2017) reported up to 90% biodegradation of diclofenac by *Brevibacterium* sp. D4 for an initial diclofenac concentration of 10 mg/L in the presence of acetate as a supplementary carbon source. On the other hand, for strains *Starkeya* sp. C11 and *Rhizobium* sp. C12, Bessa *et al.* (2017) reported up to 30% degradation of carbamazepine. The addition of acetate as a supplementary carbon source did not improve the degradation of carbamazepine by strains C11 and C12. The findings suggest that the degradation of carbamazepine by strains C11 and C12 did not occur by bio-stimulation. The degradation of carbamazepine by strains C11 and C12 can possibly be improved by bio-augmentation. However, this is not explicitly accounted for in the current study nor in the work reported by Bessa *et al.* (2017).

Evidently, pharmaceutical compounds are susceptible to biodegradation by selected bacterial strains. However, their occurrence in water bodies suggests that the current design of WWTPs partially eradicate these compounds of emerging concern. Table 2.5 presents the performance of selected studies on pharmaceuticals removal in WWTPs using conventional activated sludge systems and their concentration in surface water.

Table 2.5: Occurrence of selected pharmaceutical compounds detected in influent and effluent of WWTPs.

Class of PC	Compound	WWTP influent		WWTP effluent			Reference
		Range or Mean conc. (µg/L)	Frequency of detection (%)	Range or Mean conc. (µg/L)	Frequency of detection (%)	Surface water (µg/L)	
NSAIDS	Diclofenac	0.0126 – 0.246	100	0.00556 – 0.244	100	0.6 – 8.17	(Agunbiade and Moodley 2016; Mhuka, Dube and Nindi 2020)
	Ibuprofen	0.569 – 76.377	100	<LOQ – 7.652	93.8	1.548 – 12.812	(Mhuka, Dube and Nindi 2020)
		1.06	-	1.38	-	0.445 – 0.689	(Agunbiade and Moodley 2016)
		72	-	51	-	4.8 – 11	(Madikizela, Tavengwa and Chimuka 2017)
	Ketoprofen	<LOQ – 0.0231	82.1	<LOQ – 0.0495	93.8	-	(Mhuka, Dube and Nindi 2020)
		1.7 – 6.4	-	1.2 – 4.3	-	<0.26 – 2.0	(Madikizela, Muthwa and Chimuka 2014)
	Naproxen	1.22 – 39.6	-	<LOQ – 11.4	-	<LOQ – 0.68	(Madikizela and Chimuka 2016)
		0.0169 – 0.546	100	0.0131 -0.350	100	-	(Mhuka, Dube and Nindi 2020)

Table 2.5: (Continues)

Antibiotics	Ciprofloxacin	nd – 0.27	-	0.07	-	<0.012 – 0.51	(Madikizela, Tavengwa and Chimuka 2017)
		<LOQ – 77.04	96.4	<LOQ – 5.59	18.8	-	(Mhuka, Dube and Nindi 2020)
	Sulfamethoxazole	0.0529 – 2.405	100	0.0349 – 0.504	100	-	(Matongo *et al.* 2015b)
		59.3	-	0.16	-	0.22 – 6.01	(Mhuka, Dube and Nindi 2020)
	Erythromycin	1.1	-	0.24	-	0.03 -0.26	(Matongo *et al.* 2015b)
		<LOQ	-	<LOQ – 11.89	50	-	(Mhuka, Dube and Nindi 2020)

nd – the compound was not detected.

LOQ – compound concentration was below the quantification limit.

2.5.2. Advanced Oxidation Processes (AOPs)

Advanced oxidation processes (AOPs) are characterised as near-ambient temperature and pressure water treatment processes via oxidation by hydroxyl radicals (HO•) to remove both organic and inorganic contaminants (Ying *et al.* 2015). AOPs involve the generation of highly reactive oxygen species with a low selectivity (Kanakaraju, Glass and Oelgemöller 2018), such as hydroxyl radicals produced by oxidants (e.g., H_2O_2) and/or energy sources (e.g., ultra-violent light) or catalysts (e.g., TiO_2) providing pathways for complete mineralization. Hydroxyl radicals have cemented their application in AOPs due to their non-selective nature, high reactivity, and high oxidizing capabilities. OH• radicals have the advantage of being able to attack a wide range of organic pollutants.

Moreover, the application of AOPs in water treatment is gaining attention because of its potential to reduce low concentrations of contaminants from ppm to less than 5 ppb (Ying *et al.* 2015) and its ability to mineralise contaminants to carbon dioxide, water, and inorganics, or contaminants transformation into harmless products (Patel *et al.* 2019). However, it is imperative to note that AOPs are economically attractive for aqueous streams with relatively low organic loads in terms of chemical oxygen demand (COD). Higher COD content will require large amounts of oxidants or energy sources, thus increasing operational costs (Amaral-Silva *et al.* 2016). Aqueous streams with relatively high organic loads are more conveniently treated by means of wet oxidation and/or incineration, it is noted that these technologies are not explicitly accounted for in the current study.

It is worth noting that AOPs that have cemented their application in pharmaceutical wastewater treatment include photochemical processes (i.e., ultra-violate (UV) oxidation, photo-Fenton, and photocatalysis), non-photochemical processes (i.e., Fenton, ozonation, ultrasound, sonolysis, electrochemical, and radiation), and hybrid processes (i.e., sono-photolysis, photocatalytic ozonation, sono-biphotocatalysis, photoelectrocatalysis, electroperoxone, and sono-Fenton) (Kanakaraju, Glass and Oelgemöller 2018; Mulla *et al.* 2021).

2.5.2.1. Photocatalysis

Photocatalysis is a change in the rate of a chemical reaction when the photocatalyst absorbs ultraviolet, visible, or infrared radiation (Ying *et al.* 2015). Generally, this process (Figure 2.3) is designed based on a material (photocatalyst) absorbing a photon of energy (hv) at least equal to its band gap energy (E_g) to produce a valence band of holes (h_{vb}^+) and conduction band electrons (e_{cb}^-). The valence band holes react with water to produce hydroxyl radicals characterised as reactive oxygen species capable of oxidising a wide range of contaminants. Titanium dioxide (TiO_2) has cemented its application as a semiconductor photocatalyst in water treatment due to its low cost, non-toxic nature, and high photochemical stability (Kanakaraju, Glass and Oelgemöller 2018).

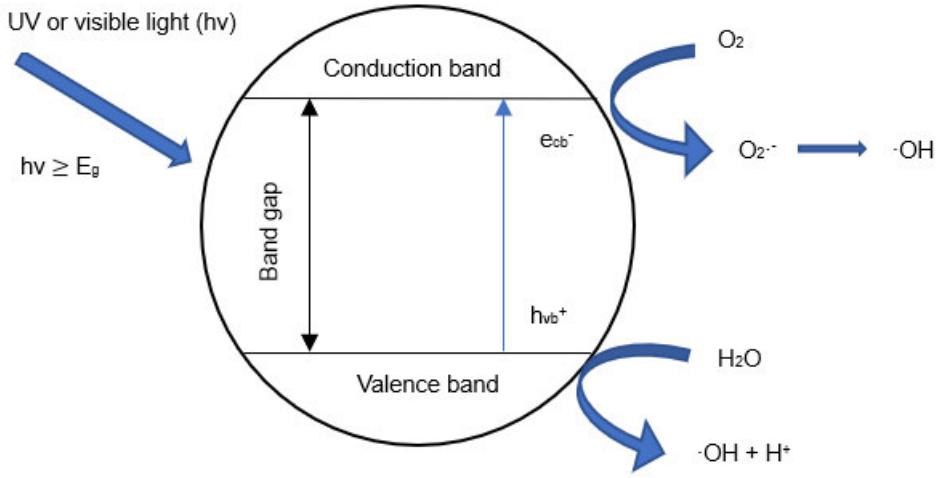

Figure 2.4: Photocatalytic mechanism for a semiconductor photocatalyst. Adapted and modified from Sujatha, Shanthakumar and Chiampo (2020).

The ultra-violent light is the most reported energy source driving photocatalytic activity with pure TiO_2 in the anatase phase possessing a band gap energy of 3.2 eV for removing organic contaminants, including pharmaceuticals (Ying *et al.* 2015). Studies (Ying *et al.* 2015; Patel *et al.* 2019) have demonstrated that naproxen, diclofenac, iopromide, sulfamethoxazole, and carbamazepine under UV/TiO_2 can be degraded by photocatalysis in the aqueous environment. Low adsorption of targeted pollutants on the catalytic surface and deactivation of the hydroxyl radicals can negatively impact the system's efficacy (Patel *et al.* 2019).

Furthermore, it is important to note that UV accounts for almost 5% of visible spectrum radiation (Ying *et al.* 2015); this is attributed to the ineffectiveness of pristine TiO_2 photocatalysts to utilize sunlight. Therefore, there is a need to reduce the wide band gap of TiO_2 by modification to allow the utilization of sunlight. Ying *et al.* (2015) reported that both metallic and non-metallic doping can reduce the energetic band gap by either raising the valence band's position or lowering the conduction band's position.

In a typical photocatalytic process, the initiating event is characterised by the absorption of the radiation, which results in the formation of electron-hole pairs (2.2). It is imperative to note that the formed electron (2.2) has considerable reducing power, allowing it to reduce some metals and dissolved oxygen by forming the superoxide radical ion. The remaining holes oxidise adsorbed H_2O or HO^- to reactive hydroxyl radicals (2.3) and (2.4).

$$TiO_2 \xrightarrow{hv} e^- + h^+ \quad (2.2)$$

$$TiO_2(h^+) + H_2O \rightarrow TiO_2 + HO^{\cdot} + H^+ \quad (2.3)$$

$$TiO_2(h^+) + HO^- \rightarrow TiO_2 + HO^{\cdot} \quad (2.4)$$

Equations (2.2) to (2.4) are significant reactions in oxidative degradation AOPs of contaminants due to the high concentration of H_2O and HO^- adsorbed on the particle surface. Hydroxyl radicals react with organic contaminants by either hydrogen abstraction i.e., from C-H, N-H, or H groups (2.5) or radical-radical interaction resulting in the formation of the peroxyl radical (2.6) or by direct electron transfer (2.7) yielding oxidized intermediates (Kanakaraju, Glass and Oelgemöller 2018).

$$HO^{\cdot} + RH \rightarrow R^{\cdot} + H_2O \quad (2.5)$$

$$R^{\cdot} + O_2 \rightarrow RO_2^{\cdot} \quad (2.6)$$

$$HO^{\cdot} + RX \rightarrow RX^{\cdot +} + HO^- \quad (2.7)$$

In cases whereby contaminants are completely mineralised, carbon dioxide, water, and inorganic salts form products.

2.5.2.2. Photolysis Processes

Photolysis involves the interaction of light (i.e., natural or artificial) with a molecule to induce a photochemical reaction to facilitate the degradation of targeted pollutants (Ying *et al.* 2015). Drinking water disinfection by photolysis has the advantage of eliminating the formation of by-products relative to chlorination. Water disinfection by photolysis is highly dependent on ultra-violet radiation, which has been demonstrated to be effective for microbial disinfection i.e., a dose of 40 J/m^2, but ineffective for removing most pharmaceuticals such as diclofenac and sulfamethoxazole (Canonica, Meunier and Von Gunten 2008). This suggests that further studies are needed to be conducted aimed at optimising the aquatic photochemistry for selected PCs.

The UV photolysis process efficacy can be improved when incorporated with hydrogen peroxide (H_2O_2). Kim, Yamashita and Tanaka (2009) investigated the effectiveness of UV and UV/H_2O_2-based processes for removing PCs in real wastewater; insignificant removal was observed for macrolide antibiotics despite a considerable UV radiation of 2768 mJ/cm^2. For the UV/H_2O_2 process, at least 90% removal was reported for 39 PCs at a UV radiation of 923 mJ/cm^2. Using H_2O_2 facilitates the formation of highly reactive hydroxyl radicals, which can degrade a broad range of organic compounds, including PCs. Kanakaraju, Glass and Oelgemöller (2018), in their review, reported that UV/H_2O_2 processes' effectiveness is dependent on H_2O_2 concentration, rate of HO· radical formation, UV light intensity, the chemical structure of the targeted contaminant as well as solution pH.

2.5.2.3. Ozonation

Ozone-based processes have been demonstrated to efficiently treat wastewater streams containing recalcitrant organic compounds such as PCs, as reported by other authors (Michael *et al.* 2013; Sharma *et al.* 2022). Ozonated water, when compared to other existing oxidising reagents, has been considered to be more efficient in pollutant degradation, which is attributed to the fact that no secondary compounds are added to the treated water (Pera-Titus *et al.* 2004). Ozone is characterised as a selective oxidant with standard potentials of 2.07 V and 1.25 V in an acidic and basic aqueous environment, respectively (Wang and Xu 2012). In principle, there are two main oxidation mechanisms reported in literature i.e., direct electrophilic attack by molecular ozone (low pH environment) and indirect attack through the formation of hydroxyl radicals (basic aqueous solutions) (Pera-Titus *et al.* 2004; Wang and Xu 2012). At low pH, direct ozonation dominates, whereby ozone selectively reacts with compounds characterised by specific functional groups through selective reactions, whereas, at basic aqueous solutions, ozone decomposes, yielding hydroxy radicals.

The pH significantly influences the kinetics and reaction mechanism in the oxidation of pollutants in an aqueous environment, thus warranting it to be a major factor in determining the efficiency of ozonation. In an acidic environment i.e., pH < 4, direct ozonation prevails; in pH 4 to 9, both direct and indirect ozonation occurs, and indirect ozonation is more dominant above pH 9 (Pera-Titus *et al.* 2004). Moreover, during the ozonation process, regardless of the ozone decomposition pathway, the process is initiated by reactions (2.8) or (2.9), and reaction (2.10), which is characterised as a direct one-electron transfer process prevails under extreme conditions of very high pH values.

$$O_3 + OH^- \rightarrow O_2^-. + HO_2. \quad (2.8)$$

$$O_3 + OH^- \rightarrow HO_2^-. + O_2 \quad (2.9)$$

$$O_3 + OH^- \rightarrow O_3^-. + HO^{\cdot} \quad (2.10)$$

The application of ozonation in water treatment has achieved low efficiencies in the mineralization of organic compounds, particularly pharmaceuticals (Almomani *et al.* 2016; Zhao *et al.* 2017), which is attributed to the relatively low solubility and stability of ozone in an aqueous environment and the slow reaction with other organic compounds. Hence, the focus has been laid on applying catalytic ozonation and hybrid processes to improve the production of hydroxyl radicals and contaminants' degradation efficiency. Catalytic ozonation, which has become an attractive and important research area in the use of ozone, can be considered homogeneous and heterogenous catalytic ozonation. Homogenous catalytic ozonation involves ozone activation by metal ions in an aqueous solution, whereas heterogeneous catalytic ozonation is based on ozone activation in the presence of metal oxides on supports. The short life span of ozone renders this technology expensive, and its high energy demand is the major drawback to upscale for real application (Kanakaraju, Glass and Oelgemöller 2018).

Studies (Almomani *et al.* 2016; Zhao *et al.* 2017) on removing PCs from aqueous solutions by the ozonation process have reported low mineralization despite high removal efficiencies. The low mineralization of PCs is attributed to the formation of persistent by-products to further oxidation. Short-chain carboxylic acids such as oxamic acid, maleic acid, oxalic acid, formic acid, acetic acid, and pyruvic acid are formed as by-products during the partial oxidation of PCs during the ozonation process (Zhao *et al.* 2017). The aforementioned by-products are formed during the initial stage of the ozonation process, and they are not susceptible to further degradation, as reported by Zhao *et al.* (2017). It is imperative to note that for the work reported by Zhao *et al.* (2017), formic acid, acetic acid, and oxalic acid account for 40% of the by-product mixture in total organic carbon.

As alluded earlier that the pH of the solution is the major contributing factor in the degradation of target pollutants by the ozonation process. Kıdak and Doğan (2018) reported a reaction rate of 1.970 min^{-1} for a system with pH 10 for the removal of amoxicillin. The reported reaction rate was the highest when compared to acidic and neutral conditions. Such findings are attributed to the forming of significant amounts of hydroxyl radicals with increasing pH. Other operation parameters that affects the removal of PCs by ozonation are discussed in literature, such as ozone dose (Almomani *et al.* 2016), water matrix, and the presence of organic matter (Cai and Lin 2016).

2.5.2.4. Hybrid AOPs

Hybrid AOPs have attracted considerable interest in PCs removal from aqueous solutions. This is attributed to PCs' high removal and mineralization efficiencies due to the synergistic effect and increased reactive species (Kanakaraju, Glass and Oelgemöller 2018). Contaminants' degradation of targeted pollutants can occur sequentially or simultaneously, depending on the system design. There are studies (Ghafoori *et al.* 2015; Naddeo *et al.* 2015; Adityosulindro *et al.* 2017) reported in the literature on the application of hybrid AOPs for PCs removal in synthetic and real wastewater. Naddeo *et al.* (2015) investigated the treatment efficiency of ozonation in combination with ultrasound to degrade diclofenac, carbamazepine, and sulfamethoxazole. For the hybrid ozonation-ultrasound process, a degradation efficiency of 94% was reported for both diclofenac and sulfamethoxazole while 61% degradation was reported for carbamazepine. Adityosulindro *et al.* (2017) studied the performance of an ultrasonic-Fenton process to remove ibuprofen in synthetic water and municipal wastewater. Adityosulindro *et al.* (2017) reported a positive synergy in mineralization yield of the model PCs for the ultrasonic-Fenton process.

Ghafoori *et al.* (2015) investigated the performance of oncolysis-photolysis (sono-photolysis) in a pilot-scale external loop airlift sono-photoreactor for the degradation of chloramphenicol, diclofenac, paracetamol, and salicylic acid in synthetic wastewater. For the work reported by Ghafoori *et al.* (2015), the reactor effluent was characterised by total organic carbon percent removal as a surrogate parameter; results obtained indicated that total organic carbon removal was significantly affected by both H_2O_2

dosage and ultrasound power. Table 2.6 summarizes other AOPs investigated for PC removal from an aqueous environment.

2.5.3. Chitosan-based adsorbents

Chitosan is characterized as the most abundant biopolymer after cellulose produced from the deacetylation of chitin derived from crustaceans and fungi (Abd El-Monaem *et al.* 2022). A typical chitin structure (Figure 2.4a) compromises 2-acetamide-2-deoxy-β-D-glucopyranose units and very few 2-amino-2-deoxy-β-D-glucopyranose units. The deacetylation reaction in chitin increases the 2-amino-2-deoxy-β-D-glucopyranose typically by not less than 50% producing chitosan (Figure 2.4b) (de Farias *et al.* 2019; Shah *et al.* 2022). The increase in 2-amino-2-deoxy-β-D-glucopyranose provides chitosan biopolymer with excellent properties such as solubility under acidic conditions, gelling, antimicrobial, film forming, biocompatibility, as well as non-toxicity (de Farias *et al.* 2019; Zhang *et al.* 2022). Moreover, according to Zhang *et al.* (2022), the chitosan amino and hydroxyl groups are highly active, making them excellent chelating sites for targeted pollutants in aqueous environments. The presence of amino and hydroxyl groups makes chitosan susceptible to chemical modification and cemented its application as a potential adsorbent for emerging contaminants removal from water and wastewater streams (Zhao *et al.* 2020; Zhang *et al.* 2022). The growing interest in chitosan-based adsorbents is also attributed to its distinctive properties such as low processing costs, biodegradability, biocompatibility, hydrophilicity, and nontoxicity, making chitosan to be environmentally friendly (green) (Shah *et al.* 2022).

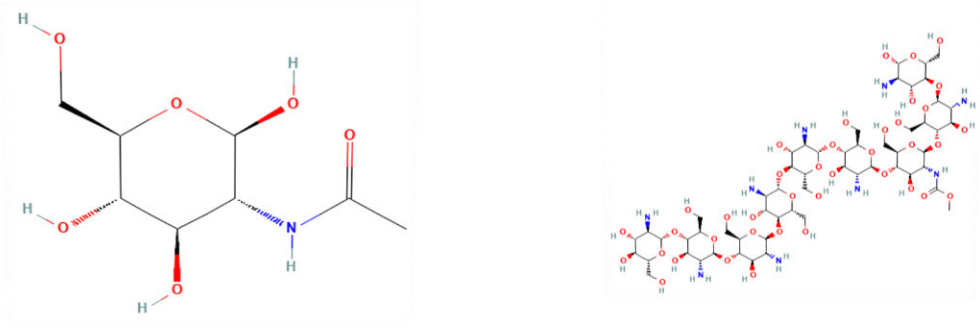

a **b**

Figure 2.5: Chemical structure of chitin **(a)** and chitosan **(b)** obtained from https://pubchem.ncbi.nlm.nih.gov (assessed on 25 April 2023).

Table 2.6: AOPs that are reported in literature for the degradation of PCs.

AOP	Brief description	Advantage	Limitation	Reference
Sonolysis	Ultrasounds (20 kHz – 2 MHz) generate radicals for degradation of molecules.	No need of additional reagents	Degradation efficiency is not satisfactory. The technology requires high energy usage	(Kanakaraju, Glass and Oelgemöller 2018; Sharma *et al.* 2022)
Fenton based process	Reaction of Fe^{2+} and H_2O_2 produce free radicals which degrade the micropollutants	No chlorinated compounds formed and complex formation promote coagulation of suspended solids	Narrow pH range operation, slow degradation	
Electrochemical oxidation	Electrochemical oxidation in the presence of a suitable electrolyte and electric current (2 – 20 A)	More suitable for point source remediation of pharmaceuticals	Accumulation of hazardous by products i.e., chlorate and perchlorate	
Ozone/H_2O_2	H_2O_2 enhances the hydroxyl radical production and hence degradation	High conversion yield	Energy intense process which makes it to be expensive	
UV/H_2O_2	H_2O_2 enhances the hydroxyl radical production and degradation.	Better removal efficiencies for PCs with poor UV absorption	Low degradation efficiency at a pH of more than 3	(Juang, Tseng and Yang 1997; Kanakaraju, Glass and Oelgemöller 2018)

Chitosan modification by physical and/or chemical techniques can be used to improve the weak mechanical strength of pristine chitosan adsorbents which is crucial in the application of chitosan-based composite in water treatment. Several studies have demonstrated that the weak mechanical strength of chitosan adsorbents can be improved by incorporating nanomaterials characterised with high mechanical strength. Table 2.7 and Table 2.8 present selected studies reported in the literature on the application of chitosan-based adsorbents on antibiotics and NSAIDs removal from wastewater.

Table 2.7: Studies conducted on antibiotics adsorption on chitosan-based composites.

Antibiotic	**Adsorbent**	**Max. Capacity**	**Kinetic model**	**Reference**
Amoxicillin	Leached carbon black waste (LCBW)-chitosan	205 mg/g	Pseudo-second-order	(Yaqubi *et al.* 2021)
	Chitosan-Fe/Ni nanoparticles	Not reported	Pseudo-first-order	(Weng *et al.* 2013)
	Fe_3O_4-acticated carbon-chitosan nanocomposite	178.57 mg/g	Pseudo-second-order	(Danalıoğlu *et al.* 2017)
Tetracycline	LCBW-chitosan	205 mg/g	Pseudo-second-order	(Yaqubi *et al.* 2021)
	Chitosan-olive pomace	1.6 mg/g	Not reported	(Rizzi *et al.* 2019a)
	Metal-organic frameworks-chitosan beads	495 mg/g	Pseudo-second-order	(Zhao *et al.* 2020)
Erythromycin	Chitosan-Fe_3O_4	52.32 µmol/g	Pseudo-first-order	(Ou *et al.* 2015)
		Not reported	Pseudo-second-order	(Ghodrat and Asrari 2018)
		215.31 mg/g	Not reported	(Ahamad *et al.* 2020)
	Fe_3O_4-acticated carbon-chitosan nanocomposite	178.57 mg/g	Pseudo-second-order	(Danalıoğlu *et al.* 2017)
Norfloxacin	MgO-graphene oxide-chitosan composite	1000 mg/g	Pseudo-second-order	(Nazraz, Yamini and Asiabi 2019)
	Chitosan-hydroxyapatite nanocomposite	625 mg/g	Pseudo-first-order	(Nayak, Bhushan and Kotnala 2022)
Ciprofloxacin	Magnetic imprinted chitosan polymer nanocomposites	142 mg/g	Pseudo-second-order	(Rasoulzadeh *et al.* 2019)
	Chitosan-biochar hydrogel beads	>76 mg/g	Pseudo-second-order	(Afzal *et al.* 2018)

Table 2.7: (continues)

Ciprofloxacin	Ethylenediaminetetraacetic Acid-Functionalized β-Cyclodextrin-Chitosan	24 mg/g	Pseudo-second-order	(Verma *et al.* 2021)
Triclosan	Graphene-oxide-magnetic-chitosan-organoclay composite	40 mg/g	Not reported	(de Almeida *et al.* 2022)
Sulfanilamide	Starch-chitosan-UiO-66-COOH	Not reported	Pseudo-second-order	(Jia *et al.* 2021)

Apart from antibiotics, NSAIDs are one of the most used pharmaceuticals in human and animal diseases, mostly for analgesic, anti-inflammatory, and antipyretic actions (Ahmed 2017; Fernandes *et al.* 2021).

Table 2.8: Studies conducted on nonsteroidal anti-inflammatory drug removal from an aqueous environment using chitosan-adsorbents.

Compound	**Adsorbent**	**Max. Capacity**	**Kinetic Model**	**Reference**
Ibuprofen	Magnetic chitosan/activated biochar	21.2 mg/g	Not reported	(Mojiri, Andasht Kazeroon and Gholami 2019)
	Chitosan modified rubber	70 mg/g	Pseudo-second-order	(Phasuphan, Praphairaksit and Imyim 2019)
Diclofenac	Chitosan modified rubber	17.7 mg/g	Pseudo-second-order	
	Chitosan-Fe_3O_4 composite	469.48 mg/g	Pseudo-second-order	(Liang *et al.* 2019)
	Chitosan-film	10 mg/g	Pseudo-second-order	(Rizzi *et al.* 2019b)
Naproxen	Chitosan modified rubber	2.3 mg/g	Pseudo-second-order	(Phasuphan, Praphairaksit and Imyim 2019)
Ketoprofen	Chitosan-film	Not reported	Pseudo-second-order	(Rizzi *et al.* 2019b)

Based on the studies presented in Table 2.7 and Table 2.8, it is apparent that the application of biopolymer adsorbents, particularly chitosan-based adsorbents, has received great attention in their application for PCs remediation in aqueous environments. This is attributed to the chitosan physicochemical properties characterised by its polycationic, cationic, and high functional groups (i.e.,

NH_2 and OH) features providing it with peculiar binding capacity for a range of macromolecules including organic and inorganic pollutants (Karimi-Maleh *et al.* 2021). The application of modified-chitosan adsorbents over pristine chitosan adsorbents is attributed to the poor physicochemical properties of chitosan, such as low porosity, low surface area, swelling in water, high crystallinity, less hydrophilicity, and hydrolysability in acid medium (Qiu *et al.* 2020; Karimi-Maleh *et al.* 2021). The high crystallinity of chitosan hinders the accessibility of adsorption sites, particularly for organic and inorganic pollutants characterised as large molecules (Qiu *et al.* 2020). Therefore, chitosan modification is necessary to minimise the aforementioned drawbacks and achieve desirable physicochemical properties. Moreover, from the studies presented in Table 2.7 and Table 2.8, it is evident that the application of modified chitosan adsorbents in water treatment has demonstrated good results, making it an environmentally green technology.

Furthermore, the thermodynamic interaction mechanism between targeted pollutants and adsorbents can be elucidated by applying adsorption kinetic models, as shown in Table 2.8. According to Largitte and Pasquier (2016), a typical adsorption mechanism consists of three steps; the initial step is the external mass transfer of the adsorbate from the bulk solution to the surface of the adsorbent, which is presided over by the internal diffusion of the adsorbate to sorption sites of the adsorbent and, lastly the sorption itself. Yoro *et al.* (2020) demonstrated that diffusion is the most limiting mechanism, which includes external and intraparticle mass transfer. The interaction mechanism for the reported studies in Table 2.7 and Table 2.8 is characterized by the pseudo models, which suggests that sorption of model contaminants occurs on localised sites, the energy of adsorption is not dependent on surface coverage, and the maximum adsorption corresponds to a saturated monolayer of adsorbates on the adsorbent surface.

2.6. Future Perspectives

Furthermore, based on the reviewed studies, AOPs have demonstrated high removal efficiencies of pharmaceuticals from wastewater. However, more work still needs to be done to improve the mineralisation of pharmaceuticals during their degradation by AOPs. The reported literature suggests that persistent by-products such as carboxylic acids are formed during the remediation of pharmaceuticals by AOPs; hence there is a need to investigate the toxicity levels of the aforementioned by-products. AOPs have been successfully applied to degrade pharmaceuticals; however, the focus has been on pilot-scale studies using synthetic wastewater due to high operational costs in producing hydroxyl radicals. These processes can be applied at an industrial scale when effectiveness factors are optimised, particularly for hybrid processes that eliminate drawbacks associated with individual AOPs to achieve maximum mineralisation of targeted contaminants at minimal energy usage.

The application of chitosan-based adsorbents on pharmaceutical removal from wastewater has been extensively investigated as a green chemistry technology. From the reviewed literature, a significant amount of work has been reported on the thermodynamic interaction mechanisms during their remediation by chitosan-based adsorbents. However, the reported literature is based on laboratory-scale studies; there is a need to conduct further investigations on applying chitosan-based adsorbents at the industrial scale as a tertiary treatment step to eradicate the occurrence of pharmaceuticals in WWTP effluent. Moreover, there is still a gap in the application of chitosan-based technologies; no work has been conducted on the techno-economic evaluations of the process, particularly when it comes to handling the adsorbent post-treatment since no mineralisation of contaminants has been reported during solid-liquid adsorption. The available literature suggest that no work has been done on multi-component adsorption aimed at investigating the effect of competing pollutants in the uptake of the targeted contaminant. Despite the occurrence of microplastics in water bodies which has become an environmental threat, no work has been done aimed at investigating the interaction of microplastics and antibiotics relative to water.

2.7. Conclusions

The current study has demonstrated the occurrence of pharmaceuticals in water bodies and the potential application of biological processes, AOPs, and chitosan-based adsorbents on the removal of pharmaceuticals in wastewater. The study provides a holistic review of the occurrence of pharmaceuticals in water bodies, and it is apparent that their environmental occurrence is not solely attributed to human consumption of pharmaceuticals but also anthropogenetic activities such as farming. Detecting pharmaceuticals in WWTPs effluent suggests that current WWTPs are the entry point of these emerging contaminants into the environment. Despite the advances made in the bioremediation of pharmaceuticals by novel bacterial strains as reported in the literature (Larcher and Yargeau 2011; Amorim *et al.* 2014; Reis *et al.* 2014; Bessa *et al.* 2017; Pan *et al.* 2017; Mulla *et al.* 2018; Pan *et al.* 2018), further investigation needs to be conducted to optimise the degradation mechanism for targeted pharmaceuticals. The application of mixed consortia of bacteria has been demonstrated to be ineffective in biodegrading specific pharmaceuticals, as reported by Larcher and Yargeau (2011). The reported literature suggests that further investigations need to be done aimed at the optimisation of operating conditions to maximise pharmaceutical biodegradation efficiencies by bacterial strain.

References

Abd El-Monaem, E. M., Eltaweil, A. S., Elshishini, H. M., Hosny, M., Abou Alsoaud, M. M., Attia, N. F., El-Subruiti, G. M. and Omer, A. M. 2022. Sustainable adsorptive removal of antibiotic residues by chitosan composites: An insight into current developments and future recommendations. *Arabian Journal of Chemistry*: 103743.

Adityosulindro, S., Barthe, L., González-Labrada, K., Haza, U. J. J., Delmas, H. and Julcour, C. 2017. Sonolysis and sono-Fenton oxidation for removal of ibuprofen in (waste) water. *Ultrasonics sonochemistry*, 39: 889-896.

Afzal, M. Z., Sun, X.-F., Liu, J., Song, C., Wang, S.-G. and Javed, A. 2018. Enhancement of ciprofloxacin sorption on chitosan/biochar hydrogel beads. *Science of the Total Environment*, 639: 560-569.

Agunbiade, F. O. and Moodley, B. 2016. Occurrence and distribution pattern of acidic pharmaceuticals in surface water, wastewater, and sediment of the Msunduzi River, Kwazulu-Natal, South Africa. *Environmental Toxicology and Chemistry*, 35 (1): 36-46.

Ahamad, T., Naushad, M., Al-Shahrani, T., Al-Hokbany, N. and Alshehri, S. M. 2020. Preparation of chitosan based magnetic nanocomposite for tetracycline adsorption: Kinetic and thermodynamic studies. *International journal of biological macromolecules*, 147: 258-267.

Ahmed, M. J. 2017. Adsorption of non-steroidal anti-inflammatory drugs from aqueous solution using activated carbons. *Journal of Environmental Management*, 190: 274-282.

Ali, A. M., Rønning, H. T., Alarif, W., Kallenborn, R. and Al-Lihaibi, S. S. 2017. Occurrence of pharmaceuticals and personal care products in effluent-dominated Saudi Arabian coastal waters of the Red Sea. *Chemosphere*, 175: 505-513.

Almomani, F. A., Shawaqfah, M., Bhosale, R. R. and Kumar, A. 2016. Removal of emerging pharmaceuticals from wastewater by ozone-based advanced oxidation processes. *Environmental Progress & Sustainable Energy*, 35 (4): 982-995.

Amaral-Silva, N., Martins, R. C., Castro-Silva, S. and Quinta-Ferreira, R. M. 2016. Ozonation and perozonation on the biodegradability improvement of a landfill leachate. *Journal of environmental chemical engineering*, 4 (1): 527-533.

Amorim, C. L., Moreira, I. S., Maia, A. S., Tiritan, M. E. and Castro, P. M. 2014. Biodegradation of ofloxacin, norfloxacin, and ciprofloxacin as single and mixed substrates by Labrys portucalensis F11. *Applied microbiology and biotechnology*, 98 (7): 3181-3190.

Amos Sibeko, P., Naicker, D., Mdluli, P. S. and Madikizela, L. M. 2019. Naproxen, ibuprofen, and diclofenac residues in river water, sediments and Eichhornia crassipes of Mbokodweni river in South Africa: an initial screening. *Environmental Forensics*, 20 (2): 129-138.

Arvaniti, O., Arvaniti, E., Gyparakis, S., Sabathianakis, I., Karagiannis, E., Pettas, E., Gkotsis, G., Nika, M., Thomaidis, N. and Manios, T. 2023. Occurrence of pharmaceuticals in the wastewater of a Greek hospital: Combining consumption data collection and LC-QTOF-MS analysis. *Science of The Total Environment*, 858: 160153.

Balakrishna, K., Rath, A., Praveenkumarreddy, Y., Guruge, K. S. and Subedi, B. 2017. A review of the occurrence of pharmaceuticals and personal care products in Indian water bodies. *Ecotoxicology and environmental safety*, 137: 113-120.

Bártíková, H., Podlipná, R. and Skálová, L. 2016. Veterinary drugs in the environment and their toxicity to plants. *Chemosphere*, 144: 2290-2301.

Becker, B. and Cooper, M. A. 2013. Aminoglycoside antibiotics in the 21st century. *ACS chemical biology*, 8 (1): 105-115.

Bessa, V., Moreira, I., Tiritan, M. and Castro, P. 2017. Enrichment of bacterial strains for the biodegradation of diclofenac and carbamazepine from activated sludge. *International Biodeterioration & Biodegradation*, 120: 135-142.

Bilal, M., Mehmood, S., Rasheed, T. and Iqbal, H. M. 2020. Antibiotics traces in the aquatic environment: persistence and adverse environmental impact. *Current opinion in environmental science & health*, 13: 68-74.

Borquaye, L. S., Ekuadzi, E., Darko, G., Ahor, H. S., Nsiah, S. T., Lartey, J. A., Mutala, A.-H., Boamah, V. E. and Woode, E. 2019. Occurrence of antibiotics and antibiotic-resistant bacteria in landfill sites in Kumasi, Ghana. *Journal of Chemistry*, 2019.

Cai, M.-J. and Lin, Y.-P. 2016. Effects of effluent organic matter (EfOM) on the removal of emerging contaminants by ozonation. *Chemosphere*, 151: 332-338.

Canonica, S., Meunier, L. and Von Gunten, U. 2008. Phototransformation of selected pharmaceuticals during UV treatment of drinking water. *Water research*, 42 (1-2): 121-128.

Chang, D., Mao, Y., Qiu, W., Wu, Y. and Cai, B. 2023. The Source and Distribution of Tetracycline Antibiotics in China: A Review. *Toxics*, 11 (3): 214.

Chang, P.-H., Jiang, W.-T., Li, Z., Jean, J.-S. and Kuo, C.-Y. 2015. Antibiotic tetracycline in the environments—a review. *Research & Reviews: Journal of Pharmaceutical Analysis*, 4 (3): 86-111.

Chen, W.-T., Haque, M. A., Lu, T., Aierzhati, A. and Reimonn, G. 2020. A perspective on hydrothermal processing of sewage sludge. *Current opinion in environmental science & health*, 14: 63-73.

Chung, H. S., Lee, Y.-J., Rahman, M. M., Abd El-Aty, A., Lee, H. S., Kabir, M. H., Kim, S. W., Park, B.-J., Kim, J.-E. and Hacımüftüoğlu, F. 2017. Uptake of the veterinary antibiotics chlortetracycline, enrofloxacin, and sulphathiazole from soil by radish. *Science of the total Environment*, 605: 322-331.

Coman, C. 2016. Antibiotic resistance: not only the clinician's problem. *Danube News*, 18 (34): 2-5.

Cristóvão, M., Torrejais, J., Janssens, R., Luis, P., Van der Bruggen, B., Dubey, K., Mandal, M., Bronze, M., Crespo, J. and Pereira, V. 2019. Treatment of anticancer drugs in hospital and wastewater effluents using nanofiltration. *Separation and Purification Technology*, 224: 273-280.

Danalıoğlu, S. T., Bayazit, Ş. S., Kuyumcu, Ö. K. and Salam, M. A. 2017. Efficient removal of antibiotics by a novel magnetic adsorbent: Magnetic activated carbon/chitosan (MACC) nanocomposite. *Journal of Molecular Liquids*, 240: 589-596.

de Almeida, A. d. S. V., de Figueiredo Neves, T., da Silva, M. G. C., Prediger, P. and Vieira, M. G. A. 2022. Synthesis of a novel magnetic composite based on graphene oxide, chitosan and organoclay and its application in the removal of bisphenol A, 17α-ethinylestradiol and triclosan. *Journal of Environmental Chemical Engineering*, 10 (1): 107071.

de Farias, B. S., Grundmann, D. D. R., Rizzi, F. Z., Martins, N. S. S., Junior, T. R. S. A. C. and de Almeida Pinto, L. A. 2019. Production of low molecular weight chitosan by acid and oxidative pathways: Effect on physicochemical properties. *Food Research International*, 123: 88-94.

Dinh, Q. T., Moreau-Guigon, E., Labadie, P., Alliot, F., Teil, M.-J., Blanchard, M. and Chevreuil, M. 2017. Occurrence of antibiotics in rural catchments. *Chemosphere*, 168: 483-490.

Felis, E., Kalka, J., Sochacki, A., Kowalska, K., Bajkacz, S., Harnisz, M. and Korzeniewska, E. 2020. Antimicrobial pharmaceuticals in the aquatic environment-occurrence and environmental implications. *European Journal of Pharmacology*, 866: 172813.

Fernandes, J. P., Almeida, C. M. R., Salgado, M. A., Carvalho, M. F. and Mucha, A. P. 2021. Pharmaceutical compounds in aquatic environments—Occurrence, fate and bioremediation prospective. *Toxics*, 9 (10): 257.

Folarin, O., Otitoloju, A., Amaeze, N. and Saliu, J. 2019. Occurrence of acetaminophen, amoxicillin, diclofenac and methylparaben in Lagos and Ologe lagoons, Lagos, Nigeria. *Journal of Applied Sciences and Environmental Management*, 23 (12): 2143-2149.

Gelband, H., Miller, P., Molly, Pant, S., Gandra, S., Levinson, J., Barter, D., White, A. and Laxminarayan, R. 2015. The state of the world's antibiotics 2015. *Wound healing southern africa*, 8 (2): 30-34.

Ghafoori, S., Mowla, A., Jahani, R., Mehrvar, M. and Chan, P. K. 2015. Sonophotolytic degradation of synthetic pharmaceutical wastewater: Statistical experimental design and modeling. *Journal of environmental management*, 150: 128-137.

Ghirardini, A., Grillini, V. and Verlicchi, P. 2020. A review of the occurrence of selected micropollutants and microorganisms in different raw and treated manure–environmental risk due to antibiotics after application to soil. *Science of the Total Environment*, 707: 136118.

Ghodrat, M. and Asrari, E. 2018. Comparative study of the performance of chitosan and chitosan adsorbents modified with Fe3O4 to eliminate erythromycin from aqueous solutions. *Iranian Journal of Health and Environment*, 10 (4): 471-482.

Grenni, P., Ancona, V. and Caracciolo, A. B. 2018. Ecological effects of antibiotics on natural ecosystems: A review. *Microchemical Journal*, 136: 25-39.

Hanekamp, J. C. and Bast, A. 2015. Antibiotics exposure and health risks: Chloramphenicol. *Environmental toxicology and pharmacology*, 39 (1): 213-220.

Haripriyan, U., Gopinath, K., Arun, J. and Govarthanan, M. 2022. Bioremediation of organic pollutants: a mini review on current and critical strategies for wastewater treatment. *Archives of Microbiology*, 204 (5): 286.

Harrower, J., McNaughtan, M., Hunter, C., Hough, R., Zhang, Z. and Helwig, K. 2021. Chemical fate and partitioning behavior of antibiotics in the aquatic environment—A review. *Environmental toxicology and chemistry*, 40 (12): 3275-3298.

He, Y., Zhang, W., Xu, M., Tong, X., Sun, F., Wang, J., Huang, S., Zhu, P. and He, X. 2015. Long-term combined chemical and manure fertilizations increase soil organic carbon and total nitrogen in aggregate fractions at three typical cropland soils in China. *Science of the Total Environment*, 532: 635-644.

Hendriksen, R. S., Munk, P., Njage, P., Van Bunnik, B., McNally, L., Lukjancenko, O., Röder, T., Nieuwenhuijse, D., Pedersen, S. K. and Kjeldgaard, J. 2019. Global monitoring of antimicrobial resistance based on metagenomics analyses of urban sewage. *Nature communications*, 10 (1): 1-12.

Hlengwa, N. and Mahlambi, P. 2020. SPE-LC-PDA method development and application for the analysis of selected pharmaceuticals in river and wastewater samples from South Africa. *Water SA*, 46 (3): 514-522.

Hou, J., Chen, Z., Gao, J., Xie, Y., Li, L., Qin, S., Wang, Q., Mao, D. and Luo, Y. 2019. Simultaneous removal of antibiotics and antibiotic resistance genes from pharmaceutical wastewater using the combinations of up-flow anaerobic sludge bed, anoxic-oxic tank, and advanced oxidation technologies. *Water research*, 159: 511-520.

Hu, Y., Yan, X., Shen, Y., Di, M. and Wang, J. 2018. Antibiotics in surface water and sediments from Hanjiang River, Central China: occurrence, behavior and risk assessment. *Ecotoxicology and Environmental Safety*, 157: 150-158.

Janusch, F., Scherz, G., Mohring, S. A. and Hamscher, G. 2014. Determination of fluoroquinolones in chicken feces–A new liquid–liquid extraction method combined with LC–MS/MS. *Environmental toxicology and pharmacology*, 38 (3): 792-799.

Jechalke, S., Heuer, H., Siemens, J., Amelung, W. and Smalla, K. 2014. Fate and effects of veterinary antibiotics in soil. *Trends in microbiology*, 22 (9): 536-545.

Jia, X., Zhang, B., Chen, C., Fu, X. and Huang, Q. 2021. Immobilization of chitosan grafted carboxylic Zr-MOF to porous starch for sulfanilamide adsorption. *Carbohydrate polymers*, 253: 117305.

Juang, L.-C., Tseng, D.-H. and Yang, S.-C. 1997. Treatment of petrochemical wastewater by UV/H2O2 photodecomposed system. *Water science and technology*, 36 (12): 357-365.

Jurado, A., Pujades, E., Walther, M. and Diaz-Cruz, M. S. 2022. Occurrence, fate, and risk of the organic pollutants of the surface water watch List in European groundwaters: a review. *Environmental Chemistry Letters*, 20 (5): 3313-3333.

K'oreje, K., Vergeynst, L., Ombaka, D., De Wispelaere, P., Okoth, M., Van Langenhove, H. and Demeestere, K. 2016. Occurrence patterns of pharmaceutical residues in wastewater, surface water and groundwater of Nairobi and Kisumu city, Kenya. *Chemosphere*, 149: 238-244.

Kaczala, F. and Blum, S. 2015. *The occurrence of veterinary pharmaceuticals in the environment: a review. Curr Anal Chem 12: 169–182*.

Kanakaraju, D., Glass, B. D. and Oelgemöller, M. 2018. Advanced oxidation process-mediated removal of pharmaceuticals from water: a review. *Journal of environmental management*, 219: 189-207.

Karimi-Maleh, H., Ayati, A., Davoodi, R., Tanhaei, B., Karimi, F., Malekmohammadi, S., Orooji, Y., Fu, L. and Sillanpää, M. 2021. Recent advances in using of chitosan-based adsorbents for removal of pharmaceutical contaminants: A review. *Journal of Cleaner Production*, 291: 125880.

Khairy, M. A., Noonan, G. O. and Lohmann, R. 2019. Uptake of hydrophobic organic compounds, including organochlorine pesticides, polybrominated diphenyl ethers, and perfluoroalkyl acids in fish

and blue crabs of the lower Passaic River, New Jersey, USA. *Environmental toxicology and chemistry*, 38 (4): 872-882.

Khan, A. H., Khan, N. A., Ahmed, S., Dhingra, A., Singh, C. P., Khan, S. U., Mohammadi, A. A., Changani, F., Yousefi, M. and Alam, S. 2020. Application of advanced oxidation processes followed by different treatment technologies for hospital wastewater treatment. *Journal of Cleaner Production*, 269: 122411.

Khumalo, S. M., Lasich, M., Bakare, B. F. and Rathilal, S. 2022. Sorption of Perfluorinated and Pharmaceutical Compounds in Plastics: A Molecular Simulation Study. *Water*, 14 (12): 1951.

Kıdak, R. and Doğan, Ş. 2018. Medium-high frequency ultrasound and ozone based advanced oxidation for amoxicillin removal in water. *Ultrasonics sonochemistry*, 40: 131-139.

Kim, I., Yamashita, N. and Tanaka, H. 2009. Performance of UV and UV/H2O2 processes for the removal of pharmaceuticals detected in secondary effluent of a sewage treatment plant in Japan. *Journal of hazardous materials*, 166 (2-3): 1134-1140.

Kovalakova, P., Cizmas, L., McDonald, T. J., Marsalek, B., Feng, M. and Sharma, V. K. 2020. Occurrence and toxicity of antibiotics in the aquatic environment: A review. *Chemosphere*, 251: 126351.

Krause, K. M., Serio, A. W., Kane, T. R. and Connolly, L. E. 2016. Aminoglycosides: an overview. *Cold Spring Harbor perspectives in medicine*, 6 (6): a027029.

Krzeminski, P., Tomei, M. C., Karaolia, P., Langenhoff, A., Almeida, C. M. R., Felis, E., Gritten, F., Andersen, H. R., Fernandes, T. and Manaia, C. M. 2019. Performance of secondary wastewater treatment methods for the removal of contaminants of emerging concern implicated in crop uptake and antibiotic resistance spread: A review. *Science of the Total Environment*, 648: 1052-1081.

Kwon, M. J., Yun, S.-T., Ham, B., Lee, J.-H., Oh, J.-S. and Jheong, W.-W. 2017. Impacts of leachates from livestock carcass burial and manure heap sites on groundwater geochemistry and microbial community structure. *PloS one*, 12 (8): e0182579.

Lappin, M., Blondeau, J., Boothe, D., Breitschwerdt, E., Guardabassi, L., Lloyd, D., Papich, M., Rankin, S., Sykes, J. and Turnidge, J. 2017. Antimicrobial use guidelines for treatment of respiratory tract disease in dogs and cats: Antimicrobial Guidelines Working Group of the International Society for Companion Animal Infectious Diseases. *Journal of Veterinary Internal Medicine*, 31 (2): 279-294.

Larcher, S. and Yargeau, V. 2011. Biodegradation of sulfamethoxazole by individual and mixed bacteria. *Applied microbiology and biotechnology*, 91 (1): 211-218.

Largitte, L. and Pasquier, R. 2016. A review of the kinetics adsorption models and their application to the adsorption of lead by an activated carbon. *Chemical engineering research and design*, 109: 495-504.

Liang, X. X., Omer, A., Hu, Z.-h., Wang, Y. g., Yu, D. and Ouyang, X.-k. 2019. Efficient adsorption of diclofenac sodium from aqueous solutions using magnetic amine-functionalized chitosan. *Chemosphere*, 217: 270-278.

Liu, J.-L. and Wong, M.-H. 2013. Pharmaceuticals and personal care products (PPCPs): a review on environmental contamination in China. *Environment international*, 59: 208-224.

Liu, S., Pu, S., Deng, D., Huang, H., Yan, C., Ma, H. and Razavi, B. S. 2020. Comparable effects of manure and its biochar on reducing soil Cr bioavailability and narrowing the rhizosphere extent of enzyme activities. *Environment international*, 134: 105277.

Liu, X., Zhang, H., Li, L., Fu, C., Tu, C., Huang, Y., Wu, L., Tang, J., Luo, Y. and Christie, P. 2016. Levels, distributions and sources of veterinary antibiotics in the sediments of the Bohai Sea in China and surrounding estuaries. *Marine Pollution Bulletin*, 109 (1): 597-602.

Lopera, A. E.-C., Ruiz, S. G. and Alonso, J. M. Q. 2019. Removal of emerging contaminants from wastewater using reverse osmosis for its subsequent reuse: pilot plant. *Journal of Water Process Engineering*, 29: 100800.

Lyu, J., Yang, L., Zhang, L., Ye, B. and Wang, L. 2020. Antibiotics in soil and water in China–a systematic review and source analysis. *Environmental Pollution*, 266: 115147.

Mackuľak, T., Černanský, S., Fehér, M., Birošová, L. and Gál, M. 2019. Pharmaceuticals, drugs, and resistant microorganisms—environmental impact on population health. *Current Opinion in Environmental Science & Health*, 9: 40-48.

Madikizela, L. M. and Chimuka, L. 2016. Determination of ibuprofen, naproxen and diclofenac in aqueous samples using a multi-template molecularly imprinted polymer as selective adsorbent for solid-phase extraction. *Journal of pharmaceutical and biomedical analysis*, 128: 210-215.

Madikizela, L. M. and Chimuka, L. 2017. Simultaneous determination of naproxen, ibuprofen and diclofenac in wastewater using solid-phase extraction with high performance liquid chromatography. *Water Sa*, 43 (2): 264-274.

Madikizela, L. M., Muthwa, S. F. and Chimuka, L. 2014. Determination of triclosan and ketoprofen in river water and wastewater by solid phase extraction and high performance liquid chromatography. *South African journal of chemistry*, 67 (1): 143-150.

Madikizela, L. M., Tavengwa, N. T. and Chimuka, L. 2017. Status of pharmaceuticals in African water bodies: occurrence, removal and analytical methods. *Journal of environmental management*, 193: 211-220.

Makhathini, T. P., Mulopo, J. and Bakare, B. F. 2020. Effective biotreatment of acidic mine water and hospital wastewater using fluidized-bed reactors. *Journal of Water Process Engineering*, 37: 101505.

Martin-Laurent, F., Topp, E., Billet, L., Batisson, I., Malandain, C., Besse-Hoggan, P., Morin, S., Artigas, J., Bonnineau, C. and Kergoat, L. 2019. Environmental risk assessment of antibiotics in agroecosystems: ecotoxicological effects on aquatic microbial communities and dissemination of antimicrobial resistances and antibiotic biodegradation potential along the soil-water continuum. *Environmental Science and Pollution Research*, 26 (18): 18930-18937.

Matongo, S., Birungi, G., Moodley, B. and Ndungu, P. 2015a. Occurrence of selected pharmaceuticals in water and sediment of Umgeni River, KwaZulu-Natal, South Africa. *Environmental Science and Pollution Research*, 22 (13): 10298-10308.

Matongo, S., Birungi, G., Moodley, B. and Ndungu, P. 2015b. Pharmaceutical residues in water and sediment of Msunduzi River, kwazulu-natal, South Africa. *Chemosphere*, 134: 133-140.

Mhuka, V., Dube, S. and Nindi, M. M. 2020. Occurrence of pharmaceutical and personal care products (PPCPs) in wastewater and receiving waters in South Africa using LC-Orbitrap™ MS. *Emerging Contaminants*, 6: 250-258.

Michael, I., Rizzo, L., McArdell, C., Manaia, C., Merlin, C., Schwartz, T., Dagot, C. and Fatta-Kassinos, D. 2013. Urban wastewater treatment plants as hotspots for the release of antibiotics in the environment: a review. *Water research*, 47 (3): 957-995.

Miguel, G. C., Orlando, E. A. and Simionato, A. V. C. 2013. Quantification of beta-lactam antibiotics in veterinary drugs: amoxicillin and ampicillin determination by high performance liquid chromatography. *Química Nova*, 36: 1214-1221.

Milić, N., Milanović, M., Letić, N. G., Sekulić, M. T., Radonić, J., Mihajlović, I. and Miloradov, M. V. 2013. Occurrence of antibiotics as emerging contaminant substances in aquatic environment. *International journal of environmental health research*, 23 (4): 296-310.

Mlunguza, N. Y., Ncube, S., Mahlambi, P. N., Chimuka, L. and Madikizela, L. M. 2019. Adsorbents and removal strategies of non-steroidal anti-inflammatory drugs from contaminated water bodies. *Journal of Environmental Chemical Engineering*, 7 (3): 103142.

Mojiri, A., Andasht Kazeroon, R. and Gholami, A. 2019. Cross-linked magnetic chitosan/activated biochar for removal of emerging micropollutants from water: Optimization by the artificial neural network. *Water*, 11 (3): 551.

Mueller, T. 2016. The correlation between regulatory conditions and antibiotic consumption within the WHO European Region. *Health Policy*, 120 (8): 882-889.

Mulla, S. I., Bagewadi, Z. K., Faniband, B., Bilal, M., Chae, J.-C., Bankole, P. O., Saratale, G. D., Bhargava, R. N. and Gurumurthy, D. M. 2021. Various strategies applied for the removal of emerging micropollutant sulfamethazine: a systematic review. *Environmental Science and Pollution Research*: 1-15.

Mulla, S. I., Hu, A., Sun, Q., Li, J., Suanon, F., Ashfaq, M. and Yu, C.-P. 2018. Biodegradation of sulfamethoxazole in bacteria from three different origins. *Journal of environmental management*, 206: 93-102.

Naddeo, V., Uyguner-Demirel, C. S., Prado, M., Cesaro, A., Belgiorno, V. and Ballesteros, F. 2015. Enhanced ozonation of selected pharmaceutical compounds by sonolysis. *Environmental technology*, 36 (15): 1876-1883.

Nayak, A., Bhushan, B. and Kotnala, S. 2022. Fabrication of chitosan-hydroxyapatite nano-adsorbent for removal of norfloxacin from water: Isotherm and kinetic studies. *Materials Today: Proceedings*, 61: 143-149.

Nazraz, M., Yamini, Y. and Asiabi, H. 2019. Chitosan-based sorbent for efficient removal and extraction of ciprofloxacin and norfloxacin from aqueous solutions. *Microchimica Acta*, 186 (7): 1-9.

O'Flynn, D., Lawler, J., Yusuf, A., Parle-McDermott, A., Harold, D., Mc Cloughlin, T., Holland, L., Regan, F. and White, B. 2021. A review of pharmaceutical occurrence and pathways in the aquatic environment in the context of a changing climate and the COVID-19 pandemic. *Analytical Methods*, 13 (5): 575-594.

Ou, H., Chen, Q., Pan, J., Zhang, Y., Huang, Y. and Qi, X. 2015. Selective removal of erythromycin by magnetic imprinted polymers synthesized from chitosan-stabilized Pickering emulsion. *Journal of hazardous materials*, 289: 28-37.

Pan, L.J., Li, J., Li, C.X., Yu, G.W. and Wang, Y. 2018. Study of ciprofloxacin biodegradation by a Thermus sp. isolated from pharmaceutical sludge. *Journal of hazardous materials*, 343: 59-67.

Pan, L.J., Tang, X.-d., Li, C.X., Yu, G.W. and Wang, Y. 2017. Biodegradation of sulfamethazine by an isolated thermophile–Geobacillus sp. S-07. *World Journal of Microbiology and Biotechnology*, 33 (5): 1-8.

Pan, M. and Chu, L. 2017. Leaching behavior of veterinary antibiotics in animal manure-applied soils. *Science of the Total Environment*, 579: 466-473.

Park, J., Cho, K. H., Ligaray, M. and Choi, M.-J. 2019. Organic matter composition of manure and its potential impact on plant growth. *Sustainability*, 11 (8): 2346.

Patel, M., Kumar, R., Kishor, K., Mlsna, T., Pittman Jr, C. U. and Mohan, D. 2019. Pharmaceuticals of emerging concern in aquatic systems: chemistry, occurrence, effects, and removal methods. *Chemical reviews*, 119 (6): 3510-3673.

Pera-Titus, M., García-Molina, V., Baños, M. A., Giménez, J. and Esplugas, S. 2004. Degradation of chlorophenols by means of advanced oxidation processes: a general review. *Applied Catalysis B: Environmental*, 47 (4): 219-256.

Phasuphan, W., Praphairaksit, N. and Imyim, A. 2019. Removal of ibuprofen, diclofenac, and naproxen from water using chitosan-modified waste tire crumb rubber. *Journal of Molecular Liquids*, 294: 111554.

Pilli, S., Sellamuthu, B., Pandey, A. K. and Tyagi, R. 2020. Treatment of wastewater containing pharmaceuticals: biological treatment. In: *Current developments in biotechnology and Bioengineering*. Elsevier, 463-520.

Prescott, J. F. 2013. Other Beta-lactam Antibiotics: Beta-lactamase Inhibitors, Carbapenems, and Monobactams. *Antimicrobial therapy in veterinary medicine*: 175-187.

Qiu, W., Vakili, M., Cagnetta, G., Huang, J. and Yu, G. 2020. Effect of high energy ball milling on organic pollutant adsorption properties of chitosan. *International journal of biological macromolecules*, 148: 543-549.

Rajapaksha, A. U., Vithanage, M., Lim, J. E., Ahmed, M. B. M., Zhang, M., Lee, S. S. and Ok, Y. S. 2014. Invasive plant-derived biochar inhibits sulfamethazine uptake by lettuce in soil. *Chemosphere*, 111: 500-504.

Rasoulzadeh, H., Mohseni-Bandpei, A., Hosseini, M. and Safari, M. 2019. Mechanistic investigation of ciprofloxacin recovery by magnetite–imprinted chitosan nanocomposite: isotherm, kinetic, thermodynamic and reusability studies. *International journal of biological macromolecules*, 133: 712-721.

Reis, P. J., Reis, A. C., Ricken, B., Kolvenbach, B. A., Manaia, C. M., Corvini, P. F. and Nunes, O. C. 2014. Biodegradation of sulfamethoxazole and other sulfonamides by Achromobacter denitrificans PR1. *Journal of hazardous materials*, 280: 741-749.

Rizzi, V., Lacalamita, D., Gubitosa, J., Fini, P., Petrella, A., Romita, R., Agostiano, A., Gabaldón, J. A., Gorbe, M. I. F. and Gómez-Morte, T. 2019a. Removal of tetracycline from polluted water by chitosan-olive pomace adsorbing films. *Science of The Total Environment*, 693: 133620.

Rizzi, V., Romanazzi, F., Gubitosa, J., Fini, P., Romita, R., Agostiano, A., Petrella, A. and Cosma, P. 2019b. Chitosan film as eco-friendly and recyclable bio-adsorbent to remove/recover diclofenac, ketoprofen, and their mixture from wastewater. *Biomolecules*, 9 (10): 571.

Rogers Van Katwyk, S., Grimshaw, J. M., Nkangu, M., Nagi, R., Mendelson, M., Taljaard, M. and Hoffman, S. J. 2019. Government policy interventions to reduce human antimicrobial use: a systematic review and evidence map. *PLoS medicine*, 16 (6): e1002819.

Scaria, J., Anupama, K. and Nidheesh, P. 2021. Tetracyclines in the environment: An overview on the occurrence, fate, toxicity, detection, removal methods, and sludge management. *Science of The Total Environment*, 771: 145291.

Shah, A. M., Qazi, I. H., Matra, M. and Wanapat, M. 2022. Role of Chitin and Chitosan in Ruminant Diets and Their Impact on Digestibility, Microbiota and Performance of Ruminants. *Fermentation*, 8 (10): 549.

Sharma, M., Yadav, A., Mandal, M. and Dubey, K. 2022. TiO2 based photocatalysis: a valuable approach for the removal of pharmaceuticals from aquatic environment. *International Journal of Environmental Science and Technology*: 1-16.

Silori, R. and Tauseef, S. M. 2022. A review of the occurrence of pharmaceutical compounds as emerging contaminants in treated wastewater and aquatic environments. *Current Pharmaceutical Analysis*, 18 (4): 345-379.

Solliec, M., Roy-Lachapelle, A., Gasser, M.-O., Coté, C., Généreux, M. and Sauvé, S. 2016. Fractionation and analysis of veterinary antibiotics and their related degradation products in agricultural soils and drainage waters following swine manure amendment. *Science of The Total Environment*, 543: 524-535.

Song, L., Yang, S., Gong, Z., Wang, J., Shi, X., Wang, Y., Zhang, R., Wu, Y. and Wager, Y. Z. 2022. Antibiotics and Antibiotic Resistant Genes in Municipal Solid Waste Landfills: Current situation and Perspective. *Current Opinion in Environmental Science & Health*: 100421.

Sujatha, G., Shanthakumar, S. and Chiampo, F. 2020. UV light-irradiated photocatalytic degradation of coffee processing wastewater using TiO2 as a catalyst. *Environments*, 7 (6): 47.

Tasho, R. P. and Cho, J. Y. 2016. Veterinary antibiotics in animal waste, its distribution in soil and uptake by plants: A review. *Science of the Total Environment*, 563: 366-376.

Thalla, A. K. and Vannarath, A. S. 2020. Response to letter to the editor on the paper "occurrence and environmental risks of nonsteroidal anti-inflammatory drugs in urban wastewater in the southwest monsoon region of India". *Environmental Monitoring and Assessment*, 192 (9): 1-5.

Tiseo, K., Huber, L., Gilbert, M., Robinson, T. P. and Van Boeckel, T. P. 2020. Global trends in antimicrobial use in food animals from 2017 to 2030. *Antibiotics*, 9 (12): 918.

Tran, N. H., Reinhard, M. and Gin, K. Y.-H. 2018. Occurrence and fate of emerging contaminants in municipal wastewater treatment plants from different geographical regions-a review. *Water research*, 133: 182-207.

Van Boeckel, T. P., Gandra, S., Ashok, A., Caudron, Q., Grenfell, B. T., Levin, S. A. and Laxminarayan, R. 2014. Global antibiotic consumption 2000 to 2010: an analysis of national pharmaceutical sales data. *The Lancet infectious diseases*, 14 (8): 742-750.

Vasquez, M. I., Lambrianides, A., Schneider, M., Kümmerer, K. and Fatta-Kassinos, D. 2014. Environmental side effects of pharmaceutical cocktails: what we know and what we should know. *Journal of Hazardous Materials*, 279: 169-189.

Verma, M., Lee, I., Sharma, S., Kumar, R., Kumar, V. and Kim, H. 2021. Simultaneous Removal of Heavy Metals and Ciprofloxacin Micropollutants from Wastewater Using Ethylenediaminetetraacetic Acid-Functionalized β-Cyclodextrin-Chitosan Adsorbent. *ACS omega*, 6 (50): 34624-34634.

Wang, J. L. and Xu, L. J. 2012. Advanced oxidation processes for wastewater treatment: formation of hydroxyl radical and application. *Critical reviews in environmental science and technology*, 42 (3): 251-325.

Wang, Q., Wang, P. and Yang, Q. 2018. Occurrence and diversity of antibiotic resistance in untreated hospital wastewater. *Science of the Total Environment*, 621: 990-999.

Wang, X., Ryu, D., Houtkooper, R. H. and Auwerx, J. 2015. Antibiotic use and abuse: a threat to mitochondria and chloroplasts with impact on research, health, and environment. *Bioessays*, 37 (10): 1045-1053.

Wei, X., Zhang, Q., Cao, S., Xu, X., Chen, Y., Liu, L., Yang, R., Chen, J. and Lv, B. 2021. Removal of pharmaceuticals and personal care products (PPCPs) and environmental estrogens (EEs) from water using positively charged hollow fiber nanofiltration membrane. *Environmental Science and Pollution Research*, 28: 8486-8497.

Weng, X., Lin, S., Zhong, Y. and Chen, Z. 2013. Chitosan stabilized bimetallic Fe/Ni nanoparticles used to remove mixed contaminants-amoxicillin and Cd (II) from aqueous solutions. *Chemical engineering journal*, 229: 27-34.

Wohde, M., Berkner, S., Junker, T., Konradi, S., Schwarz, L. and Düring, R.-A. 2016. Occurrence and transformation of veterinary pharmaceuticals and biocides in manure: a literature review. *Environmental Sciences Europe*, 28 (1): 1-25.

Xing, Y., Chen, X., Wagner, R. E., Zhuang, J. and Chen, X. 2020. Coupled effect of colloids and surface chemical heterogeneity on the transport of antibiotics in porous media. *Science of The Total Environment*, 713: 136644.

Yao, L., Wang, Y., Tong, L., Deng, Y., Li, Y., Gan, Y., Guo, W., Dong, C., Duan, Y. and Zhao, K. 2017. Occurrence and risk assessment of antibiotics in surface water and groundwater from different depths of aquifers: a case study at Jianghan Plain, central China. *Ecotoxicology and Environmental Safety*, 135: 236-242.

Yaqubi, O., Tai, M. H., Mitra, D., Gerente, C., Neoh, K. G., Wang, C.-H. and Andres, Y. 2021. Adsorptive removal of tetracycline and amoxicillin from aqueous solution by leached carbon black waste and chitosan-carbon composite beads. *Journal of Environmental Chemical Engineering*, 9 (1): 104988.

Ying, M., Wu, J., Oakes, K. D. and Hu, A. 2015. Removal of pharmaceuticals and personal care products from wastewater. *Wastewater Treatment*: 81-109.

Yoro, K. O., Amosa, M. K., Sekoai, P. T., Mulopo, J. and Daramola, M. O. 2020. Diffusion mechanism and effect of mass transfer limitation during the adsorption of CO2 by polyaspartamide in a packed-bed unit. *International Journal of Sustainable Engineering*, 13 (1): 54-67.

Yuan, Q., Snow, D. D. and Bartelt-Hunt, S. L. 2013. Potential water quality impacts originating from land burial of cattle carcasses. *Science of the Total Environment*, 456: 246-253.

Zhang, K., Li, C., Sun, C. and Marmier, N. 2022. A Review of the Treatment Process of Perfluorooctane Compounds in the Waters: Adsorption, Flocculation, and Advanced Oxidative Process. *Water*, 14 (17): 2692.

Zhao, R., Ma, T., Zhao, S., Rong, H., Tian, Y. and Zhu, G. 2020. Uniform and stable immobilization of metal-organic frameworks into chitosan matrix for enhanced tetracycline removal from water. *Chemical Engineering Journal*, 382: 122893.

Zhao, Y., Kuang, J., Zhang, S., Li, X., Wang, B., Huang, J., Deng, S., Wang, Y. and Yu, G. 2017. Ozonation of indomethacin: kinetics, mechanisms and toxicity. *Journal of hazardous materials*, 323: 460-470.

CHAPTER THREE: LITERATURE REVIEW – PART II

THE OCCURRENCE AND BIOREMEDIATION OF EMERGING PERFLUORINATED COMPOUNDS IN WATER BODIES: A MINI REVIEW

3.1. Abstract

The occurrence and fate of perfluorinated compounds (PFCs) also known as per- or polyfluoroalkyl acids in the aquatic environment resulting from anthropogenic activities has become an emerging issue of environmental chemistry. PFCs have been detected in drinking water samples, aquatic life, human tissue, and blood serum. This is attributed to their xenobiotic attributes making them environmentally persistent, bio-accumulative, and globally distributed in water receiving bodies posing serious health problems to aquatic life and human health. This is attributed to PFCs peculiar physicochemical properties of being hydrophobic and oleophobic and their removal process from wastewater streams is different from any other organic pollutants. Therefore, this chapter summarises the environmental occurrence and recent developments on microbial degradation of the most detected PFCs i.e., perfluorooctanoic acid (PFOA), and perfluorooctane sulfonic acid (PFOS) in water bodies. The available literature suggests that PFOA and PFOS are susceptible to biodegradation by *Acidimicrobium* sp. strain A6, *Pseudomonas parafulva* strain YAB1, *Pseudomonas plecoglossicidia* 2.4-D, and *Pseudomonas aeruginosa* strain HJ4. Moreover, the chapter presents a summary on phytoremediation of PFOA and PFOS as a sustainable green technology. Despite the extensive work done on bioremediation of PFOA and PFOS by biological processes, the available literature suggests that a lot of work still needs to be done aimed at investigating the biodegradation pathway of PFOA and PFOS by both microbial species and plants. Moreover, available literature suggests that studies on the removal of PFOA and PFOS by solid-liquid adsorption are scanty.

3.2. Introduction

Perfluorinated compounds (PFCs) are a class of anthropogenic emerging persistent organic pollutants that consists of a fully fluorinated hydrophobic alkyl chain attached to a hydrophilic chain end group. The PFCs carbon-fluorine bond characterised by strong polarity and strength (Khumalo *et al.* 2022) make them possess peculiar physicochemical properties such as hydrophobicity, and resistance to degradation by heat and acid (Rahman, Peldszus and Anderson 2014; Cai *et al.* 2021; Lenka, Kah and Padhye 2021). Owing to their hydrophobic and lipophobic moieties, PFCs are friction resistant and are used as water and oil repellents (Lenka, Kah and Padhye 2021). Due to their peculiar chemical attributes, PFCs have cemented their application in consumer products such as stain-resistant household products, non-sticky cooking utensils, food packaging, cosmetics and personal care products etc., and

industrial application such as surface coatings for textiles, metal plating, manufacturing of leather etc., (Ahrens 2011; Rahman, Peldszus and Anderson 2014; Sun *et al.* 2018b; Abdullah Soheimi *et al.* 2021; Lenka, Kah and Padhye 2021; Khumalo *et al.* 2022). The primary purpose of using PFC treated consumer products as well as industrial products is to improve their durability (Lenka, Kah and Padhye 2021) whilst prolonging their exposure to humans and the environment. Hence, there has been an increase in levels of PFCs detected in aquatic environments (Booi *et al.* 2019; Andersson *et al.* 2019; Crone *et al.* 2019) posing serious health problems to aquatic life and humans.

Studies (Houde *et al.* 2011; Abdullah Soheimi *et al.* 2021; Lenka, Kah and Padhye 2021; McCarthy, Roark and Middleton 2021; Xie *et al.* 2021) have indicated that PFCs have been detected ubiquitously in multiple environmental spheres such as air, water bodies, and soil. Moreover, these contaminants of emerging concern have been detected in food sources, such as livestock and crustaceans (Abdullah Soheimi *et al.* 2021). Since PFCs are ubiquitous to aquatic matrices including drinking water, humans can be exposed to them through drinking water as well as dietary intake (Rahman, Peldszus and Anderson 2014; Lenka, Kah and Padhye 2021). Several works have been reported on human health effects as a result of exposure to PFCs. Xie *et al.* (2021) reported on the nexus between PFCs and human thyroid dysfunction and concluded that PFCs are endocrine-disrupting compounds. Human exposure to PFCs result in thyroid malfunction and/or hormonal imbalance, particularly in pregnant women and neonates (Xie *et al.* 2021). Health effects associated with PFC exposure include cardiovascular diseases, urine acid, thyroid diseases, paediatric atopy, immune toxicity, anxiety, liver damage, kidney disorder, obesity, peroxisome, reduced fertility, fecundity etc., (Jian *et al.* 2017; Crone *et al.* 2019; Li *et al.* 2019; Abdullah Soheimi *et al.* 2021; Lenka, Kah and Padhye 2021; Xie *et al.* 2021). Because of the aforementioned human health complications, the production and regulations of PFCs have attracted public attention. According to Jian *et al.* (2017), the 3M company together with the United States Environmental Protection Agency (USEPA) announced the phase-out of products containing PFCs with C6 and more, aimed at eliminating long chain PFCs which have attributes of being very persistent and bio-accumulative.

Hitherto, studies are still conducted aimed at understanding the environmental occurrence and fate, as well as human health complications of PFCs. This is attributed to the thousands of PFCs that have been identified and are still being manufactured and used globally (Lenka, Kah and Padhye 2021; McCarthy, Roark and Middleton 2021). It should be noted that, despite the wide pool of PFCs that have been detected in the environment, global environmental entities are interested in long chain perfluoroalkyl sulfonic acids ($C_nF_{2n+1}SO_3H$, $n \geq 6$) (PFSAs) and perfluoroalkyl carboxylic acids ($C_nF_{2n+1}COOH$, $n \geq 7$) (PFCAs) and their corresponding anions. The aforementioned PFCs have demonstrated to be more bio-accumulative as compared to their short chain analogues as reported by Rahman, Peldszus and Anderson (2014) and Buck *et al.* (2011). Perfluorooctanoic acid (PFOA) and perfluorooctane sulfonic acid (PFOS) are conventional PFCs and mostly detected perfluoroalkyl acids (PFAAs) in the

environment (Agency 2016; EPA 2016). The high levels of PFOA and PFOS in the environment is attributed to their xenobiotic attributes as reported by many researchers which makes their complete eradication almost impossible. Therefore, the current study aims at providing an overview on the occurrence of PFCs in water bodies as well as the latest development in biological remediation of PFOA and PFOS since they are characterised as xenobiotic compounds.

3.3. Occurrence of PFCs in Water Bodies

PFCs are introduced into the environment during their industrial production, application, as well as a result of leaching and their biotic or abiotic biodegradation of consumer products containing a perfluoroalkyl moiety (Buck *et al.* 2011; Rahman, Peldszus and Anderson 2014). Moreover, the discharge of industrial effluent containing PFCs into the environment contributes significantly to the occurrence of PFCs in both surface and ground water. Consequently, these PFCs enter waste water treatment plants (WWTPs) making them the major source of PFCs to surface waters as reported by Rahman, Peldszus and Anderson (2014). Generally, WWTPs have demonstrated to be ineffective in PFCs removal from aqueous streams. This is attributed to the C-F bond becoming more stable with an increasing replacement of hydrogen by fluorine at each bond, consequently making PFCs to withstand any degradation process (i.e., photolytic, and microbial) (Rahman, Peldszus and Anderson 2014). Recently done studies (Jian *et al.* 2017; Rodríguez-Gómez *et al.* 2017; Crone *et al.* 2019) have indicated that drinking water is the major exposure pathway to PFCs in communities with contaminated water. Note that, the degradation of fluorotelomer alcohols and perfluoroalkyl sulfonamides lead to PFAAs formation consequently resulting in their occurrence in water bodies. As such, they are classified as PFAAs precursors (Rahman, Peldszus and Anderson 2014). Moreover, the persistence of PFAAs in aquatic ecosystems is attributed to their chemical attributes such as simultaneous hydrophobic-hydrophilic properties, and low volatility (Buck *et al.* 2011; Sun *et al.* 2018a).

Rahman, Peldszus and Anderson (2014) and Jian *et al.* (2017) in their reviews on the occurrence and fate of PFCs in drinking water reported that apart from PFOA and PFOS, there are other frequently detected PFCs such as perfluorooctane sulfonamide, perfluorohexane sulfonic acid, perfluorobutanoic acid, perfluorohexanoic acid, perfluoroheptanoic acid, perfluorodecanoic acid and perflurononanoic acid. Despite the occurrence of the aforementioned PFCs in aquatic ecosystems, PFOA and PFOS have been detected frequently recording the highest concentration ranging from µg/L to mg/L compared to any other PFCs reported concentration levels ranging from pg/L to ng/L. Studies (Ding *et al.* 2012; Rahman, Peldszus and Anderson 2014) suggest that, due to the stringent regulations on PFOA and PFOS, there are other emerging fluorinated organics such as polyfluoroalkyl phosphates, perfluorinated phosphonic acids, and perfluorinated phosphonic acids that have been detected in water bodies.

However, the aforementioned phosphorus containing fluorinated compounds are not explicitly accounted for in this current study.

It is imperative to note that the concentration levels of PFCs in water bodies can be influenced by the location of the PFC point source from the water bodies. Studies conducted on the global distribution of PFCs have shown that higher levels of PFCs, particularly PFOA and PFOS, that have been detected in industrialised areas (Kunacheva *et al.* 2012; Rahman, Peldszus and Anderson 2014; Sun *et al.* 2018a). Consequently, PFCs have been detected in treated water at an average concentration of 30 ng/L (Rahman, Peldszus and Anderson 2014). However, there has been a large variability in PFC concentration levels from tap water as shown in Table 3.1. Eschauzier *et al.* (2013) reported PFOA and PFOS concentrations ranging from 0.6 to 6.6 ng/L and 0.1 to 11 ng/L, respectively for background contaminated tap water. On the other hand, Eschauzier *et al.* (2012) reported PFOA and PFOS concentration ranges of 22 to 519 ng/L and 3 to 22 ng/L, respectively, for highly industrialised, and/or agricultural areas. As a matter of health concern, the USEPA issued a limit for PFOA and PFOS in drinking water of 70 ng/L for both individual and combined (Crone *et al.* 2019; Wang *et al.* 2021).

Based on the reported PFOA and PFOS concentration levels presented in Table 3.1 it is apparent that PFOA and PFOS in drinking water is below the 70 ng/L limit at least for many regions but Africa. The high PFOA and PFOS concentrations in drinking water from the African region suggests that drinking water can cause imminent human health risk due to PFCs contamination. Due to the occurrence of PFCs in tap water, Eschauzier *et al.* (2013) reported that PFOA has been detected in tap water based beverages (e.g., cola and coffee) at a concentration of 4 ng/L. The lower PFC concentration from tap water beverages is attributed to the pre-treatment of tap water prior to being used for production. Moreover, a review study by Rahman, Peldszus and Anderson (2014) has indicated that high PFOA concentration levels ranging from 487 – 10 100 ng/L has been detected in aquatic environments near point sources.

Table 3.9: Concentrations of PFOA and PFOS detected in tap water.

Region	**Country**	**PFOA, ng/L**	**PFOS, ng/L**	**Reference**
Africa	Ghana	68.1 – 190	62.1 – 168.3	(Essumang *et al.* 2017)
Oceania	Australia	0 – 16	0 – 9.7	(Thompson, Eaglesham and Mueller 2011)
America	Canada	3 – 32	2 – 12	(Tabe *et al.* 2010)
	Brazil	0.35 – 2.82	0.58 – 6.70	(Domingo and Nadal 2019)
	USA	5 – 30	1 – 57	(Thompson, Eaglesham and Mueller 2011)
Asia	China	115 – 151	0.1 – 11.2	(Tan *et al.* 2017)
	Japan	6.5 – 48	1.3 – 3.7	(Domingo and Nadal 2019)

Table 3.1: Continues

Europe	France	8.7 -18	3 – 11.99	(Schwanz *et al.* 2016)
	Germany	0 – 6.1	0 – 4.7	(Gellrich, Brunn and Stahl 2013)
	Netherlands	0.6 – 6.6 <0.3 – 11	0.1 – 11 <0.03 – 0.41	(Eschauzier *et al.* 2013) (Gebbink, Van Asseldonk and Van Leeuwen 2017)
	Sweden	0.302 – 8.56	0.397 – 8.81	(Schwanz *et al.* 2016)
	Spain	3.8 – 29	2.4 – 140	(Schwanz *et al.* 2016)

Early studies (Eschauzier *et al.* 2012) on the global distribution of PFCs in aquatic environments suggest that water receiving bodies located in low population density areas have low levels of PFCs. This can be attributed to fewer industrial activities. It is worth noting that PFCs toxicity values vary significantly from one standard to another as indicate in Table 3.2. The variability in toxicity values can be attributed to the lack of federal maximum contaminants level.

Table 3.10: PFOA and PFOS drinking water guideline levels.

Regulatory body	**PFC**	**Advisory level, ng/L**	**Toxicological endpoint**	**Reference**
U.S. EPA, 2016, Health Advisory Level	PFOA	70	Developmental	(Cordner *et al.* 2019)
	PFOS	70	Reduced pup body weight	
Alaska DEC[1], 2016, ground water clean-up level	PFOA	400	Developmental	
	PFOS	400	Reduced pup body weight	
Maine DEP[2], 2016, Remedial action guideline	PFOA	130	Liver	
	PFOS	560	Thyroid effects	
New Jersey DEP, 2017, Maximum contaminant level	PFOA	14	Liver	
	PFOS	13	Immune response	
German Drinking Water Commission	PFOA	1500	N/A	(Rahman, Peldszus and Anderson 2014)
	PFOS	600	N/A	
Drinking water inspectorate, UK	PFOA	>300	N/A	
	PFOS	>300	N/A	

[1]DEC, Department of Environmental Conservation; [2]DEP, Department of Environmental Protection

In the subsequent sections, the recent developments on biological remediation of PFCs are summarised despite being characterised as xenobiotic compounds.

3.4. Degradation and Fate of PFCs in the Environment

3.4.1. Bacterial biodegradation

Conventional WWTPs use biological techniques to treat water and wastewater streams for reuse. During biological treatment of aqueous streams, biodegradable material consisting of organics in dissolved form such as starches, alcohols, acids, aldehydes, and esters, are utilised for food by microorganisms, thus decontaminating aqueous streams. It is worth noting that microbial utilization of dissolved organics can be accompanied by oxidation which is the deletion of hydrogen from elements of an organic molecule, or by reduction which is addition of hydrogen to elements of the organic molecule (Peavy, Rowe and Tchobanoglous 1985). However, several previously done studies suggests that the biodegradation pathways and fate of PFCs is unknown to a large extent. This is attributed to the general believe that the strength of the C-F bond is the limiting factor on PFC biodegradability. However, early evidence suggests that organohalogen compounds including PFCs are susceptible to microbial degradation despite their high stability as reported by Parsons *et al.* (2008). The biodegradation of organohalogen compounds and PFCs are relatively slow due to their kinetic stability because of the carbon-halogen bond, thus contributing significantly to their long-term environmental fate.

Hitherto, dehalogenation is the thermodynamically recognised reaction mechanism for the degradation of organohalogen compounds. Early studies (Parsons *et al.* 2008; Zhang, Lai and Kong 2011) suggest that under aerobic conditions, organohalogen compounds are degraded by catabolic pathways similar to those for nonhalogenated analogues. There are a number of dehalogenation mechanisms that are reported in literature for both aliphatic and aromatic substrates i.e., haloacid dehalogenation, halohydrin dehalogenation, haloalkane dehalogenation, and reductive dehalogenation (Parsons *et al.* 2008). However, there is very little information reported on the degradation of PFCs particularly PFOA and PFOS. This is attributed to the biodegradation mechanism of 8:2 fluorotelomer alcohol by OH radicals which yields PFOA and other perfluorinated carboxylic acids as products (Rahman, Peldszus and Anderson 2014). Fluorotelomer alcohols have been reported to biodegrade under aerobic and anaerobic environments (Parsons *et al.* 2008). In an early study conducted by Meesters and Schröder (2004), it was demonstrated that both PFOA and PFOS are xenobiotic under aerobic environments. Despite the observed removal of PFOA and PFOS under anaerobic environments, no fluoride ion concentration was detected which makes the biodegradability mechanism of PFOA and PFOS in aquatic environments to remain difficult to understand for many researchers. In the subsequent section, the biodegradation of PFOA and PFOS are explained, indicating that their xenobiotic characteristics is something of the past.

Despite the chemically challenging C-F bond cleavage, recently done studies have demonstrated that PFCs, particularly PFOA and PFOS, can be defluorinated by strong chemical oxidants as well as by microbial population (Huang and Jaffé 2019; Wackett 2021, 2022). A lot of researchers have reported limited microbial defluorination of PFCs. This is attributed to the displacement of C-F bonds which

yield a fluoride ion, F^-, which is toxic to microbial population at minute concentrations (Breaker 2012). The fluoride ion, which is produced as a result of PFCs biodegradation (i.e., defluorination), enters bacterial cells, thus poisoning them (Breaker 2012; Wackett 2021). The poisoning of bacterial cells ceases or hinders metabolic activities resulting in nonbiodegradability of PFCs. Such a biological reaction mechanism explains why fluorine concentrations are not detected during biodegradation of PFCs. The revelation of the toxicity of the fluoride ion to bacterial cells explains why PFCs are characterised as xenobiotic compounds. Moreover, the biodegradation mechanism of PFCs suggests that their xenobiotic characteristics are not solely as a result of the C-F bond, but it can be attributed to the toxicity of the fluoride ion which hinders microbial activities.

Recently, Huang and Jaffé (2019) demonstrated that PFOA and PFOS are susceptible to biodegradation by *Acidimicrobium* sp. strain A6 (an autotroph) that oxidizes ammonium to nitrite while reducing ferric iron. Both PFOA and PFOS were added as carbon sources during the oxidation of ammonium to nitrite while reducing ferric iron by *Acidimicrobium* in an anaerobic environment. It was reported that both PFOS and PFOA were metabolised recording a removal efficiency of up to 60% for both PFOS and PFOA over an incubation period of 100 days. Despite the observed biodegradation of PFOS and PFOA, it was reported that intermediate products such as perfluorobutanoic acid, perfluoroheptanoic acid, perfluoropentanoic acid, and perfluorohexanoic acid were detected in *Acidimicrobium* culture. The aforementioned intermediate products were detected for PFOA and PFOS initial concentrations of 100 mg/L. It is also worth mentioning that the initial concentration of 100 mg/L for the model PFCs was detrimental on the microbial population. A significant decline on *Acidimicrobium* population was observed from day 60 of incubation as compared to an initial concentration of 0.1 mg/L. Moreover, the findings reported by Huang and Jaffé (2019) suggests that PFOS is more detrimental to *Acidimicrobium* population as compared to PFOA. Hitherto, there is no available literature reporting on PFOA and/or PFOS optimum concentration aimed at minimising their detrimental effects on microbial population.

Ruiz-Urigüen *et al.* (2022) investigated the biodegradation of PFOA in microbial electrolysis cells using *Acidimicrobium* sp. strain A6 as an inoculum under anaerobic conditions. It was reported that a decrease in PFOA concentration was observed after 18 days of operation while producing electricity. For the work reported by Ruiz-Urigüen *et al.* (2022), the biodegradation of PFOA is not explicitly accounted for, on the basis that no PFOA measurements were conducted during operation but PFOA degradation intermediate products analogues to the one reported by Huang and Jaffé (2019) were detected. The measurement of PFOA intermediate products is attributed to the complexities of PFOA measurements which can be affected by sample handling and hemimicelle formation (Ruiz-Urigüen *et al.* 2022). For the work reported by Ruiz-Urigüen *et al.* (2022), 100 mg PFOA/L was the desired initial concentration, however, due to hemimicelle formation, the initial concentration measured was 47 mg PFOA/L.

Due to the recalcitrance and high stability of PFCs, particularly PFOA and PFOS, researchers have continued to test various microbial species aimed at testing their ability to biodegrade the aforementioned model contaminants. Based on the reviewed literature, *Acidimicrobium* sp. strain A6 (Huang and Jaffé 2019; Ruiz-Urigüen *et al.* 2022) *Pseudomonas parafulva* strain YAB1 (Yi *et al.* 2016), *Pseudomonas aeruginosa* strain HJ4 (Kwon *et al.* 2014) and *Pseudomonas plecoglossicida* 2.4-D (Chetverikov *et al.* 2017) are the only microbial species reported to biodegrade PFOA and PFOS. Yi *et al.* (2016) investigated the growth rate of YAB1 which was extracted from soil sediments near a PFCs producing plant. Yi *et al.* (2016) conducted their investigation in an aerobic environment and PFOA was added as a carbon source for YAB1. Optimal bacteria growth rate and PFOA degradation was recorded for a PFOA concentration of 500 mg/L. Interestingly, it was reported (Ruiz-Urigüen *et al.* 2022) that PFOA concentration of 1000 mg/L inhibited the growth rate of YAB1, however, the strain demonstrated considerable tolerance and growth adaptability. The findings by Yi *et al.* (2016) suggests that, higher PFOA concentrations hinder microbial activities, consequently inhibiting the bacterial proliferation. This is congruent to the work reported by Huang and Jaffé (2019) and Ruiz-Urigüen *et al.* (2022) that higher PFOA concentrations become toxic to microbial species, thus hindering microbial activities. Yi *et al.* (2016) reported a PFOA removal efficiency of 48 % which was achieved after adding yeast to promote bacterial growth rate.

The growing interest in the investigation of various microbial species to degrade PFCs has demonstrated that PFOS can be degraded by *Pseudomonas aerginosa* strain HJ4 under aerobic environment (Kwon *et al.* 2014). PFOS was added as a carbon source at an initial concentration ranging from 1400 µg/L to 1800 µg/L for the growth of strain HJ4. Kwon *et al.* (2014) reported an overall PFOS biodegradation of 67% which was recorded after adding glucose to enhance the growth rate of strain HJ4 for PFOS biodegradation. However, according to Kwon *et al.* (2014) no defluorination was observed. Fluoride ion concentration remained constant during biodegradation of PFOS. On the other hand, Chetverikov *et al.* (2017) reported 75% PFOS degradation as carbon source for the growth of *Pseudomonas plecoglossicida* 2.4-D. A significant growth rate on the 2.4-D strain was observed after adding NaCl which was maintained at less than 5% to avoid any microbial inhabitation. Chetverikov and co-workers reported fluoride ions concentration of up to 150 mg/L in the culture medium to account that indeed defluorination took place. Table 3.3 presents a summary of studies conducted to-date aimed at microbial degradation of PFOA and PFOS at laboratory scale.

Table 11.3 Microbial degradation of PFOA and PFOS.

Pollutant	Microbial Species	Matrix conditions	Concentration (mg/L)	System efficacy (%)	Incubation period (day)	Reference
PFOA	*Acidimicrobium* sp. strain A6	Anaerobic	0.1 – 100	<60	100	(Huang and Jaffé 2019)
			47	77	18	(Ruiz-Urigüen *et al.* 2022)
	Pseudomonas parafulva strain YAB1	Aerobic	500	48	5	(Yi *et al.* 2016)
PFOS	*Acidimicrobium* sp. strain A6	Anaerobic	0.1 – 100	<60	100	(Huang and Jaffé 2019)
	Pseudomonas aerginosa strain HJ4	Aerobic	1.4 – 1.8	67	2	(Kwon *et al.* 2014)
	Pseudomonas plecoglossicida 2.4-D	Aerobic	1 000	75	6	(Chetverikov *et al.* 2017)

3.4.2. Microbial degradation pathway of PFOA and PFOS

Despite the experimentally illustrated biodegradation of PFOA and PFOS by microbial species (Kwon *et al.* 2014; Yi *et al.* 2016; Huang and Jaffé 2019; Ruiz-Urigüen *et al.* 2022), there is no available literature confirming a precise biodegradation mechanism of PFOA and PFOS. The few studies that have reported on PFCs biodegradation, particularly PFOA and PFOS, the mechanism is based on the detection of intermediate metabolites. According to Zhang *et al.* (2022), this is attributed to PFOA and PFOS having a low redox potential of about − 450 mV. Typical microbial oxidisable growth substrates demonstrate redox potentials greater than − 450 mV (Wackett 2022; Zhang *et al.* 2022), therefore, at a low redox potential, the transfer of an electron from a substrate to PFCs reduction will not be thermodynamically attractive for microbial species. However, as eluded from the previous sections, studies have demonstrated that selected bacteria can degrade PFOA and PFOS under anaerobic (Huang and Jaffé 2019) and aerobic (Kwon *et al.* 2014; Yi *et al.* 2016; Ruiz-Urigüen *et al.* 2022) environments. Besides the redox potential, Wackett (2021) reported that, in order for a microbe to degrade a PFC, it needs to transport the fluorinated compound into the cell, harbour a recently evolved enzyme to catalyse the C-F bond cleavage, detect the poisonous fluoride ion generated, and protect itself against the fluoride with a fluoride-proton antiporter. However, the disadvantage in C-F bond reduction is that, it can be

selected against an evolution on the basis that it provides no benefit to the microbial species but drain cellular energy (Wackett 2022). Despite the shortcomings of C-F bond reduction, selected bacteria which have been exposed to environments with fluoride concentrations exceeding 1 ppm have developed systems to protect themselves against the toxic fluoride ion. Last *et al.* (2018) reported that bacteria can resist the toxicity of environmental fluoride by expelling the fluoride ion from its cytoplasm by the aid of a proton-coupled fluoride ion antiporter, *E. casseliflavus* being the common antiporter. The microbe attributes necessary to biodegrade PFCs suggests that bacteria that are found near PFCs producing companies or in PFC contaminated environments can develop antiporters and survive the toxic fluoride ion. It is worth noting that, the available literature reporting on PFOA and PFOS degradation by novel microbial species, all reported bacteria were harvested from PFCs contaminated sites which explains why the reported bacteria can biodegrade PFOA and PFOS.

The degradation of PFOA and PFOS by novel bacteria, as reported in literature (Kwon *et al.* 2014; Yi *et al.* 2016; Huang and Jaffé 2019; Ruiz-Urigüen *et al.* 2022), can be attributed to certain enzymes cleaving the C-F bond through either oxidation by inserting oxygen atoms or reduction by adding extra electrons to the bond (Zhang *et al.* 2022). The dictation of fluoride ions during microbial degradation of PFCs indicates that microbes can break the C-F bond under control environments which can be either aerobic or anaerobic. Yu *et al.* (2019) reported that during microbial degradation of PFCs, the C-F bond cleave occurs at the sp^2 and sp^3 C-F bonds. However, Yu *et al.* (2019) reported that, despite the tertiary sp^3 C-F bond having the lowest bond dissociation energy for the model PFCs (i.e., perfluoro (4-methylpent-2-enoic acid) and 4,5,5,5-tetrafluoro-4-(trifluoromethyl)-2-pentenoic acid), the sp^2 C-F bond was more microbially active. The production of fluoride ions (Huang and Jaffé 2019) and intermediate products (Kwon *et al.* 2014; Yi *et al.* 2016; Ruiz-Urigüen *et al.* 2022) during the biodegradation of PFOA and PFOS is an indication that the C-F bond was cleaved despite having a bond dissociation energy of up to 130 kcal/mol (Zhang *et al.* 2022). There is no available literature reporting on the specific pathways for PFOA and PFOS biodegradation. It is worth noting that the extensively reported biodegradation of fluorotelomer alcohols and other PFCs apart from PFOA and PFOS is limited to the removal of non-fluorinated moieties rather than C-F bond cleavage.

3.4.3. Factors affecting PFOA and PFOS biodegradation

It is apparent that the microbial biodegradation of PFOA and PFOS can be affected by certain factors such as the type of microbial species, initial concentration of model PFCs and co-substrates. To-date, *Acidimicrobium* sp. strain A6, *Pseudomonas parafulva* strain YAB1, *Pseudomonas aeruginosa* strain HJ4 and *Pseudomonas plecoglossicida* 2.4-D are the only reported microbial species in literature that are capable of PFOA and PFOS biodegradation. This suggests that the type of microbial species plays a significant role in the biodegradation process of PFCs which are characterized as xenobiotic during

their bio-remediation process. Moreover, the available literature on the biodegradation of PFOS and PFOA have demonstrated that higher PFC concentrations ranging between 100 mg/L and 1000 mg/L can inhibit microbial growth rate depending on the microbe strain, thus compromising PFC degradation. Moreover, selected microbes use PFOA and PFOS as carbon sources and simultaneously perform bio-defluorination (Huang and Jaffé 2019; Zhang *et al.* 2022). The presence of co-substrates can enhance microbial growth rate due to microbial preference (Kwon *et al.* 2014; Huang and Jaffé 2019; Ruiz-Urigüen *et al.* 2022).

3.4.4. Other biological remediation processes of PFOA and PFOS

Previously conducted studies have reported on a number of effective remedial technologies of PFCs from aquatic environments such as photocatalysis and electrochemical oxidation (Schaefer *et al.* 2015; Schaefer *et al.* 2017; Liang *et al.* 2018; Hou *et al.* 2022), plasma technology (Stratton *et al.* 2017; Saleem *et al.* 2020), and adsorption by granular activated carbon (Li *et al.* 2019). However, the aforementioned treatment technologies are energy-intensive, consequently resulting in high operational costs (Huang *et al.* 2021). Hence, the following subsection focuses on PFOA and PFOS remediation by phytoremediation, characterised as an environmentally green and cost-effective process.

3.4.4.1. Phytoremediation of PFOA and PFOS

The removal of organic pollutants by plants is known as phytoremediation. The mechanism of the phytoremediation process consists of 1) phytofiltration which is basically the uptake of pollutants by the plant; 2) phytovolatilization which is the conversion of pollutants to volatile form, and 3) phytodegradation which involves the participation of root exudes and microbial population (Huang *et al.* 2021). Studies reported in literature (Gobelius, Lewis and Ahrens 2017; Colomer-Vidal *et al.* 2022) have demonstrated that plants can absorb PFCs, where long chain PFCs are likely to be accumulated in roots, and short chains are more likely to be accumulated in buds, fruits and crops (Li *et al.* 2019). Gobelius, Lewis and Ahrens (2017) investigated the uptake of PFCs by various plant species, and it was reported that high concentrations of short chain PFCs were detected in leaves with PFOA and PFOS being detected in roots. It is worth mentioning that Gobelius, Lewis and Ahrens (2017) did not report on PFOA and PFOS phytovolatilization and phytodegradation. The findings suggest that only phytofiltration was observed for PFOA and PFOS phytoremediation mechanisms.

Colomer-Vidal *et al.* (2022) investigated the sorption of PFCs in the water-sediment-plant system along the Dongzhulong and Xiaoqing rivers by floating and rooted plant species. The average PFC concentration in water was reported to be 84 000 ng/L and 2 300 ng/L in sediments with PFOA

accounting for up to 97% in both water and sediment. It was reported that PFOA demonstrated high sorption affinity with floating plant species absorbing a higher concentration of PFCs as compared to rooted plants. The high uptake capacity by floating plants is attributed to large proliferation rates. Higher PFOA concentrations were detected in the roots of plant species for both floating and rooted plant species, suggesting that phytofiltration took place. The PFCs distribution analysis within the model plant species for the work reported by Colomer-Vidal *et al.* (2022) demonstrated that short chain PFCs were concentrated more in the shoots than in the roots congruent to the work reported by Gobelius, Lewis and Ahrens (2017). Short chain PFCs uptake is attributed to the water potential gradient resulting from plant transpiration consequently promoting the upward uptake of PFCs through the xylem (Colomer-Vidal *et al.* 2022). On the other-hand, the accumulation of long chain PFCs in plant roots can be attributed to the proteinphilic-linked sorption. Previously done studies on phytoremediation of PFOA and PFOS suggest that long chain PFCs bound strongly to the roots surface due to positive correlation with protein content as opposed to short chain PFCs (Wen *et al.* 2016; Colomer-Vidal *et al.* 2022).

The phytoremediation of PFOA and PFOS is strongly dependent on plant species. Wen *et al.* (2016) investigated the role of protein and lipid in the accumulation of PFOA and PFOS by different plant species i.e., alfalfa, lettuce, maize, mung bean, radish, ryegrass, and soyabeans. It was reported that, the concentration of PFOA and PFOS in the roots of the aforementioned model plant species did not follow the same trend, with ryegrass, maize, and radish roots recording the lowest PFOA and PFOS concentrations. The observed behaviour was attributed to low protein content in roots of ryegrass, maize, and radish as reported by Wen *et al.* (2016). Moreover, it was reported that the binding of PFOS to roots was stronger than that of PFOA, therefore, the transfer potential of PFOA from roots to shoots is more favourable compared to PFOS (Wen *et al.* 2016). The observed behaviour could be attributed to the relatively large molecular structure and lipophilicity of PFOS when compared to PFOA.

Based on the available literature, it is evident that PFCs can be eradicated from the environment by phytoremediation. However, the detection of PFCs in plant leaves suggests that nonedible plant species should be considered for phytoremediation of PFCs to avoid human exposure to PFCs. Moreover, the reported literature on phytoremediation focuses on the translocation of PFCs in plant species. It worth noting that, at the time in which the current study was conducted, there was no available literature reporting on the degradation of PFCs in plant tissues. The uptake of PFOA and PFOS by plant species necessitate for an urgent need for their complete eradication from surface water.

3.5. Conclusions and Future Perspectives

The reviewed literature has demonstrated that PFCs, particularly PFOA and PFOS, are susceptible to degradation by certain microbial species. The metabolism mechanism of PFOA and PFOS follows a

peculiar path relative to the degradation of fluorotelomer alcohols and organohalogens. The available literature (Know *et al.* 2014; Yi *et al.* 2016; Huang and Jaffe 2019; Ruiz-Uriguen *et al.* 2022) suggests that certain microbial species (i.e., *Acidimicrobium* sp. strain A6, *Pseudomonas parafulva* strain YAB1, *Pseudomonas plecoglossicidia* 2.4-D, and *Pseudomonas aeruginosa* strain HJ4) which can develop antiporters to protect themselves from the toxic fluoride ions can biodegrade PFOA and PFOS. Despite the novel developments on PFOA and PFOS degradation by microbial species, further investigation needs to be done aimed at optimising PFOA and PFOS microbial degradation. Based on the reported literature, it is apparent that certain bacteria can use PFOA and PFOS as a carbon source, however, high concentrations of the aforementioned compounds can hinder microbial growth rate, thus compromising the treatment efficiency. Such observations warrant further investigation aimed at optimising microbial growth rate under high PFOA and PFOS concentration levels. Moreover, further investigation needs to be done on the co-substrate dose for different microbial species in enhancing microbial growth rate. The available literature suggests that there is lack of cellular benefits from PFC biodegradation, hence microbial species require a co-substrate to facilitate their growth for effective PFC removal.

Moreover, the current study has demonstrated that it is apparent that phytoremediation of PFOA and PFOS is one of the promising sustainable green technologies which can be utilized in eradicating PFCs in water bodies. Further investigation needs to be conducted on the biotransformation of PFOA and PFOS in plant tissues. Currently, there is very little information reported on the degradation of PFOA and PFOS in plant tissues. In conclusion, the reported PFOA and PFOS removal by microbial species and phytoremediation is associated with a high retention time which makes it difficult for PFOA and PFOS remediation in receiving water bodies. Genetically engineered microbes need to be considered in order to eradicate the occurrence of PFCs in water bodies. Moreover, there is a need to explore other technologies such as solid-liquid adsorption using environmental green adsorbents such as chitosan composites.

References

Abdullah Soheimi, S. S., Abdul Rahman, A., Abd Latip, N., Ibrahim, E. and Sheikh Abdul Kadir, S. H. 2021. Understanding the impact of perfluorinated compounds on cardiovascular diseases and their risk factors: a meta-analysis study. *International journal of environmental research and public health*, 18 (16): 8345.

U.S. Environmental Protection Agency. *Drinking Water Health Advisory for Perfluorooctanoic Acid (PFOA)*; Report 822-R-16-005; UEP Agency: Washington, DC, USA,2016.

Ahrens, L. 2011. Polyfluoroalkyl compounds in the aquatic environment: a review of their occurrence and fate. *Journal of Environmental Monitoring*, 13 (1): 20-31.

Andersson, E. M., Scott, K., Xu, Y., Li, Y., Olsson, D. S., Fletcher, T. and Jakobsson, K. 2019. High exposure to perfluorinated compounds in drinking water and thyroid disease. A cohort study from Ronneby, Sweden. *Environmental research*, 176: 108540.

Booi, X., Mudumbi, J., Ntwampe, S., Omodanisi, E., Daso, A., Sheldon, M. and Odisitse, S. Quantification of Perfluoroalkyl Compounds in Drinking Water Sources of the Western Cape, South Africa. In *Proceedings of the 17th Johannesburg International Conference on Science, Engineering, Technology and Waste Management (SETWM-19)* November 18 - 19, 2019 Johannesburg, South Africa.

Breaker, R. 2012. New insight on the response of bacteria to fluoride. *Caries research*, 46 (1): 78-81.

Buck, R. C., Franklin, J., Berger, U., Conder, J. M., Cousins, I. T., De Voogt, P., Jensen, A. A., Kannan, K., Mabury, S. A. and van Leeuwen, S. P. 2011. Perfluoroalkyl and polyfluoroalkyl substances in the environment: terminology, classification, and origins. *Integrated environmental assessment and management*, 7 (4): 513-541.

Cai, Y., Wang, Q., Zhou, B., Yuan, R., Wang, F., Chen, Z. and Chen, H. 2021. A review of responses of terrestrial organisms to perfluorinated compounds. *Science of the Total Environment*, 793: 148565.

Chetverikov, S. P., Sharipov, D. A., Korshunova, T. Y. and Loginov, O. 2017. Degradation of perfluorooctanyl sulfonate by strain Pseudomonas plecoglossicida 2.4-D. *Applied Biochemistry and Microbiology*, 53 (5): 533-538.

Colomer-Vidal, P., Jiang, L., Mei, W., Luo, C., Lacorte, S., Rigol, A. and Zhang, G. 2022. Plant uptake of perfluoroalkyl substances in freshwater environments (Dongzhulong and Xiaoqing Rivers, China). *Journal of Hazardous Materials*, 421: 126768.

Cordner, A., De La Rosa, V. Y., Schaider, L. A., Rudel, R. A., Richter, L. and Brown, P. 2019. Guideline levels for PFOA and PFOS in drinking water: the role of scientific uncertainty, risk assessment

decisions, and social factors. *Journal of exposure science & environmental epidemiology*, 29 (2): 157-171.

Crone, B. C., Speth, T. F., Wahman, D. G., Smith, S. J., Abulikemu, G., Kleiner, E. J. and Pressman, J. G. 2019. Occurrence of per-and polyfluoroalkyl substances (PFAS) in source water and their treatment in drinking water. *Critical reviews in environmental science and technology*, 49 (24): 2359-2396.

Ding, H., Peng, H., Yang, M. and Hu, J. 2012. Simultaneous determination of mono-and disubstituted polyfluoroalkyl phosphates in drinking water by liquid chromatography–electrospray tandem mass spectrometry. *Journal of Chromatography A*, 1227: 245-252.

Domingo, J. L. and Nadal, M. 2019. Human exposure to per-and polyfluoroalkyl substances (PFAS) through drinking water: A review of the recent scientific literature. *Environmental research*, 177: 108648.

U.S. Environmental Protection Agency. *Drinking Water Health Advisory for Perfluorooctane Sulfonate (PFOS)*; Office of Water (4304T), Health and Ecological Criteria Division EPA: Washington, DC, USA, 2016.

Eschauzier, C., Hoppe, M., Schlummer, M. and de Voogt, P. 2013. Presence and sources of anthropogenic perfluoroalkyl acids in high-consumption tap-water based beverages. *Chemosphere*, 90 (1): 36-41.

Eschauzier, C., Voogt, P. d., Brauch, H.-J. and Lange, F. T. 2012. Polyfluorinated chemicals in European surface waters, ground-and drinking waters. *Polyfluorinated chemicals and transformation products*: 73-102.

Essumang, D. K., Eshun, A., Hogarh, J. N., Bentum, J. K., Adjei, J. K., Negishi, J., Nakamichi, S., Habibullah-Al-Mamun, M. and Masunaga, S. 2017. Perfluoroalkyl acids (PFAAs) in the Pra and Kakum River basins and associated tap water in Ghana. *Science of the Total Environment*, 579: 729-735.

Gebbink, W. A., Van Asseldonk, L. and Van Leeuwen, S. P. 2017. Presence of emerging per-and polyfluoroalkyl substances (PFASs) in river and drinking water near a fluorochemical production plant in the Netherlands. *Environmental science & technology*, 51 (19): 11057-11065.

Gellrich, V., Brunn, H. and Stahl, T. 2013. Perfluoroalkyl and polyfluoroalkyl substances (PFASs) in mineral water and tap water. *Journal of Environmental Science and Health, Part A*, 48 (2): 129-135.

Gobelius, L., Lewis, J. and Ahrens, L. 2017. Plant uptake of per-and polyfluoroalkyl substances at a contaminated fire training facility to evaluate the phytoremediation potential of various plant species. *Environmental Science & Technology*, 51 (21): 12602-12610.

Hou, J., Li, G., Liu, M., Chen, L., Yao, Y., Fallgren, P. H. and Jin, S. 2022. Electrochemical destruction and mobilization of perfluorooctanoic acid (PFOA) and perfluorooctane sulfonate (PFOS) in saturated soil. *Chemosphere*, 287: 132205.

Houde, M., De Silva, A. O., Muir, D. C. and Letcher, R. J. 2011. Monitoring of perfluorinated compounds in aquatic biota: an updated review: PFCs in aquatic biota. *Environmental science & technology*, 45 (19): 7962-7973.

Huang, D., Xiao, R., Du, L., Zhang, G., Yin, L., Deng, R. and Wang, G. 2021. Phytoremediation of poly-and perfluoroalkyl substances: A review on aquatic plants, influencing factors, and phytotoxicity. *Journal of Hazardous Materials*, 418: 126314.

Huang, S. and Jaffé, P. R. 2019. Defluorination of perfluorooctanoic acid (PFOA) and perfluorooctane sulfonate (PFOS) by Acidimicrobium sp. strain A6. *Environmental science & technology*, 53 (19): 11410-11419.

Jian, J.-M., Guo, Y., Zeng, L., Liang-Ying, L., Lu, X., Wang, F. and Zeng, E. Y. 2017. Global distribution of perfluorochemicals (PFCs) in potential human exposure source–a review. *Environment international*, 108: 51-62.

Khumalo, S. M., Lasich, M., Bakare, B. F. and Rathilal, S. 2022. Sorption of perfluorinated and pharmaceutical compounds in plastics: a molecular simulation study. *Water*, 14 (12): 1951.

Kunacheva, C., Fujii, S., Tanaka, S., Seneviratne, S., Lien, N. P. H., Nozoe, M., Kimura, K., Shivakoti, B. R. and Harada, H. 2012. Worldwide surveys of perfluorooctane sulfonate (PFOS) and perfluorooctanoic acid (PFOA) in water environment in recent years. *Water Science and Technology*, 66 (12): 2764-2771.

Kwon, B. G., Lim, H.-J., Na, S.-H., Choi, B.-I., Shin, D.-S. and Chung, S.-Y. 2014. Biodegradation of perfluorooctanesulfonate (PFOS) as an emerging contaminant. *Chemosphere*, 109: 221-225.

Last, N. B., Stockbridge, R. B., Wilson, A. E., Shane, T., Kolmakova-Partensky, L., Koide, A., Koide, S. and Miller, C. 2018. A CLC-type F-/H+ antiporter in ion-swapped conformations. *Nature structural & molecular biology*, 25 (7): 601-606.

Lenka, S. P., Kah, M. and Padhye, L. P. 2021. A review of the occurrence, transformation, and removal of poly-and perfluoroalkyl substances (PFAS) in wastewater treatment plants. *Water research*, 199: 117187.

Li, P., Zhi, D., Zhang, X., Zhu, H., Li, Z., Peng, Y., He, Y., Luo, L., Rong, X. and Zhou, Y. 2019. Research progress on the removal of hazardous perfluorochemicals: A review. *Journal of environmental management*, 250: 109488.

Liang, S., Pierce Jr, R. D., Lin, H., Chiang, S. Y. and Huang, Q. J. 2018. Electrochemical oxidation of PFOA and PFOS in concentrated waste streams. *Remediation Journal*, 28 (2): 127-134.

McCarthy, C. J., Roark, S. A. and Middleton, E. T. 2021. Considerations for toxicity experiments and risk assessments with PFAS mixtures. *Integrated environmental assessment and management*, 17 (4): 697-704.

Meesters, R. J. and Schröder, H. F. 2004. Perfluorooctane sulfonate-a quite mobile anionic anthropogenic surfactant, ubiquitously found in the environment. *Water Science and Technology*, 50 (5): 235-242.

Parsons, J. R., Sáez, M., Dolfing, J. and Voogt, P. D. 2008. Biodegradation of perfluorinated compounds. *Reviews of Environmental Contamination and Toxicology Vol 196*: 53-71.

Peavy, H. S., Rowe, D. R. and Tchobanoglous, G. 1985. *Environmental engineering*. McGraw-Hill New York.

Rahman, M. F., Peldszus, S. and Anderson, W. B. 2014. Behaviour and fate of perfluoroalkyl and polyfluoroalkyl substances (PFASs) in drinking water treatment: A review. *Water research*, 50: 318-340.

Rodríguez-Gómez, R., Martín, J., Zafra-Gómez, A., Alonso, E., Vílchez, J. and Navalón, A. 2017. Biomonitoring of 21 endocrine disrupting chemicals in human hair samples using ultra-high performance liquid chromatography–tandem mass spectrometry. *Chemosphere*, 168: 676-684.

Ruiz-Urigüen, M., Shuai, W., Huang, S. and Jaffé, P. R. 2022. Biodegradation of PFOA in microbial electrolysis cells by Acidimicrobiaceae sp. strain A6. *Chemosphere*, 292: 133506.

Saleem, M., Biondo, O., Sretenović, G., Tomei, G., Magarotto, M., Pavarin, D., Marotta, E. and Paradisi, C. 2020. Comparative performance assessment of plasma reactors for the treatment of PFOA; reactor design, kinetics, mineralization and energy yield. *Chemical Engineering Journal*, 382: 123031.

Schaefer, C. E., Andaya, C., Burant, A., Condee, C. W., Urtiaga, A., Strathmann, T. J. and Higgins, C. P. 2017. Electrochemical treatment of perfluorooctanoic acid and perfluorooctane sulfonate: Insights into mechanisms and application to groundwater treatment. *Chemical Engineering Journal*, 317: 424-432.

Schaefer, C. E., Andaya, C., Urtiaga, A., McKenzie, E. R. and Higgins, C. P. 2015. Electrochemical treatment of perfluorooctanoic acid (PFOA) and perfluorooctane sulfonic acid (PFOS) in groundwater impacted by aqueous film forming foams (AFFFs). *Journal of Hazardous Materials*, 295: 170-175.

Schwanz, T. G., Llorca, M., Farré, M. and Barceló, D. 2016. Perfluoroalkyl substances assessment in drinking waters from Brazil, France and Spain. *Science of the total environment*, 539: 143-152.

Stratton, G. R., Dai, F., Bellona, C. L., Holsen, T. M., Dickenson, E. R. and Mededovic Thagard, S. 2017. Plasma-based water treatment: efficient transformation of perfluoroalkyl substances in prepared solutions and contaminated groundwater. *Environmental science & technology*, 51 (3): 1643-1648.

Sun, M., Zhou, H., Xu, B. and Bao, J. 2018a. Distribution of perfluorinated compounds in drinking water treatment plant and reductive degradation by UV/SO3 2− process. *Environmental Science and Pollution Research*, 25 (8): 7443-7453.

Sun, R., Wu, M., Tang, L., Li, J., Qian, Z., Han, T. and Xu, G. 2018b. Perfluorinated compounds in surface waters of Shanghai, China: source analysis and risk assessment. *Ecotoxicology and environmental safety*, 149: 88-95.

Tabe, S., Yang, P., Zhao, X., Hao, C., Seth, R., Schweitzer, L. and Jamal, T. 2010. Occurrence and removal of PPCPs and EDCs in the Detroit River watershed. *Water practice and technology*, 5 (1)

Tan, K.-Y., Lu, G.-H., Piao, H.-T., Chen, S., Jiao, X.-C., Gai, N., Yamazaki, E., Yamashita, N., Pan, J. and Yang, Y.-L. 2017. Current contamination status of perfluoroalkyl substances in tapwater from 17 cities in the Eastern China and their correlations with surface waters. *Bulletin of Environmental Contamination and Toxicology*, 99 (2): 224-231.

Thompson, J., Eaglesham, G. and Mueller, J. 2011. Concentrations of PFOS, PFOA and other perfluorinated alkyl acids in Australian drinking water. *Chemosphere*, 83 (10): 1320-1325.

Wackett, L. P. 2021. Why is the biodegradation of polyfluorinated compounds so rare? *Msphere*, 6 (5): e00721-00721.

Wackett, L. P. 2022. Nothing lasts forever: understanding microbial biodegradation of polyfluorinated compounds and perfluorinated alkyl substances. *Microbial biotechnology*, 15 (3): 773-792.

Wang, X., Chen, Z., Wang, Y. and Sun, W. 2021. A review on degradation of perfluorinated compounds based on ultraviolet advanced oxidation. *Environmental Pollution*, 291: 118014.

Wen, B., Wu, Y., Zhang, H., Liu, Y., Hu, X., Huang, H. and Zhang, S. 2016. The roles of protein and lipid in the accumulation and distribution of perfluorooctane sulfonate (PFOS) and perfluorooctanoate (PFOA) in plants grown in biosolids-amended soils. *Environmental Pollution*, 216: 682-688.

Xie, W., Zhong, W., Appenzeller, B. M., Zhang, J., Junaid, M. and Xu, N. 2021. Nexus between perfluoroalkyl compounds (PFCs) and human thyroid dysfunction: A systematic review evidenced from laboratory investigations and epidemiological studies. *Critical Reviews in Environmental Science and Technology*, 51 (21): 2485-2530.

Yi, L., Chai, L., Xie, Y., Peng, Q. and Peng, Q. 2016. Isolation, identification, and degradation performance of a PFOA-degrading strain. *Genet. Mol. Res*, 15 (2): 235-246.

Yu, Y., Zhang, K., Li, Z., Ren, C., Liu, J. and Men, Y. 2019. Microbial cleavage of C–F bonds in per- and polyfluoroalkyl substances via dehalorespiration. In: *ChemRxiv. Preprint*.

Zhang, X.-J., Lai, T.-B. and Kong, R. Y.-C. 2011. Biology of fluoro-organic compounds. *Fluorous chemistry*: 365-404.

Zhang, Z., Sarkar, D., Biswas, J. K. and Datta, R. 2022. Biodegradation of per-and polyfluoroalkyl substances (PFAS): A review. *Bioresource technology*, 344: 126223.

CHAPTER FOUR: ANTIBIOTICS ADSORPTION STUDIES

SINGLE AND MULTICOMPONENT ADSORPTION OF AMOXICILLIN, CIPROFLOXACIN, AND SULFAMETHOXAZOLE ON CHITOSAN-CARBON NANOTUBES HYDROGEL BEADS FROM AQUEOUS SOLUTIONS: KINETICS, ISOTHERMS, AND THERMODYNAMIC PARAMETERS

4.1. Abstract

The removal of antibiotics in water receiving bodies is an integral part in eradicating antimicrobial resistance which has become a major threat to public health. Solid-liquid adsorption has demonstrated to be an effective technique in the removal of antibiotics from aqueous environments. Herein, chitosan-carbon nanotube (chitosan-CNT) hydrogel beads were synthesised for the adsorption of amoxicillin (AMX), ciprofloxacin (CIP) and sulfamethoxazole (SMX) from aqueous solution. Adsorption kinetics, isotherms and thermodynamic parameters were systematically investigated at a solution pH of 7. Single adsorption kinetics findings suggest that experimental data for AMX, CIP and SMX was better fitted by the nonlinear pseudo-first order model with calculated maximum adsorption capacities of 23.1 $mg.g^{-1}$, 23.7 $mg.g^{-1}$ and 25.17 $mg.g^{-1}$, respectively. Moreover, findings from the Weber-Morris kinetic model suggest that multiple processes were limiting the overall adsorption rate of AMX, CIP and SMX on chitosan-CNT. Adsorption isotherm results indicated that single adsorption experimental data was better fitted by the nonlinear Freundlich isotherm model, while binary and ternary system experimental data were better fitted by the nonlinear competitive extended Sips adsorption isotherm models. Moreover, results for binary and ternary adsorption showed that multicomponent adsorption systems exhibited both antagonistic and synergistic adsorption of AMX, CIP and SMX. From the thermodynamic fundings, it was evident that the adsorption of AMX, CIP and SMX from solution is an endothermic process governed by both physical and chemical adsorption mechanisms. Based on the findings of the current study, it was concluded that chitosan-CNT has potential as a green technology for the removal of antibiotics from solution.

4.2. Introduction

Antibiotics have been successfully used to treat common infectious diseases making them crucial drugs for medical interventions particularly for human and agricultural use. As such, there has been a noticeable global increase of about 65% in the consumption of antibiotics (Manjunath, Baghel and Kumar 2020). Recently (Patel *et al.* 2020), meat producers in the United States of America have been identified as the largest users of antibiotics, far more intensely than do their counterparts in other

countries. Sadly, other countries like India and China have demonstrated an upward trend in the consumption of antibiotics (Van Boeckel *et al.* 2014). The same trend has been observed for developing countries like South Africa and Brazil (Gelband *et al.* 2015). Unfortunately for developing countries, the upward trend in antibiotic consumption is expected to increase until 2030 due to rapid population growth (Gelband *et al.* 2015). On the other hand, different classes of antibiotics have been detected in wastewater streams (Karthikraj *et al.* 2017; Mhuka, Dube and Nindi 2020), surface water (Madikizela, Tavengwa and Chimuka 2017; Mhuka, Dube and Nindi 2020), ground water (Zainab *et al.* 2020; Zeng *et al.* 2022) as well as in soil (Gothwal and Shashidhar 2015) at trace amounts ranging from ng/L to µg/L. The environmental occurrence of antibiotics is ascribed to their continuous release from different point sources such as households, hospitals, pharmaceuticals manufacturing and agricultural industries (Almomani *et al.* 2016). These environmental contaminants of emerging concerns are introduced into the environment via human secretion through urine and faeces, improper disposal of antibiotics, antibiotic metabolites, use of animal manure etc. The common practice of using animal organic excretion (i.e., faeces) as an option for manure (fertiliser) to enhance plant growth can cause veterinary antibiotics to end up in the environment particularly in surface and ground water systems through runoff and percolation (Yao *et al.* 2017). It is worth noting that antibiotics are pseudo-persistent in nature. As such, their presence in the aquatic environment triggers antimicrobial resistance against pathogens subsequently leading to ecotoxicity (Manjunath, Baghel and Kumar 2020; Patel *et al.* 2020). According to Patel *et al.* (2020), globally, about seven hundred thousand people each year die from infection with antibiotic-resistant organisms, with one-third being children under the age of five years. This number is projected to 10 million deaths per year globally by the year 2050 (Patel *et al.* 2020). Therefore, there is a need for antibiotic removal from aqueous environments on the basis that antibiotic resistance is being considered as one of the emerging health challenges.

Hitherto, a variety of biological and physicochemical treatment technologies have been used for the removal of antibiotics from aqueous environments ranging from biodegradation using novel bacteria strains (Bessa *et al.* 2017; Pan *et al.* 2017; Pan *et al.* 2018); advanced oxidation process (Anjali and Shanthakumar 2019; Cuerda-Correa, Alexandre-Franco and Fernández-González 2019); membrane technology (Yin *et al.* 2021; Nasrollahi, Vatanpour and Khataee 2022); chemical coagulation (Alexander, Hai and Al-Aboud 2012); and solid-liquid adsorption (Dutta and Mala 2020; Mangla, Sharma and Ikram 2022). However, most of these technologies are associated with some drawbacks such as being expensive (i.e., membrane technology), energy intensive (i.e., advanced oxidation and electro-coagulation), as well as slow processing or having high hydraulic retention time (biodegradation) (Karimi-Maleh *et al.* 2021). The increasing appetite in finding effective technologies for antibiotic removal can be ascribed to their detection in wastewater treatment plants (WWTPs) effluent streams (Madikizela, Tavengwa and Chimuka 2017; Mhuka, Dube and Nindi 2020), which is evident that conventional wastewater treatment techniques cannot completely eliminate antibiotics at

least in the context of South Africa. Amongst the emerging technologies, solid-liquid adsorption has been the preferred technology for antibiotic removal from aqueous environments owing to its advantages for being cost effective, easy to operate without any sludge or byproduct generation, its reusability and online operation (Karimi-Maleh *et al.* 2021). It is worth noting that there has been a paradigm shift in the use of non-renewable sources of adsorbents such as, polymers, bitumen, petroleum residues as well as activated carbon from coal on the basis that they render this process expensive. As such, this has compelled researchers within the scientific community to explore the use of low-cost adsorbents for the removal of emerging contaminants of environmental concern. A variety of low-cost adsorbents have been evaluated for the removal of antibiotics from aqueous environments such as sugarcane bagasse (Jais *et al.* 2021), walnut shell (Teixeira, Delerue-Matos and Santos 2019), coffee residue (Zhang *et al.* 2020), Siris seed pods (Ahmed and Theydan 2013), bamboo biochar (Wang *et al.* 2015), rice husk ash (Kaur, Singh and Rajor 2021), porous carbonaceous material (Ayati *et al.* 2023), etc.

Recently, the application of carbonaceous adsorbents in eradicating pharmaceutical compounds from aqueous solutions has been extensively investigated precisely for the uptake of ibuprofen (Ahmadpour *et al.* 2023; Ayati *et al.* 2023; Osman *et al.* 2023). The appetite in carbonaceous adsorbents is attributed to the existence of carbonaceous materials in various zero-, one-, two-, and three-dimensional structures such as fullerenes, activated carbon, biochar, graphene-based adsorbents, carbon nanotubes (CNTs) and clay which have demonstrated remarkable results for the uptake of pharmaceutical compounds from aqueous solutions (Ahmadpour *et al.* 2023; Ayati *et al.* 2023; Osman *et al.* 2023). Moreover, other emerging nanocomposite materials have been reported in literature such as polyvinyl-alcohol-zinc oxide-silver iodide-chlorophyll nanocomposites (Soltaninejad *et al.* 2021); geopolymer paste synthesised from agricultural waste materials (Maleki *et al.* 2020) and halloysite nanotubes (Hajizadeh *et al.* 2020) with the potential of being tested for pharmaceutical remediation from aqueous solutions. Despite the high removal efficiencies demonstrated by the aforementioned adsorbents in antibiotic removal, the quest for environmentally green and economically feasible adsorbents is still not yet over. As such, there has been a growing appetite for the application of chitosan-based composites for the removal of antibiotics from aqueous environments (Danalıoğlu *et al.* 2017; Rizzi *et al.* 2019; Ahamad *et al.* 2020; Zhao *et al.* 2020; Yaqubi *et al.* 2021) which is the primary focus of the present work.

Chitosan is characterised as an amino polysaccharide obtained from the deacetylation of chitin i.e., poly-*N*-acetyl-D-glucosamine which is by far the second most abundant biopolymer in nature after cellulose (Karimi-Maleh *et al.* 2021). Chitin is derived from crustaceans such as crabs, lobsters, shrimps, etc., as well as insects and fungi. Owing to its distinct properties of chitosan such as low processing cost, biodegradability, hydrophobicity, biocompatibility, and non-toxicity, it has cemented its application as a biosorbent in wastewater treatment processes (Danalıoğlu *et al.* 2017; Rizzi *et al.* 2019; Ahamad *et al.* 2020; Jais *et al.* 2021). The presence of highly active amino and hydroxyl

functional groups within the chitosan structure potentiate it to be an excellent biosorbent with chelating sites for targeted contaminants in aqueous environments. However, it is worth noting that the physicochemical properties of chitosan may differ by source as well as preparation methods thus affecting its functional groups (Karimi-Maleh *et al.* 2021). Despite the desirable features of chitosan, the use of pristine chitosan-based adsorbents is associated with drawbacks such as low stability, weak mechanical strength, low porosity, low surface area, hydrolystability in acid medium, and high crystallinity (Karimi-Maleh *et al.* 2021; Abd El-Monaem *et al.* 2022). The presence of amino and hydroxyl groups makes chitosan susceptible to modification through grafting, cross-linking, composites, and other chemical and physical techniques subsequently tackling the undesirable features. In the context of the present study, for an adsorbent to be considered economically feasible, the preparation and application of the material ought to require easy processing steps, consume minimal energy, have abundant sources from nature, and possess byproduct-free ability. As such, chitosan meets these criteria and it has been acknowledged as a low-cost feedstock to develop novel adsorbents as reported by Long *et al.* (2019).

Owing to the lack of studies focusing on the removal of different classes of antibiotics from multicomponent systems, this chapter focuses on the removal of three commonly detected classes of antibiotics i.e., amoxicillin (AMX), ciprofloxacin (CIP), and sulfamethoxazole (SMX) from aqueous solution using chitosan-carbon nanotube (chitosan-CNT) hydrogel beads. Available literature suggest that no studies have been conducted on multicomponent adsorption for the removal of AMX, CIP and SMX from solution using chitosan-CNT hydrogel beads. Due to the remarkable features of CNTs such as high tensile strength, large surface area, and low density, for the present study CNTs potentiate as ideal nanofillers in tackling the undesirable features of pristine chitosan composites in the context of water treatment. The scope of this chapter entails the study of adsorption kinetics by utilising nonlinear adsorption empirical models, the study of adsorption isotherms for single, binary and ternary adsorption systems to elucidate the synergistic and/or antagonistic effects of the sorption of one antibiotic in the presence of other antibiotics, and the evaluation of thermodynamic adsorption parameters.

4.3. Material and Methods

4.3.1. Materials

All chemicals used in the current study were of analytical grade and no further purification was done. Amoxicillin (≥95% anhydrous basis), ciprofloxacin (≥98% pure), sulfamethoxazole (HPLC grade), and multi-wall carbon nanotubes (>98% carbon basis) were supplied by Lasec laboratories, Durban, South Africa. Chitosan powder from shrimp shells with a degree of deacetylation of ≥75%, sodium hydroxide (NaOH) pellets (≥99.5% pure), methanol (CH_3OH) (≥99.9% pure), and sulfuric acid

(H_2SO_4) (98% pure) were supplied by Sigma-Aldrich, South Africa. Glacial acetic acid ($C_2H_4O_2$) (≥99.7% pure) was supplied by Shalom Laboratories, South Africa.

4.3.2. Adsorbent preparation

The chitosan-CNT hydrogel beads were synthesised by using acid modified multi-wall carbon nanotubes. The natural chemistry of pristine CNTs is that they bundle together and become inseparable is solution. On the other hand, the success of CNTs application in aqueous environments is strongly dependent on the capability of disbanding them into individual nanotubes, thus making them homogenous and stable suspensions (Sobczak-Kupiec *et al.* 2021). Hence for the current study, CNT modification was done by soaking a specific amount of CNTs in a solution of concentrated sulfuric acid (99%) and nitric acid (65%) at a volume ratio of 1:2, respectively for 24 hours. It is worth noting that the use of an acid containing oxygen molecules, result in the attachment of functional groups such as carboxylic and hydroxyl groups on the CNT surface which are essential for antibiotics removal from aqueous solution (Sobczak-Kupiec *et al.* 2021). Thereafter, the acid functionalised CNTs were rinsed with deionised water until a pH of 7 was achieved for the filtrate. The pH of the filtrate was measured using a HANNA HI 9828 pH meter. Furthermore, CNTs were functionalised to obtain a more hydrophilic surface as compared to pristine CNTs.

Thereafter, 100 g of chitosan was dissolved in 400 mL of 1 %v/v of glacial acetic acid solution. It is noted that chitosan has a low solubility in water but relatively high solubility in weak acidic aqueous environments. The chitosan-glacial acetic acid mixture was then vortexed using a magnetic stirrer at 200 rpm for 24 hours at room temperature to allow for complete dissolution of chitosan due to its low solubility. Thus, prolonged periods of agitation are necessary. During vortexing, the mixture of chitosan-glacial acetic acid was covered with aluminium foil to minimise any evaporation since glacial acetic acid is relatively volatile. Thereafter, 5 wt% (with respect to chitosan) of functionalised multiwall CNTs were added into the chitosan-glacial acetic acid mixture and vortexed at 200 rpm for 2 hours. This was done to obtain a homogeneous distribution of CNTs in the mixture. The viscous chitosan-CNT mixture was allowed to degas in a vacuum desiccator at room temperature until all air bubbles disappeared (i.e., disappearance of air pockets within the viscous mixture). Chitosan-CNTs microbead composite was synthesised by adding the viscous chitosan-CNT gel dropwise in a solution of 15 wt.% NaOH and 95%(v/v) methanol at a volume ratio of 4:1, respectively, using a 10 mL syringe which precipitated into chitosan-CNT beads. The chitosan-CNT beads were soaked in the NaOH-methanol solution for 24 hours, then rinsed with deionised water until a pH of 7 was obtained from the filtrate prior to being utilised for adsorption studies. The Fourier transform infrared spectrophotometry (FTIR, VERTEX 70) was used to analyse the presence of functional groups.

4.3.3. Batch studies

The adsorption profile of AMX, CIP and SMX on chitosan-CNT hydrogel beads was investigated by adopting the batch adsorption standard method as presented by Zhou *et al.* (2022). Experiments for adsorption kinetics were conducted using 50 mL clear bottles with screw caps, each having a sample size of 50 mL for a predetermined initial concentration of 40 mg/L of AMX, CIP and SMX at a fixed solution pH of 7. The solution pH was adjusted using 1.0 M NaOH and 1.0 M H_2SO_4. A predetermined quantity of 1.5 g/L of chitosan-CNT hydrogel beads was added into the respective AMX, CIP and SMX aqueous solutions and placed in a water bath shaker and agitated for 12 hours at a rate of 150 rpm at 293 K. At a set time interval, samples were drawn and filtered using a 0.45 μm syringe filter, thereafter, transferred into a 10 mL sample tube. The filtered samples were centrifuged at 5000 rpm for 10 minutes. Thereafter, a supernatant solution of the centrifuged sample was analysed for the residual of AMX, CIP and SMX concentration using a Uv-vis spectrophotometer (UV-1900i, Shimadzu, South Africa).

Adsorption isotherm studies were conducted at a temperature range of 283 K, 293 K and 303 K for an initial concentration range of 5 mg/L to 50 mg/L for AMX, CIP and SMX at a fixed solution pH of 7 for an interaction time of 24 hours. For both binary and ternary systems, an equal parts solution in terms of adsorbate initial concentration was prepared for each system i.e., AMX+CIP; AMX+SMX; CIP+SMX; and AMX+CIP+SMX. The adsorbent dose was maintained at 1.5 g/L of chitosan-CNT. The amount of antibiotics adsorbed by the chitosan-CNT adsorbent and adsorption efficiency were calculated using equations (4.1) and (4.2).

$$q_{e,i} = \frac{(C_o - C_e)}{m} \times V \tag{4.1}$$

$$Adsorption\ \% = \left[\frac{C_o - C_e}{C_o}\right] \times 100 \tag{4.2}$$

Where C_o is the initial adsorbate concentration measured in mol/L; C_e is the concentration of the adsorbate in solution after adsorption equilibrium; m is the mass of adsorbent on a dry basis; and V is the volume of the adsorbate solution with the initial concentration measured in L. It is worth noting that calculations for kinetics studies, the concentration of each antibiotic was presented in $mg.L^{-1}$ and adsorption capacity q_t was presented in $mg.g^{-1}$. The subsequent subsection presents the kinetics, isotherms, thermodynamic and statistical analysis empirical models used in this study.

4.3.4. Adsorption empirical models

4.3.4.1. Adsorption kinetics

Adsorption kinetics for the present study were studied for single adsorption systems by applying the pseudo-first order (PFO) (4.3) and pseudo-second order (PSO) (4.4) nonlinear empirical models.

$$q_t = q_{e_1}[1 - exp(-k_t t)] \tag{4.3}$$

$$q_t = \frac{q_{e_2}^2 k_2 t}{\left[k_2 q_{e_2} t + 1\right]} \tag{4.4}$$

where q_t is the adsorption capacity in mg.g^{-1} at time t; k_1 and q_{e_1} are the PFO rate constant in min^{-1} and adsorption capacity at equilibrium in mg.g^{-1}; k_2 and q_{e_2} are the PSO rate constant in g.mg^{-1}.min^{-1}, and the adsorption capacity at equilibrium in mg.g^{-1}, respectively. Kinetic model validation was conducted by employing the Bayesian Information Criterion (BIC) (4.5), residual sum of squares (RSS) (4.6), and coefficient of determination (R^2) (4.7).

$$BIC = nLn\left(\frac{RSS}{n}\right) + pLn(n) \tag{4.5}$$

$$RSS = \sum_{i=1}^{n}\left(q_{i_{exp}} - q_{i_{model}}\right)^2 \tag{4.6}$$

$$R^2 = \left(\frac{\sum_i^n \left(q_{i_{exp}} - \bar{q}_{i_{exp}}\right)^2 - \sum_i^n \left(q_{i_{exp}} - q_{i_{model}}\right)^2}{\sum_i^n \left(q_{i_{exp}} - \bar{q}_{i_{exp}}\right)^2}\right) \tag{4.7}$$

Where n is the number of experiments; $q_{i_{exp}}$ and $q_{i_{model}}$ are the experimental value and the theoretical value predicted by the model, respectively; $\bar{q}_{i_{exp}}$ is the average of all experimental values measured; and p is the number of parameters in the fitting model (Lima *et al.* 2021). The difference of the BIC value of PFO and BIC value of PSO (i.e., ΔBIC) was employed in evaluating the best model fit. According to Lima *et al.* (2021), values of $\Delta BIC \leq 2.0$ suggest an insignificant difference between the two models applied i.e., PFO and PSO kinetic models, a range of $2.0 < \Delta BIC < 6.0$ suggest that the model with lower BIC is most suitable; a BIC range of $6 < \Delta BIC < 10$ suggest that a model with lower BIC value best fit the adsorption data. Moreover, a $\Delta BIC \geq 10$ suggest that the model with a lower BIC value is better fitted.

4.3.4.2. Model Selection

The nonlinear kinetic models of the PFO (4.3) and PSO (4.4) were employed for the current study on the basis that it is not mathematically possible to compare the values of R^2 of the linearised PFO (4.8) and PSO (4.9) models due to the different values of the "Y" variable.

$$\ln\left(q_{e_1} - q_t\right) = \ln q_{e_1} - k_1 t \tag{4.8}$$

$$\frac{t}{q_t} = \frac{1}{k_2\left(q_{e_2}\right)^2} + \frac{1}{q_{e_2}} t \tag{4.9}$$

It is worth noting that the coefficient of determination of a standard linear equation (4.10) is given by equation (4.11).

$$Y = a + bX \tag{4.10}$$

$$R^2 = \left(\frac{\sum_i^n \left(Y_{i_{exp}} - \bar{Y}_{i_{exp}}\right)^2 - \sum_i^n \left(Y_{i_{exp}} - Y_{i_{model}}\right)^2}{\sum_i^n \left(Y_{i_{exp}} - \bar{Y}_{i_{exp}}\right)^2} \right) \tag{4.11}$$

Where $Y_{i_{exp}}$ is the experimentally measured Y variable; $\bar{Y}_{i_{exp}}$ is the average of all measured experimental values of Y; and $Y_{i_{model}}$ is the predicted Y value by the fitted model. It is apparent from equations (4.8) and (4.9) that the Y variables are not the same, hence it is mathematically incorrect to make a comparison of plots with different Y scales i.e., $\ln\left(q_{e_1} - q_t\right)$ (4.8) and t/q_t (4.9). However, the Y variable is given by q_t (mg.g^{-1}) for the nonlinearized PFO (4.3) and PSO (4.4) which makes it possible to compare the values of R^2.

4.3.4.3. Adsorption isotherms

Moreover, herein, two-parameter nonlinear adsorption isotherm equations (4.12) – (4.14) and three-parameter nonlinear adsorption isotherm equations (4.15) – (4.24) were applied in modelling single adsorption experimental data at equilibrium. The nonlinear adsorption isotherms were employed in order to eliminate the errors associated with linearised adsorption isotherm models as discussed by Mudhoo and Pittman Jr (2023) and Lima *et al.* (2021).

Equation (4.12) presents the Freundlich empirical model which describes the heterogeneous adsorption mechanism (Yeo *et al.* 2023):

$$q_{e,i} = K_{F,i} C_{e,i}^{n_{F,i}} \tag{4.12}$$

Where $K_{F,i}$ is the Freundlich constant for compound i measured in [(mol/kg)/(mol/L)^{nF}]; n_F is the dimensionless Freundlich's constant representing surface heterogeneity.

Langmuir model:

$$q_{e,i} = \frac{Q_{L,i} K_{L,i} C_{e,i}}{1 + K_{L,i} C_{e,i}} \tag{4.13}$$

Where $Q_{L,i}$ (mol/kg) and $K_{L,i}$ (L/mol) are the Langmuir maximum monolayer adsorption capacity and the Langmuir equilibrium constant for compound i, respectively.

Modified Langmuir model

$$q_{e,i} = \frac{Q_{ML,i} K_{ML,i} C_{e,i}}{(C_{s,i} - C_{e,i}) + K_{ML,i} C_{e,i}} \tag{4.14}$$

Where $Q_{ML,i}$ (mol/kg) and $K_{ML,i}$ are the modified Langmuir maximum adsorption capacity of the model adsorbent and the dimensionless modified Langmuir equilibrium constant for compound i, respectively, and $C_{s,i}$ (mol/L) is the saturation concentration of antibiotics in concentration.

Langmuir-Freundlich model:

$$q_{e,i} = \frac{Q_{LF} (K_{LF} C_e)^{n_{LF}}}{1 + (K_{LF} C_e)^{n_{LF}}} \tag{4.15}$$

Where $Q_{LF,i}$ (mol/kg), $K_{LF,i}$ (L/mol) and $n_{LF,i}$ are the Langmuir-Freundlich maximum adsorption capacity of adsorbent, equilibrium constant, and dimensionless exponent, respectively.

Modified Langmuir-Freundlich model:

$$q_{e,i} = \frac{Q_{MLF,i} \left(K_{MLF,i} C_{e,i}\right)^{n_{MLF,i}}}{\left(C_{s,i} - C_{e,i}\right)^{n_{MLF,i}} + \left(K_{MLF,i} C_{e,i}\right)^{n_{MLF,i}}} \tag{4.16}$$

Where $Q_{MLF,i}$ (mol/kg), $K_{MLF,i}$,and $n_{MLF,i}$ are the modified Langmuir-Freundlich adsorption capacity of the model adsorbent, dimensionless constant, and dimensionless exponent of the modified Langmuir-Freundlich model, respectively.

Sips model:

$$q_{e,i} = \frac{Q_{Sips,i} K_{Sips,i} C_e^{n_{Sips},i}}{1 + K_{Sips,i} C_{e,i}^{n_{Sips,i}}} \tag{4.17}$$

Where $Q_{Sips,i}$ (mol/kg) is the Sips adsorption capacity of the model adsorbent; $K_{Sips,i}$ is the Sips equilibrium constant measured in $(L/mol)^{n_{Sips}}$; and n_{Sips} is the dimensionless exponent of the Sips model.

Liu model:

$$q_{e,i} = \frac{Q_{Liu,i} C_{e,i}^{n_{Liu}}}{K_{Liu}^{n_{Liiu}} + C_{e,i}^{n_{Liu}}} \tag{4.18}$$

Where $Q_{Liu,i}$ (mol/kg) is the Liu adsorption capacity of adsorbent; K_{Liu} (mol/L) is the Liu constant; and n_{Liu} is the dimensionless exponent of the Liu model.

Khan model:

$$q_{e,i} = \frac{Q_{Khan} K_{Khan} C_{e,i}}{\left(1 + K_{Khan} C_{e,i}\right)^{n_{Khan}}} \tag{4.19}$$

Where Q_{Khan} (mol/kg) is the Khan maximum adsorption capacity of adsorbent; K_{Khan} (L/mol) and n_{Khan} are the Khan equilibrium constant and dimensionless exponent of the Khan model.

Hill model:

$$q_{e,i} = \frac{Q_{Hill} C_e^{n_{Hill}}}{K_{Hill} + C_e^{n_{Hill}}} \tag{4.20}$$

Where Q_{Hill} (mol/kg) is the Hill maximum adsorption capacity of adsorbent; K_{Hill} $(mol/L)^{n_{Hill}}$ and $1/K_{Hill}$ $[(L/mol)^{n_{Hill}}]$ are the Hill model constant, and the Hill equilibrium constant, respectively; and n_{Hill} is the dimensionless exponent if the Hill model.

Equation (4.21) represents the Toth model which is a modified Langmuir model that generally fits well on sub-monolayer adsorption system.

$$q_{e,i} = \frac{Q_{Toth} K_{Toth} C_e}{\sqrt[n_{Toth}]{1 + (K_{Toth} C_e)^{n_{Toth}}}} \tag{4.21}$$

Where Q_{Toth} (mol/kg), K_{Toth} (L/mol) and n_{Toth} are the maximum adsorption capacity, the Toth equilibrium constant, and the dimensionless exponent of the Toth model, respectively.

Redlich-Peterson model:

$$q_{e,i} = \frac{K_{RP} C_e}{1 + a_{RP} C_e^{n_{RP}}} \tag{4.22}$$

Where K_{RP} (L/kg), a_{RP} $(L/mol)^{n_{RP}}$ and n_{RP} are the Redlich-Peterson constant, Redlich-Peterson equilibrium constant, and the dimensionless exponent of the Redlich-Peterson model. According to Tran *et al.* (2021), the dimensionless exponent of the Redlich-Peterson model ranges from 0 to 1.

Koble-Corrigan Model:

$$q_{e,i} = \frac{A_{KC} C_e^{n_{KC}}}{1 + K_{KC} C_e^{n_{KC}}} \tag{4.23}$$

Where A_{KC} $[(L/mol)^{n_{KC}}(mol/kg)]$ and K_{KC} $(L/mol)^{n_{KC}}$ are the Koble-Corrigan constant and equilibrium constant, respectively; the Koble-Corrigan maximum adsorption capacity is given by $Q_{KC}(mol/kg) = A_{KC}/K_{KC}$; and n_{KC} is the dimensionless exponent od the Koble-Corrigan model.

Radke-Prausnitz model:

$$q_{e,i} = \frac{abC_e^{m,i}}{a + bC_e^{m-1}} \tag{4.24}$$

Multi-adsorption isotherms were studied by applying the Extended Langmuir (4.25) and Extended Sips (4.26).

$$q_{e,i} = \frac{Q_{ELi} K_{EL,i} C_{e,i}}{1 + \sum_{j=1}^{N} K_{EL,j}\, C_{e,j}} \tag{4.25}$$

$$q_{e,i} = \frac{Q_{ES,i} K_{ES,i} C_{e,i}^{\frac{1}{n_i}}}{1 + \sum_{j=1}^{N} K_{ES,j} C_{e,j}^{\frac{1}{n_j}}} \tag{4.26}$$

Where Q_{max} is the theoretical maximum biosorption capacity measured in mol.kg^{-1} , $K_{EL,i}$ (L.mol^{-1}) and $K_{EL,j}$ (L.mol^{-1}) are the competitive Extended-Langmuir constants of components i and j, respectively; $C_{e,j}$ (mol.L^{-1}) is the equilibrium concentration of component j; $q_{m,i}$ (mol.kg^{-1}) is the theoretical maximum binary adsorption capacity of component i; $K_{ES,i}$ (L.mol^{-1})$^{1/n}$ and $K_{ES,j}$ (L.mol^{-1})$^{1/n}$ are the Sips constants of components i and j, respectively; n_i and n_j are the Sips constants for components i and j, respectively obtained by fitting of experimental data for the binary adsorption system.

4.3.4.4. Thermodynamic models

The nature of the adsorption interaction between model contaminants and adsorbent was determined from the thermodynamic parameters i.e., standard Gibbs free energy change ($\Delta G°$), standard enthalpy

change ($\Delta H°$) as well as the standard entropy change ($\Delta S°$) as shown from equations (4.27) to (4.30) (Pauletto *et al.* 2021).

$$\Delta G° = -RT \ln(K_e^{\circ}) \tag{4.27}$$

$$\Delta G° = \Delta H° - T\Delta S° \tag{4.28}$$

$$lnK_e^{\circ} = \left(\frac{-\Delta H°}{R}\right)\frac{1}{T} + \frac{\Delta S°}{R} \tag{4.29}$$

$$K_e^{\circ} = \frac{K_{model} C°}{\gamma_{Adsorbate}} \tag{4.30}$$

Where R is the universal gas constant [8.3145 J/(mol.K)]; T is the absolute temperature (K); K_e° is the standard thermodynamic equilibrium constant; K_{model} is the equilibrium constant of the adsorption isotherm model measured in (L/mol); $C°$ is the standard state of solute equivalent to 1 mol/L; and $\gamma_{Adsorbate}$ is the activity coefficient of adsorbate in solution (Tran *et al.* 2023). Equation (4.29) is the linear form of the van't Hoff equation obtained by substituting equation (4.27) into equation (4.28). In the linear form of the van't Hoff equation, $\Delta H°$ and $\Delta S°$ are the slope and intercept of the plot of lnK_{eq}° as a function of 1/T, respectively.

4.4. Results and Discussion

4.4.1. Adsorbent surface characterisation

The functional groups of chitosan-CNT active sites involved in the adsorption of AMX, CIP and SMX were studied using the FTIR at a spectrum range of 650 cm^{-1} to 4000 cm^{-1}, as depicted in Figure 4.1. From the peaks, it is evident that the adsorbent surface contains functional groups which are essential for the adsorption of antibiotics. Chitosan stretching vibrations were detected such as C-N at 1379 cm^{-1}, C-O-C bending vibration at 1070 cm^{-1} as well as C=N stretching vibration at 1559 cm^{-1}. Similar functional groups on chitosan composites have been reported by Ngo *et al.* (2023).

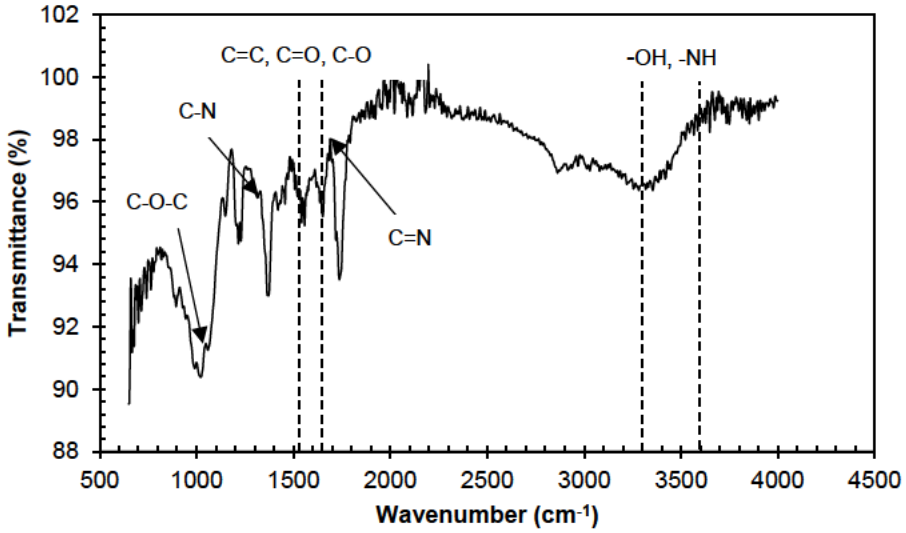

Figure 4.6: FTIR analysis of chitosan-CNT composite.

4.4.2. Effect of solution pH on the adsorption of AMX, CIP and SMX on chitosan-CNT

The solution pH plays a vital role in the protonation and/or deprotonation of the adsorbent surface charge as well as the speciation of the model contaminants. As such, for the current study, the one-factor-at-a-time approach was applied in ascertaining the effect of solution pH for the sorption of AMX, CIP and SMX (Figure 4.2) at a pH range of 2 – 11 at a fixed AMX, CIP and SMX initial concentration (40 mg/L) and adsorbent dose of 1.5 g/L. Highest removal efficiencies of 84% for CIP, 73 % for AMX, and 72 % for (SMX) were recorded for a solution pH of 6 for CIP and 7 for both AMX and SMX.

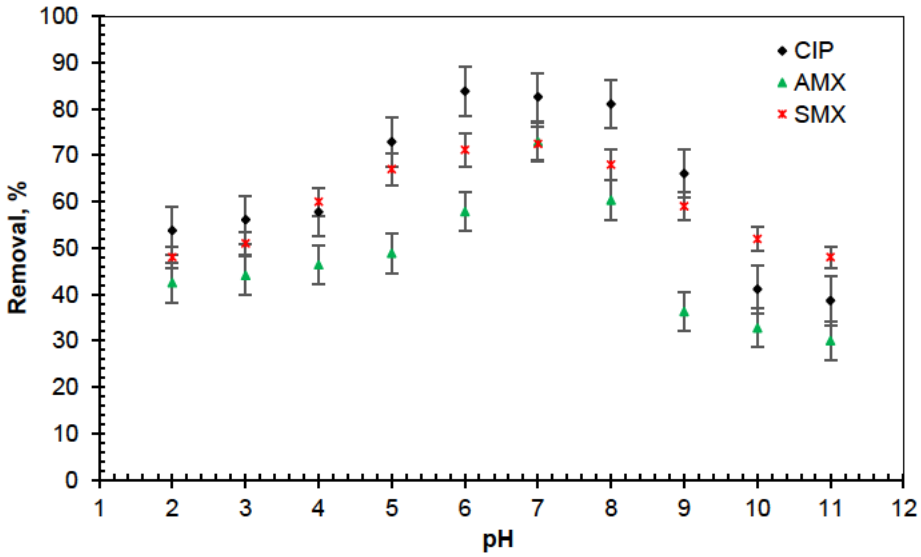

Figure 4.7: The effect of pH on the sorption of AMX, CIP and SMX from solution.

The observed behaviour on the removal of CIP with varying solution pH (Figure 4.2) can be ascribed to the mere fact that CIP is characterised with a carboxylic acid functional group (-COOH) and an amine functional group (-NH_2) on the piperazine moiety with corresponding pK_a values of 6.1 and 8.7, respectively (Wang *et al.* 2016). Therefore, the CIP pK_a values suggest that at solution pH greater than 6.1 and 8.7 the carboxylic and amine functional groups, respectively, within the chemical structure of CIP becomes deprotonated (i.e., negatively charged). It is worth noting that the point of zero charge (pH_{pzc}) for chitosan-CNT was found to be 8.5 suggesting that the surface of chitosan-CNT is positively charged at a solution pH less than the pH_{pzc}. When traversing the sorption of CIP from Figure 4.2, it is apparent that CIP removal was significant at a solution pH range of 6 and 8. These removal efficiencies can be ascribed to the deprotonation of CIP (i.e., at a solution pH range between 6 and 8), thus initiating the electrostatic interaction mechanism as the major adsorption mechanism as opposed to pore filling. The low removal efficiencies between a pH range of 2 – 5 can be ascribed to CIP being in an undissociated form (Manjunath, Baghel and Kumar 2020), suggesting that the adsorption of CIP was initiated by the pore filling mechanism. Moreover, at a solution pH of greater than the model adsorbent's pH_{pzc}, the surface of the adsorbent becomes deprotonated with a negative charge. As such, the π-electron interaction between the adsorbate and the adsorbent is destabilised due to charge repulsion thus compromising the adsorption efficacy of the targeted pollutant (Ngo *et al.* 2023).

It is worth noting that available literature (Ngo *et al.* 2023) suggest that the π- π bond is crucial in the sorption mechanism of SMX molecules from solution. This is ascribed to the benzene rings as well as amine groups within the chemical structure of antibiotics allowing them to accept π-electrons. From the FTIR results it is evident that the chitosan-CNT composite adsorbent contains functional groups which can give strong π-electrons such as C=C, C=O as well as C=N as suggested by Ngo *et al.* (2023). On the other hand, Liu, Nie and Yu (2021) reported that the ring π-electron interaction between SMX and double bonds on the adsorbent surface forms π-π electron coupling. For the current study, it is apparent that the highest SMX removal percentage was achieved at a solution pH range of 5 - 8. The observed trend can be ascribed to SMX having a pKa of 5.6 suggesting that at a solution pH greater than 5.6, it deprotonates, releasing an -OH functional group which interacts with the adsorbent functional groups. The release of the -OH functional groups promote the sorption of the model antibiotic by the electron interaction between the negatively charged antibiotic and the positively charged adsorbent (Fan *et al.* 2012). Moreover, the high removal efficiencies can be ascribed to π-electron interaction between the adsorbent and SMX. It is worth noting that from the thermodynamic results presented in Table 4.6 to Table 4.19 4.8 (*see subsection 4.4.6*), it is apparent that the sorption of SMX on chitosan-CNT can also be characterised by the physical adsorption mechanism as the high removal efficiencies at a solution pH of 5 can be ascribed to pore filling.

From Figure 4.2, it is apparent that the uptake of AMX by chitosan-CNT adsorbent was the least as compared to CIP and SMX. According to Verma and Subbiah (2019), at a solution pH of 7, about 60%

of amoxicillin exists as a zwitterionic form and 40 % exists as a cationic with a pKa value of 7.2. From Figure 4.2 the highest removal of AMX at a solution pH of 7 can be ascribed to electrostatic force interaction between the positively charged adsorbent with the negatively charged adsorbate. Moreover, at a solution pH of less than 9, a significant decline in the sorption of AMX on chitosan-CNT was observed which can be ascribed to the destabilised π-electron interaction due to charge repulsion between the negatively charged AMX and the adsorbent surface.

4.4.3. Effects of initial adsorbate concentration and adsorbent dosage on the sorption of AMX, CIP and SMX on chitosan-CNT adsorbent

For the present study, the effect of varying the adsorbate and adsorbent dose on the removal efficiency of AMX, CIP and SMX was conducted at an adsorbent dose range of 40 mg/L to 240 mg/L for each antibiotic and at an adsorbent dose range of 0.5 g/L to 3 g/L. The solution pH was maintained constant at 7 for a contact time of 24 hours. When traversing Figure 4.3a, it is apparent that the adsorption efficiency decreased to an asymptotic value with an increase in the initial adsorbate concentration for a fixed adsorbate dose of 1.5 g/L. According to Chandrasekaran *et al.* (2020), the observed trend can be ascribed to the limited number of adsorption sites on the adsorbate surface which eventually become saturated under higher adsorbate (i.e., AMX, CIP and SMX) concentration. On the other hand, the high removal efficiencies under low adsorbate concentrations can be ascribed to the availability of vacant adsorption sites thus adsorbing a higher composition of the adsorbate from solution. It is worth noting that the number of vacant sites acts as a driving force for the adsorption efficiency of the model adsorbent. It is evident that as the initial adsorbate concentration increases, the number of available adsorption sites decreases subsequently reducing the adsorption removal efficiency.

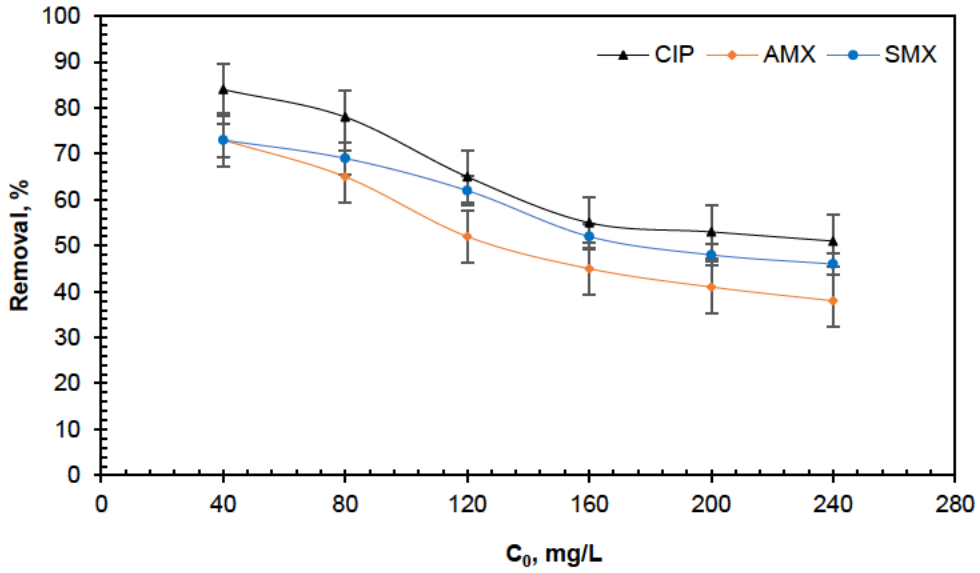

Figure 4.8a: The influence of varying adsorbate initial concentration on the adsorption efficiency of AMX, CIP and SMX on chitosan-CNTs.

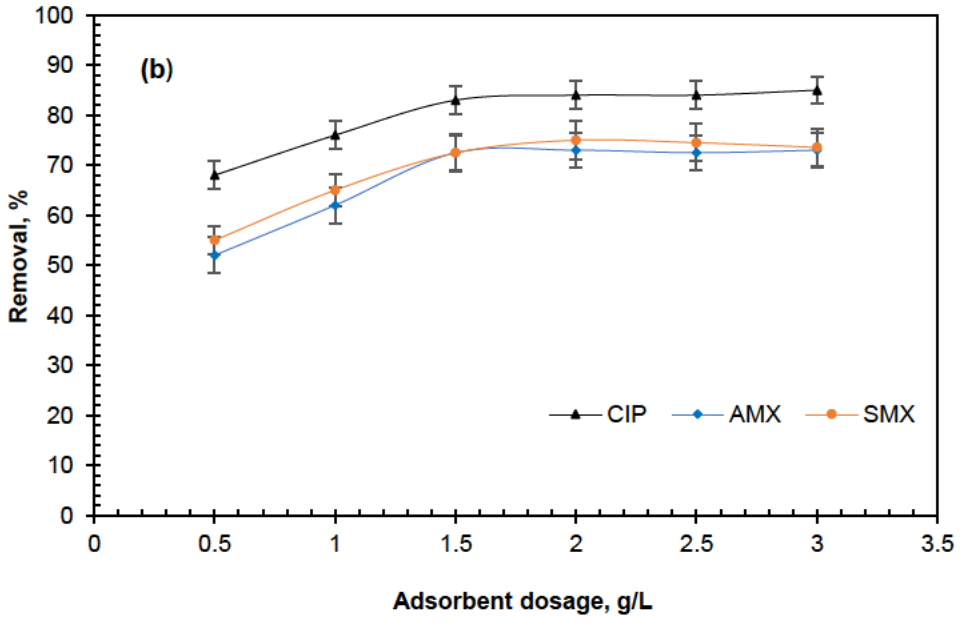

Figure 9.3b: Influence of varying adsorbent dosage on the adsorption efficiency of AMX, CIP and SMX on chitosan-CNTs.

On the other hand, the adsorption efficiency increased up to an asymptotic value with an increase in adsorbent dosage for a fixed adsorbate concentration of 40 mg/L. From Figure 4.3b, it can be observed that maximum removal efficiencies were achieved at an adsorbent dose of 1.5 g/L recording removal

efficiencies of above 70% for the model adsorbates. The observed trend on the adsorption efficiency can be ascribed to an increase in adsorption available sites with an increase in the adsorbent dose subsequently increasing the composition of the model antibiotics adsorbed. Chandrasekaran *et al.* (2020) reported that when the adsorbent dose increases at a fixed adsorbate concentration, the distribution of the adsorbate molecules in the adsorbent active sites will decrease. This will subsequently increase the rate of mass transfer resulting in higher loading of the model adsorbate in the adsorbent active sites. However, a further increase in the adsorbent dose will result in an increase in the availability of active sites subsequently resulting in a decrease in the rate of mass transfer to a point where mass transfer will cease, hence the adsorption efficiency will reach an asymptotic value as depicted in Figure 4.3b.

4.4.4. Single adsorption kinetics

The underlying sorbate-adsorbent interaction kinetics for the single adsorption system was studied using the nonlinear PFO, PSO as well as the Weber-Morris kinetic models. The adsorption kinetic parameters, coefficient of determination values as well as the difference of the BIC values for the competing PFO and PSO empirical models are presented in Table 4.1. The PFO rate constant (k_1) values suggest that the sorption rate for the model antibiotics was in the order of CIP (0.0039 min^{-1}) > AMX (0.0032 min^{-1}) > SMX (0.0024 min^{-1}). Moreover, it is worth noting that for the PFO kinetic model the difference between experimental and model predicted adsorption capacities at equilibrium was not significant, recording standard deviations in the order of ±1.37 $mg.g^{-1}$ for CIP < ±2.83 $mg.g^{-1}$ for AMX < ±4.32 $mg.g^{-1}$ for SMX. The low standard deviations and high R^2 values of greater than 0.98 for all model antibiotics suggest that experimental data was best fitted by the PFO kinetic model. On the other hand, for the PSO kinetic model, it is apparent from Table 4.1 that for the single adsorption system, there was a significant difference between the experimental and predicted adsorption capacities at equilibrium, with standard deviations in the order of ±7.39 $mg.g^{-1}$ (CIP) < ±10.15 $mg.g^{-1}$ (AMX) < ±14.18 $mg.g^{-1}$ (SMX). Despite the high R^2 values of greater than 0.97 recorded for the PSO kinetic model for all model antibiotics, the significant difference between experimental and predicted adsorption capacities at equilibrium, suggest that the PSO kinetic model failed to fit the single adsorption experimental data well.

Moreover, it is worth noting that the competing PFO and PSO kinetic models cannot simply be validated by the coefficient of determination alone. For the present study, the PFO and PSO kinetic models were validated by applying the difference of the BIC values of the PFO and BIC values of the PSO kinetic models. The guidelines outlined by Raftery (1995) and Lima *et al.* (2021) were used in assessing the PFO and PSO as discussed in the materials and methods section. Herein, ΔBIC values of 2.44 and 5.44

were obtained for the adsorption systems of CIP and SMX, respectively, suggesting that the PFO was the suitable empirical model in fitting experimental data for the single adsorption system.

Table 4.12: AMX, CIP and SMX adsorption kinetics parameters.

		Antibiotics		
Model	**Parameters**	**AMX**	**CIP**	**SMX**
PFO	$q_{e,exp}$ (mg.g^{-1})	19.1	21.8	19.05
	q_e (mg.g^{-1})	23.1	23.74	25.174
	k_1 (min^{-1})	0.003188	0.003851	0.00238
	R^2	0.9840	0.9991	0.9802
	BIC	-3.28	-26.52	0.75
PSO	$q_{e,exp}$ (mg.g^{-1})	19.1	21.8	19.05
	q_e (mg.g^{-1})	33.46	32.25	39.11
	k_2 (g.mg^{-1}.min^{-1})	7.16E-05	1.02E-04	4.1E-05
	R^2	0.9768	0.9932	0.9777
	BIC	5.57	-24.08	6.19
	ΔBIC	8.86	2.44	5.44

Moreover, the single adsorption system of AMX gave a ΔBIC value of 8.86 suggesting that the experimental data was better fitted by the PFO kinetic model. The supremacy of the PFO kinetic model in fitting the experimental data is cemented by the relatively high R^2 values demonstrated by the PFO model when compared to the PSO model. Figure S4.1 to Figure S4.3 (*see supplementary data*), clearly depicts that the experimental data was better fitted by the PFO kinetic model. From Figure S4.1 to S4.3 it is apparent that the adsorption of the model antibiotics on chitosan-CNT hydrogel beads was rapid during the initial stage (i.e., within 500 minutes) of the process subsequently slowed down over time as a consequence of decreasing active adsorption sites within the surface of the adsorbent. On the other hand, the fast adsorption rate within the first 500 minutes of the process can be partly ascribed to the presence of mesopores in the adsorbent which can be accessible to the adsorbates. Note that the aforementioned mechanism is not explicitly accounted for in the present work.

Herein, the findings of the current study on the adsorption kinetics studies were compared with studies reported in literature for the adsorption of AMX, CIP and SMX on chitosan-based composites (see Table 4.2).

Table 4.13: Literature studies on antibiotics adsorption on chitosan-based composites.

Antibiotic	**Adsorbent**	**Kinetic model**	**Reference**
Amoxicillin	Leached carbon black waste chitosan	Nonlinear-PFO	(Yaqubi *et al.* 2021)
	Chitosan-Fe/Ni nanocomposite	Linear-PFO	(Weng *et al.* 2013)
	Fe_3O_4-activated carbon-chitosan nanocomposite	Linear-PSO	(Danalıoğlu *et al.* 2017)
	Chitosan-CNT	Nonlinear-PFO	Present study
Ciprofloxacin	Magnetic imprinted chitosan polymer nanocomposites	Linear-PSO	(Rasoulzadeh *et al.* 2019)
	Chitosan-biochar hydrogel beads	Nonlinear-PSO	(Afzal *et al.* 2018)
	Ethylenediaminetetraacetic Acid-Functionalized β-Cyclodextrin-Chitosan	Linear-PSO	(Verma *et al.* 2021)
	Chitosan-CNT	Nonlinear-PFO	Present study
Sulfamethoxazole	Starch-chitosan-UiO-66-COOH	Linear-PSO	(Jia *et al.* 2021)
	Graphitic carbon nitride embedded chitosan-polyvinyl alcohol	Nonlinear-PSO	(Zhou *et al.* 2022)
	Chitosan-CNT	Nonlinear-PFO	Present study

For the work reported by Weng *et al.* (2013), it is noted that only the linearised PFO model was used to fit experimental data on the basis that it was assumed that the reduction of AMX by chitosan-Fe/Ni was a solid-liquid interphase reaction. As such, Weng *et al.* (2013) reported that such a reaction can be modelled in accordance with the linear PFO kinetic model. It is apparent that Wang and co-workers did not consider the PFO and PSO empirical kinetics model as competing models therefore no statistical analysis was used for the model selection. Similarly, Danalıoğlu *et al.* (2017) modelled experimental data for the sorption of AMX on Fe_3O_4-activated carbon-chitosan nanocomposite using a linear PSO kinetic model without any comparison with the PFO. It was reported that the linear PSO kinetic model best fitted the experimental with an R^2 value 0.9344. On the other hand, in the context of AMX sorption on chitosan-based composites Yaqubi *et al.* (2021) reported that the nonlinear-PFO empirical model best fitted the experimental data (R^2 >0.995) when compared with the PSO for the sorption of AMX on leached carbon black waste chitosan. The validity of the nonlinear-PFO model for the work reported by Yaqubi *et al.* (2021) was confirmed by the insignificant disparity between the experimental and

calculated values of the adsorption capacities at equilibrium. Therefore, the findings of the current study are congruent with the work reported by Yaqubi *et al.* (2021).

Rasoulzadeh *et al.* (2019) reported the supremacy of the linearised PSO kinetic model over the linearised PFO model on the sorption of CIP on magnetic imprinted chitosan polymer nanocomposites recording an R^2 value of 0.99. Model selection and validation was based on the R^2 values as well as comparison between experimental and calculated values of adsorption capacities at equilibrium. Similarly Verma *et al.* (2021) employed the nonlinear PSO and PFO kinetic models and concluded that experimental data for the sorption of CIP on ethylenediaminetetraacetic acid-functionalized β-cyclodextrin-chitosan was best fitted by the linearised PSO model recording an R^2 value of 0.999. Model validation was conducted by evaluating the chi square test, χ^2. However, it is noted that within the scientific community, the comparison of the linearised PFO and PSO is strongly discouraged (Tran *et al.* 2017; Mudhoo and Pittman Jr 2023) despite the approach being deeply-rooted in the practice and literature of adsorption science. The short comings of comparing the linearised PFO and PSO kinetic models are discussed in the materials and methods section. On the other hand, Afzal *et al.* (2018) reported that experimental data for the sorption of CIP on chitosan-biochar hydrogel beads was best fitted by the nonlinearized PSO empirical model. It is worth noting that, for the work reported by Afzal *et al.* (2018), the nonlinearized PFO model demonstrated a better fit in terms of R^2 values for an initial adsorbate concentration in the range of 5 $mg.g^{-1}$ to 30 $mg.g^{-1}$ when compared to the nonlinearized PSO model. However, for initial concentration of 50 $mg.g^{-1}$ and 80 $mg.g^{-1}$, the nonlinearized PSO model recorded higher R^2 values of 0.980 and 0.982, respectively. It should be noted that no other statistical tool was used for the model selection and validation apart from the coefficient of determination. As such, the findings of the present study are similar to the work reported by Afzal *et al.* (2018) for an initial adsorbate concentration range of 5 $mg.g^{-1}$ to 30 $mg.g^{-1}$. The difference in terms of selecting the nonlinear PSO model can be ascribed to the lack of model validation statistical tool apart from the coefficient of determination.

Zhou *et al.* (2022) and Jia *et al.* (2021) conducted studies on the sorption of SMX and sulfanilamide from aqueous solutions on graphitic carbon nitride embedded chitosan-polyvinyl alcohol and starch-chitosan-UiO-66-COOH composites, respectively. For the work reported by Zhou *et al.* (2022), the nonlinear PSO model was selected as the best model to fit the experimental solely on the basis of the recorded higher coefficients of determination when compared to the nonlinear PFO. On the other hand Jia *et al.* (2021) applied the linearised PFO and PSO model to study the kinetics of SMX sorption on the model antibiotics. It was concluded that the linearised PSO kinetic model with the higher coefficient of determination presented a preferable fit than that of a PFO. Moreover, the linearised PSO model was selected on the basis of the insignificant differences between simulated and experimental equilibrium adsorption capacities. However, for the present study, the nonlinearized PFO kinetic model gave a better fit of the experimental data. Model selection and validation was not limited to the coefficient of

determination, but a statistical tool was adopted in terms of ΔBIC in determining the most appropriate kinetic model since both the PFO and PSO models were treated as competing models. Based on the comparison studies presented in Table 4.2, it is evident that there is a need for rigorous statistical analysis as the basis of model selection and validation.

Furthermore, a typical adsorption process involves four stages i.e., adsorbate transport from bulk solution to adsorbent surface; diffusion through a boundary layer to the adsorbent surface; adsorption onto active adsorbing sites of surface; and intraparticle diffusion of adsorbate into the interior pores of the adsorbent. As such, the Weber-Morris (4.31) kinetic model was applied in ascertaining the rate control mechanism for the adsorption process of the model antibiotics on chitosan-CNT hydrogel beads as proposed by Weber Jr and Morris (1963).

$$q_t = k_i t^{0.5} + C \tag{4.31}$$

Where k_i (mg.g^{-1}.min$^{-1/2}$) is the intraparticle diffusion rate constant and C is a dimensionless constant which gives information related to the film thickness and relates to the adsorbate concentration on the adsorbent's surface. It is noted that a number of studies that are reported in literature (Zhou *et al.* 2022) have employed mg.g^{-1} as the units of C and it appears dubious to have mg.g^{-1} as the units of C if it is a boundary layer thickness. However, one has to acknowledge that, despite the mismatch in the units of the constant C with its physical meaning as a boundary layer thickness it does not result in a dimensional inconsistency if one agrees that the units of the boundary layer thickness can be mg.g^{-1} and not meters.

According to Sahoo and Prelot (2020) and Weber Jr and Morris (1963), in a typical solid-liquid adsorption process, intraparticle diffusion is involved during the adsorption process if the plot of q_t as a function of $t^{0.5}$ yields a straight line. It is noted that multilinear plots indicate that multiple processes are limiting the overall adsorption rate. Figure 4.4 presents single adsorption system experimental data for the adsorption of AMX, CIP and SMX on chitosan-CNT hydrogel beads fitted using the Weber-Morris kinetic model. From Figure 4.4, it is apparent that experimental data for the current study gave multilinear plots for all three model antibiotics i.e., AMX, CIP and SMX suggesting that multiple processes were limiting the overall adsorption rate of the antibiotics on chitosan-CNT hydrogel beads.

Traversing Figure 10.4 from left to right, the very first segment of the plot with the highest slope depicts a zone that is controlled by external mass transfer. In the external mass transfer zone (Figure 10.4), the constant C of the fitted model is approximately zero indicating insignificant effects of the boundary layer diffusion on the adsorption of AMX, CIP and SMX but the antibiotics were adsorbed on the surface of the model adsorbent i.e., chitosan-CNT hydrogel beads. The subsequent segment represents a zone controlled by intraparticle mass transfer, suggesting that the model antibiotics were gradually diffused into the model adsorbent, and the last segment which is almost plateau denotes an incipient of an equilibrium state indicating that the model antibiotics were adsorbed in the active sites of the model

adsorbent. As such, it is apparent that the last two zones were the rate-limiting steps for the adsorption process for the model antibiotics on the chitosan-CNT adsorbent. It is worth noting that the findings of the current study are congruent to the work reported by Zhou *et al.* (2022) for the adsorption of sulfamethoxazole on graphitic carbon nitride embedded chitosan-polyvinyl alcohol composite with light regeneration.

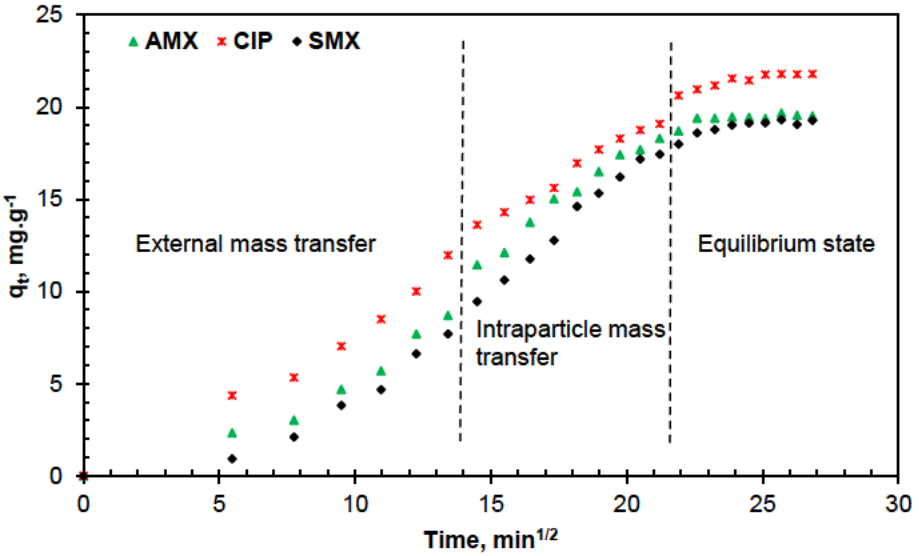

Figure 10.4: Weber-Morris kinetic model curves for AMX, CIP and SMX sorption on CCNT.

However, it is noted that the adsorption mechanism for any adsorption process cannot be explicitly explained by the PFO and PSO kinetic empirical models. As such, available literature (Lima *et al.* 2021; Tran *et al.* 2023) suggests that adsorption mechanisms are solely established using analytical techniques e.g., FTIR, scanning electron microscopy, X-Ray diffraction analysis etc., and having a clear chemical nature of the adsorbate and adsorbent, adsorbent's surface, and chemical or physical interactions between the adsorbent and adsorbate.

4.4.5. Equilibrium isotherms.

Most of studies reported in literature on solid-liquid adsorption are presented in units of mg.L^{-1} for concentrations and mg.g^{-1} for the sorption capacities. Similarly, most discharge regulations of pharmaceutical wastewater are presented on a mass basis. However, for dimensional consistency in modelling thermodynamic parameters, the isotherm units are presented on a mole basis as recommended by Tran *et al.* (2021). Recently done studies (Lima *et al.* 2021) have discussed new approaches on applying adsorption isotherms in calculating thermodynamic parameters for solid-liquid adsorption studies, requiring constants to be expressed in mole basis. Moreover, herein the nonlinear technique in modelling and evaluating the relevant adsorption isotherm parameters was applied on the

basis that the conversional linear approach has been associated with some error functions (i.e., over-linearisation) during modelling as discussed by Tran *et al.* (2017) and Lima *et al.* (2021).

4.4.5.1. Single adsorption isotherms

Table 4.3 presents the nonlinear fitting results for the selected two parameter and three parameter adsorption isotherm models. Model parameter values were optimised by performing sensitivity analyses i.e., (1) initialisation of the model parameters with the minimum possible value of the objective function through the evaluation of the sum of square error (SSE); (2) nonlinear regression analysis was performed to ascertain the optimal solution which minimised the objective function (SSE); (3) thereafter, the perturbation concept was applied, by modifying one parameter at a time while keeping other parameters constant. This approach was used to implicate a sensitivity analysis to each model parameter; (4) lastly, re-evaluation of the objective function (SSE) was done for each perturbation. It should be noted that the global minimum was obtained if the perturbation for all model parameters was zero. Higher values i.e., values greater than zero denotes poor nonlinear regression analysis of the values of the model parameters. A similar approach was reported by Al-Ghouti and Da'ana (2020) in their recent work where they discuss the guidelines for the use and interpretation of adsorption isotherm models.

Based on the chi square test values (χ^2) of less than 0.0 and high values of the coefficient of determination of greater than 0.9 it is apparent that the single adsorption studies experimental data was well fitted with almost all the models investigated, but not with the Sips (R^2 = 0.7771), Hill (R^2 = 0.7814), and Koble-Corrigan (R^2 = 0.773) for the AMX system. Despite the recommended low coefficients of determination values, the chi square test gave values of less than 0.01 for all systems studied.

Table 4.14: Isotherm constants for the removal of AMX, CIP and SMX using chitosan-CNT in single-component adsorption system.

			Antibiotic		
Model	**Model Parameters**	**Units**	**AMX**	**CIP**	**SMX**
Freundlich model	K_F	$(mol/kg)/(mol/L)^{nF}$	33.732	4.348	68.25
	n_F	--	0.615	0.395	0.6769
	R^2	--	0.9928	0.9529	0.9920
	χ^2		2.45E-07	0.00135	4.20E-07
Langmuir model	Q_L	mol/kg	0.07514	0.0791	0.09718
	K_L	L/mol	81 336	180 734	65 464
	R^2	--	0.9342	0.9559	0.8736
	χ^2		0.000118	0.00251	6.42E-04

Table 4.3: Continues

Modified Langmuir model	Q_{ML}	mol/kg	0.07215	0.0795	0.1762
	K_{ML}	--	1 773	3 673	19.11
	R^2	--	0.9206	0.968	0.9896
	χ^2		0.000165	4.11E-05	3.20E-05
Langmuir-Freundlich model	Q_{LF}	mol/kg	0.07026	0.0759	0.09145
	K_{LF}	L/mol	96 852	259 713	57 142
	n_{LF}	--	1.0339	1.103	1.8102
	R^2	--	0.9169	0.9610	0.9389
	χ^2		0.000155	3.150E-05	0.0001
Modified Langmuir-Freundlich model	Q_{MLF}	mol/kg	0.07165	0.0759	0.09145
	K_{MLF}	--	1 781	4 126	59.78
	n_{MLF}	--	1.0349	1.103	1.7054
	R^2	--	0.9247	0.9611	0.9442
	χ^2		0.000129	3.13E-05	7.17E-04
Sips model	Q_{Sips}	mol/kg	0.0727	0.0819	0.1006
	K_{Sips}	$(L/mol)^{nSips}$	1 403	12 329	2.4E07
	n_{Sips}	--	0.6245	0.7572	1.5751
	R^2	--	0.7771	0.9265	0.9593
	χ^2		0.000779	4.05E-04	7.99E-05
Liu model	Q_{Liu}	mol/kg	0.07083	0.0759	0.09521
	K_{Liu}	mol/L	1.15E-05	3.851E-06	1.93E-05
	n_{Liu}	--	1.2365	1.1034	1.6547
	R^2	--	0.9451	0.9610	0.9511
	χ^2		1.15E-06	3.14E-05	5.47E-04
Khan model	Q_{Khan}	mol/kg	0.06870	0.0792	0.0830
	K_{Khan}	L/mol	370629	122 201	39 570
	n_{Khan}	--	0.4020	0.8539	0.6201
	R^2	--	0.9373	0.9312	0.9908
	χ^2		0.00127	0.00133	1.77E-05
Hill model	Q_{Hill}	mol/kg	0.07272	0.0818	0.0939
	K_{Hill}	$(mol/L)^{nHill}$	6.58E-04	6.96E-05	1.08E-08
	n_{Hill}	--	0.6316	0.7698	1.679
	R^2	--	0.7814	0.9302	0.9455
	χ^2		0.00077	3.77E-04	4.52E-05
Toth model	Q_{Toth}	mol/kg	0.06066	0.0797	0.0927
	K_{Toth}	L/mol	36 417	965 689	25 271

Table 4.3: Continues

Toth model	n_{Toth}	--	546	0.6026	3.4209
	R^2	--	0.9040	0.8683	0.9755
	χ^2		0.00134	6.31E-04	1.25E-04
Redlich-Peterson model	K_{RP}	L/kg	2.19E09	8.75E08	2.85E09
	a_{RP}	$(L/mol)^{nRP}$	6.22E07	2.01E08	4.17E07
	n_{RP}	--	0.385	0.605	0.3229
	R^2	--	0.993	0.9529	0.992
	χ^2		1.03E-06	0.00134	4.35E-07
Koble-Corrigan model	A_{KC}	$(mol/kg)(L/mol)^{nKC}$	36.7781	729	218
	K_{KC}	$(L/mol)^{nKC}$	448	7 734	2003
	Q_{KC}	mol/kg	0.08195	0.0942	0.8045
	n_{KC}	--	0.5467	0.7533	0.6993
	R^2	--	0.7773	0.9747	0.8045
	χ^2		0.000826	1.06E-04	0.0011
Radke-Prausnitz model	a	L/kg	4.5E06	20 075	6 486
	b	$(mol/kg)/(mol/L)^m$	34.927	0.3795	19.55
	m	--	0.615	0.1530	0.5208
	R^2	--	0.9927	0.9629	0.9922
	χ^2		3.31E-07	0.00205	1.47E-06

When considering the R^2 and χ^2 values for the investigated two parameter adsorption isotherm models i.e., the Freundlich, Langmuir, and Modified-Langmuir models, the best fitting models for AMX were in the order of Freundlich model (R^2 = 0.9928; χ^2 = 2.45E-07) > Langmuir model (R^2 = 0.9342; χ^2 = 1.18E-04) > Modified-Langmuir model (R^2 = 0.9206; χ^2 = 1.65E-04); for CIP were in the order of Modified-Langmuir model (R^2 = 0.9680; χ^2 = 4.11E-05) > Langmuir model ≈ Freundlich model recording R^2 and χ^2 values of 0.9959, 0.9529, 0.00251, and 0.00135, respectively. For SMX Freundlich model (R^2 = 0.9920; χ^2 = 4.2E-07) > Modified-Langmuir model (R^2 = 0.9896; χ^2 = 3.20E-05) > Langmuir model (R^2 = 0.8736; χ^2 = 6.42E-04). From the single adsorption two parameter isotherm models it is apparent that both AMX and SMX experimental data were well fitted in the Freundlich model with CIP experimental data favouring the Modified-Langmuir model.

Based on the Freundlich model demonstrating supremacy in the sorption of AMX and SMX, the findings of the current study suggest the heterogeneity of the surface as well as the exponential distribution of the active sites for the model adsorbent. As such, the Freundlich adsorption isotherm model suggests that AMX and SMX were adsorbed by firstly occupying the stronger binding sites of the adsorbent; subsequently an exponential decline in the adsorption energy occurred upon completion of the adsorption process. Despite the relatively high values of R^2 (>0.9) and χ^2 values of less than 0.01

suggesting a good fit, the values of $1/n_F$ of greater than 1 (i.e., $1/n_F$ = 1.626 for AMX and $1/n_F$ = 1.477 for SMX) suggest a weak surface heterogeneity of the model adsorbent indicating the lack of adsorption intensity of AMX and SMX on chitosan-CNT adsorbent. According to Al-Ghouti and Da'ana (2020), the parameter $1/n_F$ is the intensity of the adsorption or surface heterogeneity indicating the energy relative distribution and the adsorbate sites' heterogeneity.

On the other hand, the adsorption isotherms result in Table 4.3, which suggests that CIP experimental data was well fitted by the Modified-Langmuir isotherm model. The model suggest that the thickness of the adsorbed layer is a single molecule i.e., monolayer adsorption, suggesting that the adsorption of CIP on chitosan-CNT adsorbent occurred at identical and equivalent definite localised sites. Therefore, without explicitly accounting for the sorption mechanism of CIP, the findings suggest that no steric hindrance manifested on adjacent sites, nor between the adsorbed molecules of CIP. According to Kundu and Gupta (2006) and Al-Ghouti and Da'ana (2020), the observed behaviour for the single adsorption of CIP on chitosan-CNT suggest that adsorbent sites had equal affinity towards the model antibiotic without any transmigration in the adsorbent surface plane. Within the framework of the Modified-Langmuir model, the separation factor (R_{ML}) for the CIP adsorption system was 0.9557 suggesting that the adsorption process of CIP on chitosan-CNT hydrogel beads was favoured. Al-Ghouti and Da'ana (2020) reported that the variation of the suitable area and porosity of an adsorbent can be correlated with the separation factor suggesting that higher adsorption capacities can be achieved from large surface area and pore volume. On the other hand, Weber and Chakravorti (1974) reported that, the nature of the adsorption process can be indicated by the separation factor to be either linear when R_{ML} = 1, irreversible when R_{ML} = 0, unfavourable when R_{ML} > 1, and/or favourable when R_{ML} ranges between 0 and 1. Based on the work reported by Weber and Chakravorti (1974), the obtained R_{ML} value of 0.9557 is evident that CIP sorption on the model adsorbent was favoured.

Furthermore, single adsorption experimental data was also fitted in three parameter adsorption isotherm models. AMX experimental data was well fitted in the order of Redlich-Peterson model (R^2 = 0.9930; χ^2 = 1.03E-06) ≈ Radke-Prausnitz model (R^2 = 0.9927; χ^2 = 3.31E-07) > Liu model (R^2 = 0.9451; χ^2 = 1.15E-06) > Khan model (R^2 = 0.9373; χ^2 = 1.27E-03) > modified Langmuir-Freundlich model (R^2 = 0.9247; χ^2 = 1.65E-04) ≈ Langmuir-Freundlich model (R^2 = 0.9930; χ^2 = 1.55E-04) > Toth model (R^2 = 0.9040; χ^2 = 0.00134) > Hill model (R^2 = 0.7814; χ^2 = 0.06066) > Koble-Corrigan model (R^2 = 0.7773; χ^2 = 8.26E-04) ≈ Sips model (R^2 = 0.7771; χ^2 = 7.79E-04). From the results presented in Table 4.3Table 4.14, it is apparent that that the Redlich-Peterson isotherm model best fitted the experimental data for the single sorption of AMX on the model adsorbent. It is worth noting that the Redlich-Peterson model is characterised as a hybrid model featuring the Freundlich and Langmuir isotherm models making it to have three parameters. The adsorption isotherm results in terms of the Redlich-Peterson model suggest that the sorption of AMX on the model adsorbent did not follow an ideal monolayer adsorption. This is ascribed to the mere fact that the favoured three parameter model

is a versatile isotherm model which can be applied to heterogeneous and homogeneous systems. It should be noted that for the two-parameter model, the AMX single sorption experimental data was well fitted in the Freundlich model, which is one of the isotherm models from which the Redlich-Peterson model was derived. Moreover, from the results presented in Table 4.3, SMX sorption experimental data was best fitted by the Redlich-Peterson isotherm model with an R^2 value of 0.9920 and χ^2 = 4.35E-07. Hence, the findings become instructive that the sorption of SMX on chitosan-CNT hydrogel beads from aqueous solutions was analogous to that of AMX.

CIP experimental data was fitted using the three parameter model and the model was well fitted in the order of Koble-Corrigan model (R^2 = 0.9747; χ^2 = 1.06E-04) > Redke-Prausnitz model (R^2 = 0.9629; χ^2 = 0.00205) > modified Langmuir-Freundlich model (R^2 = 0.9611; χ^2 = 3.13E-05) ≈ Langmuir-Freundlich model (R^2 = 0.9610; χ^2 = 3.15E-05) ≈ Liu model (R^2 = 0.9610; χ^2 = 3.14E-05) > Redlich-Peterson model (R^2 = 0.9526; χ^2 = 0.00134) > Khan model (R^2 = 0.9312; χ^2 = 0.00133) ≈ Hill model (R^2 = 0.9302; χ^2 = 0.0797). On the basis of the values of R^2 and χ^2, it is evident that the CIP single adsorption experimental data was best fitted in the Koble-Corrigan isotherm model which is a three-parameter model derived from the combination of the Freundlich and Langmuir isotherm models. The Koble-Corrigan isotherm gave a relatively high value of R^2 despite the low value of n_{KC} of 0.7533. According to Majd *et al.* (2022), the obtained n_{KC} value of less than a unit suggest that the Koble-Corrigan isotherm model was unable to specify the CIP experimental data due to a high concentration coefficient thus compelling the model to become a Freundlich isotherm at high concentration. This is evident from the relatively high R^2 value of 0.9529 obtained from the Freundlich isotherm model for the single sorption of CIP from aqueous solutions.

4.4.5.2. Binary and Ternary Adsorption Isotherms

The study of multicomponent sorption is crucial for optimal wastewater remediation on the basis that wastewater is associated with numerous organic and inorganic pollutants which may have a significant effect on the sorption of the targeted pollutant. Herein, the nonlinear extended Langmuir and extended Sips competitive adsorption isotherms were applied to elucidate the competitive adsorption of AMX, CIP, and SMX on chitosan-CNT hydrogel beads. Herein, the traditional models for mono-adsorption systems where modified in order to account for the adsorbates involved and interactions between them i.e., binary and ternary adsorption as recommended by Martín-Lara *et al.* (2016). Multicomponent competitive isotherms that are commonly used can be classified into two groups i.e., 1) competitive isotherms related only with parameters of single isotherms which are the competitive Langmuir model (extended Langmuir model), competitive Freundlich model (extended Freundlich model), competitive Sips model (extended Sips model) etc., and 2) competitive isotherms related with parameters of single isotherms and correction factors which are the competitive modified Langmuir model, competitive

modified Freundlich model, etc. (Martín-Lara *et al.* 2016). The extended Langmuir adsorption isotherm model is based on the traditional Langmuir isotherm, which assumes that the surface sites are uniform, and the monolayer adsorption prevails.

Table 4.4 presents adsorption isotherm parameters for both binary and ternary systems, on the other hand Figure 4.5 a to Figure 4.5f present the adsorption profile of AMX, CIP, and SMX on chitosan-CNT hydrogel beads. Based on the relatively high values of R^2 and χ^2 values of less than 0.01, the experimental data for both the binary and ternary system was best fitted by the competitive extended-Langmuir and extended-Sips isotherm models. It is worth noting that both isotherms demonstrated supremacy for different systems i.e., the extended-Sips isotherm model best fitted experimental data for the sorption of AMX in AMX+CIP; AMX in AMX+SMX; CIP in AMX+CIP and CIP in SMX+CIP. On the other hand, the extended-Langmuir isotherm model best fitted experimental data for the sorption of SMX in AMX+SMX and SMX in CIP+SMX. Furthermore, the ternary sorption of AMX in AMX+CIP+SMX was best fitted by the extended-Langmuir isotherm model (R^2 = 0.9847), while the ternary sorption of CIP in AMX+CIP+SMX and SMX in AMX+CIP+SMX was best fitted by the extended-Sips isotherm model recording R^2 values of 0.9942 and 0.8980, respectively.

The efficacy of the competitive extended-Langmuir and extended-Sips isotherm models was cemented by the insignificant difference between the experimental and calculated maximum adsorption capacities as depicted in Table 4.4. In a typical multiple adsorption system, the mixture of the model compounds can exhibit three possible behaviours i.e., antagonism, synergism, and non-interaction (Martín-Lara *et al.* 2016). These behaviours were measured by the ratio of the maximum adsorption capacity of one compound in the presence of another $Q_{m,i}$ to the maximum adsorption capacity of the same compound when it is present alone in solution $Q_{s,i}$. A ratio of less than 1 indicates that the adsorption process is suppressed by the presence of the other compound (i.e., antagonism); a ratio of more than 1 indicates that the adsorption process is promoted by the presence of the other compounds (synergism); and lastly a ratio of 1 indicates that there is no observable net interaction between the compounds in solution during their adsorption (Martín-Lara *et al.* 2016).

When studying Table 4.4, Figure 4.5a and Figure 4.5b, it is apparent that the binary sorption of AMX in AMX+CIP recorded a higher maximum adsorption capacity as compared to the single, binary (i.e., AMX in AMX+SMX), and ternary (i.e., AMX in AMX+CIP+SMX) adsorption systems. The $Q_{m,i}/Q_{s,i}$ ratio of 1.31 for the sorption of AMX in AMX+CIP suggest a synergistic effect of CIP on the sorption of AMX from solution i.e., the sorption of AMX was promoted by the presence of CIP. The observed behaviour can be ascribed to an increase in the adsorption capacity of AMX in the AMX +CIP system. On the other hand, from Figure 4.5b there was a slight decrease in the sorption of AMX from AMX+SMX with an increase in initial concentration when compared to the single sorption system. The $Q_{m,i}/Q_{s,i}$ of 0.930 suggest that SMX had an antagonistic (i.e., competitive) effect on the sorption of

AMX. Similarly, from Figure 4.5a to Figure 4.5f when comparing the results of the mono and/or single adsorption of the model antibiotics to the binary and ternary sorption system, there was a considerable decrease in the uptake of AMX, CIP and SMX but AMX in AMX+CIP, whereas a significant decline in AMX, CIP and SMX uptake by chitosan-CNT as a model adsorbent was observed for the ternary adsorption system recording $Q_{m,i}/Q_{s,i}$ values of 0.319, 0.169 and 0.132, respectively. Both the binary and ternary findings suggest that the presence of other antibiotics has an antagonistic effect on the uptake of the targeted antibiotic which can be ascribed to competition of antibiotics for the limited binding sites over the model adsorbent.

Table 15.4: Binary and ternary adsorption isotherm parameters

Model	Parameter	Binary Adsorption						Ternary Adsorption		
		AMX in AMX+CIP	**AMX in AMX+SMX**	**CIP in AMX+CIP**	**CIP in CIP+SMX**	**SMX in AMX+SMX**	**SMX in CIP+SMX**	**AMX in AMX+CIP+SMX**	**CIP in AMX+CIP+SMX**	**SMX in AMX+CIP+SMX**
	$Q_{max,exp}$ ($mol.kg^{-1}$)	0.0861	0.0610	0.0633	0.0666	0.0427	0.0454	0.02095	0.01308	0.01224
Extended Langmuir	Q_{max} ($mol.kg^{-1}$)	0.09298	0.0796	0.0668	0.0668	0.0698	0.05902	0.02945	0.01845	0.01754
	K_{EL}	102 367	89 172	91 986	77 828	19 795	31 926	23 872	28 495	17 00
	R^2	0.7848	0.9687	0.8975	0.8965	0.9873	0.9809	0.9847	0.9915	0.8798
	χ^2	4.31E-04	7.43E-04	4.90E-04	3.84E-04	1.32E-05	9.56E-06	7.63E-08	2.57E-06	1.55E-06
Extended Sips	Q_{max} ($mol.kg^{-1}$)	0.08759	0.07418	0.06705	0.06749	0.0432	0.04620	0.02129	0.01501	0.014
	K_{ES}	2.02E08	184 273	28 290	2.1E07	1.12E07	946 459	5.9E07	5.1E07	9.7E06
	n_{ES}	0.6002	0.9458	0.3645	0.6605	0.665	0.7928	0.5985	0.89	0.6297
	R^2	0.8323	0.9690	0.9673	0.9427	0.9438	0.9572	0.9654	0.9942	0.8980
	χ^2	1.11E-04	1.701E-05	7.62E-05	1.58E-05	5.32E-06	6.81E-05	2.02E-06	1.79E-06	9.79E-07
	$Q_{m,i}/Q_{s,i}$	1.31	0.930	0.818	0.861	0.461	0.491	0.319	0.169	0.132

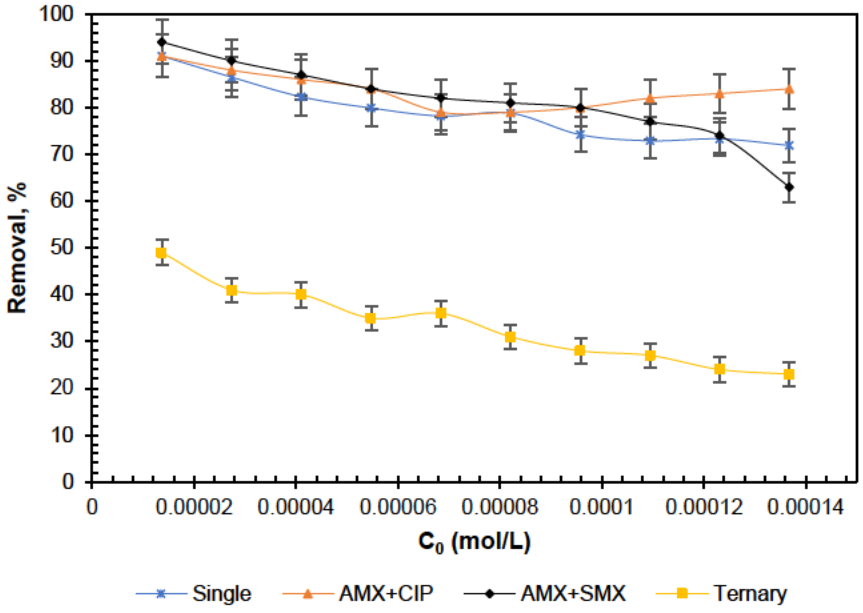

Figure 4.11a: Single, binary, and ternary percentage removal profile of AMX.

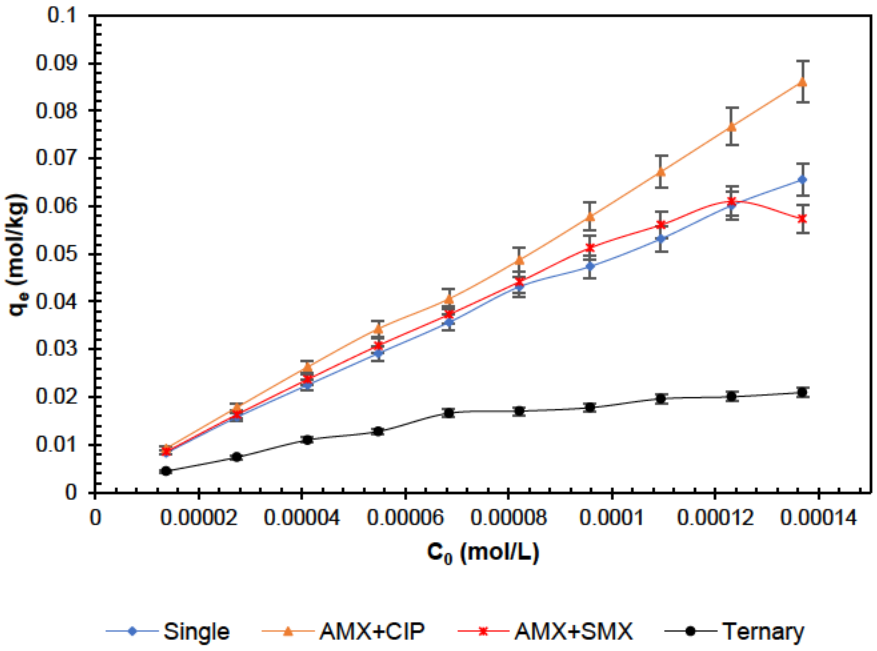

Figure 4.12b: Single, binary and ternary adsorption profile of AMX.

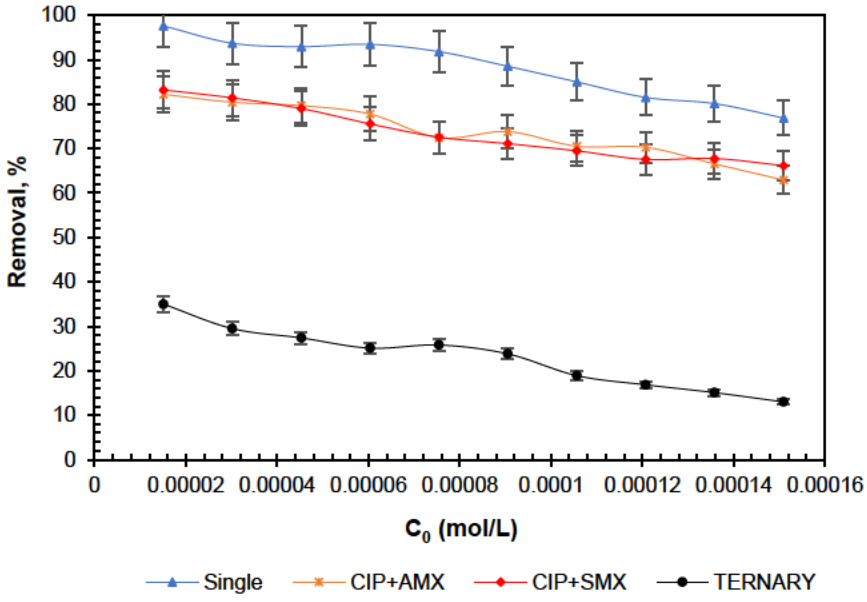

Figure 4.13c: Single, binary, and ternary percentage removal profile of CIP.

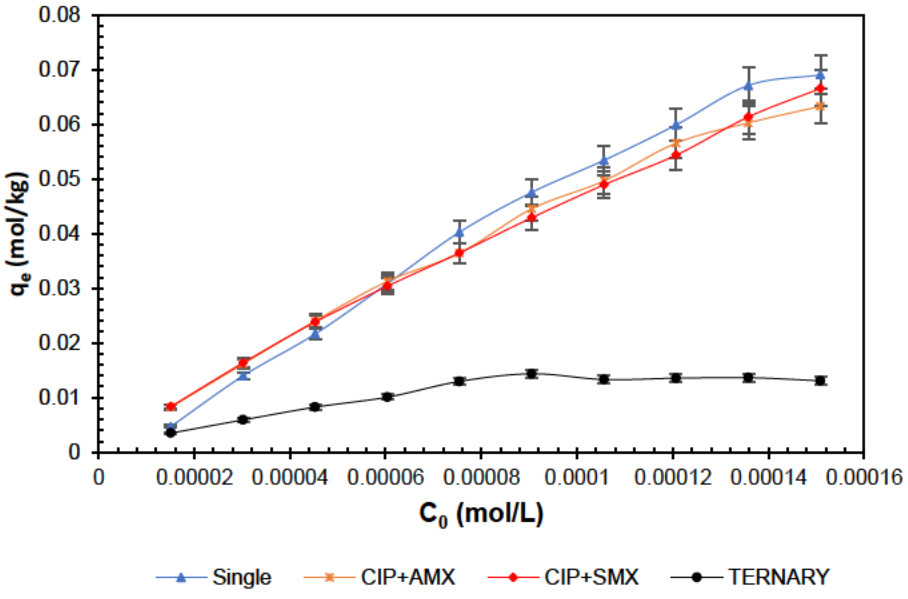

Figure 4.14d: Single, binary, and ternary adsorption profile of CIP.

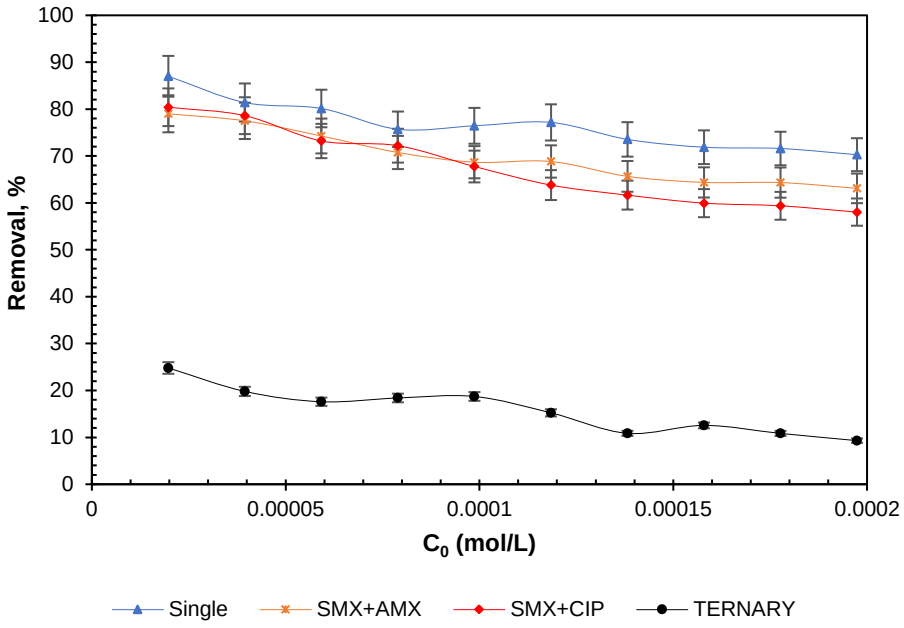

Figure 4.15e: Single, binary, and ternary percentage removal profile of SMX.

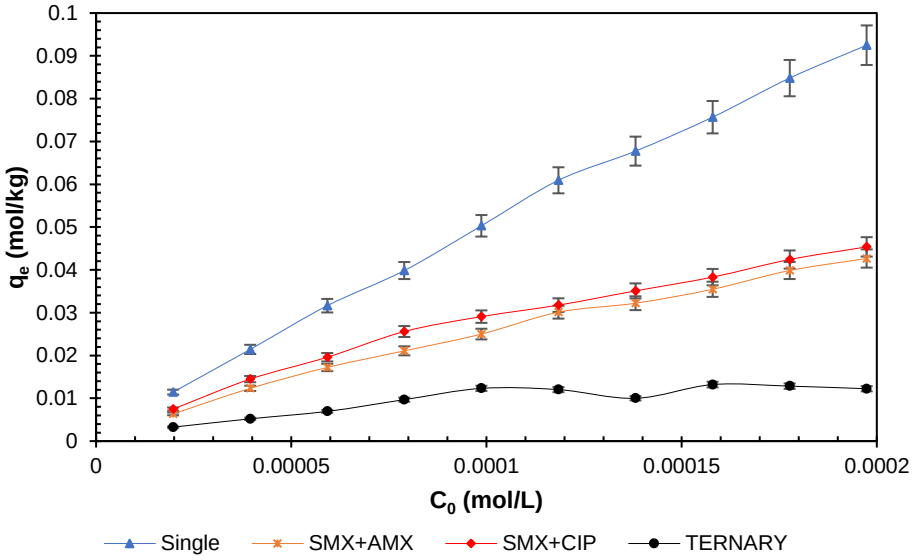

Figure 4.16f: Single, binary, and ternary adsorption profile of CIP

Similar findings have been reported by Manjunath, Baghel and Kumar (2020) on the sorption of sulfadiazine, metronidazole and tetracycline on potassium hydroxide activated Prosopis juliflora activated carbon (KPAC). It was reported that the observed decline in antibiotics uptake on KPAC in multicomponent adsorption systems can be ascribed to the mere fact that the finite number of adsorption sites present on the KPAC surface became saturated at higher antibiotic concentrations in a multicomponent system in

comparison with single adsorption systems. Hence, the findings of the current study are congruent to the work reported by Manjunath, Baghel and Kumar (2020).

Moreover, the percentage removal of AMX, CIP and SMX for the single, binary and ternary adsorption systems were statistically analysed using the single factor analysis of variance (ANOVA). In the single factor ANOVA test, one continuous dependent mean variable (adsorbate percentage removal) is compared with the mean of one categorical independent variable (initial concentration of adsorbate) with two hypotheses i.e., 1) null hypothesis: assumes that there is no statistically significant difference that exists between the means, and 2) alternative hypothesis: assumes that there is a statistical difference between the means. Herein, the investigated adsorption systems gave p-values of less than 0.05 (see Table 4.5) indicating that the mean differences between the compared variables were statistically significant. Therefore, the ANOVA results presented in Table 4.5 suggest that there was a significant variation in the percentage removal of the model antibiotics with a change in the adsorbate initial concentration. Moreover, the mean differences were further confirmed at 95% confidence level by the F-values of more than 1 for all adsorption systems. The relatively high F-values and sum of squares (SS) values statistically confirm that there was a significant uptake of AMX, CIP and SMX with varying adsorbate initial concentration. The low p-, F- and SS-values for ternary adsorption systems statistically confirm that there was a relatively low uptake of the model antibiotics in ternary adsorption systems when compared to single and binary adsorption systems due to the antagonistic effects caused by the co-existing antibiotics.

Table 4.16: ANOVA results for the percentage removal of AMX, CIP and SMX on chitosan-CNTs.

Compound	**System**	**SS**	**F-value**	**P-value**
AMX	AMX in Solution	31125.9	1572.202	5.59E-19
	AMX in AMX+CIP	34944.74	4544.836	4.3E-23
	AMX in AMX+SMX	32967.14	865.532	1.13E-16
	AMX in AMX+CIP+SMX	5577.78	160.28	2.12E-10
CIP	CIP in Solution	38849.79	1625.129	4.23E-19
	CIP in CIP+AMX	27124.61	1355.78	2.12E-18
	CIP in CIP+SMX	26920.22	1442.868	1.22E-18
	CIP in CIP+AMX+SMX	2655.414	109.7327	4.35E-09
SMX	SMX in Solution	29271.71	2182.818	3.05E-20
	SMX in SMX+AMX	24255.22	1515.349	7.89E-19
	SMX in SMX+CIP	22780.16	678.2488	9.68E-16
	SMX in SMX+AMX+CIP	1249.841	103.3647	6.92E-09

4.4.6. Adsorption thermodynamic studies

The thermodynamic equilibrium constant K_e° is the most imperative parameter in the evaluation of the thermodynamic parameters as discussed by Tran *et al.* (2021). As such, attention must be paid in selecting the relevant adsorption isotherm equilibrium constant as well as in the derivation of the thermodynamic equilibrium constant. Herein, eleven adsorption isotherm models were considered in the derivation of the thermodynamic equilibrium constant. The approach that was used in the derivation of K_e° values is congruent to the work reported by Tran *et al.* (2021), where K_e° was considered to be equal to K_{model} for all adsorption isotherm models in which the units of K_{model} are expressed in L/mol as presented in equation (30). However, it is worth noting that the equilibrium constants for the modified Langmuir and modified Langmuir-Freundlich adsorption isotherm models are dimensionless, as such they were considered tantamount to K_e° and appropriate to be applied directly in evaluating the thermodynamic parameters as reported in literature (Zuyi and Taiwei 2000; Zhou and Zhou 2014; Ghosal and Gupta 2017). Moreover, the equilibrium constants for the Sips, Liu, Hill, Redlich-Peterson, and Koble-Carrigan adsorption isotherm models were first converted from dimensional to dimensionless constants using equations S1-S5 prior to being used in the evaluation of the thermodynamic parameters.

4.4.6.1. Thermodynamic parameters

Herein, thermodynamic studies for the solid-liquid adsorption of AMX, CIP and SMX on chitosan-CNT hydrogel beads were conducted to study the adsorption mechanism of the model antibiotics on chitosan-CNT. Table 4.6 to Table 4.8 present the thermodynamic properties for the single adsorption of model antibiotics under different temperature conditions of 283 K, 293 K, and 303 K. The Gibb's free energy change parameter was used to determine the spontaneity of the adsorption process of AMX, CIP and SMX in chitosan-CNT. All three single adsorption systems gave negative results in terms of the Gibb's free energy change suggesting that the adsorption of AMX, CIP and SMX on chitosan-CNT is spontaneous. The negative Gibb's free energy change results is an indication of the feasibility and spontaneity of the adsorption of the model antibiotics on chitosan-CNT within a temperature range of 283 K to 303 K. Moreover, when studying Table 4.6 to Table 4.8, it is apparent that the Gibb's free energy change decreased with an increase in temperature for the adsorption of AMX, CIP and SMX on chitosan-CNT. The observed decrease in the Gibb's free energy change with temperature increase is an indication that the adsorption process of the model antibiotics is more favourable with an increase in temperature i.e., from 283 K to 303 K. This can be ascribed to the mere fact that the mobility of adsorbate molecules in solution increases noticeably with an increase in temperature thus resulting in an increase in the affinity of the model

antibiotics on chitosan-CNT hydrogel beads. However, it is worth noting that higher temperatures can compromise the adsorption process efficacy depending on the properties of the adsorbate and adsorbent as well as the adsorption process mechanism. Liu, Nie and Yu (2021) reported low adsorption efficacy of SMX on genipin crosslinked carboxyalkyl-chitosan combined with sulfonated graphene oxide at an operating temperature of 310 K and above. The poor adsorption efficiency was ascribed to the exothermic nature of the adsorption process thus compromising the adsorption affinity of the model adsorbent for the sulfonamide antibiotic at temperatures of 310 K and above. Furthermore, an increase in temperature results in an increase in the solubility of the adsorbate species resulting in stronger interaction forces between the adsorbate and the solvent than those between the adsorbate and adsorbent compelling the adsorbate to be more difficult to adsorb.

Table 4.17: Thermodynamic studies for the sorption of AMX on chitosan-CNT.

Model	**Temp. (K)**	**Model Parameters**			**Thermodynamic Parameters**		
		K_{Eq}°	R^2	χ^2	ΔG° (kJ/mol)	ΔH° (kJ/mol)	ΔS° (kJ/mol.K)
Langmuir model	283	47 424	0.7352	1.4E-03	-25.3		
	293	81 336	0.9342	1.2E-04	-27.5	53.2	0.277
	303	2.12E05	0.9588	7.0E-06	-30.9		
Modified Langmuir	283	948	0.7306	1.4E-04	-16.1		
	293	1 773	0.9206	1.7E-04	-18.2	52.3	0.242
	303	4 131	0.9588	6.9E-06	-21.0		
Langmuir-Freundlich	283	54 717	0.9298	2.4E-04	-25.7		
	293	96 852	0.9169	1.6E-04	-28.0	47.8	0.259
	303	209 563	0.9589	2.4E-06	-30.9		
Modified Langmuir Freundlich	283	1 064	0.9300	2.5E-04	-16.4		
	293	1 780	0.9247	1.3E-04	-18.2	47.8	0.226
	303	4 079	0.9586	2.52E-06	-20.9		
Sips	283	4.41E04	0.9663	7.9E-08	-25.2		
	293	1.09E05	0.7771	7.8E-04	-28.3	49.5	0.264
	303	1.76E05	0.9662	5.4E-05	-30.4		
Liu	283	4.83E04	0.9557	2.7E-07	-25.4		
	293	8.70E04	0.9451	1.2E-06	-27.7	50.2	0.267
	303	1.98E05	0.9598	2.7E-05	-30.7		
Khan	283	29 303	0.9461	4.7E-04	-24.2		
	293	37 629	0.9373	1.3E-03	-25.7	64.3	0.311
	303	180 867	0.9690	4.4E-05	-30.5		
Hill	283	5.55E04	0.8830	8.2E-04	-25.7		
	293	1.09E05	0.7814	7.7E-04	-28.3	46.8	0.256
	303	2.06E05	0.9593	6.0E-06	-30.8		
Toth	283	22 221	0.9687	1.4E-04	-23.6		
	293	36 417	0.9040	1.3E-03	-25.6	49.4	0.257
	303	89 389	0.8702	4.6E-04	-28.7		
Redlich-Peterson	283	1.47E24	0.8428	9.1E-04	-131		
	293	3.28E24	0.9927	1.0E-06	-138	-659	-1.84

Table 4.6: Continues

	303	1.09E16	0.9659	1.2E-05	-93.0		
Koble-Corrigan	283	1 610	0.9665	6.7E-05	-17.4		
	293	71 000	0.7773	8.3E-04	-27.2	133	0.537
	303	64 600	0.9765	1.2E-07	-27.9		

Herein, the enthalpy, ΔH° parameter was evaluated to determine the nature of the adsorption of AMX, CIP, and SMX on the model adsorbent which is chitosan-CNT hydrogel beads. The investigated isotherm models gave positive enthalpy values except for the Redlich-Peterson isotherm model.

Table 4.18: Thermodynamic studies for the sorption of CIP on chitosan-CNT.

Model	**Temp. (K)**	**Model Parameters**			**Thermodynamic Parameters**		
		K°_{Eq}	R^2	χ^2	ΔG° (kJ/mol)	ΔH° (kJ/mol)	ΔS° (kJ/mol.K)
Langmuir model	283	12 996	0.8889	2.2E-04	-22.3		
	293	1.80E05	0.9559	2.5E-03	-29.5	123.9	0.518
	303	411 805	0.9365	1.5E-05	-32.6		
Modified Langmuir	283	207	0.8889	2.2E-04	-12.5		
	293	3 673	0.9682	4.11E-05	-20.0	109.7	0.435
	303	4 360	0.9421	1.4E-05	-21.1		
Langmuir-Freundlich	283	66 219	0.9769	6.1E-06	-26.1		
	293	259 713	0.9610	3.15E-05	-30.4	61.5	0.311
	303	367 243	0.9417	2.1E-05	-32.3		
Modified Langmuir Freundlich	283	1 052	0.9769	6.1E-06	-16.4		
	293	4 125	0.9611	3.13E-05	-203	53.8	0.249
	303	4 692	0.9417	2.0E-05	-21.3		
Sips	283	65 900	0.9769	6.2E-06	-26.1		
	293	254 000	0.9265	4.05E-04	-30.3	61.5	0.311
	303	366 000	0.9417	2.1E-05	-32.3		
Liu	283	1.5E-05	0.9769	6.1E-06	-26.1		
	293	3.85E-06	0.9610	3.14E-05	-30.4	61.5	0.311
	303	2.7E-06	0.9415	4.0E-06	-32.3		
Khan	283	38 145	0.8818	1.8E-04	-24.8		
	293	122 201	0.9312	1.3E-03	-28.5	79.6	0.369
	303	355 221	0.9424	1.5E-05	-32.2		
Hill	283	74 100	0.8837	1.08E-03	-26.4	57.5	0.298
	293	252 000	0.9302	3.8E-04	-30.3		
	303	369 000	0.9417	2.2E-05	-32.3		
Toth	283	30 774	0.9267	2.3E-04	-24.3		
	293	965 689	0.8683	6.3E-04	-33.6	85.2	0.393
	303	319 260	0.9420	1.8E-05	-31.9		
Redlich-Peterson	283	3.7E09	0.8636	9.1E-05	-253		
	293	8.8E08	0.9529	1.3E-03	-82.9	-277	-8.99
	303	6.8E08	0.9159	2.1E-05	-77.2		

Table 4.7: Continues

Koble-Corrigan	283	2.7E12	0.9722	8.2E-05	-25.9		
	293	7 734	0.9747	1.07E-04	-29.0	47.1	0.259
	303	10 799	0.9403	4.0E-07	-31.1		

The positive enthalpy values suggest that the adsorption phenomenon of the model antibiotics on chitosan-CNTs is an endothermic process. The findings of the present study suggest that the model adsorbate species must displace more than one water molecule during their adsorption on chitosan-CNTs resulting in the endothermicity of the adsorption process. It is worth noting that the solid-liquid adsorption process is typically a combination of two processes which are the desorption of the solvent (in many cases water acts as a solvent) molecules previously adsorbed by the model adsorbent, and the adsorption of the adsorbate molecule. On the other hand, the negative enthalpy values recorded from the Redlich-Peterson isotherm model for all adsorbate species suggest that the adsorption phenomenon can be considered as an exothermic process.

Table 4.19: Thermodynamic studies for the sorption of SMX on chitosan-CNT.

Model	**Temp. (K)**	**Model Parameters**			**Thermodynamic Parameters**		
		K°_{Eq}	R^2	χ^2	ΔG° (kJ/mol)	ΔH° (kJ/mol)	ΔS° (kJ/mol.K)
Langmuir model	283	32 693	0.6589	1.1E-03	-24.4		
	293	65 464	0.8736	6.4E-04	-27.0	35.8	0.213
	303	88 794	0.8726	5.2E-05	-28.7		
Modified Langmuir	283	31.9	0.6911	1.1E-03	-8.81		
	293	19.1	0.9896	3.2E-05	-7.19	38.1	0.161
	303	95.2	0.8777	3.9E-05	-11.5		
Langmuir-Freundlich	283	26 367	0.9419	3.7E-06	-24.0		
	293	57 142	0.9389	1.0E-04	-26.7	37.7	0.219
	303	75 552	0.8991	6.5E-04	-28.3		
Modified Langmuir Freundlich	283	27.1	0.9490	4.3E-04	-7.76		
	293	59.8	0.9442	7.2E-04	-9.97	40.0	0.169
	303	82.9	0.9000	6.4E-04	-11.1		
Sips	283	23 200	0.9562	2.1E-04	-23.7		
	293	48 500	0.9593	8.0E-05	-26.3	43.2	0.237
	303	77 800	0.8975	2.3E-04	-28.4		
Liu	283	25 300	0.9492	4.3E-04	-23.9		
	293	51 800	0.9511	5.5E04	-26.4	40.6	0.227
	303	78 100	0.8978	2.2E-04	-28.4		
Khan	283	16 444	0.8950	6.2E-04	-22.8		
	293	39 570	0.9908	1.8E-05	-25.8	42.0	0.230
	303	53 202	0.9309	3.3E-04	-27.4		
Hill	283	26 100	0.8703	3.9E-04	-23.9		
	293	55 400	0.9455	4.5E-05	-26.6	37.3	0.217
	303	74 000	0.8837	1.0E-03	-28.2		

Table 4.8: Continues

Toth	283	12 307	0.9443	3.2E-05	-22.2		
	293	25 271	0.9755	1.3E-04	-24.7	45.2	0.238
	303	43 649	0.9095	2.9E-04	-26.9		
Redlich-Peterson	283	2.24E37	0.9443	1.1E-04	-202		
	293	1.91E29	0.9920	4.4E-07	-164	-1103	-3.190
	303	8.59E23`	0.9497	4.1E-05	-138		
Koble-Corrigan	283	16 900	0.6702	3.1E-06	-22.9		
	293	52 700	0.8045	1.1E-03	-26.5	57.2	0.284
	303	83 600	0.8053	1.9E-03	-28.6		

In the context of adsorption studies, in an exothermic process, the amount of energy absorbed during bond breaking is less than the energy released during the formation of bonds between the adsorbate and adsorbent, thus releasing extra energy in a form of heat. Moreover, according to Saha and Chowdhury (2011), the magnitude of the enthalpy may give some insight on the type of sorption if one considers the heat evolved during physical adsorption to be the same order of magnitude as the heat of condensation typically ranging from 2.1 kJ/mol to 20.9 kJ/mol, while the heat of chemisorption falls in the range of 80 kJ/mol to 200 kJ/mol. Therefore, based on the enthalpy findings presented in Table 4.6 to Table 4.8, the sorption of AMX, CIP and SMX on chitosan-CNT adsorbent cannot be explicitly classified as chemical or a physical process, however, the sorption of the model antibiotics can be attributed to a physico-chemical adsorption process.

For the present study, the entropy parameter was evaluated to determine the affinity of chitosan-CNT hydrogel beads towards the AMX, CIP and SMX. According to Saha and Chowdhury (2011), positive entropy values suggest an increase in randomness at the solid-liquid interface with some structural changes in the adsorbate and the adsorbent. Therefore, the positive entropy values obtained from all investigated adsorption isotherms, but the Redlich-Peterson adsorption isotherm suggest high affinity of the chitosan-CNT adsorbent towards the model antibiotics. The positive entropy values for the single adsorption studies suggest that water molecules as the adsorbed solvent were displaced by the antibiotics molecules, allowing the water molecules to gain more translational entropy than is lost by the antibiotic molecules allowing for the prevalence of randomness within the system. On the other hand, the negative entropy values recorded from the Redlich-Peterson isotherm model suggest that the adsorption process of AMX, CIP, and SMX is enthalpy driven. Saha and Chowdhury (2011) reported that a negative value of the entropy change is an indication of a decreased disorder at the solid-liquid interface during the adsorption process resulting in the adsorbate molecules escaping from the solid phase to the liquid phase, thus compromising the amount of adsorbate that can be adsorbed.

4.4.6.2. Activation Parameters

Herein, the thermodynamic activation parameters such as activation of enthalpy ΔH*, free energy of activation ΔG*, and activation entropy ΔS* were evaluated aimed at getting more insight on the adsorption mechanism of AMX, CIP and SMX on chitosan-CNT hydrogel beads. The Eyring equation (S6) and (S7) were employed in calculating the thermodynamic activation parameters, and results are presented in Table 4.9.

Table 4.20: Thermodynamic activation parameters.

			Activation Parameters			
Antibiotic	**T (K)**	K°_{Eq}	**ΔG***	**ΔH***	**ΔS***	**R^2**
AMX	283	47 424	-88.3			
	293	81 336	-94.4	85.8	0.615	0.8956
	303	212 000	-100.6			
CIP	283	12 996	-81.0			
	293	180 000	-95.5	330	1.45	0.8722
	303	411 805	-100.1			
SMX	283	32 693	-86.9			
	293	65 464	-91.1	31.7	0.419	0.9599
	303	88 800	-95.3			

The free energy of activation for all three systems gave negative results suggesting that the adsorption of AMX, CIP and SMX on the model adsorbent does not require energy from an external source in order to initiate the adsorption process. On the other hand, all three systems have positive activation of enthalpy values suggesting that the adsorption process of the model antibiotics is an endothermic process. The conclusion drawn from the activation enthalpy values is congruent to the conclusion drawn from the enthalpy results presented in Table 4.6 to Table 4.8, thus cementing the fact that the sorption process of AMX, CIP and SMX on chitosan-CNT hydrogel beads is an endothermic process. Moreover, the positive values of the activation entropy implies that the adsorption process of the model antibiotics on the model adsorbent involves a dissociative mechanism (Saha and Chowdhury 2011). It is worth noting that adsorption systems that are characterised with a dissociative mechanism are not favoured under high temperatures as demonstrated in literature by Liu, Nie and Yu (2021).

4.3. Future Perspectives

Based on the findings presented in the current study, it is evident that chitosan-CNT composites have demonstrated high removal efficiencies for antibiotics removal from aqueous solution. However, more work still needs to be done in investigating the effect of competing ions and/or inorganic pollutants on adsorbent efficiency in the removal of antibiotics. Moreover, the focus on the assessment of resurfacing

adsorbents on antibiotics removal has been on synthetic wastewater and on pilot scale studies. As such there is a need for studies in multicomponent adsorption studies using urban wastewater and on techno-economics assessment to report on the cost implications of upscaling chitosan-based adsorption processes for the removal of antibiotics and any other emerging contaminants of environmental concerned particularly when it comes to handling the adsorbent post-treatment. Moreover, herein adsorption isotherms were conducted at 283 K, 293 K and 303 K. Available literature (Liu, Nie and Yu 2021) suggests that at operating temperature conditions of 310 K and above, the adsorption of antibiotics on chitosan-based adsorbents is compromised. As such, more work needs to be done on temperature optimisation for the adsorption of antibiotics on chitosan-based adsorbents.

4.4. Conclusion

Herein, the single, binary, and ternary adsorption of AMX, CIP and SMX on chitosan-CNT from aqueous solution was investigated. FTIR adsorbent characterisation results exhibited the potential of chitosan-CNT as an adsorbent for the removal of antibiotics from solution. Single adsorption studies indicated that the affinity of chitosan-CNTs on the model antibiotics was in the order of CIP > AMX > SMX while the nonlinear PFO kinetic model best fitted the experimental adsorption data. Moreover, from the Weber-Morris equation, it was evident that multiple processes were limiting the overall adsorption rate of AMX, CIP and SMX on chitosan-CNTs hydrogel beads. The nonlinear Freundlich isotherm model gave a better fit for the single adsorption experimental data for AMX and SMX suggesting the heterogeneity of the surface as well as the exponential distribution of the active sites for the model adsorbent. On the other hand, the nonlinear modified Langmuir isotherm model gave a better fit for the adsorption of CIP on chitosan-CNT suggesting that the adsorption of CIP on chitosan-CNT adsorbent occurred at identical and equivalent definite localised sites. From the binary and ternary adsorption studies, the findings of the current study explicitly indicated that multicomponent adsorption systems exhibit both antagonistic and synergistic effects due to competition of AMX, CIP and SMX to occupy vacant adsorption sites on chitosan-CNT. Moreover, the findings of the current study explicitly indicated that the uptake of AMX, CIP and SMX decreased significantly in the ternary adsorption system as compared to single adsorption. From the thermodynamic study results, it is evident that the adsorption process of AMX, CIP and SMX on chitosan-CNTs is a physico-chemical adsorption process. As such, the current study suggests that chitosan-CNT has potential as a green technology for the removal of antibiotics from solution.

References

Abd El-Monaem, E. M., Eltaweil, A. S., Elshishini, H. M., Hosny, M., Abou Alsoaud, M. M., Attia, N. F., El-Subruiti, G. M. and Omer, A. M. 2022. Sustainable adsorptive removal of antibiotic residues by chitosan composites: An insight into current developments and future recommendations. *Arabian journal of chemistry*, 15 (5): 103743.

Afzal, M. Z., Sun, X.-F., Liu, J., Song, C., Wang, S.-G. and Javed, A. 2018. Enhancement of ciprofloxacin sorption on chitosan/biochar hydrogel beads. *Science of the Total Environment*, 639: 560-569.

Ahamad, T., Naushad, M., Al-Shahrani, T., Al-Hokbany, N. and Alshehri, S. M. 2020. Preparation of chitosan based magnetic nanocomposite for tetracycline adsorption: Kinetic and thermodynamic studies. *International journal of biological macromolecules*, 147: 258-267.

Ahmadpour, A., Tanhaei, B., Khoshkho, S. M., Ayati, A., Krivoshapkin, P. and Sillanpää, M. 2023. Dual-purpose magnetic κ-carrageenan/montmorillonite hydrogel for carrying and removal of tetracycline from aqueous medium. *Inorganic Chemistry Communications*, 156: 111274.

Ahmed, M. J. and Theydan, S. K. 2013. Microwave assisted preparation of microporous activated carbon from Siris seed pods for adsorption of metronidazole antibiotic. *Chemical Engineering Journal*, 214: 310-318.

Al-Ghouti, M. A. and Da'ana, D. A. 2020. Guidelines for the use and interpretation of adsorption isotherm models: A review. *Journal of hazardous materials*, 393: 122383.

Alexander, J. T., Hai, F. I. and Al-Aboud, T. M. 2012. Chemical coagulation-based processes for trace organic contaminant removal: Current state and future potential. *Journal of environmental management*, 111: 195-207.

Almomani, F. A., Shawaqfah, M., Bhosale, R. R. and Kumar, A. 2016. Removal of emerging pharmaceuticals from wastewater by ozone-based advanced oxidation processes. *Environmental Progress & Sustainable Energy*, 35 (4): 982-995.

Anjali, R. and Shanthakumar, S. 2019. Insights on the current status of occurrence and removal of antibiotics in wastewater by advanced oxidation processes. *Journal of environmental management*, 246: 51-62.

Ayati, A., Tanhaei, B., Beiki, H., Krivoshapkin, P., Krivoshapkina, E. and Tracey, C. 2023. Insight into the adsorptive removal of ibuprofen using porous carbonaceous materials: A review. *Chemosphere*, 323: 138241.

Bessa, V. S., Moreira, I. S., Tiritan, M. E. and Castro, P. M. L. 2017. Enrichment of bacterial strains for the biodegradation of diclofenac and carbamazepine from activated sludge. *International Biodeterioration & Biodegradation*, 120: 135-142.

Chandrasekaran, A., Patra, C., Narayanasamy, S. and Subbiah, S. 2020. Adsorptive removal of Ciprofloxacin and Amoxicillin from single and binary aqueous systems using acid-activated carbon from Prosopis juliflora. *Environmental Research*, 188: 109825.

Cuerda-Correa, E. M., Alexandre-Franco, M. F. and Fernández-González, C. 2019. Advanced oxidation processes for the removal of antibiotics from water. An overview. *Water*, 12 (1): 102.

Danalıoğlu, S. T., Bayazit, Ş. S., Kuyumcu, Ö. K. and Salam, M. A. 2017. Efficient removal of antibiotics by a novel magnetic adsorbent: Magnetic activated carbon/chitosan (MACC) nanocomposite. *Journal of Molecular Liquids*, 240: 589-596.

Dutta, J. and Mala, A. A. 2020. Removal of antibiotic from the water environment by the adsorption technologies: A review. *Water science and technology*, 82 (3): 401-426.

Fan, L., Luo, C., Sun, M., Li, X., Lu, F. and Qiu, H. 2012. Preparation of novel magnetic chitosan/graphene oxide composite as effective adsorbents toward methylene blue. *Bioresource technology*, 114: 703-706.

Gelband, H., Miller, P., Molly, Pant, S., Gandra, S., Levinson, J., Barter, D., White, A. and Laxminarayan, R. 2015. The state of the world's antibiotics 2015. *Wound healing southern africa*, 8 (2): 30-34.

Ghosal, P. S. and Gupta, A. K. 2017. Determination of thermodynamic parameters from Langmuir isotherm constant-revisited. *Journal of Molecular Liquids*, 225: 137-146.

Gothwal, R. and Shashidhar, T. 2015. Antibiotic pollution in the environment: a review. *Clean–Soil, Air, Water*, 43 (4): 479-489.

Hajizadeh, Z., Valadi, K., Taheri-Ledari, R. and Maleki, A. 2020. Convenient Cr (VI) removal from aqueous samples: executed by a promising clay-based catalytic system, magnetized by Fe3O4 nanoparticles and functionalized with humic acid. *ChemistrySelect*, 5 (8): 2441-2448.

Jais, F. M., Chee, C. Y., Ismail, Z. and Ibrahim, S. 2021. Experimental design via NaOH activation process and statistical analysis for activated sugarcane bagasse hydrochar for removal of dye and antibiotic. *Journal of Environmental Chemical Engineering*, 9 (1): 104829.

Jia, X., Zhang, B., Chen, C., Fu, X. and Huang, Q. 2021. Immobilization of chitosan grafted carboxylic Zr-MOF to porous starch for sulfanilamide adsorption. *Carbohydrate polymers*, 253: 117305.

Karimi-Maleh, H., Ayati, A., Davoodi, R., Tanhaei, B., Karimi, F., Malekmohammadi, S., Orooji, Y., Fu, L. and Sillanpää, M. 2021. Recent advances in using of chitosan-based adsorbents for removal of pharmaceutical contaminants: A review. *Journal of Cleaner Production*, 291: 125880.

Karthikraj, R., Vasu, A. K., Balakrishna, K., Sinha, R. K. and Kannan, K. 2017. Occurrence and fate of parabens and their metabolites in five sewage treatment plants in India. *Science of the Total Environment*, 593: 592-598.

Kaur, G., Singh, N. and Rajor, A. 2021. Ofloxacin adsorptive interaction with rice husk ash: Parametric and exhausted adsorbent disposability study. *Journal of Contaminant Hydrology*, 236: 103737.

Kundu, S. and Gupta, A. K. 2006. Arsenic adsorption onto iron oxide-coated cement (IOCC): Regression analysis of equilibrium data with several isotherm models and their optimization. *Chemical Engineering Journal*, 122 (1): 93-106.

Lima, E. C., Sher, F., Guleria, A., Saeb, M. R., Anastopoulos, I., Tran, H. N. and Hosseini-Bandegharaei, A. 2021. Is one performing the treatment data of adsorption kinetics correctly? *Journal of Environmental Chemical Engineering*, 9 (2): 104813.

Liu, Y., Nie, P. and Yu, F. 2021. Enhanced adsorption of sulfonamides by a novel carboxymethyl cellulose and chitosan-based composite with sulfonated graphene oxide. *Bioresource Technology*, 320: 124373.

Long, L., Hu, X., Yan, J., Zeng, Y., Zhang, J. and Xue, Y. 2019. Novel chitosan–ethylene glycol hydrogel for the removal of aqueous perfluorooctanoic acid. *Journal of Environmental Sciences*, 84: 21-28.

Madikizela, L. M., Tavengwa, N. T. and Chimuka, L. 2017. Status of pharmaceuticals in African water bodies: Occurrence, removal and analytical methods. *Journal of Environmental Management*, 193: 211-220.

Majd, M. M., Kordzadeh-Kermani, V., Ghalandari, V., Askari, A. and Sillanpää, M. 2022. Adsorption isotherm models: A comprehensive and systematic review (2010− 2020). *Science of The Total Environment*, 812: 151334.

Maleki, A., Mohammad, M., Emdadi, Z., Asim, N., Azizi, M. and Safaei, J. 2020. Adsorbent materials based on a geopolymer paste for dye removal from aqueous solutions. *Arabian Journal of Chemistry*, 13 (1): 3017-3025.

Mangla, D., Sharma, A. and Ikram, S. 2022. Critical review on adsorptive removal of antibiotics: Present situation, challenges and future perspective. *Journal of Hazardous Materials*, 425: 127946.

Manjunath, S., Baghel, R. S. and Kumar, M. 2020. Antagonistic and synergistic analysis of antibiotic adsorption on Prosopis juliflora activated carbon in multicomponent systems. *Chemical Engineering Journal*, 381: 122713.

Martín-Lara, M., Blázquez, G., Calero, M., Almendros, A. and Ronda, A. 2016. Binary biosorption of copper and lead onto pine cone shell in batch reactors and in fixed bed columns. *International Journal of Mineral Processing*, 148: 72-82.

Mhuka, V., Dube, S. and Nindi, M. M. 2020. Occurrence of pharmaceutical and personal care products (PPCPs) in wastewater and receiving waters in South Africa using LC-Orbitrap™ MS. *Emerging Contaminants*, 6: 250-258.

Mudhoo, A. and Pittman Jr, C. U. 2023. Adsorption Data Modeling and Analysis Under Scrutiny: A Clarion Call to Redress Recently Found Troubling Flaws. *Chemical Engineering Research and Design*,

Nasrollahi, N., Vatanpour, V. and Khataee, A. 2022. Removal of antibiotics from wastewaters by membrane technology: Limitations, successes, and future improvements. *Science of the Total Environment*, 838: 156010.

Ngo, H. H., Guo, W., Nguyen, T. H., Luong, T. M. L., Nguyen, X. H., Phan, T. L. A., Nguyen, M. P. and Nguyen, M. K. 2023. New chitosan-biochar composite derived from agricultural waste for removing sulfamethoxazole antibiotics in water. *Bioresource Technology*: 129384.

Osman, A. I., Ayati, A., Farghali, M., Krivoshapkin, P., Tanhaei, B., Karimi-Maleh, H., Krivoshapkina, E., Taheri, P., Tracey, C. and Al-Fatesh, A. 2023. Advanced adsorbents for ibuprofen removal from aquatic environments: a review. *Environmental Chemistry Letters*: 1-46.

Pan, L.-j., Li, J., Li, C.-x., Tang, X.-d., Yu, G.-w. and Wang, Y. 2018. Study of ciprofloxacin biodegradation by a Thermus sp. isolated from pharmaceutical sludge. *Journal of Hazardous Materials*, 343: 59-67.

Pan, L.-j., Tang, X.-d., Li, C.-x., Yu, G.-w. and Wang, Y. 2017. Biodegradation of sulfamethazine by an isolated thermophile–Geobacillus sp. S-07. *World Journal of Microbiology and Biotechnology*, 33: 1-8.

Patel, S. J., Wellington, M., Shah, R. M. and Ferreira, M. J. 2020. Antibiotic stewardship in food-producing animals: challenges, progress, and opportunities. *Clinical therapeutics*, 42 (9): 1649-1658.

Pauletto, P. S., Lütke, S. F., Dotto, G. L. and Salau, N. P. G. 2021. Adsorption mechanisms of single and simultaneous removal of pharmaceutical compounds onto activated carbon: Isotherm and thermodynamic modeling. *Journal of Molecular Liquids*, 336: 116203.

Raftery, A. E. 1995. Bayesian model selection in social research. *Sociological methodology*: 111-163.

Rasoulzadeh, H., Mohseni-Bandpei, A., Hosseini, M. and Safari, M. 2019. Mechanistic investigation of ciprofloxacin recovery by magnetite–imprinted chitosan nanocomposite: isotherm, kinetic, thermodynamic and reusability studies. *International journal of biological macromolecules*, 133: 712-721.

Rizzi, V., Lacalamita, D., Gubitosa, J., Fini, P., Petrella, A., Romita, R., Agostiano, A., Gabaldón, J. A., Gorbe, M. I. F. and Gómez-Morte, T. 2019. Removal of tetracycline from polluted water by chitosan-olive pomace adsorbing films. *Science of The Total Environment*, 693: 133620.

Saha, P. and Chowdhury, S. 2011. Insight into adsorption thermodynamics. *Thermodynamics*, 16: 349-364.

Sahoo, T. R. and Prelot, B. 2020. Adsorption processes for the removal of contaminants from wastewater: the perspective role of nanomaterials and nanotechnology. In: *Nanomaterials for the detection and removal of wastewater pollutants*. Elsevier, 161-222.

Sobczak-Kupiec, A., Drabczyk, A., Florkiewicz, W., Głąb, M., Kudłacik-Kramarczyk, S., Słota, D., Tomala, A. and Tyliszczak, B. 2021. Review of the applications of biomedical compositions containing hydroxyapatite and collagen modified by bioactive components. *Materials*, 14 (9): 2096.

Soltaninejad, V., Ahghari, M. R., Taheri-Ledari, R. and Maleki, A. 2021. Bifunctional PVA/ZnO/AgI/chlorophyll nanocomposite film: Enhanced photocatalytic activity for degradation of pollutants and antimicrobial property under visible-light irradiation. *Langmuir*, 37 (15): 4700-4713.

Teixeira, S., Delerue-Matos, C. and Santos, L. 2019. Application of experimental design methodology to optimize antibiotics removal by walnut shell based activated carbon. *Science of The Total Environment*, 646: 168-176.

Tran, H. N., Bollinger, J.-C., Lima, E. C. and Juang, R.-S. 2023. How to avoid mistakes in treating adsorption isotherm data (liquid and solid phases): Some comments about correctly using Radke-Prausnitz nonlinear model and Langmuir equilibrium constant. *Journal of Environmental Management*, 325: 116475.

Tran, H. N., Lima, E. C., Juang, R.-S., Bollinger, J.-C. and Chao, H.-P. 2021. Thermodynamic parameters of liquid–phase adsorption process calculated from different equilibrium constants related to adsorption isotherms: A comparison study. *Journal of Environmental Chemical Engineering*, 9 (6): 106674.

Tran, H. N., You, S.-J., Hosseini-Bandegharaei, A. and Chao, H.-P. 2017. Mistakes and inconsistencies regarding adsorption of contaminants from aqueous solutions: A critical review. *Water Research*, 120: 88-116.

Van Boeckel, T. P., Gandra, S., Ashok, A., Caudron, Q., Grenfell, B. T., Levin, S. A. and Laxminarayan, R. 2014. Global antibiotic consumption 2000 to 2010: an analysis of national pharmaceutical sales data. *The Lancet infectious diseases*, 14 (8): 742-750.

Verma, M., Lee, I., Sharma, S., Kumar, R., Kumar, V. and Kim, H. 2021. Simultaneous removal of heavy metals and ciprofloxacin micropollutants from wastewater using ethylenediaminetetraacetic acid-functionalized β-cyclodextrin-chitosan adsorbent. *ACS omega*, 6 (50): 34624-34634.

Verma, V. K. and Subbiah, S. 2019. Sericin-coated polymeric microfiltration membrane for removal of drug-based micropollutants. *Journal of Chemical Technology & Biotechnology*, 94 (11): 3625-3636.

Wang, F., Yang, B., Wang, H., Song, Q., Tan, F. and Cao, Y. 2016. Removal of ciprofloxacin from aqueous solution by a magnetic chitosan grafted graphene oxide composite. *Journal of Molecular Liquids*, 222: 188-194.

Wang, Y., Lu, J., Wu, J., Liu, Q., Zhang, H. and Jin, S. 2015. Adsorptive removal of fluoroquinolone antibiotics using bamboo biochar. *Sustainability*, 7 (9): 12947-12957.

Weber Jr, W. J. and Morris, J. C. 1963. Kinetics of adsorption on carbon from solution. *Journal of the sanitary engineering division*, 89 (2): 31-59.

Weber, T. W. and Chakravorti, R. K. 1974. Pore and solid diffusion models for fixed-bed adsorbers. *AIChE Journal*, 20 (2): 228-238.

Weng, X., Lin, S., Zhong, Y. and Chen, Z. 2013. Chitosan stabilized bimetallic Fe/Ni nanoparticles used to remove mixed contaminants-amoxicillin and Cd (II) from aqueous solutions. *Chemical engineering journal*, 229: 27-34.

Yao, L., Wang, Y., Tong, L., Deng, Y., Li, Y., Gan, Y., Guo, W., Dong, C., Duan, Y. and Zhao, K. 2017. Occurrence and risk assessment of antibiotics in surface water and groundwater from different depths of aquifers: A case study at Jianghan Plain, central China. *Ecotoxicology and Environmental Safety*, 135: 236-242.

Yaqubi, O., Tai, M. H., Mitra, D., Gerente, C., Neoh, K. G., Wang, C.-H. and Andres, Y. 2021. Adsorptive removal of tetracycline and amoxicillin from aqueous solution by leached carbon black waste and chitosan-carbon composite beads. *Journal of Environmental Chemical Engineering*, 9 (1): 104988.

Yeo, J. Y. J., Khaerudini, D. S., Soetaredjo, F. E., Waworuntu, G. L., Ismadji, S., Putranto, A. and Sunarso, J. 2023. Experimental and modelling study of adsorption isotherms of amoxicillin, ampicillin and

doripenem on bentonite-chitosan composite. *South African Journal of Chemical Engineering*, 43 (1): 38-45.

Yin, F., Lin, S., Zhou, X., Dong, H. and Zhan, Y. 2021. Fate of antibiotics during membrane separation followed by physical-chemical treatment processes. *Science of the Total Environment*, 759: 143520.

Zainab, S. M., Junaid, M., Xu, N. and Malik, R. N. 2020. Antibiotics and antibiotic resistant genes (ARGs) in groundwater: A global review on dissemination, sources, interactions, environmental and human health risks. *Water research*, 187: 116455.

Zeng, H., Li, J., Zhao, W., Xu, J., Xu, H., Li, D. and Zhang, J. 2022. The current status and prevention of antibiotic pollution in groundwater in China. *International Journal of Environmental Research and Public Health*, 19 (18): 11256.

Zhang, X., Zhang, Y., Ngo, H. H., Guo, W., Wen, H., Zhang, D., Li, C. and Qi, L. 2020. Characterization and sulfonamide antibiotics adsorption capacity of spent coffee grounds based biochar and hydrochar. *Science of the Total Environment*, 716: 137015.

Zhao, R., Ma, T., Zhao, S., Rong, H., Tian, Y. and Zhu, G. 2020. Uniform and stable immobilization of metal-organic frameworks into chitosan matrix for enhanced tetracycline removal from water. *Chemical Engineering Journal*, 382: 122893.

Zhou, A., Yang, K., Wu, X., Liu, G., Zhang, T. C., Wang, Q. and Luo, F. 2022. Functionally-Designed Chitosan-based hydrogel beads for adsorption of sulfamethoxazole with light regeneration. *Separation and Purification Technology*, 293: 120973.

Zhou, X. and Zhou, X. 2014. The unit problem in the thermodynamic calculation of adsorption using the langmuir equation. *Chemical Engineering Communications*, 201 (11): 1459-1467.

Zuyi, T. and Taiwei, C. 2000. On the Applicability of the Langmuir Equation to Estimation of Adsorption Equilibrium Constants on a Powdered Solid from Aqueous Solution. *Journal of Colloid and Interface Science*, 231 (1): 8-12.

Supplementary Material

Figures S4.1 – S4.3 present the adsorption kinetics profile of AMX, CIP, and SMX on chitosan-CNT adsorbent.

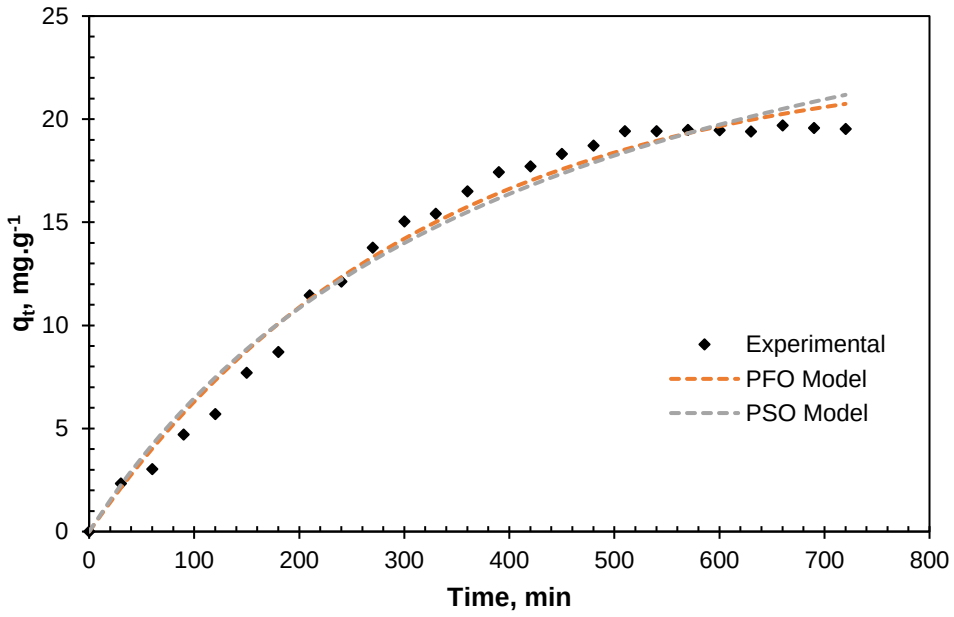

Figure S17.1: Adsorption kinetics for AMX

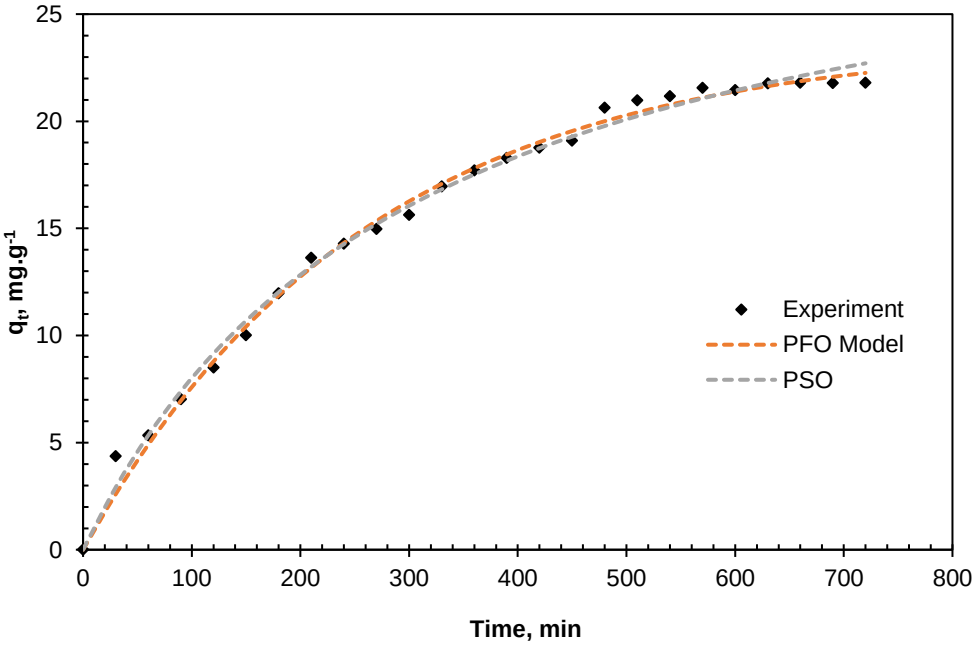

Figure S18.2: Adsorption kinetics for CIP

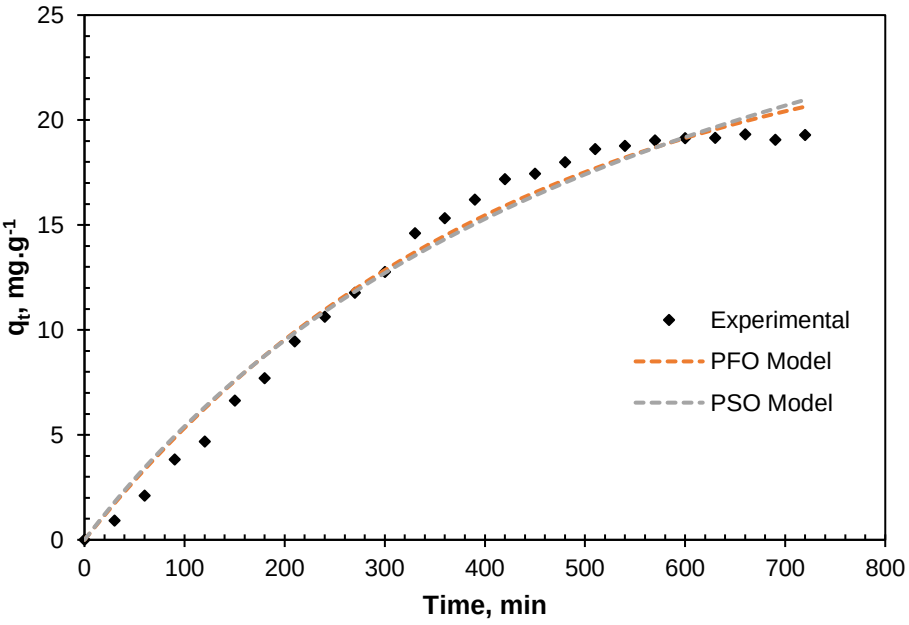

Figure S19.3: Adsorption kinetics for SMX

Equations S1 – S5 were used to convert the equilibrium constants i.e., K_{Sips}, K_{Liu}, K_{Hill}, K_{RP}, and K_{KC} from dimensional to dimensionless on the basis that the units of the aforementioned adsorption constants are dependent on the selection of the units of an adsorption isotherm model. It is worth noting that for equilibrium constants with their units containing exponent i.e., K_{Sips} and K_{Hill} their unit conversion was obtained by taking into consideration the relationship between the equilibrium constant and exponent in each adsorption isotherm model.

Sips isotherm

$$K_e^\circ = \sqrt[n_{Sips}]{K_{Sips}} \times \frac{C_{adsorbate}^\circ}{\gamma_{adsorbate}} \quad (S1)$$

Liu isotherm

$$K_e^\circ = \frac{1}{K_{Liu}} \times \frac{C_{adsorbate}^\circ}{\gamma_{adsorbate}} \quad (S2)$$

Hill isotherm

$$K_e^\circ = \frac{1}{\sqrt[n_{Hill}]{K_{Hill}}} \times \frac{C_{adsorbate}^\circ}{\gamma_{adsorbate}} \quad (S3)$$

Redlich-Peterson

$$K_e^\circ = \sqrt[n_{RP}]{K_{RP}} \times \frac{C_{adsorbate}^\circ}{\gamma_{adsorbate}} \quad (S4)$$

Koble-Corrigan

$$K_e^\circ = \sqrt[n_{KC}]{K_{KC}} \times \frac{C_{adsorbate}^\circ}{\gamma_{adsorbate}} \quad (S5)$$

CHAPTER FIVE: EFFECT OF COMPETING IONS

THE EFFECT OF COMPETING IONS ON THE SORPTION OF AMOXICILLIN, CIPROFLOXACIN, AND SULFAMETHOXAZOLE ON CHITOSAN-CARBON NANOTUBE HYDROGEL BEADS

5.1. Abstract

This chapter pertains to the synthesis of chitosan-carbon nanotube (CCNT) hydrogel beads using a two-step process for the uptake of amoxicillin (AMX), ciprofloxacin (CIP) and sulfamethoxazole (SMX) in the presence of varying concentration of sodium chloride (NaCl) and humic acid (HA) from 0 mg/L to 40 mg/L as competing ions. From the results obtained it was concluded that the increase in NaCl or HA concentration demonstrated antagonistic effects in the uptake of AMX, CIP and SMX on the synthesised CCNT hydrogel beads due to the formation of aggregates with an increase in ionic strength. Moreover, NaCl demonstrated the least effects on the uptake of the model antibiotics as compared to HA, indicating that NaCl ions exhibit minimal competitive effects with adsorbate molecules for active adsorption sites on CCNT hydrogel beads. Similarly, from the single factor analysis of variance results, p-values of less than 0.05 were recorded for the uptake of AMX, CIP and SMX on CCNT hydrogel beads, explicitly indicating that there was a statistical difference between the means for the independent and dependent variables, thus cementing the negative effect of increasing ionic strength on the uptake of model adsorbates. Moreover, the findings of the present work suggest that there is need for a pretreatment stage aimed at eliminating co-existing contaminants prior to the application of solid-liquid adsorption for complete eradication of contaminants of emerging concern, particularly antibiotics.

5.2. Introduction

Recently, there has been a significant increase in the use of antibiotics for human consumption and agricultural use particularly in poultry farming, animal husbandry, beekeeping, aquaculture as well as livestock as growth promoters (Manjunath, Baghel and Kumar 2020; Khumalo *et al.* 2023). The comprehensive use of antibiotics can be ascribed to their ability to minimise the burden of common infectious diseases qualifying them to be crucial for medical interventions as elucidated by Manjunath, Baghel and Kumar (2020). Sadly, there has been a noticeable global increase in the consumption of antibiotics of 65% between year 2000 and 2015 from 21.1 to 34.8 billion defined daily dose, while the antibiotic consumption rate increase has been reported to move from 11.3 to 15.7 daily dose per 1000

inhabitants per day as elucidated by Manjunath, Baghel and Kumar (2020) and Klein *et al.* (2018). Due to the increase in the consumption rate of antibiotics, they have been detected in water bodies at minute concentrations ranging from ng/L to µg/L (Khumalo *et al.* 2023).

The occurrence of antibiotics in water receiving bodies is ascribed to human secretion through urine and faeces, from original compounds, as its metabolites and/or as conjugates glucuronic and sulfuric acid, as well as the use of animal manure (i.e., mixture of faeces, urine and bedding material) (Tran, Reinhard and Gin 2018; Ghirardini, Grillini and Verlicchi 2020; Khumalo *et al.* 2023). It is worth noting that approximately 50 – 90 percent of antibiotics administered by humans or animals are excreted via urine and faeces as a mixture of the parent compound as well as in its metabolite form (Tran, Reinhard and Gin 2018), which are then sent into wastewater treatment plants (WWTPs) as urban wastewater. However, the occurrence of antibiotics in water receiving bodies is evident enough that the current WWTPs cannot completely eradicate these emerging contaminants of environmental concern as reported in literature (Madikizela and Chimuka 2017; Kovalakova *et al.* 2020). Moreover, antibiotics are characterised as pseudo-persistent compounds; as such their occurrence in aquatic environment triggers antimicrobial resistance against pathogens subsequently leading to ecotoxicity. Available literature (Patel *et al.* 2020) suggests that, about one-third of children under the age of five years have succumbed to infection with antibiotic-resistant organisms. Therefore, there is an urgent need for antibiotics removal from water bodies on the basis that antibiotic resistance is being considered as one of the emerging health challenges.

A number of techniques have been investigated for the removal of antibiotics from wastewater ranging from advanced oxidation (Wang *et al.* 2023), membrane technology (Nasrollahi, Vatanpour and Khataee 2022), biodegradation (Han *et al.* 2020), as well as solid-liquid adsorption (Manjunath, Baghel and Kumar 2020). However, hitherto, solid-liquid adsorption has been one of the most preferred technologies for antibiotic removal from aqueous environments as compared to the other aforementioned technologies. The growing appetite in the application of solid-liquid adsorption is ascribed to its advantages i.e., cost effective, easy operation without any sludge nor byproducts generation, reusability as well as online operation (Manjunath, Baghel and Kumar 2020; Karimi-Maleh *et al.* 2021). There has been a paradigm shift in the application of conventional adsorbents derived from non-renewable resources such as polymers since they render the adsorption process expensive. As such, most researchers within the scientific community are exploring new avenues in the application of low-cost adsorbents derived from agricultural waste for complete eradication of emerging contaminants of environmental concern.

The current study focuses on the application of chitosan-based adsorbent for the removal of amoxicillin (AMX), ciprofloxacin (CIP) and sulfamethoxazole (SMX) from aqueous solutions. Chitosan is characterised as a natural polysaccharide that can be easily obtained from crustacean (i.e., lobster, crabs,

shrimps as well as insects and fungi) chitin by thermo-chemical deacetylation (Yaqubi *et al.* 2021). Owing to its environmentally complacent properties such as being inexpensive, biocompatible, non-toxicity, hydrophobicity as well as biodegradability, it has cemented its application as a biosorbent in wastewater treatment processes (Khumalo, Bakare and Rathilal 2024). According to Khumalo, Bakare and Rathilal (2024), the presence of active amino and hydroxyl functional groups within the chitosan structure allows it to be an excellent biosorbent with chelating sites for targeted compounds in aqueous environments. Chitosan can be easily modified to gels, beads and films with enhanced mechanical strength, diffusion capacity as well as swelling (Yaqubi *et al.* 2021). Due to the versatility of chitosan is makes it an excellent material to develop novel composites with a wide range of functional groups.

Due to the lack of studies focusing on the uptake of antibiotics from solution in the presence of competing ions, herein chitosan-carbon nanotube (CCNT) hydrogel beads were synthesised via precipitation in an alkaline solution as discussed by Khumalo, Bakare and Rathilal (2024). The adsorption efficacy of CCNT hydrogel beads was investigated for the uptake of AMX, CIP and SMX in the presence of sodium chloride (NaCl) and humic acid (HA) as competing ions.

5.3. Materials and Methods

5.3.1. Materials

All chemicals used in the present study were not subjected to any purification process and were used as received from respective suppliers. Amoxicillin (≥95% anhydrous basis), ciprofloxacin (≥98% pure), sulfamethoxazole (HPLC grade), and multi-walled carbon nanotubes (>98% carbon basis) were supplied by Lasec laboratories, Durban, South Africa. Chitosan powder from shrimp shells (≥75% deacetylation), sodium hydroxide (NaOH) pellets (≥99.5% pure), methanol (CH_3OH) (≥99.9% pure), 98% pure sulfuric acid (H_2SO_4), HPLC grade NaCl salt and humic acid ($C_{187}H_{186}O_{89}N_9S_1$) salt were supplied by Sigma-Aldrich, South Africa. Glacial acetic acid ($C_2H_4O_2$) (≥99.7% pure) was supplied by Shalom Laboratories, South Africa.

5.3.2. Adsorbent synthesis

CCNT hydrogel beads were synthesized by adopting the procedure as outlined in Chapter Four (Khumalo, Bakare and Rathilal 2024). Multiwall-CNTs were first modified by soaking a specific amount of CNTs in a solution of concentrated sulfuric acid (99%) and nitric acid (65%) at a volume ratio of 1:2, respectively for 24 hours. The acid modification of CNTs was imperative for the attachment of functional groups such as carboxylic and hydroxyl groups on the CNTs surface. Functionalized CNTs were rinsed with ultra-pure

deionized water until a filtrate pH of 7 was achieved. Thereafter, 100 g of chitosan powder was dissolved in 400 mL of 1 %v/v of $C_2H_4O_2$ solution on the basis that chitosan has a relatively high solubility in weak acidic aqueous environments (Khumalo *et al.* 2023a). The chitosan-$C_2H_4O_2$ mixture was then vortexed using a magnetic stirrer bar at 200 rpm for 24 hours at room temperature to allow for complete dissolution of chitosan due to its low solubility. Thereafter, 5 wt.% with respect to chitosan of functionalized multiwall-CNTs were added into the chitosan-$C_2H_4O_2$ mixture and vortexed at 200 rpm for 2 hours to obtain a homogeneous distribution of CNTs in the mixture. CCNT hydrogel beads were synthesized by adding the viscous CCNT gel dropwise in a solution of 15 wt.% NaOH and 95 %v/v methanol at a volume ratio of 4:1, respectively, using a 10 mL syringe which precipitated into CCNT hydrogel beads. The CCNT hydrogel beads were soaked in the NaOH-methanol solution for 24 hours, then rinsed with deionised water until a pH of 7 was obtained from the filtrate prior to being utilised for adsorption studies.

5.3.3. Adsorption batch studies

The adsorption efficacy of the model adsorbent was investigated by conducting batch adsorption experiments using 50 mL clear bottles with screw caps. A sample size of 50 mL for a predetermined initial concentration 40 mg/L of AMX, CIP and SMX at a fixed solution pH of 7 was used. The solution pH was adjusted using 1.0 M NaOH and 1.0 M H_2SO_4. A predetermined quantity of 1.5 g/L of CCNT hydrogel beads was added into respective AMX, CIP and SMX aqueous solutions and in a shaker for 24 hours at a rate of 150 rpm at 293 K. Samples were then drawn and filtered using a 0.45 µm syringe filter, thereafter, transferred into a 10 mL sample tube. Filtered samples were centrifuged at 5000 rpm for 10 minutes. Thereafter, the supernatant solution of the centrifuged sample was analysed for the residual of AMX, CIP and SMX concentration using a UV-vis spectrophotometer (UV-1900i, Shimadzu, South Africa). The amount of antibiotics adsorbed on CCNT hydrogel beads and adsorption efficacy were calculated using equations (5.1) and (5.2) below.

$$\mathrm{q}_{e,i} = \frac{(C_0 - C_e)}{m} \times V \tag{5.1}$$

$$Adsorption\ \% = \left[\frac{C_0 - C_e}{C_0}\right] \times 100 \tag{5.2}$$

Where $\mathrm{q}_{e,i}$ is the adsorption capacity at equilibrium of component i measured in mg/g; C_0 is the initial adsorbate concentration of component, i measured in mol/L; C_e is the concentration of the adsorbate in solution after adsorption equilibrium measured in mol/L; m is the mass of adsorbent on a dry basis measured in g; and V is the volume of the adsorbate solution with the initial concentration measured in L.

5.4. Results and Discussion

5.4.1. Effect of NaCl and HA on the uptake of AMX, CIP and SMX on CCNT hydrogel beads.

Salts are abundant from natural as well as anthropogenic sources. As such the salinity of surface water and groundwater may vary considerably. NaCl is one of the most detected salts in surface water due to its application in the manufacturing process of plastics and as a food preservative which subsequently enters water receiving bodies. On the other hand, human acid (HA) is ubiquitous in aquatic environments highly concentrated in sediments of terrestrial (Zhao *et al.* 2019), thus playing a role on the fate of co-existing organic contaminants through interaction by cation exchange, complexation, and/or hydrogen bonding. Herein, the influence of varying NaCl and HA concentration (i.e., 0 mg/L to 50 mg/L) on the uptake of AMX (Figure 5.1), CIP (Figure 5.2) and SMX (Figure 5.3) on CCNT hydrogel beads was investigated at a fixed adsorbate concentration of 40 mg/L. From the findings of the present work, it can be inferred from Figure 5.1 to Figure 5.3 that NaCl had a minimal negative effect on the uptake of the model adsorbate as compared to HA. In the context of NaCl, it is worth noting that the uptake of AMX, CIP and SMX did not change for a NaCl concentration of less than 15 mg/L. However, the decrease in the uptake of the model adsorbates (i.e., AMX from 53 mmol/kg to 43 mmol/kg; CIP from 64 mmol/kg to 50.14 mmol/kg; and SMX from 75 mmol/kg to 52.09 mmol/kg) with increasing NaCl concentration can be attributed to the mere fact that an increase in ionic strength weakens the electrostatic attraction between the adsorbate and adsorbent thus compromising the efficacy of the adsorbent. Moreover, the decrease in the uptake of the model adsorbate with increasing NaCl concentration suggests that they were competitive effects between the adsorbate and Na^+ on the adsorbate active sites.

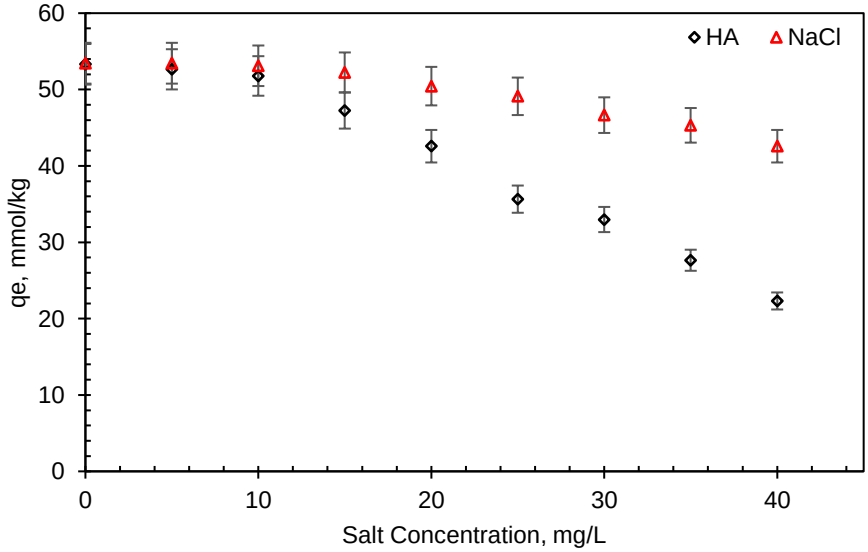

Figure 5.20: Effect of HA and NaCl on the sorption of AMX on CCNT.

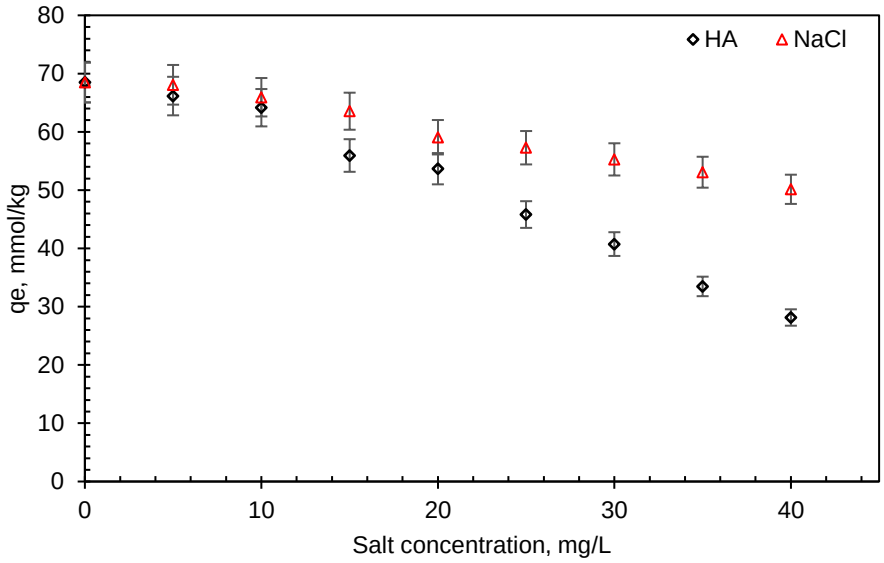

Figure 5.21: Effect of HA and NaCl on the sorption of CIP on CCNT.

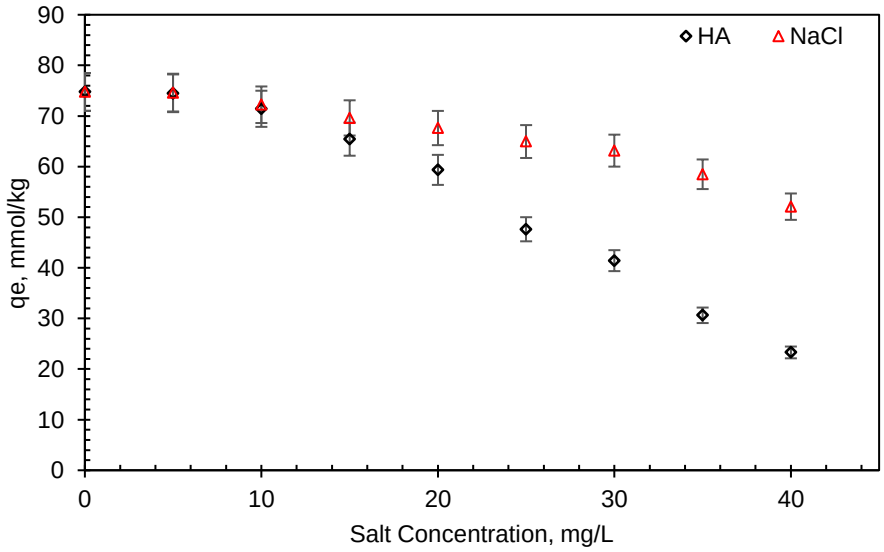

Figure 5.22: Effect of HA and NaCl on the sorption of SMX on CCNT.

It is worth noting that the results obtained suggest that the adsorption system in the presence of NaCl and HA exhibit intermolecular aggregation. Generally, intermolecular forces such as van der Waals forces, ion-dipole and dipole-dipole forces exist between organic molecules in solution (Zhang *et al.* 2019). These forces increase upon an increase in salt concentration facilitating the aggregation of organic substances. However, for the present work it can be inferred from Figure 5.1 to Figure 5.3 that the uptake of AMX, CIP and SMX on CCNT hydrogel beads is not promoted by the addition of NaCl and HA due to aggregation. In the context of HA, the significant decrease in the adsorption of the model adsorbates can be attributed to

the formation of HA aggregates in solution which are adsorbed on CCNT active sites. The adsorption of large HA aggregates hinders any further adsorption of isolated adsorbate molecules on CCNT hydrogel beads active sites, subsequently resulting in a significant decrease on the efficacy of the adsorbent. Moreover, the significant decrease in the uptake of AMX, CIP and SMX with increasing HA concentration can also be ascribed to cation bridging which is a crucial mechanism that triggers the aggregation of humic molecules into large colloidal structures as elucidated by Zhang *et al.* (2019). The findings of the present study suggest that humic molecule aggregates were adsorbed on CCNT hydrogel beads, initiating charge neutralization of negatively charged adsorbate molecules subsequently suppressing the adsorption process through electrostatic attraction. The findings of the present study are congruent to similar studies reported in literature (Afzal *et al.* 2018). However, it is worth noting that, in some cases an increase in ionic strength can improve the uptake of organic adsorbates on carbonaceous adsorbents due to the effect of salting-out. An increase in ionic strength can result in a decrease in the solubility of the adsorbate, thus allowing the dominance of the uptake of model adsorbate by hydrophobic interaction between the adsorbate and adsorbent (Yu, Deng and Yu 2008).

5.4.2. Analysis of variance

The percentage removal of AMX, CIP and SMX on CCNT hydrogel beads with varying HA (Figure 5.4) and NaCl (Figure 5.5) concentration were statistically examined using the single factor analysis of variance (ANOVA). The ANOVA results are presented in Table 5.1. In the ANOVA analysis, a single continuous dependent variable (i.e., adsorbate percentage removal) was compared with the mean of the initial concentrations of NaCl and HA as independent variables. Herein, two hypotheses were formulated i.e., 1) null hypothesis: assuming that there is no statistically significant difference that exist between the means of the independent and dependent variables, and 2) alternative hypothesis: assuming that there is a statistical difference between the means. For both model competing ions adsorption systems, the findings of the current study recorded p-values of less than 0.05 indicating that there was a statistical difference between the means of the independent and dependent variables rejecting the null hypothesis.

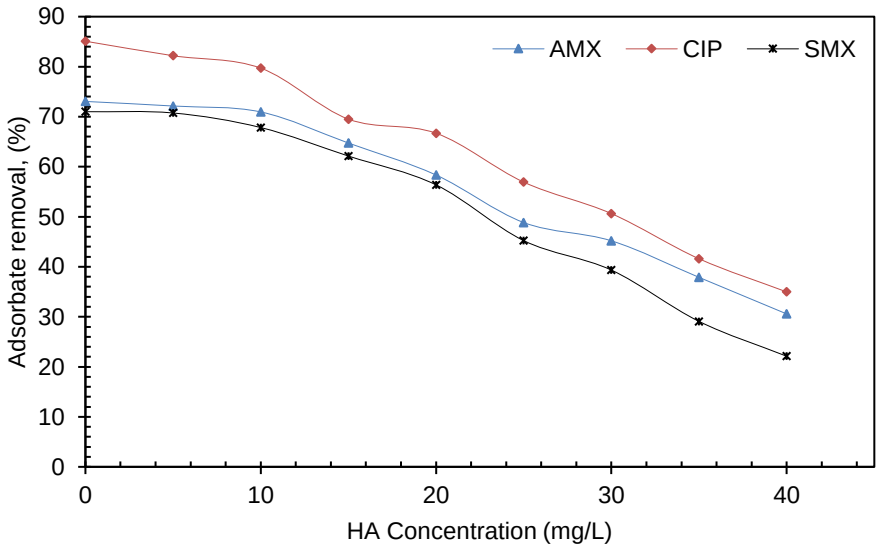

Figure 5.23: Effect of HA on the percentage removal of AMX, CIP and SMX.

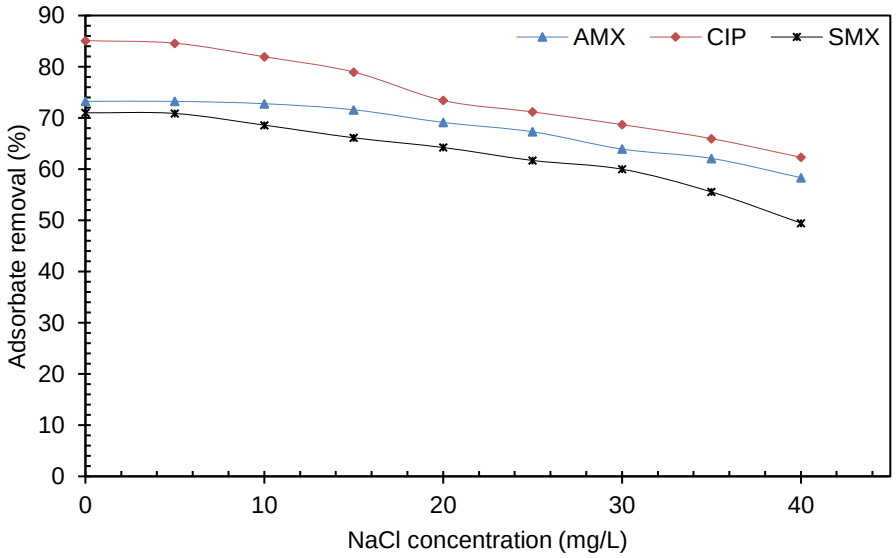

Figure 24.5: Effect of NaCl on the percentage removal of AMX, CIP and SMX.

Table 5.21: Single factor ANOVA results for the percentage removal of AMX, CIP and SMX on CCNT hydrogel beads

	Humic acid (HA)			Sodium chloride (NaCl)		
Compound	**SS**	**F-value**	**p-value**	**SS**	**F-value**	**p-value**
AMX	5750	26.29	0.000101	10 349	95.32	3.83E-08
CIP	8 334	32.33	3.38E-05	13 454	104.67	2.0E-08
SMX	4476	17.02	0.000792	8 342	69360	3.21E-07

Therefore, the ANOVA results suggest that there was a variation in the uptake of the model adsorbates with varying HA and/or NaCl concentration. Moreover, the mean differences were further confirmed at 95% confidence level by the recorded F-values of less than 1 as presented in Table 5.1. Similarly, the uptake of AMX, CIP and SMX in the presence of NaCl recorded relatively high sum of squares (SS) values when compared to the uptake of the model antibiotics in the presence of HA. The ANOVA results on the recorded SS values suggests that the uptake of AMX, CIP and SMX in the presence of NaCl was relatively high regardless of the increase in concentration as compared to the uptake of the aforementioned adsorbates in the presence of HA. The relatively low SS values in the presence of HA suggest that HA had significant antagonistic effects in the uptake of AMX, CIP and SMX with increasing concentration. As such, it can the inferred from the ANOVA results that there was a statistical decline in the percentage uptake of AMX, CIP and SMX with an increase in HA or NaCl concentration.

5.5. Conclusion

From the findings of the current work, it can be inferred that the presence of competing ions in the form of NaCl and HA have antagonistic effects in the uptake of antibiotics on CCNT hydrogel beads from aqueous solutions. Moreover, it is apparent that the uptake of AMX, CIP and SMX is not facilitated by an increase in ionic strength particularly in the presence of NaCl and HA due to the formation of aggregates with increasing NaCl and HA concentration subsequently compromising the efficacy of carbonaceous adsorbents. Therefore, there is need for a pretreatment stage aimed at eliminating co-existing contaminants prior to the application of solid-liquid adsorption from complete eradication of contaminants of emerging concern, particularly antibiotics.

References

Afzal, M. Z., Sun, X.-F., Liu, J., Song, C., Wang, S.-G. and Javed, A. 2018. Enhancement of ciprofloxacin sorption on chitosan/biochar hydrogel beads. *Science of the Total Environment*, 639: 560-569.

Ghirardini, A., Grillini, V. and Verlicchi, P. 2020. A review of the occurrence of selected micropollutants and microorganisms in different raw and treated manure – Environmental risk due to antibiotics after application to soil. *Science of The Total Environment*, 707: 136118.

Han, Y., Yang, L., Chen, X., Cai, Y., Zhang, X., Qian, M., Chen, X., Zhao, H., Sheng, M. and Cao, G. 2020. Removal of veterinary antibiotics from swine wastewater using anaerobic and aerobic biodegradation. *Science of the Total Environment*, 709: 136094.

Karimi-Maleh, H., Ayati, A., Davoodi, R., Tanhaei, B., Karimi, F., Malekmohammadi, S., Orooji, Y., Fu, L. and Sillanpää, M. 2021. Recent advances in using of chitosan-based adsorbents for removal of pharmaceutical contaminants: A review. *Journal of Cleaner Production*, 291: 125880.

Khumalo, S. M., Bakare, B. F. and Rathilal, S. 2024. Single and Multicomponent Adsorption of Amoxicillin, Ciprofloxacin, and Sulfamethoxazole on Chitosan-Carbon Nanotubes Hydrogel Beads from Aqueous Solutions: Kinetics, Isotherms, and Thermodynamic Parameters. *Journal of Hazardous Materials Advances*: 100404.

Khumalo, S. M., Makhathini, T. P., Bwapwa, J. K., Bakare, B. F. and Rathilal, S. 2023b. The occurrence and fate of antibiotics and nonsteroidal anti-inflammatory drugs in water treatment processes: A review. *Journal of Hazardous Materials Advances*, 10: 100330.

Klein, E. Y., Van Boeckel, T. P., Martinez, E. M., Pant, S., Gandra, S., Levin, S. A., Goossens, H. and Laxminarayan, R. 2018. Global increase and geographic convergence in antibiotic consumption between 2000 and 2015. *Proceedings of the National Academy of Sciences*, 115 (15): E3463-E3470.

Kovalakova, P., Cizmas, L., McDonald, T. J., Marsalek, B., Feng, M. and Sharma, V. K. 2020. Occurrence and toxicity of antibiotics in the aquatic environment: A review. *Chemosphere*, 251: 126351.

Madikizela, L. M. and Chimuka, L. 2017. Simultaneous determination of naproxen, ibuprofen and diclofenac in wastewater using solid-phase extraction with high performance liquid chromatography. *Water Sa*, 43 (2): 264-274.

Manjunath, S., Baghel, R. S. and Kumar, M. 2020. Antagonistic and synergistic analysis of antibiotic adsorption on Prosopis juliflora activated carbon in multicomponent systems. *Chemical Engineering Journal*, 381: 122713.

Nasrollahi, N., Vatanpour, V. and Khataee, A. 2022. Removal of antibiotics from wastewaters by membrane technology: Limitations, successes, and future improvements. *Science of the Total Environment*, 838: 156010.

Patel, S. J., Wellington, M., Shah, R. M. and Ferreira, M. J. 2020. Antibiotic stewardship in food-producing animals: challenges, progress, and opportunities. *Clinical therapeutics*, 42 (9): 1649-1658.

Tran, N. H., Reinhard, M. and Gin, K. Y.-H. 2018. Occurrence and fate of emerging contaminants in municipal wastewater treatment plants from different geographical regions-a review. *Water Research*, 133: 182-207.

Wang, X., Jing, J., Zhou, M. and Dewil, R. 2023. Recent advances in H2O2-based advanced oxidation processes for removal of antibiotics from wastewater. *Chinese Chemical Letters*, 34 (3): 107621.

Yaqubi, O., Tai, M. H., Mitra, D., Gerente, C., Neoh, K. G., Wang, C.-H. and Andres, Y. 2021. Adsorptive removal of tetracycline and amoxicillin from aqueous solution by leached carbon black waste and chitosan-carbon composite beads. *Journal of Environmental Chemical Engineering*, 9 (1): 104988.

Yu, Q., Deng, S. and Yu, G. 2008. Selective removal of perfluorooctane sulfonate from aqueous solution using chitosan-based molecularly imprinted polymer adsorbents. *Water Research*, 42 (12): 3089-3097.

Zhang, Y., Zhu, C., Liu, F., Yuan, Y., Wu, H. and Li, A. 2019. Effects of ionic strength on removal of toxic pollutants from aqueous media with multifarious adsorbents: A review. *Science of the Total Environment*, 646: 265-279.

Zhao, L., Liu, J., Wang, H. and Dong, Y.-h. 2019. Sorption of copper and norfloxacin onto humic acid: effects of pH, ionic strength, and foreign ions. *Environmental Science and Pollution Research*, 26: 10685-10694.

CHAPTER SIX: ADSORPTION KINETICS, ISOTHERMS AND THERMODYNAMIC PARAMETERS

SINGLE AND BINARY ADSORPTION OF PERFLUOROOCTANOIC ACID AND PERFLUOROOCTANE SULFONIC ACID ON CHITOSAN-CARBON NANOTUBES HYDROGEL BEADS: OPTIMIZATION, KINETICS, ISOTHERMS, THERMODYNAMIC PARAMETERS AND EFFECT OF COMPETING IONS

6.1. Abstract

The occurrence of perfluorooctanoic acid (PFOA) and perfluorooctane sulfonic acid (PFOS) in water receiving bodies have posed significant health risks to human and aquatic life. Herein, the adsorption of PFOA and PFOS on chitosan-carbon nanotube (CCNT) hydrogel beads from aqueous solutions for an adsorbate concentration range of 1.208E-05 $mol.L^{-1}$ to 1.208E-04 $mol.L^{-1}$ for PFOA and 9.997E-06 $mol.L^{-1}$ to 9.997E-05 $mol.L^{-1}$ for PFOS was studied. Findings on the adsorption kinetic studies suggest that experimental data were well fitted by the nonlinear pseudo-first order kinetic model for a contact time of 48 hours and adsorbent dose of 1.5 $g.L^{-1}$ for both PFOA and PFOS. Single adsorption isotherms data were well fitted by the nonlinear Freundlich isotherm model recording R^2 values of 0.991 for PFOA and 0.997 for PFOS suggesting that the uptake of PFOA and PFOS on CCNT hydrogel beads was not restricted to the monolayer adsorption process. On the other hand, binary adsorption isotherm data were well fitted by the extended-Langmuir isotherm model ($R^2 = 0.996$ for PFOA and $R^2 = 0.995$ for PFOS) and extended-Sips isotherm model ($R^2 = 0.996$ for PFOA and $R^2 = 0.997$ for PFOS). From binary adsorption studies, it was inferred that the uptake of one adsorbate (i.e., PFOA or PFOS) in the presence of the other resulted in antagonistic effects, thus compromising the overall efficacy of the model adsorbent. Thermodynamic studies explicitly indicated that the uptake of PFOA and PFOS on CCNT hydrogel beads is an endothermic process and it cannot be explicitly classified as a chemical nor physical adsorption process but as a physiochemical adsorption process. The presence of sodium chloride as a competing ion gave synergistic effects in the uptake of PFOA and PFOS from aqueous solutions. It was concluded that the hydrophobic interaction and electrostatic attraction were the predominant mechanisms in the uptake of PFOA and PFOS on CCNT hydrogel beads.

6.2. Introduction

Per- or poly-fluoroalkyl substances (PFAS) are a class of anthropogenic emerging persistent organo-fluorine compounds characterised with a fully or partially fluorinated alkyl chain terminated by a polar acid

group i.e., carboxylate, sulphonate, or phosphonate (Garg *et al.* 2021). PFAS have inimitable properties which are ascribed to their carbon-fluorine (C-F) bond characterised by strong polarity and strength having a binding energy of 116 kcal/mol in the fluorinated chain (Elanchezhiyan *et al.* 2021; Khumalo, Bakare and Rathilal 2022). The stable C-F bond has cemented the application of PFAS as industrial detergents, in fire-fighting foams, polymerisation agent, as raw material for the production of water- and grease-repellent materials for all areas of use, coating agents, non-stick cookware as well as food packaging (Kotthoff *et al.* 2015; Elanchezhiyan *et al.* 2021; Khumalo, Bakare and Rathilal 2022). Despite their impeccable industrial applications, PFAS have been considered as contaminants of global environmental concern due to their environmental persistence, high bioaccumulation factors ascribed to their strong protein-affinity which has resulted in PFAS toxicity in humans, flora, and fauna. Due to their stability, PFAS have been detected in many environmental matrices globally, perfluorooctanoic acid (PFOA) and perfluorooctane sulfonic acid (PFOS) being the most detected PFAS as reported by Elanchezhiyan *et al.* (2021). The occurrence of PFAS in water bodies and their health hazards due to long term exposure to both PFOA and PFOS have been discussed in literature (Cui *et al.* 2009; Tsuda 2016; Li *et al.* 2017; Liu, Yin and Faiola 2018; Tarapore and Ouyang 2021; Khumalo, Bakare and Rathilal 2022; Wee and Aris 2023). Owing to the reproductive toxicity, neurotoxicity, and immunotoxicity of PFOA and PFOS in human health, developed countries like the United States of American through its Environmental Protection Agency (EPA), has stipulated a health advisory concentration of 70 ng/L for the individual and/or combined PFOA and PFOS in drinking water bodies (Park *et al.* 2020; Elanchezhiyan *et al.* 2021; Khumalo, Bakare and Rathilal 2022). According to Jian *et al.* (2017) the 3M company, together with the EPA in the United States of America, announced the phase-out of products containing PFAS with C6 and more, aimed at eliminating long-chain PFAS which have attributes of being very persistent and bio-accumulative. As such, there is an urgent need to explore effective and environmentally stable technologies to remove PFOA and PFOS from drinking water bodies since they have been characterized with a high frequency detection factor.

It is worth noting that several technologies have been reported in literature for the removal of PFAS from aqueous environments such as advanced oxidation (Cui, Gao and Deng 2020; Parenky *et al.* 2020; Yuan *et al.* 2020), electroflotation (Hubert *et al.* 2023; Li *et al.* 2023), nanofiltration and membrane processes (Franke *et al.* 2019; Xiong *et al.* 2021; Liu *et al.* 2022), chemical precipitation (Zhang *et al.* 2021), biodegradation (Yi *et al.* 2016; Huang and Jaffé 2019; Ruiz-Urigüen *et al.* 2022) as well as solid-liquid adsorption processes (Park *et al.* 2020; Elanchezhiyan *et al.* 2021). The degradation of PFAS either by advanced oxidation or biological processes result in the formation of undesirable byproducts such as the fluorine ion (F^-) and shorter chain PFAS compounds that are even more toxic and harder to remove from an aqueous environment than the parent PFAS (Long *et al.* 2019). Similarly, the degradation of PFAS by

advanced oxidation requires a series of chemical reactions activated by the hydroxyl radical and sulfate radical, which requires high energy usage for the regeneration of these radicals, thus rendering the process expensive for industrial applications (Gomez-Ruiz *et al.* 2018; Long *et al.* 2019). Membrane processes have demonstrated to be effective for the removal of PFAS from aqueous solutions, however, this technology is associated with some drawbacks such as membrane fouling which can be minimised by incorporating with a nanofiltration or reverse osmosis process thus rendering the process expensive and energy intensive (Vieira *et al.* 2020). Conventional biodegradation techniques have demonstrated to be ineffective in degrading PFAS under ambient conditions (Zhang *et al.* 2011). However, available literature (Zhang *et al.* 2011; Yi *et al.* 2016; Huang and Jaffé 2019; Ruiz-Urigüen *et al.* 2022) suggests that there has been a breakthrough in the biodegradation of PFOA and PFOS using novel bacterial strain. These technologies are still at infant stages for a practical application. On the other hand, solid-liquid adsorption has demonstrated to be effective in the removal of PFOA and PFOS (Long *et al.* 2019). The application of various conventional adsorbents for the removal of PFAS have been reported in literature such as activated carbon, carbon nanotubes, polymeric resins, and zeolite (Zhang *et al.* 2011; Gong *et al.* 2016). However, the use of the aforementioned adsorbents has been associated with a number of drawbacks such as not being easily available which may expose the risk of depleted resources, nonbiodegradability, being expensive, as well as the potential to form secondary contaminants that may harm the environment (Zakaria *et al.* 2022). Therefore, there is an urgent need for the development of low cost and environmentally green adsorbents for the removal of PFAS.

Recently, there has been a growing appetite for the application of low cost and environmentally friendly adsorbents such as chitosan-based composites for the removal of PFOA and PFOS from aqueous solutions (Zhang *et al.* 2010; Zhang *et al.* 2011; Long *et al.* 2019; Elanchezhiyan *et al.* 2021; Zakaria *et al.* 2022). The increase in the application of chitosan-based adsorbents is ascribed to the high content of amino, acetaminophen, as well as primary and secondary hydroxyl functional groups on the chitosan structure making it an excellent chelation site for targeted compounds (Elanchezhiyan *et al.* 2021). Chitosan is characterised as a polymeric β(1 → 4) glucosamine and *N*-acetyl-D-glucosamine derived from chitin by *N*-deacetylation which is the most abundant biopolymer after cellulose (Elanchezhiyan *et al.* 2021). Chitin, which is deacetylated into chitosan, is extracted from crustacean shells, including crab and shrimp shells, and fungal mycelia, which is beneficial for its various applications in environmental remediation technologies (Long *et al.* 2019). In the context of the present study, one will recall that, for an adsorbent to be considered economically feasible, the preparation and application of the material ought to require easy processing steps, consume minimal energy, have abundant sources from nature, and possess byproduct-free ability. As such, chitosan meets these criteria and it has been acknowledged as a low-cost feedstock to

develop novel adsorbents as reported by Long *et al.* (2019). The interest on chitosan-based adsorbents is also ascribed to its inherent features such as excellent biocompatibility, biodegradability, antibacterial activity, non-toxicity, ease of modification. It comprises multiple functional groups as reported by Zakaria *et al.* (2022) in their latest review on the recent advances in applications of hybrid natural polymers as adsorbents. It is worth noting that chitosan hydrogels have gained popularity for their application in wastewater treatment processes. However, the application of pristine chitosan flakes or hydrogel beads is associated with some drawbacks due to their rigidness because of their slow adsorption kinetic and high solubility in acidic aqueous solutions (Elanchezhiyan *et al.* 2021). These undesirable features of pristine chitosan can be tackled by incorporating carbonaceous material into chitosan matrix to enhance its insoluble nature in low-acidic aqueous solutions and increase its adsorption capacity (Elanchezhiyan *et al.* 2021; Khumalo *et al.* 2023).

This chapter presents the findings of the present study on investigating the efficacy of chitosan-carbon nanotube (CCNT) hydrogel beads as an adsorbent for the removal of PFOA and PFOS from an aqueous solution. Due to the remarkable features of carbon nanotubes (CNTs) such as high tensile strength, large surface area, and low density, CNTs potentiate as ideal nanofillers in tackling the undesirable features of pristine chitosan composites in the context of water treatment. The scope of this chapter entails the study of adsorption kinetics using the nonlinear pseudo empirical models, study of adsorption isotherms for single and binary systems aimed at elucidating the synergistic and/or antagonistic effects of the sorption of one PFAS in the presence of another. Furthermore, this chapter focuses in the evaluation of thermodynamic adsorption parameters to study the dominant adsorption mechanism, studying the effect of competing ions on the sorption of the PFOA and PFOS as well as process parametric optimisation using the central composite design (CCD) in response surface methodology (RSM).

6.3. Materials and Methods

6.3.1. Chemical reagents

Chitosan powder from shrimp shells with a degree of deacetylation of ≥75%, sodium hydroxide (NaOH) pellets (≥95% anhydrous basis), sodium chloride (NaCl), methanol (CH_3OH) (≥99.9% pure), 98% pure sulfuric acid (H_2SO_4), and glacial acetic acid ($C_2H_4O_2$) (≥99.7% pure) were supplied by Sigma-Aldrich, South Africa. PFOA ($C_8HF_{15}O_2$), PFOS ($C_8HF_{17}O_3S$), and multi-wall CNTs (>98% carbon basis) were supplied by Lasec laboratories, Durban, South Africa. All chemicals were of analytical grade, and were used without any additional purification. Synthetic solutions were prepared using ultra-pure water.

6.3.2. Adsorbent preparation

CCNT hydrogel beads used in the present study were synthesised using acid modified multi-wall CNTs as elucidated in chapters four and five. It is worth noting that the natural chemistry of pristine CNTs is that they bundle together and become inseparable in solution. On the other hand, the success of CNTs application in water treatment is strongly dependent on the capability of disbanding them into individual nanotubes, which makes them homogenous and stable as reported by Sobczak-Kupiec *et al.* (2021). As such, for the present work, CNT modification was done by soaking a specific amount of CNTs in a solution of concentrated H_2SO_4 and nitric acid at a volume ratio of 1:2, respectively for 24 hours. The use of an acid containing oxygen molecules result in the attachment of functional groups such as carboxylic and hydroxyl groups on the surface of CNTs which are essential in the removal of the model contaminants in aqueous solutions. Thereafter, the acid functionalised CNTs were rinsed with ultrapure deionised water until a filtrate pH of 7 was achieved. The filtrate pH was measured using a HANNA HI 9828 pH meter. Moreover, it is worth noting that the functionalisation of CNTs was necessary to ascertain a more hydrophilic surface as compared to pristine CNTs.

CCNT hydrogel beads were then synthesised by dissolving 100 g of chitosan in 400 mL of 1 %v/v solution of glacial acetic acid. Pure chitosan has a low solubility in water which is improved in weak acidic aqueous environments. Thereafter, the chitosan-glacial acetic acid mixture was vortexed using a magnetic stirrer at 200 rpm for 24 hours at room temperature to allow for complete dissolution of chitosan due to its low solubility at room temperature, thus prolonged periods of vortexing are necessary. During vortexing, the chitosan-CNT mixture was covered with an aluminium foil to minimise any evaporation since glacial acetic acid is relatively volatile. Thereafter, 5 wt.% of the functionalised CNTs with respect to chitosan were added into the chitosan-glacial acetic acid mixture and vortexed at 200 rpm for 2 hours. This was done to obtain a homogeneous distribution of CNTs in the mixture. The viscous CCNT mixture was allowed to degas in a vacuum desiccator until all air bubbles disappeared (i.e., disappearance of air pockets within the viscous mixture). CCNT hydrogel beads were synthesised by adding the viscous CCNT mixture dropwise in a solution of 15 wt.% NaOH and 95 %v/v CH_3OH at a volume ratio of 4:1, respectively, using a 10 mL syringe. The CCNT gel precipitated into CCNT beads and were allowed to soak in the NaOH-CH_3OH solution for 24 hours. Thereafter, CCNT beads were rinsed with deionised water until a filtrate pH of 7 was obtained prior to being used for adsorption studies. The Fourier transform infrared spectrophotometry (FTIR, VERTEX 70) was used to analyse the presence of functional groups.

6.3.3. Batch studies

Experiments for adsorption kinetics for the sorption of PFOA and PFOS on CCNT hydrogel beads were conducted at adsorbent and adsorbate loads of 1.5 g/L and 5 mg/L, respectively, at a fixed solution pH of 7. The adsorbent and adsorbate load were determined using the CCD in RSM. Experiments were conducted using 50 mL clear bottles with screw caps having a sample volume of 50 mL for both PFOA and PFOS. Sample bottles were placed in a water bath shaker and agitated for 48 hours at a rate of 150 rpm at 293 K. At a set time interval, samples were drawn and filtered using a 0.45 µm syringe filter and transferred into a 10 mL sample tube. The filtered samples were centrifuged at 5000 rpm for 10 minutes Thereafter, the supernatant solution of the centrifuged sample was analysed for the residual PFOA and PFOS using a UV-vis spectrophotometer (UV-1900i, Shimadzu, South Africa) at a wavelength of 365 nm and 360 nm, respectively. The removal rate of the model contaminants was calculated based on the difference between the initial and final aqueous concentration using equation (6.1).

$$\text{Adsorption } \% = \left[\frac{C_o - C_f}{C_o}\right] \times 100 \tag{6.1}$$

Where C_o and C_f are the initial and final adsorbate concentrations measured in mg.L^{-1}. Moreover, adsorption isotherms studies were conducted for a temperature values of 283 K, 293 K and 303 K for an initial concentration range of 5 mg.L^{-1} to 50 mg.L^{-1} for both PFOA and PFOS at a fixed solution pH of 7 for an interaction time of 168 hours (7 days). For binary adsorption studies, equal part solutions in terms of the adsorbate initial concentration were prepared for a concentration range of 1.21E-05 mol.L^{-1} to 1.21E-04 mol.L^{-1} for PFOA and 9.998E-06 mol.L^{-1} to 9.998E-05 mol.L^{-1} for PFOS in solution. The adsorbent dose was maintained at 1.5 g.L^{-1}. The amount of PFOA and/or PFOS adsorbed at equilibrium was calculated using equation (6.2).

$$q_{e,i} = \frac{(C_o - C_e)}{m} \times V \tag{6.2}$$

Where $q_{e,i}$ is the adsorption capacity of species i at equilibrium measured in mol.kg^{-1}; C_0 is the initial adsorbate concentration measured in mol.L^{-1}; C_e is the concentration of the adsorbate in solution after adsorption at equilibrium in mol.L^{-1}; m is the mass of adsorbent on a dry basis measured in kg, and V is the volume of the adsorbate solution with the initial concentration measured in L.

6.3.4. Adsorption empirical models

6.3.4.1. Adsorption kinetics studies

The nonlinear pseudo-first order (PFO) (6.3), pseudo-second order (PSO) (6.4), and the Weber-Morris (6.5) empirical models were employed in studying the adsorption kinetics for the present study.

$$q_t = q_{e_1}[1 - exp(-k_1 t)] \tag{6.3}$$

$$q_t = \frac{q_{e_2}^2 k_2 t}{\left[k_2 q_{e_2} t + 1\right]} \tag{6.4}$$

$$q_t = k_i t^{0.5} + C \tag{6.5}$$

Where q_t is the adsorption capacity in mg.g^{-1} at time t; k_1 and q_{e_1} are the PFO rate constant in min^{-1} and adsorption capacity at equilibrium in mg.g^{-1}, respectively; k_2 and q_{e_2} are the PSO rate constant in g.mg^{-1}.min^{-1}, and the adsorption capacity at equilibrium in mg.g^{-1}, respectively; k_i is the intraparticle diffusion rate constant measured in mg.g^{-1}.min$^{-1/2}$, and C is a dimensionless constant which gives information related to the film thickness and relates to the adsorbate concentration on the adsorbent surface. Adsorption kinetics model validation was conducted by employing the Bayesian Information Criterion (BIC) (6.6), the residual sum of squares (RSS) (6.7), coefficient of determination (R^2) (6.8), the chi square test (χ^2) (6.9) and adjusted R^2 (adj.R^2) (6.10).

$$\text{BIC} = n \ln\left(\frac{RSS}{n}\right) + p \ln(n) \tag{6.6}$$

$$RSS = \sum_{i=1}^{n} \left(q_{i_{exp}} - q_{i_{model}}\right)^2 \tag{6.7}$$

$$R^2 = \left(\frac{\sum_i^n \left(q_{i_{exp}} - \bar{q}_{i_{exp}}\right)^2 - \sum_i^n \left(q_{i_{exp}} - q_{i_{model}}\right)^2}{\sum_i^n \left(q_{i_{exp}} - \bar{q}_{i_{exp}}\right)^2}\right) \tag{6.8}$$

$$\chi^2 = \sum \frac{\left(q_{e,exp} - q_{e,model}\right)^2}{q_{e,model}} \tag{6.9}$$

$$adj.R^2 = 1 - \left[\frac{(1-R^2)(n-1)}{n-p-1}\right] \quad (6.10)$$

Where n is the number of experiments; p is the number of parameters in the fitting model; $q_{i_{exp}}$ and $q_{i_{model}}$ are the experimental values and the theoretical values predicted by the model, respectively; $\bar{q}_{i_{exp}}$ is the average of all experimental values measured.

6.3.4.2. Adsorption isotherms studies

Herein, the adsorption equilibrium is represented by nonlinear isotherms relating the amount of adsorbate retained on the surface of CCNT as a model adsorbent with the residual concentration of adsorbate (PFOA and PFOS) in aqueous solution under isothermal conditions (Pauletto *et al.* 2021). As such, one-parameter (6.11), two-parameter (6.12 – 6.13), and three-parameter (6.14 – 6.19) nonlinear adsorption isotherm empirical models were applied in modelling single adsorption experimental data at equilibrium as recommended by Tran *et al.* (2021).

Henry model

$$q_{e,i} = K_{Henry} C_e \quad (6.11)$$

Where K_{Henry} is the Henry constant measured in L/kg.

Langmuir model

$$q_{e,i} = \frac{Q_{L,i} K_{L,i} C_{e,i}}{1 + K_{L,i} C_{e,i}} \quad (6.12)$$

Where $Q_{L,i}$ (mol.kg^{-1}) and $K_{L,i}$ (L.mol^{-1}) are the Langmuir maximum adsorption capacity and the Langmuir equilibrium constant for compound i, respectively.

Freundlich model

$$q_{e,i} = K_{F,i} C_{e,i}^{n_{F,i}} \quad (6.13)$$

Where $K_{F,i}$ is the Freundlich constant for compound i measured in [(mol.kg^{-1})/(mol.L^{-1})^{nF}]; n_F is the dimensionless Freundlich's constant.

Langmuir-Freundlich model

$$q_{e,i} = \frac{Q_{LF}(K_{LF}C_e)^{n_{LF}}}{1 + (K_{LF}C_e)^{n_{LF}}} \tag{6.14}$$

Where $Q_{LF,i}$, (mol.kg^{-1}), $K_{LF,i}$ (L.mol^{-1}) and $n_{LF,i}$ are the Langmuir-Freundlich maximum adsorption capacity of adsorbent, equilibrium constant, and dimensionless exponent of the Langmuir-Freundlich model, respectively.

Sips model

$$q_{e,i} = \frac{Q_{Sips,i}K_{Sips,i}C_e^{n_{Sips},i}}{1 + K_{Sips,i}C_{e,i}^{n_{Sips,i}}} \tag{6.15}$$

Where $Q_{Sips,i}$ (mol.kg^{-1}) is the Sips adsorption capacity of the model adsorbent; $K_{Sips,i}$ is the Sips equilibrium constant measured in $(L.mol^{-1})^{n_{Sips}}$; and n_{Sips} is the dimensionless exponent of the Sips model.

Liu model

$$q_{e,i} = \frac{Q_{Liu,i}C_{e,i}^{n_{Liu}}}{K_{Liu}^{n_{Liiu}} + C_{e,i}^{n_{Liu}}} \tag{6.16}$$

Where $Q_{Liu,i}$ (mol.kg^{-1}) is the Liu adsorption capacity of adsorbent; K_{Liu} (mol.L^{-1}) is the Liu constant; and n_{Liu} is the dimensionless exponent of the Liu model.

Khan model

$$q_{e,i} = \frac{Q_{Khan}K_{Khan}C_{e,i}}{\left(1 + K_{Khan}C_{e,i}\right)^{n_{Khan}}} \tag{6.17}$$

Where Q_{Khan} (mol.kg^{-1}) is the Khan maximum adsorption capacity of adsorbent; K_{Khan} (L.mol^{-1}) and n_{Khan} are the Khan equilibrium constant and dimensionless exponent of the Khan model.

Hill model

$$q_{e,i} = \frac{Q_{Hill}C_e^{n_{Hill}}}{K_{Hill} + C_e^{n_{Hill}}} \tag{6.18}$$

Where Q_{Hill} (mol.kg^{-1}) is the Hill maximum adsorption capacity of adsorbent; K_{Hill} $(mol.L^{-1})^{n_{Hill}}$ and $1/K_{Hill}$ $(L.mol^{-1})^{n_{Hill}}$ is the Hill model constant, and the Hill equilibrium constant, respectively; and n_{Hill} is the dimensionless exponent of the Hill model.

Toth model

$$q_{e,i} = \frac{Q_{Toth} K_{Toth} C_e}{\sqrt[n_{Toth}]{1 + (K_{Toth} C_e)^{n_{Toth}}}} \tag{6.19}$$

Where Q_{Toth} (mol.kg^{-1}), K_{Toth} (L.mol^{-1}) and n_{Toth} are the maximum adsorption capacity, the Toth equilibrium constant, and the dimensionless exponent of the Toth model, respectively.

Binary adsorption isotherm studies for the sorption of PFOA and PFOS on CCNT hydrogel beads from aqueous solutions were conducted by employing the competitive extended Langmuir model (6.20) and extended Sips model (6.21) as recommended by Reynel-Avila *et al.* (2016).

$$q_{e,i} = \frac{Q_{ELi} K_{EL,i} C_{e,i}}{1 + \sum_{j=1}^{N} K_{EL,j}\, C_{e,j}} \tag{6.20}$$

$$q_{e,i} = \frac{Q_{ES,i} K_{ES,i} C_{e,i}^{\frac{1}{n_i}}}{1 + \sum_{j=1}^{N} K_{ES,j} C_{e,j}^{\frac{1}{n_j}}} \tag{6.21}$$

Where $Q_{EL,i}$ and $Q_{ES,i}$ are the theoretical maximum biosorption capacities for the extended-Langmuir model and extended Sips model, respectively, measured in mol.kg^{-1}; $K_{EL,i}$ (L.mol^{-1}) and $K_{EL,j}$ (L.mol^{-1}) are the competitive Extended-Langmuir constants for components i and j, respectively; $C_{e,j}$ (mol.L^{-1}) is the equilibrium concentration of component j; $K_{ES,i}$ (L.mol^{-1})$^{1/n}$ and $K_{ES,j}$ (L.mol^{-1})$^{1/n}$ are the Sips constants for component i and j, respectively; n_i and n_j are the Sips constants for component i and j, respectively obtained by fitting of experimental data for the binary adsorption system (Reynel-Avila *et al.* 2016).

6.3.4.3. Thermodynamic studies

According to Zakaria *et al.* (2022), in any typical adsorption process, temperature is one of the crucial parameters that should be optimised using thermodynamic studies for the design of an effective adsorption process. Thermodynamic studies provide essential information related to the nature of the adsorption interaction between model contaminants and adsorbent i.e., determining whether the process involves

exothermic, endothermic, spontaneous or non-spontaneous state (Zakaria *et al.* 2022; Tran *et al.* 2023). Herein, the standard Gibbs free energy change ($\Delta G°$), standard enthalpy change ($\Delta H°$) as well as the standard entropy change ($\Delta S°$) were determined using equations (6.22) to (6.25) (Tran *et al.* 2021).

$$\Delta G° = -RT \ln\left(K_e^{\circ}\right) \tag{6.22}$$

$$\Delta G° = \Delta H° - T\Delta S° \tag{6.23}$$

$$lnK_e^{\circ} = \left(\frac{-\Delta H°}{R}\right)\frac{1}{T} + \frac{\Delta S°}{R} \tag{6.24}$$

$$K_e^{\circ} = \frac{K_{model} C°}{\gamma_{Adsorbate}} \tag{6.25}$$

Where R is the universal gas constant [8.3145 J.mol^{-1}.K^{-1}]; T is the absolute temperature (K); K_e° is the standard thermodynamic equilibrium constant; K_{model} is the equilibrium constant of the adsorption isotherm model measured (L.mol^{-1}); $C°$ is the standard state of solute equivalent to 1 mol.L^{-1}; and $\gamma_{Adsorbate}$ is the activity coefficient of adsorbate in solution (Tran *et al.* 2023). Equation (6.24) is the linear form of the van't Hoff equation obtained by substituting equation (6.22) into equation (6.23), in the linear form of the van't Hoff equation, $\Delta H°$ and $\Delta S°$ are the slope and intercept of the plot of lnK_{eq}° as a function of 1/T, respectively.

6.3.5. Parametric optimisation studies using RSM

Herein, the effect of solution pH, adsorbate initial concentration, adsorbent dose, and interaction time were investigated by employing a standard central composite design (CCD) in RSM by adopting the procedure recommended by Karimifard and Moghaddam (2016) in Design Expert version 11. The CCD within the framework of RSM is used for fitting a quadratic surface by analysing the interactions between selected parameters and optimising the conditions with minimum experiments. Furthermore, the CCD allows for sensitive data for testing the lack of fit without involving a large number of design points which has cemented its application in process optimisation studies (Karimifard and Moghaddam 2016; Madondo, Rathilal and Bakare 2022; Khumalo *et al.* 2023). The codes, ranges, and levels of the investigated parameters which were considered for PFOA and PFOS removal model optimisation are as depicted in Table 6.1.

Table 6.22: Experimental range and levels of independent process variables

Factor	Units	Code	Range and level of factors	
			Low	High
			-1	+1
pH	--	A	4	10
Initial adsorbate concentration	mg/L	B	5	20
Adsorbent dose	g/L	C	0.05	1.5
Time	h	D	2	48

For statistical analysis, the system's response with respect to the independent variables was approximated using equation (6.26) within the framework of RSM and all process variables were coded as X_i (6.27).

$$Y = \beta_0 + \sum_{i=1}^{k} \beta_i X_i + \sum_{i=1}^{k} \beta_{ii} X_i^2 + \sum_{i=1}^{k=1} \sum_{j=i+1}^{k} \beta_{ij} X_i X_j + \varepsilon \quad (6.26)$$

$$X_i = \left(\frac{z_i - z_0}{\Delta z_i}\right)\beta_d \quad (6.27)$$

Where, Y is the predicted response, X_i and X_j are the input variables, β_0, β_i, β_{ii}, and β_{ij}, are the regression constants for the intercept, linear coefficient, quadratic coefficient, and coefficient of regression, respectively; k denotes the number of factors studied and optimized by the experiment and ε accounts for the random error (Khumalo *et al.* 2023); z_i and z_0 denotes the code and uncoded values of the ith independent variable, respectively; β_d is the major coded limit value in the matrix for each variable, and Δz_i is the step-change codification of the value between the low level (-1) and high level (+1). Codification of independent variables was conducted solely for the purpose of normalising the variables. Independent variables may have unique units and orders of magnitude. The codification ensures that all independent variables affect the specified responses evenly. The quality of the fitted model was evaluated by applying the analysis of variance (ANOVA) which compares the variation due to the change in the combination of variable levels with the variation due to random errors inherent to the measurements of the generated responses (Bezerra *et al.* 2008). Hence, from such comparison it was possible to evaluate the significance of the regression to predict the output response considering the sources of experimental variance.

6.4. Results and Discussion

6.4.1. Adsorbent characterization

Herein, the Fourier transform infrared (FTIR) spectra was used to investigate the changes in molecular vibrations of the functional groups of the model adsorbent before and after adsorption. FTIR analyses were conducted at a wavenumber range of 500 cm^{-1} to 4000 cm^{-1} and the findings are depicted in Figure 6.1. For the CCNT adsorbent, the weak absorption peak at 3297 cm^{-1} is attributed to the -OH and -NH_2 stretching vibrations of the polysaccharide within the chitosan structure. The band at 3436 cm^{-1} can be assigned to the -OH functional group resulting from incorporating CNTs. The absorption peaks 1664 cm^{-1} and 1593 cm^{-1} are attributed to the presence of the C=O and -N-H stretching vibrations, respectively confirming the existence of the chitin moiety i.e., -$NHCOCH_3$ in chitosan as a result of using partially deacetylated chitosan flakes as elucidated by Elanchezhiyan *et al.* (2021). The peak at 2884 cm^{-1} can be attributed to the -CH stretching vibration of the chitosan polymer. The peaks at 1028 cm^{-1}, 1387 cm^{-1}, and 1431 cm^{-1} can be assigned to the -C-O-C stretching vibration, -CH group deformation, and -CN stretching vibration, respectively (Elanchezhiyan and Meenakshi 2018). The peaks at 2919 cm^{-1} and 2848 cm^{-1} are attributed to asymmetric CH_2 stretching vibrations of the CNTs, and the peak at 1630 cm^{-1} is assigned to the CNTs conjugated C=C stretching vibrations. Moreover, the weak peaks at 1226 cm^{-1} and 1573 cm^{-1} correspond to C-O-H bending and C=C alkene stretching vibrations from the CNTs, respectively. The strong peaks at 1035 cm^{-1} are assigned to the C-H in-plane bending on the CNTs surface as discussed by Karimifard and Moghaddam (2016). The strong peaks of the functional groups on the surface of CCNTs are attributed to the acid functionalisation of CNTs leading to the release of carbons at the defected sites and end points of the CNTs. The intensity of the bands specifies the successful addition of the desired functional groups which enhance the adsorption performance of the model adsorbent. From the FTIR results, it is apparent that there were changes in the element content as demonstrated by the bands intensity changes, explicitly indicating that there was an uptake of PFOA and PFOS on CCNT hydrogel beads.

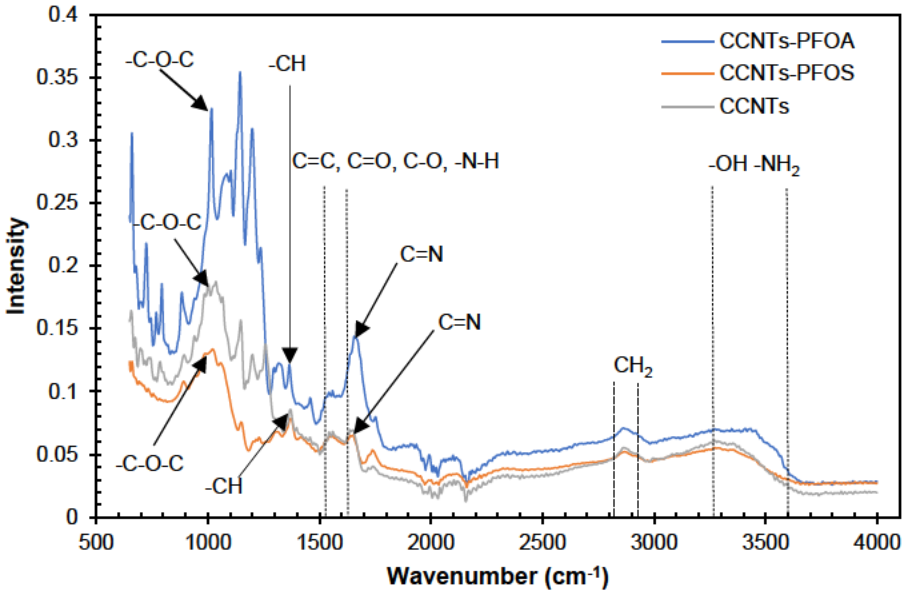

Figure 6.25: FTIR spectra of CCNTs, CCNTs-PFOA and CCNTs-PFOS

6.4.2. Parametric optimisation using CCD in RSM

6.4.2.1. Development of regression model in RSM

Herein, second order quadratic regression models were built to fit the responses of PFOA (Y_1) and PFOS (Y_2) percentage removal by studying the interactions between the dependent variables and independent variables as described by the coded equations (6.28) and (6.29), respectively.

$$Y_1 = 76.27 - 3.50A - 8.89B + 7.72C + 22.50D - 4.12BC - 6.25BD + 5.25CD - 15.11C^2 - 29.11D^2 \quad (6.28)$$

$$Y_2 = 81.70 - 2.78A - 9.22B + 7.83C + 22.72D - 4.192BC - 6.06BD + 5.06CD - 6.85A^2 - 8.35C^2 - 29.35D^2 \quad (6.29)$$

Equations (6.28) and (6.29) are useful in identifying the relative impact of terms and their interactions by comparing their coefficients (Zhan and Zhu 2024). For the coded equations built in RSM, a higher value of the absolute coefficient suggests a more significant impact. It can be inferred from equations (6.28) and (6.29) that factor A (pH) had the least absolute values suggesting the least impact it has on the removal of PFOA and PFOS from solution when compared to the other factors i.e., B (initial adsorbate concentration), C (adsorbent dose), and D (interaction time). On the other hand, based on the absolute values, it is apparent that the term D^2 had the most significant impact on the removal of PFOA and PFOS. The significance of

the models as well as the interactions between independent variables was further analysed by employing the analysis of variance (ANOVA) and model fit statistics as presented in Table 6.2 and Table 6.3.

Table 6.23: ANOVA and fit statistics of the PFOA removal predictive model

Source	**Sum of Squares**	**df**	**Mean Square**	**F-value**	**p-value**	
Model	25489.58	9	2832.18	85.53	< 0.0001	**significant**
A-pH	220.50	1	220.50	6.66	0.0179	
B-PFOA Conc.	1422.22	1	1422.22	42.95	< 0.0001	
C-CCNT dose	1073.39	1	1073.39	32.41	< 0.0001	
D-Time	9112.50	1	9112.50	275.18	< 0.0001	
BC	272.25	1	272.25	8.22	0.0095	
BD	625.00	1	625.00	18.87	0.0003	
CD	441.00	1	441.00	13.32	0.0016	
C^2	786.71	1	786.71	23.76	< 0.0001	
D^2	2919.38	1	2919.38	88.16	< 0.0001	
Residual	662.29	20	33.11			
Cor Total	26151.87	29				
Fit statistics of the quadratic model						
Std. Dev.	**R^2**	**Adjusted R^2**		**Predicted R^2**	**Adeq. Precision**	
5.75	0.9747	0.9633		0.9358	26.6460	

Table 6.24: ANOVA and fit statistics of the PFOS removal predictive model

Source	**Sum of Squares**	**df**	**Mean Square**	**F-value**	**p-value**	
Model	25626.51	10	2562.65	80.29	< 0.0001	**significant**
A-pH	138.89	1	138.89	4.35	0.0507	
B-PFOS Conc.	1530.89	1	1530.89	47.96	< 0.0001	
C-CCNT dose	1104.50	1	1104.50	34.60	< 0.0001	
D-Time	9293.39	1	9293.39	291.16	< 0.0001	
BC	280.56	1	280.56	8.79	0.0080	
BD	588.06	1	588.06	18.42	0.0004	
CD	410.06	1	410.06	12.85	0.0020	
A^2	133.29	1	133.29	4.18	0.0551	
C^2	198.03	1	198.03	6.20	0.0222	

Table 6.3: Continues

D^2	2445.71	1	2445.71	76.62	< 0.0001	
Residual	606.46	19	31.92			
Cor Total	26232.97	29				
Fit statistics of the quadratic model						
Std. Dev.	**R^2**	**Adjusted R^2**		**Predicted R^2**	**Adeq. Precision**	
5.65	0.9769	0.9647		0.9258	25.7068	

Generally, the significance of any process related parameter can be analysed by applying the sum of squares value. Within the framework of the ANOVA, higher sum of squares suggests a significant effect of the corresponding variable in the context of a typical process. It can be inferred from Table 6.2 and Table 6.3 that for the current work, the significance of individual parameters was in the order of interaction time (D) > adsorbate initial concentration (B) > adsorbent dose (C) > solution pH (A). The findings suggest that for the sorption of PFOA and PFOS from solution, the contact time had a significant effect on the adsorption of PFOA and PFOS from solution whilst the solution pH demonstrated a relatively low effect when compared to the other parameters i.e., B, C and D. The relatively low sum of squares recorded for the solution pH does not imply that this parameter had an insignificant effect in the uptake of the model adsorbates. The ANOVA results in terms of the significance of individual parameters are congruent with the physical meaning of the predictive coded models i.e., equations (6.28) and (6.29) built in RSM.

The significance of the quadratic model was evaluated by its F-value which must be higher than the rest of the parameters and its p-value which is the probability value, which must be less than 0.05 as recommended by Alimohammadi *et al.* (2017). From Table 6.2 and Table 6.24 6.3, it is apparent that both the PFOA and PFOS coded predictive models recorded F-values of 85.53 and 80.29, respectively, and p-values of less than 0.0001. The obtained predictive model F-values for both PFOA and PFOS removal implies that the models are significant i.e., there is only 0.01% chance that F-values this large could occur due to noise. Furthermore, the models p-values of less than 0.05 indicate that all model terms are significant. In the case of PFOA and PFOS predictive models i.e., equations (6.28) and (6.29), respectively, all model terms are significant with p-values of less than 0.05 except for A and A^2 having p-values of 0.0507 and 0.0551, respectively (see Table 6.3). The sightly high p-values suggest that terms A and A^2 are the least significant terms in the model i.e., equation (6.29). However, it is worth noting that only model terms with p-values of greater than 0.100 imply not being significant within the framework of RSM. As such, the model does not require any reduction when considering model terms with a p-value of 0.100 or less.

The goodness of fit for the quadratic PFOA and PFOS removal predictive models was evaluated by applying the model fit statistics within ANOVA as depicted in Table 6.2 and Table 6.3, respectively. The significance of the models was measured by considering the coefficient of determination, R^2, adjusted R^2, the adequate precision, and standard deviation (Std. Dev). In the context of ANOVA, R^2 is a statistical parameter which measures the total variation of predicted values to the mean. As such, for a model to exhibit a good prediction efficacy, the value of R^2 must be close to 1 (Montgomery 2017). Therefore, the R^2 values of 0.9747 and 0.9769 for PFOA and PFOS systems, respectively, suggest that the developed predictive models can satisfactorily predict the removal efficiencies for the model adsorbates from solution at a Std. Dev. of ±5.75% (PFOA) and ±5.65% (PFOS). The models' goodness of fit was further tested by considering the adjusted R^2 as a statistical parameter which corrects the R^2 value for a sample size and the number of terms in the model (Alimohammadi *et al.* 2017; Montgomery 2017). It is worth noting that, the value of R^2 increases with an increase in the number of terms in the model, regardless of the significance of the term, whereas values of the adjusted R^2 do not increase with the number of terms but remains smaller than the value of R^2. From the fit statistics in Table 6.2 and Table 6.3 both the PFOA and PFOS systems reported high adjusted R^2 values greater than 0.96 but remained less than the reported R^2 values, suggesting that the developed models satisfactorily predict the desired responses with minimal deviation. On the other hand, the difference of less than 0.2 between the adjusted R^2 and predicted R^2 for both systems under investigation is evident that the predicted R^2 is in agreement with the adjusted R^2. Moreover, from the ANOVA results, it is apparent that the developed models have an adequate ratio of greater than 4, implying an adequate signal. The adequate precision measures the signal to noise ratio, therefore, the obtained ratios of greater than 4 suggest that the developed models can be used to navigate the design space.

6.4.2.2. Model validation

Herein, the developed quadratic models were validated by considering the plots of model predicted PFOA or PFOS percentage removal versus the actual PFOA or PFOS percentage removal as indicated in Figure 6.2 and by conducting a diagnostic test in terms of the plot of externally studentized results versus experimental runs (see Figure 6.3). According to Montgomery (2017) and Khumalo *et al.* (2023), a good prediction can be exhibited from the plot of the responses of the predicted versus actual values which must be randomly scattered not far from the 45° line (Figure 6.26). Data points that are randomly scattered above or below the 45° line indicate areas of over or under prediction, respectively. For the present study, it can be inferred from Figure 6.2 that data points for both the PFOA and PFOS systems are randomly distributed closer to the 45° line implying a significant correlation between the independent variables (i.e., solution pH, PFOA and PFOS initial concentration, CCNT dose, and interaction time) and responses (i.e., PFOA

and PFOS percentage removals). The observed trend in Figure 6.2 is ascribed to the relatively high predicted R^2 values of 0.9358 for PFOA and 0.9258 for PFOS implying a good fit for the developed models. As such, the models demonstrate insignificant errors within the bounds of the operating parameters.

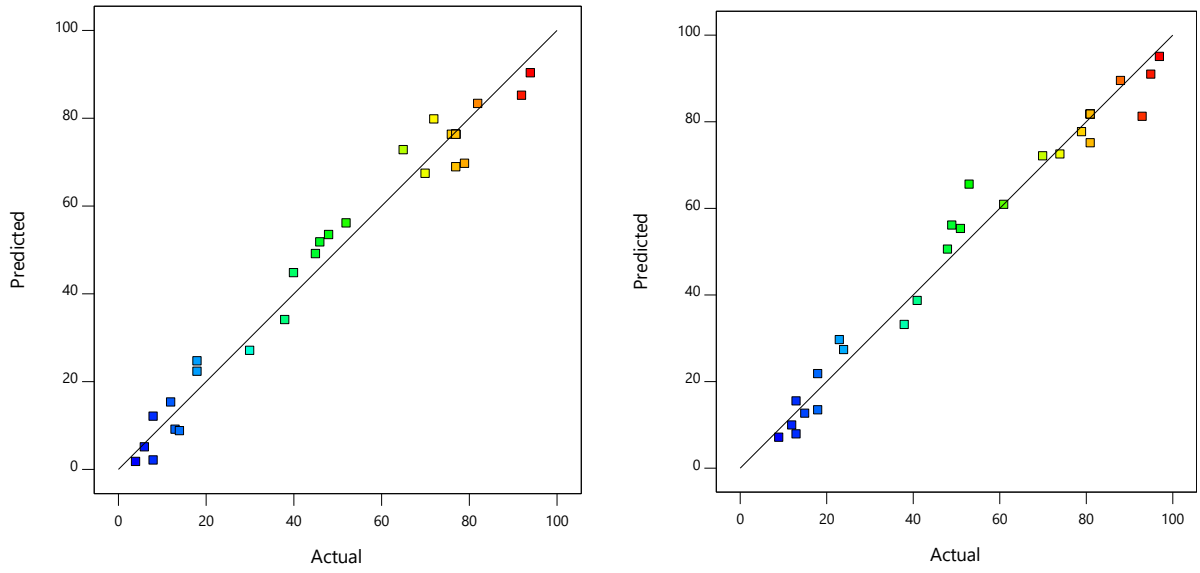

(a) PFOA (b) PFOS

Figure 6.26: Model predicted versus actual PFOA (a) and PFOS (b) removal efficiency.

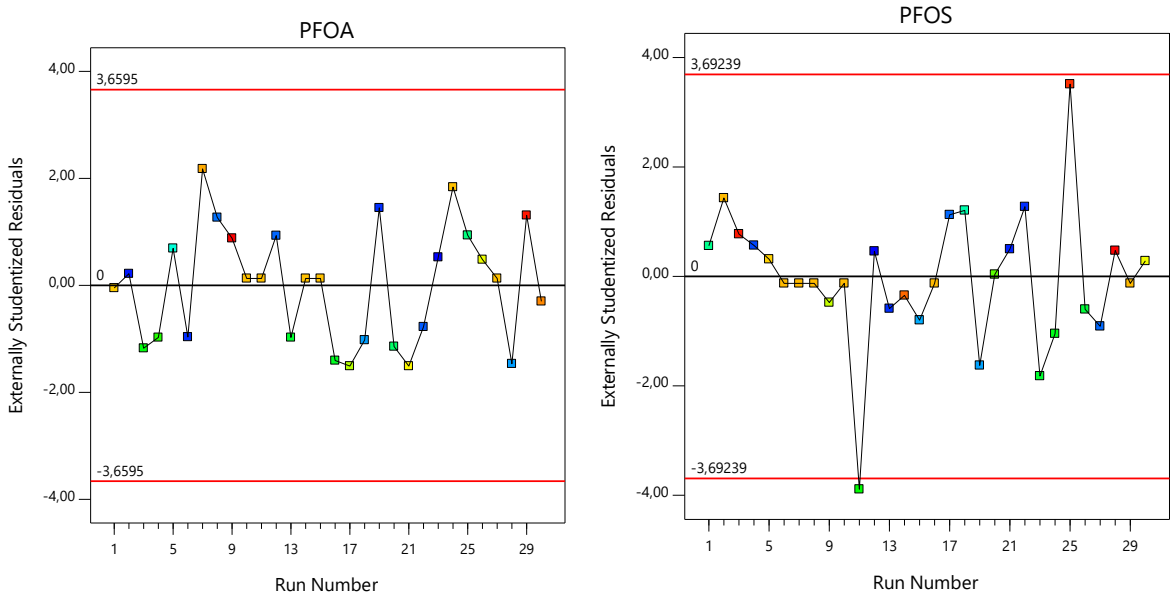

(a) **(b)**

Figure 6.27: Externally studentized residuals versus run number for PFOA (a) and PFOS (b) adsorption system.

The diagnostic plots in terms of the externally studentized residuals versus experimental runs for the adsorption systems of PFOA and PFOS as depicted in Figure 6.3 were applied to check for lurking variables that may have influenced the responses during the experiment. From a statistic point of view, a model will exhibit a good prediction efficiency if the plot of externally studentized residuals versus experimental runs is randomly scattered without demonstrating a specific trend, which is the case for the present study (Figure 6.3). On the other hand, a trend implies a time-related variable lurking in the background. Studentized residuals allow comparison of differences between the observed values and predicted target values in a typical regression model across different predictor values. In other words, an externally studentized residual greater than 4 in the context of the investigation is called an "outlier". An "outlier" or observation with a high leverage exerts influence on the fitted model, biasing the model outputs. Therefore, the developed quadratic models for the sorption of PFOA and PFOS on CCNT hydrogel beads no outliers were observed i.e., all externally studentized residuals were within the residual limit suggesting the responses in terms of PFOA and PFOS percentage removal did not require any transformation (Montgomery 2017).

6.4.2.3. Evaluation of single factor effect on PFOA and PFOS removal

Herein, the effect of single factors i.e., pH, adsorbate concentration, CCNT dose, and interaction time on the responses of PFOA and PFOS removal efficiencies were analysed using the XY plots (see Figure 6.4 and Figure 6.5) based on the predictive models developed in RSM.

Effect of solution pH

In any typical adsorption process, the solution pH plays a crucial role because it affects the degree of ionization of model adsorbates (Elanchezhiyan *et al.* 2021). Moreover, a change in solution pH can also have an effect on the surface charge of the model adsorbent. The influence of solution pH on the sorption of PFOA and PFOS on CCNT was investigated for a pH range of 4 to 10 and the results are presented in Figure 6.4. From Figure 6.4, it can be inferred that an increase in pH from 4 to 10 resulted in a decrease in the percentage removal of PFOA and PFOS implying the dependence of the adsorption process on pH. Highest percentage removals of greater than 80% for both PFOA and PFOS were recorded for a solution pH of 4, suggesting that the adsorbent (i.e., CCNT hydrogel beads) functional groups were protonated under an acidic environment enabling CCNT hydrogel beads to effectively absorb the anionic PFOA and PFOS by strong electrostatic attraction. The acid dissociation constants (pKa) of PFOA and PFOS are reported to be 2.8 and -3.27, respectively (Wang and Shih 2011) which is lower than the pH range of 4 – 10 adopted in the present study allowing PFOA and PFOS to exist in deprotonated forms. On the other hand, the point of

zero charge (pH_{pzc}) for CCNT was found to be 8.5 suggesting that the surface of CCNT is positively charged at a solution pH less than the pH_{pzc}. As such, the observed gradual decrease in PFOA and PFOS removal efficiency with an increase in pH can be ascribed to the reduction in the number of positive sites on the CCNT surface, thus compromising the uptake of PFOA and PFOS by electrostatic interaction. Moreover, CCNT is characterised with different functional groups such as carboxyl, amino, and hydroxyl which easily form a network with the anionic form of PFOA and PFOS via electrostatic interaction under acidic conditions (Elanchezhiyan *et al.* 2021). The findings of the current study are congruent to the work reported by Wang and Shih (2011) on the sorption of PFAS on alumina and Elanchezhiyan *et al.* (2021) on the sorption of PFAS on reduced graphene oxide modified zinc ferrite immobilised chitosan beads. Therefore, the observed trend may suggest the existence of a specific chemical interaction between sulfonate and the CCNT surface on the basis that both PFOA and PFOS were presumably subject to the same electrostatic influence.

However, it is worth noting that the decrease in PFOA and PFOS removal with increasing pH was not significant i.e., a removal efficiency of less than 10% was observed over a pH variation of 4 to 10. The observed trend suggests that the sorption of PFOA and PFOS on CCNT is not solely dependent on the electrostatic interaction forces but also on other sorption mechanisms such as pore-filling and hydrophobic interaction as reported in literature (Zhi and Liu 2015).

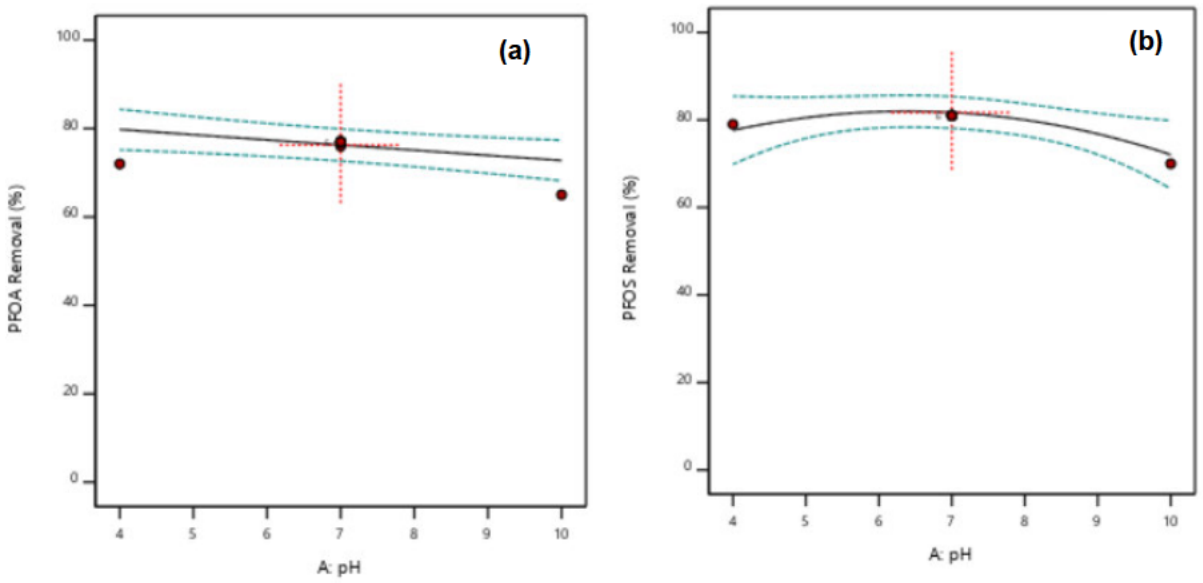

Figure 6.28: XY plots for the effect of pH on PFOA **(a)** and PFOS **(b)** percentage removal

Adsorbate initial concentration

The findings of the present study on the effect of initial adsorbate concentration on the percentage removal of PFOA and PFOS are presented in Figure 6.5. It is apparent that an increase in initial adsorbate concentration resulted in a gradual decrease on the percentage removal of PFOA and PFOS. The observed trend can be ascribed to the mere fact that at higher concentrations, the number of adsorbate molecules ratio to the available adsorption sites is relatively high subsequently compromising the removal efficiency. As such, the highest removal efficiencies for both PFOA and PFOS were recorded for an adsorbate initial concentration of 5 $mg.L^{-1}$ due to the large number of available adsorption sites compared to the adsorbate molecules to be adsorbed on the adsorbate surface. Moreover, it is apparent that the model adsorbent demonstrated higher affinity for PFOS as compared to PFOA which is ascribed to the more hydrophobic nature of PFOS as compared to PFOA suggesting that the uptake of PFOS on CCNT hydrogel beads is through hydrophobic interactions and electrostatic attraction (Zhang *et al.* 2011).

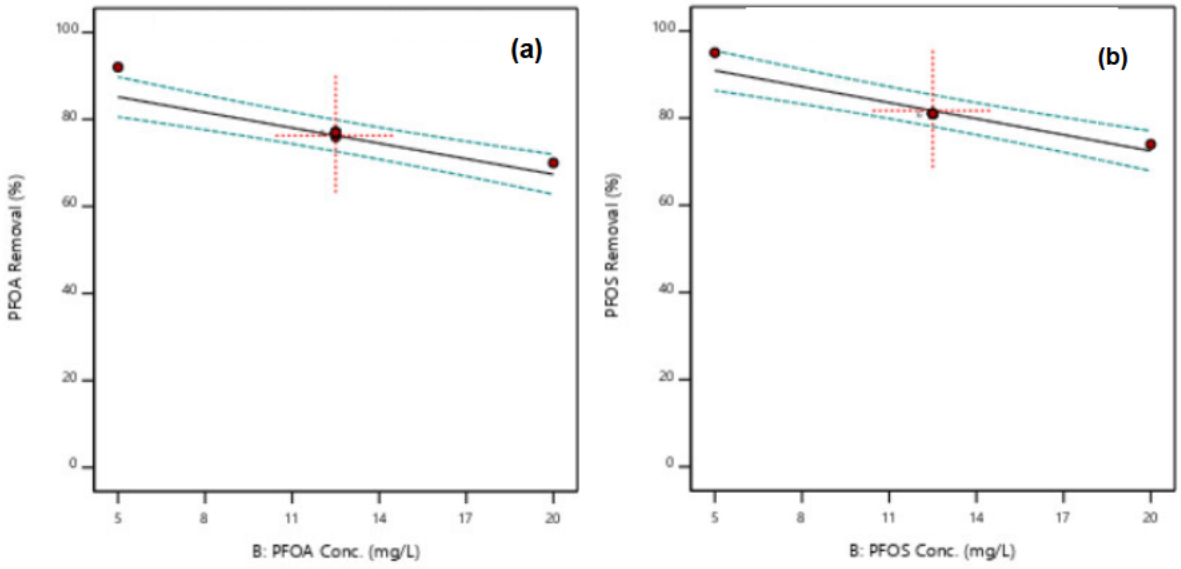

Figure 6.29: XY plots for the effect of adsorbate initial concentration on PFOA **(a)** and PFOS **(b)** percentage removal

Adsorbent dose

From Figure 6.6 it can be inferred that the percentage removal of PFOA and PFOS increased with an increase in CCNT hydrogel beads dose over a range of 0.05 $g.L^{-1}$ to 1.5 $g.L^{-1}$. The observed trend can be ascribed to the mere fact that increasing the adsorbent dosage results in an increase in the adsorption surface

area, subsequently augmenting the number of adsorption active sites available for the adsorption of the model adsorbates. It can be inferred from Figure 6.6 that the highest PFOA and PFOS percentage removal was achieved for a CCNT dose of 1.5 $g.L^{-1}$ for both PFOA and PFOS. However, it is worth noting that an increase on adsorbent dose above 0.775 $g.L^{-1}$ did not record a rapid percentage uptake of PFOA and PFOS on CCNT at a fixed adsorbate concentration. The plateau on PFOA and PFOS removal in relation to the CCNT dose variation above 0.775 $g.L^{-1}$ is evident that beyond an adsorbent dose of 0.775 $g.L^{-1}$, PFOA removal was not significantly affected any further. However, the uptake of PFOS improved by 10% when the adsorbent dose was increased from 0.775 $g.L^{-1}$ to 1.5 $g.L^{-1}$. The findings of the current study suggests that high percentage removals of PFOA and PFOS can be achieved at an adsorbent dose of 1.5 $g.L^{-1}$.

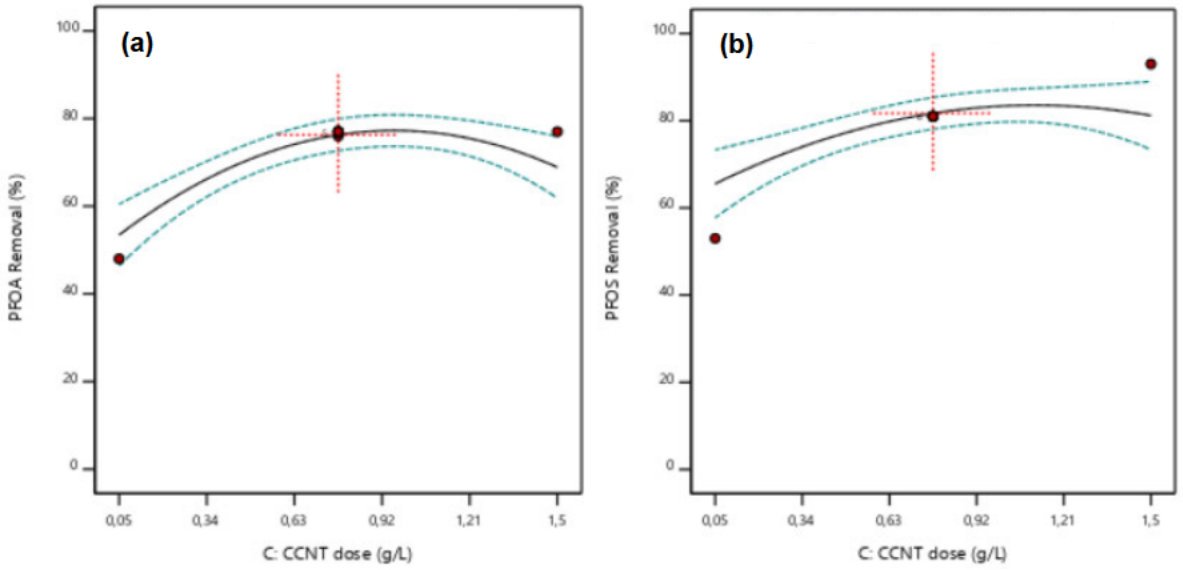

Figure 6.30: XY plots for the effect of adsorbent dose on PFOA **(a)** and PFOS **(b)** percentage removal

Contact time

The effect of contact time on the percentage removal of PFOA and PFOS from solution was investigated at a range of 2 - 48 hours as depicted in Figure 6.7. From the findings of the present study, it is apparent that the removal efficiency of PFOA and PFOS increased with an increase in contact time. As such, the observed trend can be ascribed to the fact that in a typical solid-liquid adsorption process, the rate of adsorption increases with an increase in contact time due to the availability of free adsorption sites on the surface of the model adsorbent. It was anticipated that, after a definite period, the adsorption rate decreases due to the unavailability of active sites on the adsorbent surface. Therefore, the findings of the current study on the effect of contact time suggest that for the investigated system, a large composition of CCNT active sites were occupied by PFOA and PFOS at a contact time of 25 hours. A decline in the percentage removal rate

of PFOA and PFOS was observed after 25 hours which is evident from the relatively low percentage removal rate between a contact time of 25 hours and 48 hours of contact time as depicted in Figure 6.7.

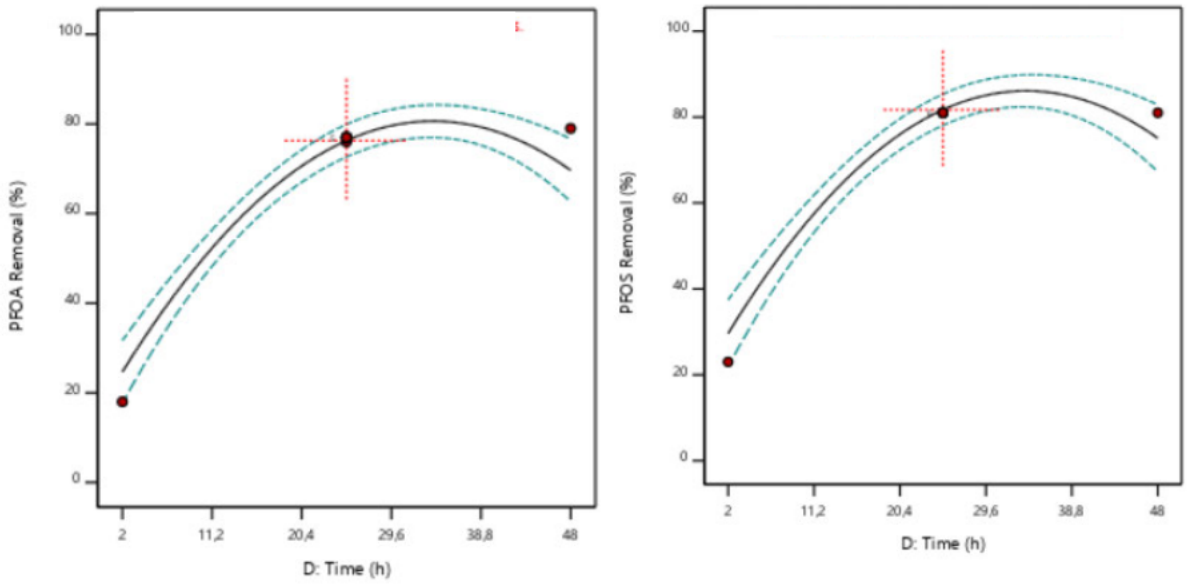

Figure 6.31: XY plots for the effect of contact time on PFOA **(a)** and PFOS **(b)** percentage removal.

6.4.2.4. Evaluating the effect of interactive factors on PFOA and PFOS removal

The interaction effect of independent variables i.e., contact time, CCNT dose, and adsorbate concentration on the removal of PFOA and PFOS was evaluated using 3D response surface plots in RSM as depicted in Figure 6.8. The fundings of the present study on the interaction effects between contact time and adsorbent dose on the removal of PFOA and PFOS are presented in Figure 6.8a and Figure 6.8b, respectively, for a contact time range of 2 – 48 hours and CCNT dose of 0.05 – 1.5 g/L. The findings of the current study suggest a strong correlation between the initial adsorbate concentration (i.e., PFOA and PFOS) and adsorbent dose, such that an increase in CCNT dose and contact time result in an increase in PFOA and PFOS removal. Highest PFOA and PFOS removals were recorded for a CCNT dose of 1.5 g/L at a contact time of 48 hours. Similarly, with the 3D surface plots there was a minimal improvement on the uptake of PFOA and PFOS post a contact time of 25 hours. This is evident from Figure 6.8a and Figure 6.8b in which the 3D plots formed almost a plateau beyond a contact time of 25 hours indicating a slow uptake rate of PFOA and PFOS. Furthermore, it can be inferred from the curved edges of the 3D surface plots that an increase in contact time and adsorbent dose results in an increase in the percentage removal of PFOA and PFOS, confirming significant interaction effects between contact time and adsorbent dose in the percentage uptake of the model adsorbates.

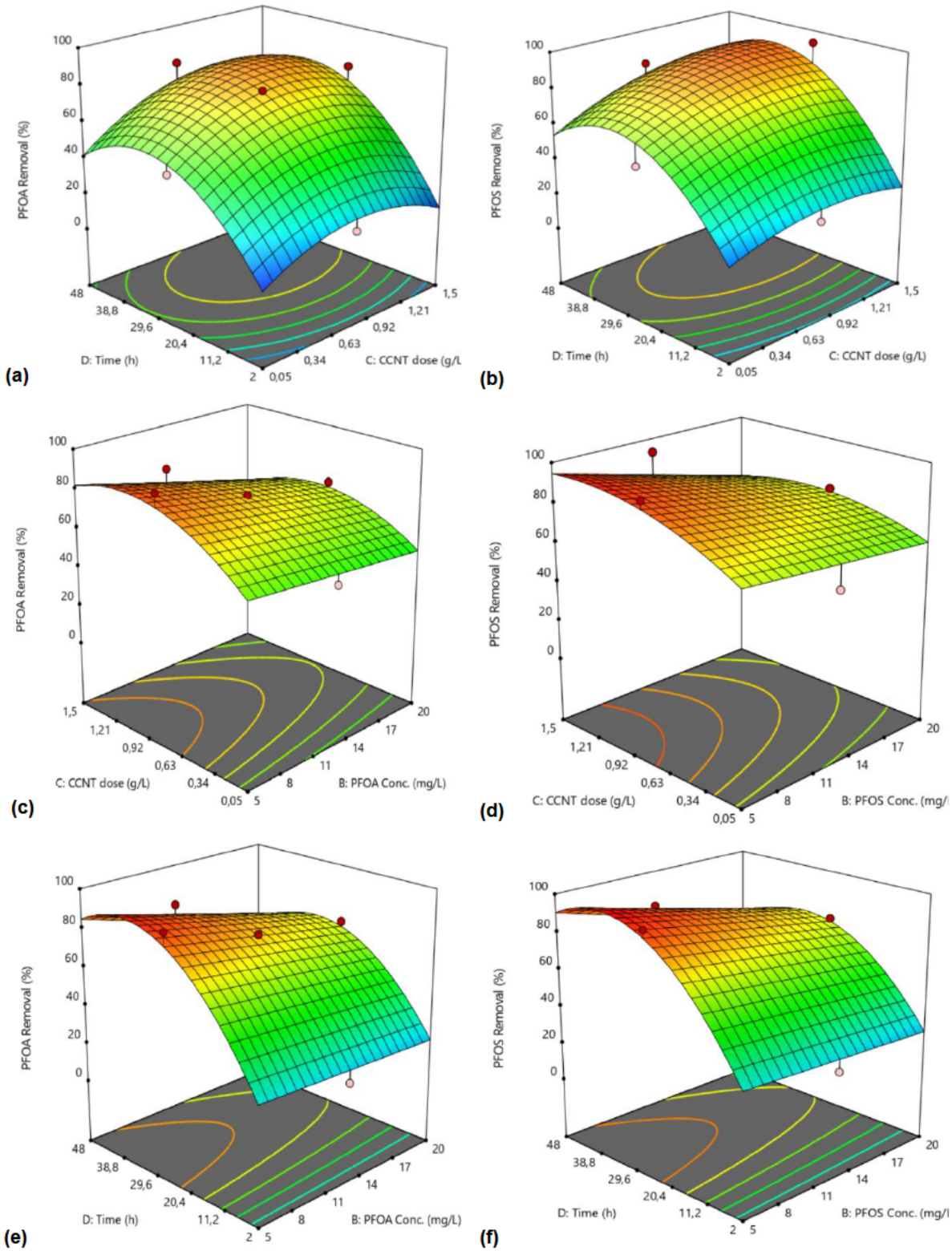

Figure 6.32: 3D surface plots for the interactions between time and CCNT dosage **(a)** and **(b)**, CCNT dose and adsorbate concentration **(c)** and **(d)**, and time and adsorbate concentration **(e)** and **(f)** on PFOA and PFOS removal.

Figure 6.8c and Figure 6.8d present the interactive effect between CCNT dosage and initial adsorbate concentration on the percentage removal of PFOA and PFOS. From the ANOVA results presented in Table 6.2 and Table 6.3, the interaction between CCNT and the adsorbate concentration recorded p-values of 0.0095 and 0.0080 for PFOA and PFOS, respectively which was less significant than the effect between time and CCNT as well as time and initial adsorbate concentration. This is evident from the 3D plots in Figure 6.8c and Figure 6.8d. An increase in PFOA and/or PFOS initial concentration from 5 $mg.L^{-1}$ to 20 $mg.L^{-1}$ with an increase in CCNT dosage did not have a significant effect on the percentage removal of PFOA or PFOS which is indicated by the flat surface of the 3D plots as indicated in Figure 6.8c and Figure 6.8d. On the other hand, there was a gradual increase in PFOA and PFOS removal with an increase in CCNT dose from 0.05 $g.L^{-1}$ to 1.5 $g.L^{-1}$ for a fixed adsorbate concentration of 5 $mg.L^{-1}$.

Similarly, it is apparent from Figure 6.8e and Figure 6.8f, for an adsorbate concentration of 5 $mg.L^{-1}$, there was a significant uptake in PFOA and PFOS with an increase in contact time up to 25 hours. Post 25 hours of contact time, no significant uptake on PFOA and/or PFOS was observed as indicated by the plateau. The observed trend from the 3D plots on the interaction between contact time and initial adsorbate concentration can be cemented by the recorded p-values of 0.0003 (PFOA) and 0.0004 (PFOS) indicating a significant effect of the interaction between contact time and adsorbate concentration for the uptake of PFOA and PFOS on CCNT hydrogel beads. Therefore, it can be inferred from Figure 6.8 and the ANOVA results in Table 6.2 and Table 6.3 that the interactions between contact time and CCNT dosage, adsorbate initial concentration and CCNT dosage as well as contact time and adsorbate initial concentration had a significant effect on the uptake of PFOA and PFOS by CCNT from solution.

6.4.2.5. Optimisation of PFOA and PFOS adsorption on CCNT hydrogel beads

Optimisation studies for the uptake of PFOA and PFOS on CCNT hydrogel beads were conducted to ascertain optimal conditions for maximum removal of PFOA and PFOS. Herein, the developed quadratic models (i.e., (28) and (29)) in RSM were used to determine the optimal levels of each factor (i.e., pH, adsorbate initial concentration, CCNT dose and contact time) for the maximum uptake of PFOA and PFOS as depicted in Figure 6.9. RSM gave 100 conditional solutions with 100% desirability at 95% confidence level. Herein, the desirability function in RSM was applied on the basis that the quality of the responses of the adsorption process having four input variables is completely unacceptable if one of the variables is outside of the desirable limit. As such, by employing the desirability function, it allows to find operating conditions that ensure compliance with the criteria of all the involved responses at the same time providing the best value of compromise in the desirable joint response as elucidated by Candioti *et al.* (2014). For the sorption of PFOA and PFOS on CCNT hydrogel beads, the desirability was achieved by converting the

multiple responses into a single one, combining the individual responses into a composite function followed by its optimisation within the framework of RSM (Candioti *et al.* 2014).

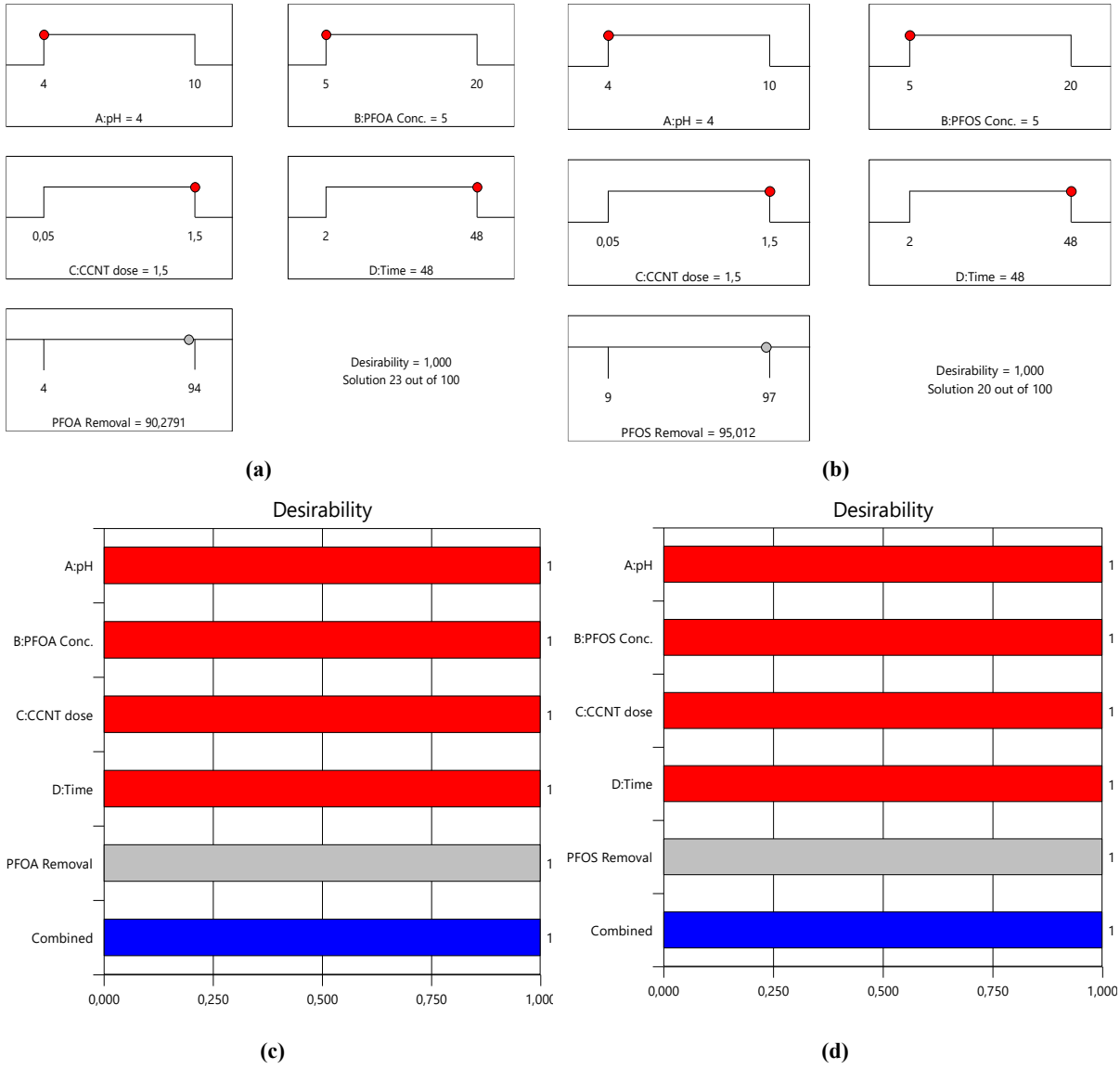

Figure 6.33: Desirability ramp plots and bar plots for the maximum removal of PFOA and PFOS.

In RSM, an individual desirability function for each response was created using the fitted response models thus establishing the optimisation criteria. It is worth noting that the desirability function opts for the values between 0 (undesirable response) and 1 (completely desirable response). Desirability intermediate values may indicate more or less desirable responses. The final optimum levels for the input factors to achieve

maximum PFOA and PFOS were generated as depicted in the ramp plots Figure 6.9a and Figure 6.9b. Moreover, the desirability plots (Figure 6.9c and Figure 6.9d) suggest that all input factors as well as the responses in terms of PFOA and PFOS uptake had a full desirability of 1, resulting in perfect combined desirability of 1.

6.4.3. Adsorption kinetic studies

6.4.3.1. Single adsorption kinetic studies

Herein, the single adsorption of pseudo-first order (PFO) and pseudo-second order (PSO) kinetic models were employed in studying the mechanism interaction of PFOA and PFOS on CCNT hydrogel beads as an adsorbent. The competing PFO and PSO kinetic models were subjected to statistical analysis to determine the kinetic model that best fitted the experimental data. The models and statistical parameters are presented in Table 6.4. From Table 6.4, Figure 6.10 and Figure 6.11. It can be inferred that for both the PFO and PSO nonlinear kinetic models, no significant difference was observed between the experimental and calculated PFOA and PFOS uptake at equilibrium (q_e) affirming that the kinetic models well fitted the experimental data. However, the nonlinear PFO kinetic model gave higher R^2 values of 0.986 and 0.982 for the uptake of PFOA and PFOS on CCNT hydrogel beads, respectively, when compared to the PSO kinetic model which gave R^2 values of less than 0.9 for both systems (i.e., PFOA and PFOS). Similarly, the difference of less than 0.2 between the R^2 values and adj. R^2 values for the PFO and PSO kinetic models suggest a reasonable agreement between the models' parameters. Therefore, the high R^2 and adj.R^2 values suggest that the nonlinear PFO kinetic model best fitted the experimental data for the sorption of PFOA and PFOS on CCNT.

Table 6.25: PFO and PSO kinetic models' parameters for PFOA and PFOS sorption on CCNT.

PFAS	**Pseudo-first order model**		**Pseudo-second-order model**	
	Parameter	**Value**	**Parameter**	**Value**
PFOA	$q_{e,exp}$ (mg.g^{-1})	2.66	$q_{e,exp}$ (mg.g^{-1})	2.66
	q_{e1} (mg.g^{-1})	2.74	q_{e2} (mg.g^{-1})	2.81
	k_1 (h^{-1})	0.079	k_2 (g.mg^{-1}.h^{-1})	0.062
	R^2	0.986	R^2	0.893
	Adj. R^2	0.985	Adj. R^2	0.883
	χ^2	6.53E-04	χ^2	5.89E-03
	BIC	-113	BIC	-62

Table 6.4: Continues

PFOS	$q_{e,exp}$ (mg.g^{-1})	2.79	q_e,exp (mg.g^{-1})	2.79
	q_{e1} (mg.g^{-1})	2.81	q_{e2} (mg.g^{-1})	2.82
	k_1 (h^{-1})	0.085	k_2 (mg.g^{-1})	0.066
	R^2	0.982	R^2	0.894
	Adj. R^2	0.981	Adj. R^2	0.884
	χ^2	8.79E-03	χ^2	0.064
	BIC	-107	BIC	-62

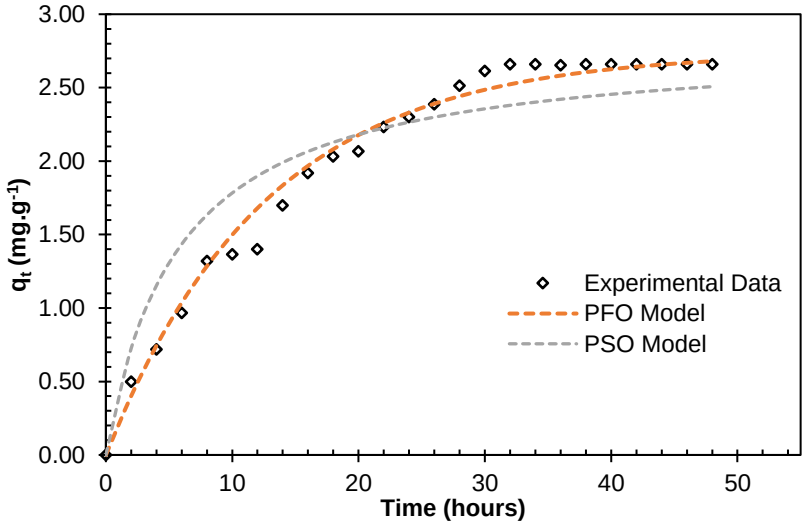

Figure 6.34: PFOA adsorption kinetics profile

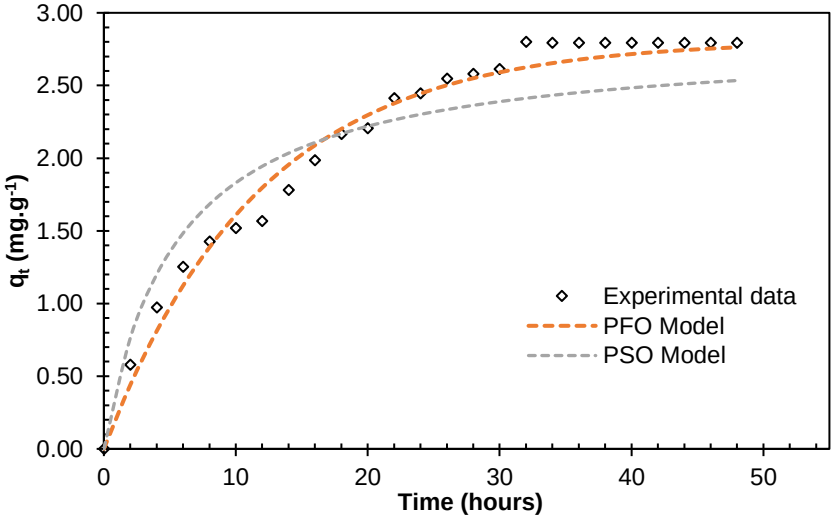

Figure 6.35: PFOS adsorption kinetics profile

Moreover, the chi-squared test and BIC were employed for model validation between the competing PFO and PSO kinetic models. In the chi-squared test, the squares of the differences between the experimental data and calculated data using the models are divided by the corresponding data obtained and then summed. Therefore, if the data obtained using a model are similar to the experimental data, the chi-squared value (χ^2) is close to zero. On the other hand, high χ^2 values suggest high biasness between the experiment and the model. From Table 6.4, it is apparent that the PFO kinetic model recorded lower χ^2 values (i.e., 6.53E-04 and 8.79E-03 for PFOA and PFOS, respectively) when compared to the PSO (i.e., 5.89E-03 and 0.064 for PFOA and PFOS, respectively) affirming that the PFO kinetic model best fitted the experimental data. Moreover, the difference of the BIC value for PFO and BIC value for PSO (i.e., ΔBIC) was employed in evaluating the best model fit as recommended by Raftery (1995). The guidelines outlined by Raftery (1995) for competing models, indicates that ΔBIC range of $1 \leq \Delta BIC \leq 3$ suggest an insignificant difference between the competing models, a range of $3 \leq \Delta BIC \leq 10$ suggest positive evidence that the model with a lower BIC is suitable, a range of $10 \leq \Delta BIC \leq 100$ suggest a strong evidence that the model with a lower BIC value is suitable, and when ΔBIC is greater than 100 it is decisive that the model with a lower BIC is suitable. For the present study ΔBIC values of 51 and 44 were obtained for the sorption of PFOA and PFOS, respectively, suggesting that the adsorption studies experimental data was best fitted by the nonlinear PFO kinetic model.

The findings of the present study suggest that the uptake of PFOA and PFOS on CCNT hydrogel beads from aqueous solutions is governed by the diffusion process as the rate-limiting step. Therefore, the uptake mechanism of the model contaminants does not depend on the concentration of both reactants (i.e., PFOA or PFOS and water) but only on the concentration of the model adsorbate, hence the PFO is considered to be controlled by physisorption (Agbovi and Wilson 2021). Herein, the Weber-Moris empirical model was applied in ascertaining the rate controlling mechanism for the uptake of PFOA and PFOS on CCNT hydrogel beads. In a typical adsorption process, if the plot of q_t as a function of $t^{0.5}$ yields a straight line, intraparticle diffusion is involved during the adsorption process (Weber Jr and Morris 1963). For the present study, the plot of the Weber-Moris empirical model (Figure 6.12) did not yield a straight line, suggesting that the uptake of PFOA and PFOS is a complex process, and that other mechanisms along with intraparticle diffusion control the process steps. During the external mass transfer phase, the constant C of the Weber-Moris model is approximately zero indicating the insignificant effects of the boundary layer diffusion on the uptake of PFOA or PFOS. However, PFOA and PFOS were adsorbed on the surface of CCNT hydrogel beads. The intraparticle phase suggests that PFOA and PFOS were diffused into the model adsorbent, and lastly, the equilibrium state indicates that PFOA and PFOS were adsorbed in the active sites of the CCNT

hydrogel beads. Therefore, it can be inferred from Figure 6.12 that the last two zones were the rate limiting steps for the sorption of PFOA and PFOS on CCNT hydrogel beads.

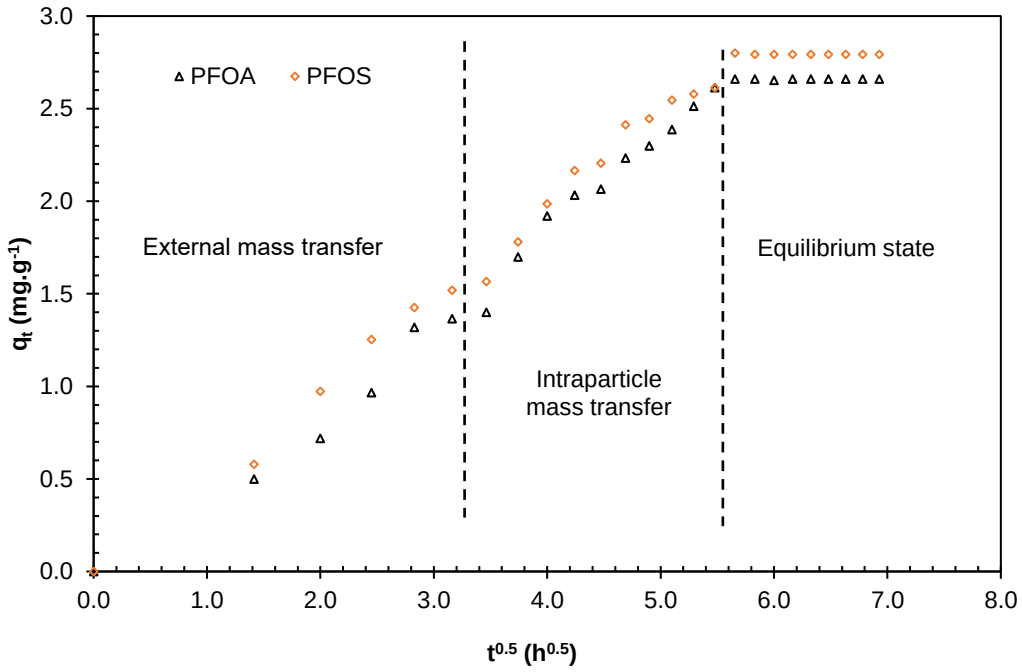

Figure 6.36: Weber-Morris kinetic model curves for PFOA and PFOS sorption of CCNT

However, it is worth noting that adsorption mechanisms cannot be directly assigned based on observing kinetic experimental data or by fitting kinetic models such as the PFO and PSO. It is necessary to confirm adsorption mechanisms by means of several analytical techniques (i.e., FTIR, scanning electron microscopy, thermogravimetric analyser, nitrogen adsorption-desorption isotherms, Raman spectroscopy and X-Ray diffraction analysis) together with adsorptive thermodynamic data (i.e., changes in enthalpy and entropy) as well as activation- and adsorption-energies as elucidated by Tran *et al.* (2017) in their recent review "*mistake and inconsistencies regarding adsorption of contaminants from aqueous solutions*".

6.4.4. Adsorption isotherm studies

6.4.4.1. Single adsorption

Herein, adsorption isotherm studies were conducted for a temperature variation of 283 K, 293 K and 303 K aimed at gaining some insight on the equilibrium performance of the adsorbent (i.e., CCNT hydrogel beads) on the uptake of PFOA and PFOS at constant temperature. Generally, predictions of the overall

adsorption behaviour can be done by modelling the isotherms data by linear analysis as a mathematical approach. However, recently done studies (Al-Ghouti and Da'ana 2020) on the guidelines for the use and interpretation of adsorption isotherm models have indicated that discrepancies between the experimental data and predictions could be caused by linear analysis of the isotherm data. As such, for the current study, experimental data were fitted in nonlinear adsorption isotherm empirical models i.e., Henry isotherm model (6.11), Langmuir isotherm model (6.12), Freundlich isotherm model (6.13), Langmuir-Freundlich isotherm model (6.14), Sips isotherm model (6.15), Liu (6.16), Khan isotherm model (6.17), Hill isotherm model (6.18) and Toth isotherm model (6.19). All model parameters are presented in Table 6.5. Herein, sensitivity analysis was conducted in assuring that isotherm model parameter values were optimised. Sensitivity analysis was performed by 1) initialising each model parameter with the minimum possible value of the objective function i.e., sum of squared error (SSE); 2) the nonlinear regression analysis was then applied aimed at finding the optimal solution that minimise the objective function; 3) the perturbation concept was then applied whereby one parameter was modified at a time while keeping other parameters constant; 4) where necessary re-estimation of the objective function was performed for each perturbation, and the global minimum was obtained when the perturbation for all model parameters was 0%. On the other hand, if the model parameter does not yield a global minimum at the 0% perturbation, that will suggest a poor non-linear regression analysis based estimation of the values of the model parameters as discussed by Al-Ghouti and Da'ana (2020) and Mukhtar *et al.* (2020). Furthermore, model evaluation was accomplished by applying the coefficient of determination (R^2), adjusted coefficient of determination (adj. R^2) and the chi-square test (χ^2).

From the isotherm tests presented in Table 6.5, it is evident that all adsorption isotherm models gave relatively high R^2 values for the single adsorption of PFOA and PFOS on CCNT hydrogel beads. PFOA experimental data was better fitted in the order of Khan ≈ Liu ≈ Freundlich > Toth > Langmuir-Freundlich > Sips ≈ Hill > Langmuir > 0.836. On the other hand, the experimental data for the uptake of PFOS was better fitted in the order of Khan ≈ Freundlich > Toth > Langmuir-Freundlich ≈ Sips ≈ Hill ≈ Liu > Langmuir > Henry. For both the uptake of PFOA and PFOS, the Freundlich adsorption isotherm recorded relatively high R^2 and adj. R^2 values (i.e., $R^2 = 0.991$ for PFOA; $R^2 = 0.997$ for PFOS; adj. $R^2 = 0.998$ for PFOA and adj. $R^2 = 0.996$ for PFOS), cementing that experimental data were better fitted by the Freundlich adsorption isotherm model. Moreover, there was an insignificant difference between the experimental and predicted adsorption capacities for both the uptake of PFOA and PFOS on CCNT hydrogel beads suggesting that the isotherm data was well fitted in all investigated isotherm models.

The supremacy of the Freundlich isotherm model suggests that the uptake of PFOA and PFOS on CCNTs was not restricted to the monolayer adsorption process. As such the adsorption heat and affinities were not

uniformly distributed on the heterogeneous surface of CCNTs as a model adsorbent (Al-Ghouti and Da'ana 2020). Moreover, the supremacy of the Freundlich adsorption isotherm model defines the heterogeneity of the CCNT hydrogel beads surface as well as the exponential distribution of the active sites together with the energy of the active sites. It is worth noting that the Freundlich adsorption isotherm model demonstrates that at varying adsorbate concentrations, the ratio of the adsorbate onto the certain adsorbent mass to the solute is not constant. As such, during the uptake of PFOA and PFOS from solution on CCNT hydrogel beads, the stronger binding sites were occupied by both PFOA and PFOS. Thereafter, an exponential decline in the adsorption energy occurred upon completing the adsorption process as elucidated by Zeldowitsch (1934) and Al-Ghouti and Da'ana (2020). From the Freundlich model parameters i.e., K_F and n_F values, the type of isotherm can be determined. It is worth noting that K_F and n_F denotes the intensity of the adsorption and/or surface heterogeneity indicating the energy relative distribution as well as the adsorbate sites' heterogeneity (Al-Ghouti and Da'ana 2020). According to Hu *et al.* (2023), the obtained n_F values of less than 1 denotes prolonged mass transfer zones due to the slow uptake of PFOA and PFOS on CCNTs. As such, for the present work, isotherm studies were conducted for a contact time of 168 hours to compensate for the slow uptake of PFOA and PFOS on CCNT hydrogel beads. Moreover, the obtained values of n_F of less than 1, suggest that the adsorption process was indeed favourable and reversible.

From Table 6.5, it can be inferred that the Khan adsorption isotherm empirical model also recorded relatively high R^2 and adj. R^2 values of 0.998 and 0.997, respectively, for the uptake of PFOA and PFOS on CCNT hydrogel beads. Similarly, the Liu isotherm adsorption model also recorded high R^2 and adj. R^2 values of 0.999 and 0.998, respectively, for the uptake of PFOA. According to Al-Ghouti and Da'ana (2020) and Ribas *et al.* (2020), the Khan and Liu isotherm models are a combination of the Langmuir and Freundlich isotherm models, with the exception that the infinite adsorption assumption from the Freundlich model and the monolayer assumption of the Langmuir model are jettisoned, suggesting that adsorbates (i.e., PFOA and PFOS) molecules were able to occupy certain active sites on the surface of CCNT hydrogel beads. This can be confirmed from the FTIR results in Figure 6.1 with the change in the absorbing intensity after adsorption. On the other hand, Al-Ghouti and Da'ana (2020) reported that when the value of the equilibrium concentration is relatively large, the Khan model reduces to the Freundlich adsorption isotherm, and it reduces to the Langmuir isotherm model when the value of n_{Khan} is tantamount to a unit. On the basis that for the present work, the values of n_{Khan} obtained with temperature variation (see Table 6.5) did not equate to a unit, the Freundlich isotherm model was considered as the governing isotherm in fitting the experimental data which was cemented by the χ^2 values of less than 0.01 and R^2 values of greater than 0.99 for the single sorption of PFOA and PFOS.

Furthermore, the Langmuir isotherm model recorded lower R^2 values when compared to the Freundlich isotherm model of 0.936 and 0.913 for the uptake of PFOA and PFOS, respectively, which are still good correlations of determination. The Langmuir isotherm model is based on four fundamental underlying assumptions i.e., 1) the monolayer adsorption occurs on the structurally homogeneous surface of the adsorbent; 2) each adsorption site can only accommodate one adsorbate molecule, 3) all adsorption sites are energetically equivalent and independent, and 4) there is no interaction between adsorbate molecules adsorbed on neighbouring sites (Hu *et al.* 2023). As such, the relatively low values of R^2 and adj. R^2 recorded by the Langmuir isotherm model as compared to the Freundlich isotherm model suggest that the aforementioned mechanisms were not dominant during the uptake of PFOA and PFOS on CCNTs. It should be noted that the aforementioned mechanisms are not explicitly accounted for in the present work. Similarly, the Toth adsorption isotherm recorded relatively high R^2 values of 0.988 and 0.978 for the uptake of PFOA and PFOS, respectively. The Toth isotherm model is an empirical modified version of the Langmuir isotherm model as explained by Al-Ghouti and Da'ana (2020). The Toth model is used for the description of heterogenous adsorption systems satisfying the low and high adsorbate concentrations (Al-Ghouti and Da'ana 2020). For the present work, the Toth dimensionless exponents are not equal to a unit for both PFOA and PFOS indicating the heterogeneity of the adsorption system under investigation (Podder and Majumder 2016), suggesting that PFOA and PFOS molecules were adsorbed onto the active sites with relatively high energy. As the adsorption process progresses, the adsorbate molecules (i.e., PFOA and PFOS) were adsorbed onto sites with decreasing energy subsequently leading to a decline in the amount adsorbed (Do 1998), thus incepting the state of equilibrium.

Moreover, the Sips adsorption isotherm model gave relatively high R^2 values of 0.968 and 0.960 for the uptake of PFOA and PFOS on CCNTs, respectively. It is worth noting that the Sips isotherm model incorporates essential characteristics of the Langmuir and Freundlich models. The parameter n_{Sips} is a measure of the system's heterogeneity which can be attributed from the solid or the adsorbate or a combination of both as indicated by Do (1998) and Hu *et al.* (2023). The n_{Sips} values of greater than 1 reported for the current work for the uptake of PFOA and PFOS confirms the heterogeneity of the system under investigation (Hu *et al.* 2023). The R^2 values of greater than 0.9 is evident enough that the Sips isotherm model was able to fit isotherms data with an increase in concentration. Similarly, the Hill adsorption isotherm gave R^2 values of greater than 0.9 for both the uptake of PFOA and PFOS on CCNTs. The Hill's model is derived on the basis that the adsorption process is a cooperative phenomenon (Al-Ghouti and Da'ana 2020). As such, the relatively high values of R^2 suggests that molecules of PFOS and PFOA were able to bind on one site on the adsorbent, subsequently influencing other binding sites on the surface of the adsorbent. Moreover, the obtained model parameter i.e., n_{Hill} of greater than 1 suggests that

the binding of the model adsorbates had a positive cooperativity thus cementing the binding of PFOA and PFOS on CCNT hydrogel beads surface.

Table 6.26: Single adsorption isotherm model parameters for the uptake of PFOA and PFOS on CCNTs.

		PFOA			PFOS		
Isotherms model	**Model parameters**	**283 K**	**293 K**	**303 K**	**283 K**	**293 K**	**303 K**
Henry model	K_{Henry} (L.kg^{-1})	1330	1409	1512	1459	1650	1823
	R^2	0.836	0.79	0.695	0.828	0.679	0.585
	Adj. R^2	0.816	0.764	0.657	0.806	0.638	0.533
	χ^2	9.63E-02	0.116	0.151	0.106	0.164	0.201
Langmuir model	Q_L (mol.kg^{-1})	0.0580	0.0540	0.0546	0.0454	0.0466	0.0481
	K_L (L.mol^{-1})	69 265	93 977	111 249	112 914	150 169	179 706
	R^2	0.936	0.914	0.934	0.913	0.946	0.951
	Adj. R^2	0.918	0.890	0.915	0.888	0.931	0.937
	χ^2	4.68E-03	1.72E-02	2.12E-02	1.52E-02	1.91E-02	2.31E-02
Freundlich model	K_F [(mol/kg)/(mol/L)^{nF}]	28.81	19.32	10.65	22.70	7.75	4.402
	n_F	0.630	0.587	0.525	0.606	0.498	0.439
	R^2	0.991	0.992	0.993	0.997	0.997	0.994
	Adj. R^2	0.988	0.990	0.991	0.996	0.996	0.992
	χ^2	4.23E-03	2.90E-03	2.29E-03	2.58E-03	1.22E-03	7.89E-05
Langmuir-Freundlich model	Q_{LF} (mol.kg^{-1})	0.0515	0.0526	0.0533	0.0440	0.0450	0.0478
	K_{LF} (L.mol^{-1})	78 237	88 997	107 318	105 563	151 369	186 818
	n_{LF}	1.666	1.586	1.443	1.536	1.23	1.06
	R^2	0.970	0.959	0.955	0.960	0.949	0.949
	Adj. R^2	0.954	0.938	0.932	0.940	0.923	0.923
	χ^2	2.59E-02	1.06E-02	1.21E-02	2.76E-02	2.66E-02	8.35E-03
Sips model	Q_{Sips} (mol.kg^{-1})	0.0511	0.0523	0.0533	0.0440	0.0459	0.0478
	K_{Sips} (L.mol^{-1})^{nSips}	1.73E08	4.6E07	9.98E06	5.2E07	2.4E06	285 438
	n_{Sips}	1.682	1.551	1.396	1.536	1.23	1.04
	R^2	0.968	0.960	0.957	0.960	0.951	0.950
	Adj. R^2	0.952	0.940	0.936	0.940	0.927	0.925
	χ^2	2.69E-02	3.06E-02	3.2E-02	2.76E-02	6.51E-03	2.42E-02
Liu model	Q_{Liu} (mol.kg^{-1})	0.0920	0.0524	0.0533	0.044	0.0453	0.0470
	K_{Liu} (mol.L^{-1})	3.64E-05	1.15E-05	9.32E-06	9.14E-06	6.46E-06	5.0E-06
	n_{Liu}	0.981	1.55	1.44	1.58	1.27	1.06
	R^2	0.999	0.960	0.955	0.958	0.948	0.945
	Adj. R^2	0.998	0.940	0.932	0.936	0.922	0.917
	χ^2	6.52E-04	3.05E-02	1.21E-02	7.95E-03	7.80E-03	4.84E-03

Table 6.5: Continues

Khan model	Q_{Khan} (mol.kg^{-1})	0.050	0.0512	0.0521	0.0430	0.0449	0.0469
	K_{Khan} (L.mol^{-1})	56 125	64 046	80 917	75 490	114 917	151 540
	n_{Khan}	0.718	0.765	0.828	0.747	0.872	0.929
	R^2	0.998	0.995	0.992	0.998	0.983	0.966
	Adj. R^2	0.997	0.993	0.988	0.997	0.974	0.949
	χ^2	4.54E-04	5.24E-03	9.58E-03	4.47E-03	1.32E-02	1.80E-02
Hill model	Q_{Hill} (mol.kg^{-1})	0.0517	0.0529	0.0530	0.0441	0.0449	0.0458
	K_{Hill} (mol.L^{-1})^{nHill}	2.58E-08	2.21E-08	1.72E-08	1.59E-08	1.09E-08	8.6E-09
	n_{Hill}	1.55	1.55	1.55	1.55	1.55	1.55
	R^2	0.968	0.960	0.952	0.958	0.930	0.900
	Adj. R^2	0.953	0.940	0.928	0.937	0.895	0.850
	χ^2	1.63E-02	8.50E-03	1.95E-02	5.45E-03	3.08E-02	5.23E-02
Toth model	Q_{Toth} (mol.kg^{-1})	0.0505	0.0517	0.0527	0.0435	0.0456	0.0476
	K_{Toth} (L.mol^{-1})	38 455	43 182	55 514	52 939	94 671	148 636
	n_{Toth}	3.133	2.686	2.03	2.487	1.514	1.144
	R^2	0.988	0.979	0.973	0.978	0.959	0.951
	Adj. R^2	0.982	0.969	0.959	0.967	0.938	0.927
	χ^2	8.64E-03	1.46E-02	2.73E-02	2.20E-02	1.10E-02	2.46E-02

6.4.4.2. Binary sorption of PFOA and PFOS on CCNTs hydrogel beads

Table 6.6, Figure 6.37 6.13 and Figure 6.14 present adsorption isotherm findings for the present study on simultaneous uptake of PFOA and PFOS on CCNT hydrogel beads from a binary mixture of equal parts i.e., PFOA+PFOS for an initial concentration range of 5 mg.L^{-1} to 50 mg.L^{-1} (i.e., 1.208E-05 mol.L^{-1} to 1.208E-04 mol.L^{-1} for PFOA and 9.997E-06 mol.L^{-1} to 9.997E-05 mol.L^{-1} for PFOS). The competitive uptake of PFOA and PFOS was evaluated using the competitive extended-Langmuir and extended-Sips adsorption isotherm models. Based on the experimental data, PFOS recorded a higher maximum adsorption capacity of 0.0339 mol.kg^{-1} at equilibrium with PFOA recording a maximum adsorption capacity of 0.0333 mol.kg^{-1}. The maximum adsorption capacities at equilibrium suggest that CCNT hydrogel beads demonstrated higher affinity towards PFOS as compared to PFOA. According to the R^2 values > 0.994; adj. R^2 values > 0.992 and χ^2 values < 0.01, it can be concluded that the isotherms experimental data were well fitted with the investigated adsorption isotherm models i.e., extended-Langmuir model and extended-Sips model as cemented in Figure 6.13 and Figure 6.14. It is worth noting that R^2 is a statistical parameter which measures the total variation of the predicted values to the mean, which increases with the model parameters. As such, herein the adj. R^2 was applied to correct the R^2 values for a sample size and the number of parameters in the model. According to Khumalo *et al.* (2023), the value of R^2 decreases with an increase in the number of model parameters. Therefore, the insignificant difference between the R^2 and adj. R^2 values further confirms that the isotherms experimental data were well fitted by the extended-Langmuir and extended-Sips isotherm model.

Table 6.27: Binary adsorption isotherm parameters for the uptake of PFOA and PFOS on CCNTs

Model	**Parameter**	**PFOA in PFOA+PFOS**	**PFOS in PFOA+PFOS**
Experimental	$Q_{max,\ exp}$ (mol.kg^{-1})	0.0333	0.0339
Extended Langmuir Model	Q_{EL} (mol.kg^{-1})	0.0544	0.0582
	$K_{EL,\ PFOA}$ (L.mol^{-1})	23 075	5.8E-05
	$K_{EL,PFOS}$ (L.mol^{-1})	1.5E-04	27 749
	R^2	0.996	0.995
	Adj. R^2	0.994	0.992
	χ^2	1.3E-03	6.3E-03
Extended Sips Model	Q_{ES} (mol.kg^{-1})	0.0518	0.0742
	$K_{ES,\ PFOA}$ (L.mol^{-1})	34 741	3 732
	$K_{ES,\ PFOS}$ (L.mol^{-1})	1.12E-05	1.36E-05
	$n_{ES,\ PFOA}$	0.970	1.18
	$n_{ES,\ PFOS}$	1.35	1.45
	R^2	0.996	0.997
	Adj. R^2	0.994	0.996
	χ^2	2.3E-03	8.6E-03

In the context of the extended-Langmuir adsorption isotherm model, the binary system adsorption findings suggest that the uptake of PFOA and PFOS from PFOA+PFOS occurred at identical and equivalent definite localized sites of the model adsorbent i.e., CCNT hydrogel beads. Therefore, the uptake of PFOA and PFOS from PFOA+PFOS did not produce any steric hindrance and lateral interaction on adjacent sites i.e., between the adsorbed molecules as elucidated by Al-Ghouti and Da'ana (2020). Moreover, the relatively high adj. R^2 for the extended-Langmuir model suggests that the adsorption process of PFOA and PFOS is homogeneous such that the sorption activation energy and constant enthalpies are possessed by each molecule. Similarly, in the context of the extended-Sips adsorption isotherm model which is a combination of both the Langmuir and Freundlich isotherm models. The high adj. R^2 values suggest that the binary adsorption system under investigation in the present work can be characterized by the presence of active sites with heterogeneous energies.

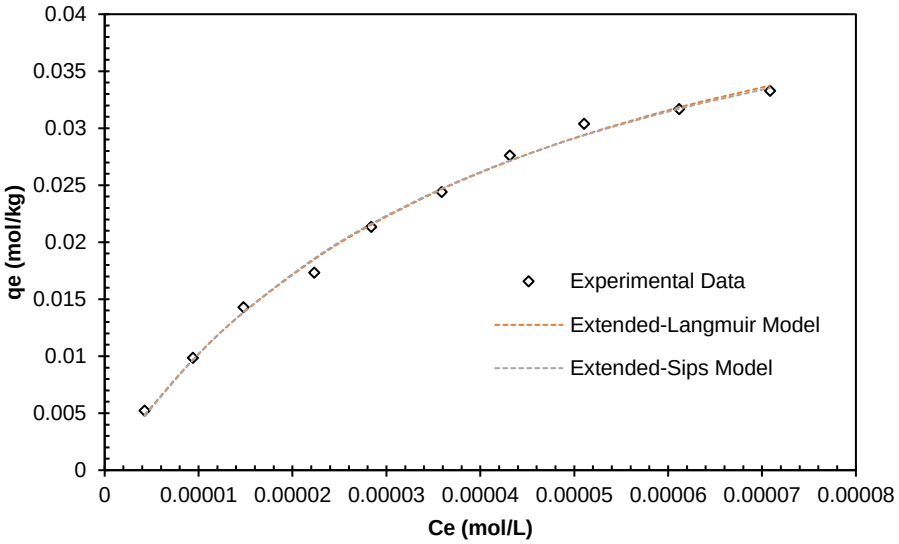

Figure 6.37: Uptake of PFOA in PFOA+PFOS at equilibrium

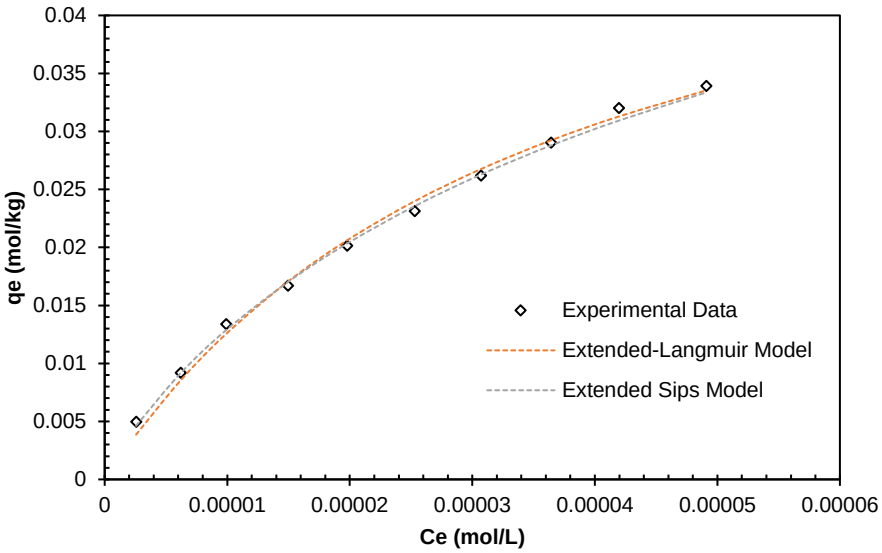

Figure 6.38: Uptake of PFOS in PFOA+PFOS at equilibrium

Furthermore, the effect of the presence of a second adsorbate on the uptake of the other was examined by calculating the ratio of the maximum adsorption capacity of one adsorbate in the presence of another $Q_{binary,i}$ to the maximum adsorption capacity of the same adsorbate when it is present alone in solution $Q_{single,i}$. According to Chandrasekaran *et al.* (2020), based on the ratio of $Q_{binary,i}/Q_{single,i}$, three possible results can be anticipated: 1) a ratio equal to 1, denotes no interaction of individual adsorbates in the binary system, 2) a ratio of less than 1, denotes antagonistic effects on the adsorption of individual species from a multicomponent mixture and 3) a ratio of more than 1, denotes a synergistic effect on the adsorption of individual component in the multicomponent mixture. Herein, the uptake of PFOA and PFOS in PFOA+PFOS gave ratios of 0.65 and 0.75, respectively, suggesting that both adsorbates demonstrated antagonistic effects on the sorption of the other. Moreover, it can be inferred from Figure 6.15 that there was a significant decline in the uptake of PFOA and PFOS for the binary mixture of PFOA and PFOS as compared to the single adsorption system with an increase in initial concentration. The antagonistic effects demonstrated by both adsorbates can be ascribed to the decrease in the number of active sites on the adsorbent due to a decrease in the ratio of number of active sites to the molecules to be adsorbed as the initial concentration of adsorbates increases. As such, the antagonistic effects on the uptake of PFOA and PFOS can be ascribed to the mere fact that the finite number of adsorption sites present on the CCNT hydrogel beads adsorbent became saturated at higher concentrations as compared to single adsorption systems.

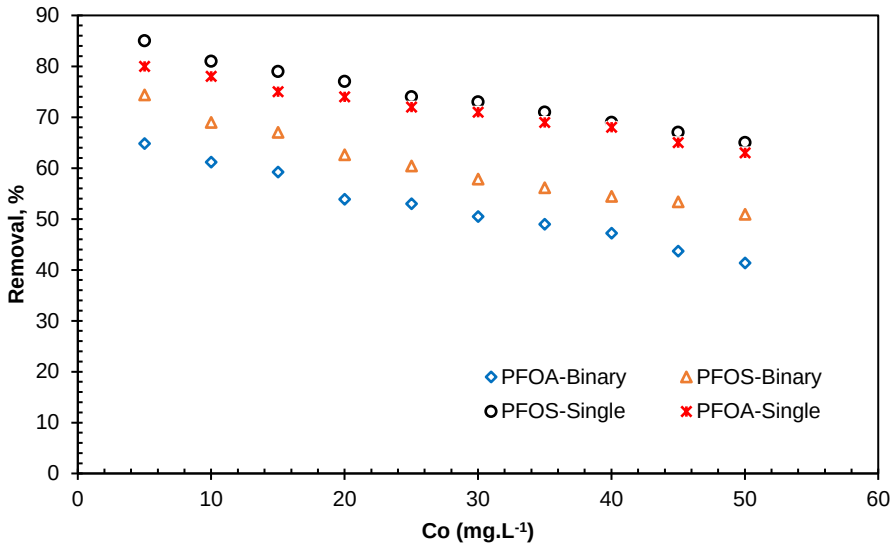

Figure 6.39: Single and binary adsorption profile of PFOA and PFOS on CCNT hydrogel beads

Furthermore, the percentage uptake of PFOA and PFOS on CCNT hydrogel beads for the single and binary systems were statistically analysed using the single factor analysis of variance (ANOVA) and the results are presented in Table 6.7Table 6.28: Single factor ANOVA results for the percentage removal of PFOA and PFOS on CCNT hydrogel beads.. Herein, within the framework of ANOVA, a single continuous dependent variable (i.e., adsorbate percentage removal) was compared with the mean of the adsorbate initial concentration (i.e., independent variable). Two hypotheses were formulated i.e., 1) null hypothesis: assuming that there is no statistically significant difference that exists between the means, and 2) alternative hypothesis: assuming that there is a statistical difference between the means. For the investigated adsorption systems, the ANOVA results recorded p-values of less than 0.05 suggesting that indeed there was a statistical difference between the mean differences of the compared variables. Furthermore, the mean differences were further confirmed at 95% confidence level by the recorded F-values of greater than 1 for all systems. It is noteworthy that from the ANOVA results, the PFOS system recorded relatively high sum of squares (SS) values when compared to the PFOA system, denoting the high affinity of the model adsorbent towards PFOS as compared to PFOA with varying initial concentration. Therefore, from the ANOVA results, it can be conferred that there was a statistical decline in the percentage removal of PFOA and/or PFOS with an increase in initial concentration of the model adsorbate.

Table 6.28: Single factor ANOVA results for the percentage removal of PFOA and PFOS on CCNT hydrogel beads.

Compound	**System**	**SS**	**F-value**	**p-value**
PFOA	Single	3094	21.56	2.02E-04
	PFOA in PFOA+PFOS	10634	76.53	6.71E-08

PFOS	Single	5483	38.25	7.74E-06
	PFOS in PFOA+PFOS	12944	86.06	2.8E-08

6.4.5. Adsorption thermodynamic studies

The derivation and application of the thermodynamic equilibrium constant K_{Eq}° equation (26) in evaluating thermodynamic parameters has been extensively discussed in literature (Romero-Gonzalez *et al.* 2005; Lima *et al.* 2021; Tran *et al.* 2021). Herein, the thermodynamic equilibrium constant K_{Eq}° is considered to be tantamount to the K_{Model} for all isotherm models with units of L/mol for K_{Model}. It is worth noting that the Henry and Freundlich constants have been used in literature to calculate thermodynamic parameters for adsorption processes. In the context of Henry's constant, it cannot be applied as K_{Eq}° on the basis of the units which are L/kg or L/g. According to Tran *et al.* (2021), the grams or kilograms refer to the quantity of the adsorbent and not of the adsorbate which is a solute. Similarly, the Freundlich constant, K_F is not a true equilibrium constant nor tantamount to K_{Eq}° because of the units i.e., [(mol/kg)/(mol/L)^{nF}]. As such, the Henry constant and Freundlich constant were not considered to be suitable for evaluating the thermodynamic parameters as recommended in recent literature (Liu 2009; Tran *et al.* 2017; Tran *et al.* 2021).

Herein, single adsorption thermodynamic studies were conducted aimed at investigating the sorption mechanism of PFOA and PFOS on CCNT hydrogel beads under three different temperature conditions i.e., 283 K, 293 K and 303 K. In a typical adsorption process, the Gibbs free energy change (ΔG°) indicates the degree of spontaneity of the adsorption process. As such, the relatively high negative values of the Gibbs free energy change for both the uptake of PFOA and PFOS (see Table 6.8 and Table 6.9) suggests that the adsorption process of PFOA and PFOS on CCNT hydrogel beads is a spontaneous process. Furthermore, it can be inferred from the thermodynamic results in Table 6.8 and Table 6.9, that an increase in temperature results in an increase in the negative values of the Gibbs free energy change, indicating a more energetically favourable adsorption process with an increase in temperature. The observed trend can be ascribed to the mere fact that the mobility of model adsorbate molecules in solution increases with temperature, subsequently resulting in an increase in the affinity of the model adsorbent towards PFOA and PFOS.

Table 6.29: Thermodynamic parameters for the sorption of PFOA on CCNT hydrogel beads

Model	**Temp. (K)**	**Model Parameters**			**Thermodynamic Parameters**		
		K_{Eq}°	R^2	**Adj. R²**	ΔG° **(kJ/mol)**	ΔH° **(kJ/mol)**	ΔS° **(kJ/mol.K)**
Langmuir	283	69 265			-26.2		
model	293	93 977	0.9791	0.9731	-27.9	16.9	0.153

	303	111 249			-29.3		
Langmuir-	283	78 237			-26.5		
Freundlich	293	88 997	0.9842	0.9760	-27.8	11.2	0.133
model	303	107 318			-29.2		
Sips model	283	79 026			-26.5		
	293	87 202	0.9714	0.9571	-27.8	9.48	0.127
	303	103 206			-29.1		
Liu model	283	27 473			-24.0		
	293	86 957	0.8758	0.8137	-27.7	48.9	0.259
	303	107 296			-29.2		
Khan	283	56 125			-25.7		
model	293	64 046	0.9683	0.9525	-27.0	13.0	0.137
	303	80 917			-28.5		
Hill model	283	78 700			-26.5		
	293	86 916	0.9761	0.9642	-27.7	57.5	0.298
	303	102 173			-29.1		
Toth model	283	38 455			-24.8		
	293	43 182	0.9483	0.9225	-26.0	85.2	0.393
	303	55 514			-27.5		

Table 6.30: Thermodynamic parameters for the sorption of PFOS on CCNT hydrogel beads

Model	**Temp. (K)**	**Model Parameters**			**Thermodynamic Parameters**		
		K_{Eq}°	R^2	**Adj. R^2**	ΔG° **(kJ/mol)**	ΔH° **(kJ/mol)**	ΔS° **(kJ/mol.K)**
Langmuir	283	112 914			-27.4		
model	293	150 169	0.9878	0.9843	-29.0	16.6	0.156
	303	179 706			-30.5		
Langmuir-	283	105 563			-27.2		
Freundlich	293	151 369	0.983	0.9745	-29.1	20.4	0.168
model	303	186 818			-30.6		
Sips model	283	105 546			-27.2		
	293	153 873	0.9402	0.9103	-29.1	18.3	0.161
	303	176 070			-30.4		
Liu model	283	109 409			-27.3		
	293	154 799	0.9955	0.9933	-29.1	21.5	0.173
	303	200 000			-30.8		
Khan	283	75 490			-26.4		
model	293	114 917	0.9903	0.9855	-28.4	24.9	0.181
	303	151 540			-30.1		
Hill model	283	107 487			-27.3		

	293	137 134	0.9876	0.9814	-28.8	14.2	0.146
	303	159 790			-30.2		
Toth model	283	52 939			-25.6		
	293	94 671	0.9972	0.9958	-27.9	36.8	0.221
	303	148 636			-30.0		

Moreover, enthalpy change, ΔH° calculations were conducted aimed at gaining some insight into the type of adsorption process. For the present study, it is apparent from Table 6.8 and Table 6.9 that the single uptake of PFOA and PFOS gave positive enthalpy change values indicating that the adsorption process of the model adsorbates is an endothermic process. As such, it can be inferred from the positive enthalpy change values that the uptake of PFOA and PFOS on the model adsorbent involve the displacement of more than one water molecule on CCNT hydrogel beads resulting in the endothermicity of the process. On the other hand, according to Liu (2009), the heat evolved during the physical adsorption process is of the same order of magnitude as the heat of condensation over a range of 2.1 $kJ.mol^{-1}$ to 20.9 $kJ.mol^{-1}$, with the heat of chemisorption falling within the range of 80 $kJ.mol^{-1}$ to 200 $kJ.mol^{-1}$. For the present work, the enthalpy changes values range from 11.2 $kJ.mol^{-1}$ to 85.2 $kJ.mol^{-1}$ for PFOA and from 14.2 $kJ.mol^{-1}$ to 36.8 $kJ.mol^{-1}$ for PFOA. Based on the enthalpy change results presented in Table 6.8 and Table 6.9, the adsorption process of PFOA and PFOS on CCNT hydrogel beads cannot be explicitly classified as physical adsorption or chemisorption, however, it can be inferred that the uptake of PFOA and PFOS on the model adsorbent is a physiochemical adsorption process i.e., a combination of physical and chemical adsorption process.

The entropy change, ΔS° was evaluated for the single adsorption process of PFOA and PFOS on CCNT hydrogel beads aimed at elucidating the affinity of the model adsorbent on PFOA and PFOS. It is worth noting that according to Saha and Chowdhury (2011) and Liu (2009), positive entropy change values suggest an increase in randomness at the solid-liquid interface with some structural changes in the adsorbate and adsorbent. Hence, the positive entropy changes values obtained for all the investigated adsorption isotherm models explicitly indicate high affinity of CCNT hydrogel beads on PFOA and PFOS. The obtained positive entropy changes values suggest that the molecules of the adsorbed solvent (i.e., water) were displaced by PFOA or PFOS, allowing the water molecules to gain more translational entropy than is lost by PFOA or PFOS molecules allowing for the prevalence of randomness within the solid-liquid adsorption system. Moreover, the goodness of fit for all the investigated adsorption models was evaluated by applying R^2 and adj. R^2 as statistical parameters. From the relatively high R^2 and adj. R^2 values of greater than 0.9, it can be inferred that the nonlinear adsorption isotherm models gave a good fit in evaluating thermodynamic parameters.

6.4.6. Effect of competing ions on the uptake of PFOA and PFOS on CCNT hydrogel beads.

According to Elanchezhiyan *et al.* (2021), salts are abundantly available from natural and anthropogenic sources, and salinity of surface water and groundwater can vary considerably. Sodium chloride (NaCl) is one of the most detected salts in water bodies. This can be ascribed to NaCl being used as a road-icing agent which subsequently enters wetlands, rivers, and lakes through runoffs. As such, herein the influence of NaCl on PFOA and PFOS sorption on CCNT hydrogel beads was investigated for a NaCl concentration range of 0.026 mol.L^{-1} to 0.171 mol.L^{-1} at a fixed PFOA and PFOS concentration of 5 mg.L^{-1} to determine their environmental fate as presented in Figure 6.16. It can be inferred from Figure 6.16 that the addition of NaCl did not have any significant improvement in the uptake of both PFOA and PFOS for a NaCl concentration of less than 0.06 mol.L^{-1}. However, a slight improvement in the uptake of PFOA from 80% to 87% and 85% to 93% for PFOS was observed as the NaCl concentration increased from 0.06 mol.L^{-1} to 0.171 mol.L^{-1}. The findings of the current study can be attributed to the salting-out effect and hydrophobic interactions between the model adsorbates and adsorbent. It is worth noting that salting-out is induced by the preferential movement of solvent molecules from their role as the solvent for ions of the nonelectrolyte or ions with a relatively low affinity for the solvent in their competition for solvent molecules, which in turn decreases the hydration and subsequently the solubility of nonelectrolyte ions (Zhang *et al.* 2019). Since salting-out increases the hydrophobic interactions compelling the adsorbate and adsorbent to bind together, it subsequently reduces the total area of contact between water molecules and hydrophobic particles as elucidated by Zhang *et al.* (2019). As such, the percentage increase in the uptake of PFOA and PFOS with NaCl concentration can be ascribed to the hydrophobic interaction between the perfluoroalkyl tails and hydrophobic moieties on the CNTs, as reported in literature, to be one of the major adsorption mechanisms for PFOA and PFOS (Zhi and Liu 2015; Elanchezhiyan *et al.* 2021; Zakaria *et al.* 2022). The findings of the current study suggest that the hydrophobic interactions are the predominant forces that significantly influence the uptake of PFOA and PFOS on CCNT hydrogel beads. The findings of the current study are congruent to the work reported by Yu, Deng and Yu (2008), Xiao *et al.* (2011) and Zhang *et al.* (2010) on the uptake of PFOA and PFOS on carbonaceous adsorbents at varying ionic strengths.

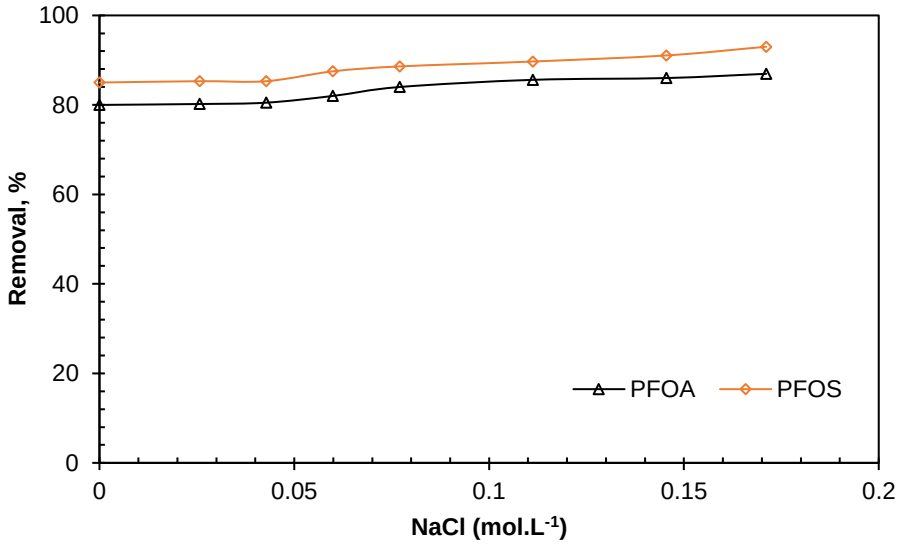

Figure 6.40: The effect of NaCl concentration on the uptake of PFOA and PFOS on CCNT hydrogel beads.

However, similar studies conducted on the uptake of PFOA and PFOS on carbonaceous adsorbents at varying anionic strength such as SO_4^{2-} and $Cr_2O_7^{2-}$ (Zhang *et al.* 2011) have reported that the presence of competitive anions have a negative effect on the sorption of PFOA and PFOS. Similarly, Elanchezhiyan *et al.* (2021) reported a decrease in the uptake of PFOA and PFOS in the presence of chloride, sulfate, and phosphate anions. The decrease in the uptake of PFOA and PFOS can be ascribed to the model anions competing with PFOA and PFOS for the protonated amino groups on the adsorbent. The insignificant uptake of PFOA and PFOS with an increase in concentration of the model anions (Zhang *et al.* 2011; Elanchezhiyan *et al.* 2021) further imply the dominance of the hydrophobic interaction forces.

6.5. Conclusion

The single adsorption experimental data explicitly indicates that the synthesized CCNT hydrogel beads demonstrated high affinity towards PFOS and PFOA with the adsorption equilibrium being reached after 48 hours of contact time. It is evident from the RSM results that the uptake of PFOA and PFOS on CCNT hydrogel beads was strongly dependent on the initial concentration of the model adsorbate. An increase in the initial concentration of PFOA and PFOS resulted in a decrease on the percentage removal rate. Moreover, kinetic studies experimental data were well fitted by the nonlinear PFO kinetic model confirming that the uptake mechanism of PFOA and PFOS does not depend on the concentration of both reactants (i.e., PFOA or PFOS and water) but only on the concentration of the model adsorbate, hence the PFO is considered to be controlled by physisorption. From the single adsorption isotherm studies, it is evident that experimental data were well fitted by the Freundlich isotherm model suggesting that the uptake of PFOA and PFOS on CCNT hydrogel beads was not restricted to the monolayer

adsorption process. As such, the adsorption heat and affinities were not uniformly distributed on the heterogeneous surface of CCNT hydrogel beads as a model adsorbent. On the other hand, the binary uptake of PFOA and PFOS experimental data were well fitted by the competitive extended-Langmuir and extended-Sips isotherm models. Both PFOA and PFOS demonstrated antagonistic effects on the uptake of either PFOA and/or PFOS in PFOA+PFOS. Furthermore, from the thermodynamic results obtained, it could be inferred that the uptake of PFOA and PFOS on CCNT hydrogel beads cannot be explicitly explained by chemical nor physical adsorption, however, it can be inferred that the uptake of PFOA and PFOS on the model adsorbent is a physiochemical adsorption process. Findings of the present work on the uptake of PFOA and PFOS in the presence of varying concentration of Na^+ (i.e., NaCl) as a competing ion demonstrated synergistic effects on both adsorbates.

References

Agbovi, H. K. and Wilson, L. D. 2021. 1 - Adsorption processes in biopolymer systems: fundamentals to practical applications. In: Kalia, S. ed. *Natural Polymers-Based Green Adsorbents for Water Treatment*. Elsevier, 1-51.

Al-Ghouti, M. A. and Da'ana, D. A. 2020. Guidelines for the use and interpretation of adsorption isotherm models: A review. *Journal of hazardous materials*, 393: 122383.

Alimohammadi, M., Saeedi, Z., Akbarpour, B., Rasoulzadeh, H., Yetilmezsoy, K., Al-Ghouti, M. A., Khraisheh, M. and McKay, G. 2017. Adsorptive removal of arsenic and mercury from aqueous solutions by eucalyptus leaves. *Water, Air, & Soil Pollution*, 228: 1-27.

Bezerra, M. A., Santelli, R. E., Oliveira, E. P., Villar, L. S. and Escaleira, L. A. 2008. Response surface methodology (RSM) as a tool for optimization in analytical chemistry. *Talanta*, 76 (5): 965-977.

Candioti, L. V., De Zan, M. M., Cámara, M. S. and Goicoechea, H. C. 2014. Experimental design and multiple response optimization. Using the desirability function in analytical methods development. *Talanta*, 124: 123-138.

Chandrasekaran, A., Patra, C., Narayanasamy, S. and Subbiah, S. 2020. Adsorptive removal of Ciprofloxacin and Amoxicillin from single and binary aqueous systems using acid-activated carbon from Prosopis juliflora. *Environmental Research*, 188: 109825.

Cui, J., Gao, P. and Deng, Y. 2020. Destruction of per-and polyfluoroalkyl substances (PFAS) with advanced reduction processes (ARPs): A critical review. *Environmental Science & Technology*, 54 (7): 3752-3766.

Cui, L., Zhou, Q.-f., Liao, C.-y., Fu, J.-j. and Jiang, G.-b. 2009. Studies on the toxicological effects of PFOA and PFOS on rats using histological observation and chemical analysis. *Archives of environmental contamination and toxicology*, 56: 338-349.

Do, D. D. 1998. *Adsorption analysis: Equilibria and kinetics (with cd containing computer MATLAB programs)*. World Scientific.

Elanchezhiyan, S. S. and Meenakshi, S. 2018. Encapsulation of metal ions between the biopolymeric layer beads for tunable action on oil particles adsorption from oily wastewater. *Journal of Molecular Liquids*, 255: 429-438.

Elanchezhiyan, S. S., Preethi, J., Rathinam, K., Njaramba, L. K. and Park, C. M. 2021. Synthesis of magnetic chitosan biopolymeric spheres and their adsorption performances for PFOA and PFOS from aqueous environment. *Carbohydrate Polymers*, 267: 118165.

Franke, V., McCleaf, P., Lindegren, K. and Ahrens, L. 2019. Efficient removal of per-and polyfluoroalkyl substances (PFASs) in drinking water treatment: nanofiltration combined with active carbon or anion exchange. *Environmental Science: Water Research & Technology*, 5 (11): 1836-1843.

Garg, S., Wang, J., Kumar, P., Mishra, V., Arafat, H., Sharma, R. S. and Dumée, L. F. 2021. Remediation of water from per-/poly-fluoroalkyl substances (PFAS)–Challenges and perspectives. *Journal of Environmental Chemical Engineering*, 9 (4): 105784.

Gomez-Ruiz, B., Ribao, P., Diban, N., Rivero, M. J., Ortiz, I. and Urtiaga, A. 2018. Photocatalytic degradation and mineralization of perfluorooctanoic acid (PFOA) using a composite TiO2− rGO catalyst. *Journal of hazardous materials*, 344: 950-957.

Gong, Y., Wang, L., Liu, J., Tang, J. and Zhao, D. 2016. Removal of aqueous perfluorooctanoic acid (PFOA) using starch-stabilized magnetite nanoparticles. *Science of the Total Environment*, 562: 191-200.

Hu, Q., Lan, R., He, L., Liu, H. and Pei, X. 2023. A critical review of adsorption isotherm models for aqueous contaminants: Curve characteristics, site energy distribution and common controversies. *Journal of Environmental Management*, 329: 117104.

Huang, S. and Jaffé, P. R. 2019. Defluorination of perfluorooctanoic acid (PFOA) and perfluorooctane sulfonate (PFOS) by Acidimicrobium sp. strain A6. *Environmental science & technology*, 53 (19): 11410-11419.

Hubert, M., Meyn, T., Hansen, M. C., Hale, S. E. and Arp, H. P. H. 2023. Per-and polyfluoroalkyl substance (PFAS) removal from soil washing water by coagulation and flocculation. *Water Research*: 120888.

Jian, J.-M., Guo, Y., Zeng, L., Liang-Ying, L., Lu, X., Wang, F. and Zeng, E. Y. 2017. Global distribution of perfluorochemicals (PFCs) in potential human exposure source–a review. *Environment international*, 108: 51-62.

Karimifard, S. and Moghaddam, M. R. A. 2016. Enhancing the adsorption performance of carbon nanotubes with a multistep functionalization method: Optimization of Reactive Blue 19 removal through response surface methodology. *Process Safety and Environmental Protection*, 99: 20-29.

Khumalo, S. M., Bakare, B. F. and Rathilal, S. 2022. The occurrence and bioremediation of emerging polyfluorinated compounds in water bodies: a mini review. *Applied Sciences*, 12 (23): 12196.

Khumalo, S. M., Bakare, B. F., Tetteh, E. K. and Rathilal, S. 2023. Application of Response Surface Methodology on Brewery Wastewater Treatment Using Chitosan as a Coagulant. *Water*, 15 (6): 1176.

Kotthoff, M., Müller, J., Jürling, H., Schlummer, M. and Fiedler, D. 2015. Perfluoroalkyl and polyfluoroalkyl substances in consumer products. *Environmental Science and Pollution Research*, 22: 14546-14559.

Li, K., Gao, P., Xiang, P., Zhang, X., Cui, X. and Ma, L. Q. 2017. Molecular mechanisms of PFOA-induced toxicity in animals and humans: Implications for health risks. *Environment international*, 99: 43-54.

Li, Y.-F., Fang, T., Lee, Y.-C., Liu, Y.-J., Hu, C.-Y. and Lo, S.-L. 2023. Cationic surfactants influencing the enhancement of energy efficiency for perfluorooctanoic acid (PFOA) removal in the electrocoagulation-flotation (ECF) system. *Chemosphere*, 318: 137932.

Lima, É. C., Dehghani, M. H., Guleria, A., Sher, F., Karri, R. R., Dotto, G. L. and Tran, H. N. 2021. Adsorption: fundamental aspects and applications of adsorption for effluent treatment. In: *Green technologies for the defluoridation of water*. Elsevier, 41-88.

Liu, C., Zhao, X., Faria, A. F., Quiñones, K. Y. D., Zhang, C., He, Q., Ma, J., Shen, Y. and Zhi, Y. 2022. Evaluating the efficiency of nanofiltration and reverse osmosis membrane processes for the removal of per-and polyfluoroalkyl substances from water: A critical review. *Separation and Purification Technology*: 122161.

Liu, S., Yin, N. and Faiola, F. 2018. PFOA and PFOS disrupt the generation of human pancreatic progenitor cells. *Environmental Science & Technology Letters*, 5 (5): 237-242.

Liu, Y. 2009. Is the free energy change of adsorption correctly calculated? *Journal of Chemical & Engineering Data*, 54 (7): 1981-1985.

Long, L., Hu, X., Yan, J., Zeng, Y., Zhang, J. and Xue, Y. 2019. Novel chitosan–ethylene glycol hydrogel for the removal of aqueous perfluorooctanoic acid. *Journal of Environmental Sciences*, 84: 21-28.

Madondo, N. I., Rathilal, S. and Bakare, B. F. 2022. Utilization of Response Surface Methodology in Optimization and Modelling of a Microbial Electrolysis Cell for Wastewater Treatment Using Box–Behnken Design Method. *Catalysts*, 12 (9): 1052.

Montgomery, D. C. 2017. *Design and analysis of experiments*. John wiley & sons.

Mukhtar, A., Saqib, S., Safdar, F., Hameed, A., Rafiq, S., Mellon, N. B., Amen, R., Khan, M. S., Ullah, S. and Assiri, M. A. 2020. Experimental and comparative theoretical study of thermal conductivity of MWCNTs-kapok seed oil-based nanofluid. *International Communications in Heat and Mass Transfer*, 110: 104402.

Parenky, A. C., de Souza, N. G., Nguyen, H. H., Jeon, J. and Choi, H. 2020. Decomposition of carboxylic PFAS by persulfate activated by silver under ambient conditions. *Journal of Environmental Engineering*, 146 (10): 06020003.

Park, M., Wu, S., Lopez, I. J., Chang, J. Y., Karanfil, T. and Snyder, S. A. 2020. Adsorption of perfluoroalkyl substances (PFAS) in groundwater by granular activated carbons: Roles of hydrophobicity of PFAS and carbon characteristics. *Water Research*, 170: 115364.

Pauletto, P. S., Lütke, S. F., Dotto, G. L. and Salau, N. P. G. 2021. Adsorption mechanisms of single and simultaneous removal of pharmaceutical compounds onto activated carbon: Isotherm and thermodynamic modeling. *Journal of Molecular Liquids*, 336: 116203.

Podder, M. and Majumder, C. 2016. Studies on the removal of As (III) and As (V) through their adsorption onto granular activated carbon/MnFe2O4 composite: isotherm studies and error analysis. *Composite Interfaces*, 23 (4): 327-372.

Raftery, A. E. 1995. Bayesian model selection in social research. *Sociological methodology*: 111-163.

Reynel-Avila, H. E., Mendoza-Castillo, D. I., Olumide, A. A. and Bonilla-Petriciolet, A. 2016. A survey of multi-component sorption models for the competitive removal of heavy metal ions using bush mango and flamboyant biomasses. *Journal of Molecular Liquids*, 224: 1041-1054.

Ribas, M. C., De Franco, M. A., Adebayo, M. A., Lima, E. C., Parkes, G. and Feris, L. A. 2020. Adsorption of Procion Red MX-5B dye from aqueous solution using homemade peach and commercial activated carbons. *Applied Water Science*, 10 (6): 1-13.

Romero-Gonzalez, J., Peralta-Videa, J., Rodrıguez, E., Ramirez, S. and Gardea-Torresdey, J. 2005. Determination of thermodynamic parameters of Cr (VI) adsorption from aqueous solution onto Agave lechuguilla biomass. *The Journal of chemical thermodynamics*, 37 (4): 343-347.

Ruiz-Urigüen, M., Shuai, W., Huang, S. and Jaffé, P. R. 2022. Biodegradation of PFOA in microbial electrolysis cells by Acidimicrobiaceae sp. strain A6. *Chemosphere*, 292: 133506.

Saha, P. and Chowdhury, S. 2011. Insight into adsorption thermodynamics. *Thermodynamics*, 16: 349-364.

Sobczak-Kupiec, A., Drabczyk, A., Florkiewicz, W., Głąb, M., Kudłacik-Kramarczyk, S., Słota, D., Tomala, A. and Tyliszczak, B. 2021. Review of the applications of biomedical compositions containing hydroxyapatite and collagen modified by bioactive components. *Materials*, 14 (9): 2096.

Tarapore, P. and Ouyang, B. 2021. Perfluoroalkyl chemicals and male reproductive health: do PFOA and PFOS increase risk for male infertility? *International journal of environmental research and public health*, 18 (7): 3794.

Tran, H. N., Bollinger, J.-C., Lima, E. C. and Juang, R.-S. 2023. How to avoid mistakes in treating adsorption isotherm data (liquid and solid phases): Some comments about correctly using Radke-Prausnitz nonlinear model and Langmuir equilibrium constant. *Journal of Environmental Management*, 325: 116475.

Tran, H. N., Lima, E. C., Juang, R.-S., Bollinger, J.-C. and Chao, H.-P. 2021. Thermodynamic parameters of liquid–phase adsorption process calculated from different equilibrium constants related to adsorption isotherms: A comparison study. *Journal of Environmental Chemical Engineering*, 9 (6): 106674.

Tran, H. N., You, S.-J., Hosseini-Bandegharaei, A. and Chao, H.-P. 2017. Mistakes and inconsistencies regarding adsorption of contaminants from aqueous solutions: a critical review. *Water research*, 120: 88-116.

Tsuda, S. 2016. Differential toxicity between perfluorooctane sulfonate (PFOS) and perfluorooctanoic acid (PFOA). *The Journal of toxicological sciences*, 41 (Special): SP27-SP36.

Vieira, W. T., de Farias, M. B., Spaolonzi, M. P., da Silva, M. G. C. and Vieira, M. G. A. 2020. Removal of endocrine disruptors in waters by adsorption, membrane filtration and biodegradation. A review. *Environmental Chemistry Letters*, 18 (4): 1113-1143.

Wang, F. and Shih, K. 2011. Adsorption of perfluorooctanesulfonate (PFOS) and perfluorooctanoate (PFOA) on alumina: Influence of solution pH and cations. *water research*, 45 (9): 2925-2930.

Weber Jr, W. J. and Morris, J. C. 1963. Kinetics of adsorption on carbon from solution. *Journal of the sanitary engineering division*, 89 (2): 31-59.

Wee, S. Y. and Aris, A. Z. 2023. Revisiting the “forever chemicals”, PFOA and PFOS exposure in drinking water. *NPJ Clean Water*, 6 (1): 57.

Xiao, F., Zhang, X., Penn, L., Gulliver, J. S. and Simcik, M. F. 2011. Effects of monovalent cations on the competitive adsorption of perfluoroalkyl acids by kaolinite: experimental studies and modeling. *Environmental science & technology*, 45 (23): 10028-10035.

Xiong, J., Hou, Y., Wang, J., Liu, Z., Qu, Y., Li, Z. and Wang, X. 2021. The rejection of perfluoroalkyl substances by nanofiltration and reverse osmosis: influencing factors and combination processes. *Environmental Science: Water Research & Technology*, 7 (11): 1928-1943.

Yi, L., Chai, L., Xie, Y., Peng, Q. and Peng, Q. 2016. Isolation, identification, and degradation performance of a PFOA-degrading strain. *Genet. Mol. Res*, 15 (2): 235-246.

Yu, Q., Deng, S. and Yu, G. 2008. Selective removal of perfluorooctane sulfonate from aqueous solution using chitosan-based molecularly imprinted polymer adsorbents. *Water Research*, 42 (12): 3089-3097.

Yuan, Y., Feng, L., Xie, N., Zhang, L. and Gong, J. 2020. Rapid photochemical decomposition of perfluorooctanoic acid mediated by a comprehensive effect of nitrogen dioxide radicals and Fe3+/Fe2+ redox cycle. *Journal of hazardous materials*, 388: 121730.

Zakaria, A. F., Yahaya, N., Raznisyafiq, M., Loh, S. H. and Kamaruzaman, S. 2022. Recent advances in applications of hybrid natural polymers as adsorbent for perfluorinated compounds removal–review paper. *Journal of Polymer Research*, 29 (1): 21.

Zeldowitsch, J. 1934. Adsorption site energy distribution. *Acta phys. chim. URSS*, 1 (1): 961-973.

Zhan, Y. and Zhu, J. 2024. Response surface methodology and artificial neural network-genetic algorithm for modeling and optimization of bioenergy production from biochar-improved anaerobic digestion. *Applied Energy*, 355: 122336.

Zhang, J., Pang, H., Gray, S., Ma, S., Xie, Z. and Gao, L. 2021. PFAS removal from wastewater by in-situ formed ferric nanoparticles: Solid phase loading and removal efficiency. *Journal of Environmental Chemical Engineering*, 9 (4): 105452.

Zhang, Q., Deng, S., Yu, G. and Huang, J. 2011. Removal of perfluorooctane sulfonate from aqueous solution by crosslinked chitosan beads: Sorption kinetics and uptake mechanism. *Bioresource Technology*, 102 (3): 2265-2271.

Zhang, X., Niu, H., Pan, Y., Shi, Y. and Cai, Y. 2010. Chitosan-coated octadecyl-functionalized magnetite nanoparticles: preparation and application in extraction of trace pollutants from environmental water samples. *Analytical Chemistry*, 82 (6): 2363-2371.

Zhang, Y., Zhu, C., Liu, F., Yuan, Y., Wu, H. and Li, A. 2019. Effects of ionic strength on removal of toxic pollutants from aqueous media with multifarious adsorbents: A review. *Science of The Total Environment*, 646: 265-279.

Zhi, Y. and Liu, J. 2015. Adsorption of perfluoroalkyl acids by carbonaceous adsorbents: Effect of carbon surface chemistry. *Environmental pollution*, 202: 168-176.

CHAPTER SEVEN: BREAKTHROUGH CURVES

SORPTION OF ANTIBIOTICS AND PERFLUOROALKYL ACIDS ON CHITOSAN-CARBON NANOTUBE HYDROGEL BEADS IN A FIXED-BED COLUMN: EFFECT OF OPERATING CONDITIONS ON BREAKTHROUGH CURVES

7.1. Abstract

Fixed-bed adsorption columns have cemented their application in eradicating emerging contaminants of environmental concern from aqueous solutions. As such, for an effective fixed-bed adsorption process design or evaluation performance, breakthrough curve models are essential in determining the breakthrough point time. Herein, the effect of three operating parameters i.e., initial adsorbate concentration, fixed-bed height, and volumetric flow rate on the breakthrough curves for the sorption of amoxicillin, ciprofloxacin, sulfamethoxazole, perfluorooctanoic acid and perfluorooctane sulfonic acid on chitosan-carbon nanotube hydrogel beads were investigated. The results obtained suggest that the breakthrough point time decreases with an increase in adsorbate initial concentration and volumetric flow rate indicating low uptake of the model adsorbates. On the other hand, it can be inferred from the results obtained that the breakthrough point time increases with a decrease in volumetric flowrate due to an increase in mass transfer zone. Moreover, breakthrough curves experimental data was well fitted by the Thomas model recording R^2 and adjusted R^2 values of more than 0.99 indicating that the breakthrough curves for the present work can be described by a symmetric function. The breakthrough points time predicted by the Thomas model was aligned with the experimentally determined breakthrough points time cementing its practical utility and superiority over the log-Gompertz and Bohart-Adams models. Therefore, from the results obtained, it can be inferred that the Thomas model can be used to investigate the dynamic behaviour of the fixed-bed adsorption system investigated in the present study.

7.2. Introduction

Despite the environmental occurrence of organic micropollutants such as pharmaceutical compounds (PCs) and perfluoroalkyl acids (PFAAs) in trace amounts ranging from ng/L to µg/L, they have the ability to disrupt ecosystems and pose serious health risks to human and aquatic flora and fauna (Chu and Hashim 2023; Khumalo, Bakare and Rathilal 2024). The environmental occurrence of pharmaceuticals particularly in aquatic environments is ascribed to their continuous release into the ecosystem from various point sources such as households, hospitals, and pharmaceutical industries (Khumalo *et al.* 2023). Antibiotics are one of the environmentally threatening groups of PCs due to their high consumption rate of 34.8 billion defined daily dose (Klein *et al.* 2018). The high consumption

rate can be ascribed to the use of antibiotics by humans and animals as primary treatment of acute illness, subsequently ending up in the environment through animal and human secretion in urine and faeces as original compounds, metabolites or as conjugates (Tran, Reinhard and Gin 2018; Khumalo *et al.* 2023; Khumalo, Bakare and Rathilal 2024). On the other hand, the two most prominent PFAA species in drinking water are perfluorooctanoic acid (PFOA) and perfluorooctane sulfonic acid (PFOS). The occurrence of PFAAs in water bodies is ascribed to the discharge of untreated and partially treated industrial effluent containing PFAAs into the environment subsequently entering wastewater treatment plants (WWTPs) making them the major source of PFAAs. In the context of the African region, PCs and PFAAs are characterized as emerging contaminants of environmental concern. As such, there has been a call for stringent regulations which is among the major driving forces to investigate treatment technologies and the fate of PCs and PFAAs in water bodies.

PFAAs, particularly PFOA and PFOS, have been widely used as surfactants, fire retardants, wetting agents, lubricants, as well as additives (Khumalo *et al.* 2022). The appetite in the application of PFAAs is ascribed to their unique chemical and physical properties such as oleophobicity, hydrophobicity, as well as extraordinary chemical stability of the carbon-fluorine (C-F) bond (Gong *et al.* 2016; Xu *et al.* 2021). Despite the chemically stable C-F bond of PFOA and PFOS, their sulfonate and carboxyl functional groups attached at the end (see Figure 7.1) makes them water soluble and mobile in aqueous systems (Xu *et al.* 2021). As such, PFOA and PFOS have been frequently detected in surface water, ground water, sediments, as well as in drinking water (Xu *et al.* 2021; Khumalo *et al.* 2022). It is worth noting that the United States of America issued health advisory levels for drinking water of 70 ng/L for PFOA and/or PFOS (Khumalo *et al.* 2022).

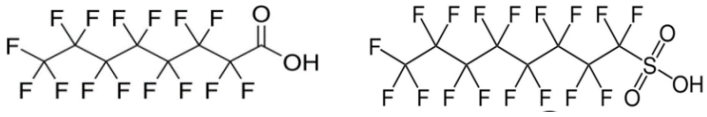

PFOA PFOS

Figure 7.41: Chemical structures of PFOA and PFOS

Similarly, antibiotics have been frequently detected in WWTP effluent streams at a range of 1536 ng/L to 3600 ng/L as reported by Yaqubi *et al.* (2021). The relatively high concentrations of antibiotics in WWTP effluent streams are evident enough that current technologies in WWTPs is not capable to completely eradicate these contaminants of emerging concern. In understanding the environmental occurrence of antibiotics, the reader is referred to Khumalo *et al.* (2023) where the occurrence and fate of antibiotics in water treatment processes is systematically discussed. It is worth noting that a number of technologies have been investigated for the removal of antibiotics and PFAAs from aqueous solutions such as solid-liquid adsorption (Gong *et al.* 2016; Yaqubi *et al.* 2021; Khumalo, Bakare and Rathilal

2024), advanced oxidation processes (Cuerda-Correa, Alexandre-Franco and Fernández-González 2019; Wang and Zhuan 2020), bioremediation (Koch *et al.* 2021; Khumalo, Bakare and Rathilal 2022) as well as reverse osmosis and nanofiltration (Lan *et al.* 2019; Zhang, Zhang and Liang 2019). However, most of these methods require advanced apparatus, consume high energy, and they have the potential to generate large amounts of waste, thus rendering these processes expensive.

By contrast, solid-liquid adsorption has demonstrated to be effective in removing a wide range of emerging contaminants of environmental concern including antibiotics (Khumalo, Bakare and Rathilal 2024) and PFAAs (Zhang, Zhang and Liang 2019) from aqueous environments. The growing appetite in the application of solid-liquid adsorption in water treatment processes is ascribed to its simplicity, economic viability as well as high efficiencies. A variety of adsorbents have been investigated such as granular activated carbon (Fan, Zheng and Hou 2019), anion-exchange resin (Wang *et al.* 2017; Parvin *et al.* 2023) as well as biomaterials and molecularly imprinted biopolymers (Zhang, Zhang and Liang 2019) for water purification. It is worth noting that chitosan has attracted the attention of many researchers within the scientific community due to the abundant availability of its source chitin which is extracted from crustacean shells and mycelia fungi (Long *et al.* 2019). The presence of highly active amino and hydroxyl functional groups within the chitosan structure potentiate it to be an excellent biosorbent with chelating sites for targeted contaminants in aqueous environments. Despite the desirable features of chitosan such as low processing cost, biodegradability, hydrophobicity, biocompatibility, and non-toxicity, the use of pristine chitosan-based adsorbents is associated with drawbacks such as low stability, weak mechanical strength, low porosity, low surface area, hydro-stability in acid medium, and high crystallinity (Khumalo, Bakare and Rathilal 2024). Due to the remarkable features of carbon nanotubes (CNTs) such as high tensile strength, large surface area, and low density, for the present study CNTs potentiate as ideal nanofillers in tackling the undesirable features of pristine chitosan composites in the context of water treatment.

It is worth noting that most of the studies in solid-liquid adsorption reported in literature are based on batch adsorption. Studies in continuous systems i.e., fixed-bed columns are scanty. Therefore, the present work focuses on investigating the effect of operating parameters on the breakthrough curves for the sorption of amoxicillin (AMX), ciprofloxacin (CIP), sulfamethoxazole (SMX), PFOA and PFOS on chitosan-carbon nanotube (CCNT) hydrogel beads in a fixed-bed column as the first case. Moreover, the present work is focusing on investigating the dynamic behaviour of the fixed-bed adsorption system by applying the Thomas model, log-Gompertz model and Bohart-Adams model. Experimental data model fit was conducted with the aid of nonlinear regression analysis in order to obtain a model with a better goodness of fit.

7.3. Materials and Methods

7.3.1. Materials

All chemicals used in the current study were used without any further purification. Multiwall carbon nanotubes (>98% carbon basis), HPLC grade of sulfamethoxazole, ≥95% anhydrous basis amoxicillin, >98% pure ciprofloxacin, PFOA ($C_8HF_{15}O_2$) and PFOS ($C_8HF_{17}O_3S$) were supplied by Lasec laboratories, Durban, South Africa. Chitosan powder from shrimp shells with a degree of deacetylation of ≥75%, sodium hydroxide (NaOH) pellets (≥95% anhydrous basis), sodium chloride (NaCl), methanol (CH_3OH) (≥99.9% pure), 98% pure sulfuric acid (H_2SO_4), and glacial acetic acid ($C_2H_4O_2$) (≥99.7% pure) were supplied by Sigma-Aldrich, South Africa.

7.3.2. Fixed-bed adsorption studies

Herein, the experimental procedure adopted in the adsorbent synthesis i.e., CCNT hydrogel beads and characterisation is well discussed in previous work (Khumalo, Bakare and Rathilal 2024) as well as in chapter four. The breakthrough curves for the uptake of AMX, CIP, SMX, PFOA and PFOS on CCNT hydrogel beads were investigated by conducting a set of experiments under constant temperature of 293 K, volumetric flow rate range of 1 $ml.min^{-1}$, 2 $ml.min^{-1}$, 3 $ml.min^{-1}$ and 4 $ml.min^{-1}$, adsorbate concentration range of 15 $mg.L^{-1}$, 20 $mg.L^{-1}$ and 25 $mg.L^{-1}$, and a bed height range of 15 cm, 25 cm, and 35 cm. A fixed amount of CCNT hydrogel beads was placed in a glass column with a height of 60 cm and an internal diameter of 1.5 cm as depicted in Figure 7.2. The bottom of the column consisted of a glass sieve to support the adsorbent. The bottom and top of the column was filled with glass beads to compact the CCNT hydrogel beads bed, minimize dead volume as well as channelling. Aqueous solutions of different adsorbate concentrations were place in a glass beaker and pumped at a specific volumetric flow rate using a peristaltic pump at a fixed volumetric flow rate. Samples were collected using a glass beaker (Figure 7.2), at a specific time interval, which were then filtered using a 0.45 µm syringe filter and transferred into a 10 mL sample tube. The filtered samples were centrifuged at 5000 rpm for 10 minutes. Thereafter, a supernatant solution of the centrifuged sample was analysed for the residual of the respective adsorbate i.e., PFOA, PFOS, AMX, CIP and SMX concentration using a UV-visible spectrophotometer (UV-1900i, Shimadzu, South Africa). Adsorption column experiments were conducted in duplicates for data validation. Samples were collected until the saturation state was reached.

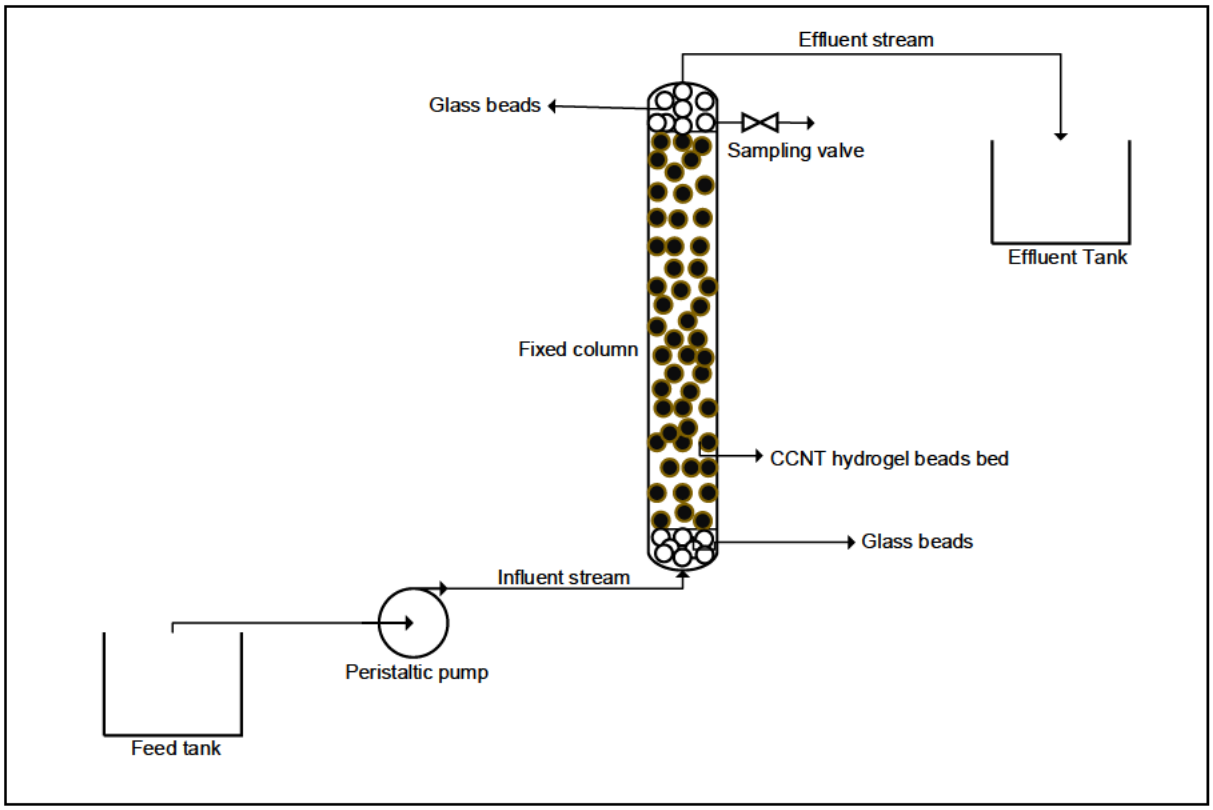

Figure 7.42: Fixed column adsorption experimental set-up

7.3.3. Fixed bed models

In a typical industrial scale wastewater treatment set-up, fixed-bed columns are widely used for continuous adsorption systems over batch operations. However, the longevity of fixed-bed columns is often overlooked as elucidated by Wang *et al.* (2023). Herein, three breakthrough curve models were applied to correlate adsorption-equilibria data.

The Thomas model

$$\frac{c_i}{c_{0i}} = \frac{1}{1 + exp\left(\frac{k_T q_0 m}{Q - k_T c_0 t}\right)} \tag{7.1}$$

The log-Gompertz model

$$\frac{c_i}{c_{0i}} = exp[-exp(k_{G1} - k_{G2} \ln t)] \tag{7.2}$$

The simplified Bohart-Adams model

$$\frac{c_i}{c_{0i}} = exp\left(k_{BA} c_0 t - \frac{k_{BA} N_0 L}{v}\right) \tag{7.3}$$

Where c_i and c_{oi} are the concentration of species i in the liquid phase at time t in mg.L^{-1} and the concentration of species i in the feed in mg.L^{-1}, respectively; k_T and k_{BA} are the rate coefficients measured in cm^3.mg^{-1}.min^{-1} for the Thomas and Bohart-Adams models, respectively; m is the amount of adsorbent in the column measured in mg; q_0 (mg.g^{-1}) is the solid loading per unit mass of adsorbent; and Q (cm^3.min^{-1}) is the volumetric flow rate; k_{G1} is a dimensionless parameter; k_{G2} is the log-Gompertz model parameter expressed in units of min^{-1}; N_0 (mg.cm^{-3}) is the adsorption capacity of the adsorbent per unit volume of the bed; L is the height of the bed in cm; and v is the superficial velocity measured in cm.min^{-1} (Chu and Hashim 2023; Wang *et al.* 2023).

7.3.3.1. Model evaluation

Herein, the error analysis approach was adopted in mathematically evaluating the goodness of fit of the experimental and computed data. For the present work, the chi-square test (χ^2), and sum of squares error (SSE)) were used together with the coefficients of determination i.e., R^2 and adjusted R^2 in evaluating the goodness of fit for the tested breakthrough curve models. For a perfect model, the error functions are relatively low, approaching zero, and the coefficients of determination are tantamount to a unity. For the present work, sensitivity analysis was performed using the four-step procedure outlined by Khumalo, Bakare and Rathilal (2024) i.e., 1) initializing each model parameters with the minimum possible value of the objective function i.e., SSE, 2) the nonlinear regression analysis was then applied aimed at finding the optimal solution that minimize the objective function, 3) the perturbation concept was then applied whereby one parameter was modified at a time while keeping other parameters constant, 4) where necessary re-estimation of the objective function was performed for each perturbation, and the global minimum was obtained when the perturbation for all model parameters was 0%. On the other hand, if the model parameter does not yield a global minimum at the 0% perturbation, that will suggest a poor non-linear regression analysis-based estimation of the values of the model parameters.

$$\chi^2 = \sum \frac{\left(c_{i,exp} - c_{i,model}\right)^2}{c_{i,model}} \tag{7.4}$$

$$SSE = \sum_{i=1}^{n} \left(c_{i_{exp}} - c_{i_{model}}\right)^2 \tag{7.5}$$

$$R^2 = \left(\frac{\sum_i^n \left(c_{i_{exp}} - \bar{c}_{i_{exp}}\right)^2 - \sum_i^n \left(c_{i_{exp}} - c_{i_{model}}\right)^2}{\sum_i^n \left(c_{i_{exp}} - \bar{c}_{i_{exp}}\right)^2} \right) \tag{7.6}$$

$$adj.R^2 = 1 - \left[\frac{(1-R^2)(n-1)}{n-p-1}\right] \quad (7.7)$$

Where p is the number of model parameters; n is the number of data set point; c_{iexp} is the experimentally measured relative concentration of species i; $\bar{c}_{i_{exp}}$ is the average of all measured experimental values of relative concentration; and $c_{i_{model}}$ is the predicted value by the fitted model (Khumalo, Bakare and Rathilal 2024).

7.4. Results and Discussion

7.4.1. The effect of volumetric flow rate on the breakthrough curves

Herein, the effect of volumetric flow rate (i.e., from 1 ml.min^{-1} to 4 ml.min^{-1}) on the breakpoint time was investigated for a fixed initial concentration and column bed height of 15 mg.L^{-1} and 35 cm, respectively for CIP, AMX and SMX as depicted in Figure 7.3a, Figure 7.3b and Figure 7.3c, respectively. Similarly, Figure 7.3d and Figure 7.3e depict the breakthrough curves for PFOS and PFOA for an initial concentration of 5 mg.L^{-1} for both PFOA and PFOS at a fixed-bed height of 35 cm. It can be observed from Figure 7.3 that high breakthrough point times were recorded for a volumetric flow rate of 1 ml.min^{-1} and the lowest breakthrough point times were recorded for a volumetric flow rate of 4 ml.min^{-1}. The findings of the present study suggest that an increase in volumetric flow rate results in a decrease in the breakthrough point time. The observed findings can be ascribed to the mere fact that, at relatively high flowrates, the film mass resistance on the surface of the model adsorbent has minimum resistance to the flow of the influent subsequently decreasing the contact time between the adsorbate and adsorbent, resulting in a decrease in the uptake of the model adsorbate. Furthermore, from the results obtained, it is evident from Figure 7.3 that, at high operating volumetric flow rates, the saturation time of the adsorbent increases, suggesting a low uptake of the model adsorbate, thus resulting in low breakthrough point times. On the other hand, the relatively high breakthrough points time under low volumetric flow rates (i.e., 1 ml.min^{-1}) suggest that there was adequate time for the model adsorbates to interact with the adsorbent active sites, subsequently improving the uptake of the model antibiotics and PFAAs.

Moreover, it is worth noting that breakthrough point times were recorded at a relative concentration (i.e., c_t/c_0) of 0.05 as recommended by Geankoplis, Hersel and Lepek (2018). It can be observed from Figure 7.3a, Figure 7.3b and Figure 7.3c that the breakthrough point times were different for a volumetric flow rate of 1 ml.min^{-1} and 4 ml.min^{-1}, CIP recorded 40 min and 14 min; AMX recorded 32 min and 6.3 min; and SMX recorded 22 min and 5.2 min, respectively. The relatively high

breakthrough points time recorded by CIP when compared to AMX and SMX, suggest that the model adsorbent demonstrated high affinity on CIP when compared to AMX and SMX. This can be ascribed to CIP consisting of a carboxylic acid functional group (-COOH) and an amine functional group (-NH_2) on the piperazine moiety which are deprotonated at a solution pH of 7 initiating the electrostatic interaction mechanism as the major adsorption mechanism as opposed to pore filling (Khumalo, Bakare and Rathilal 2024). Despite the high affinity of CCNT hydrogel beads towards CIP, the breakthrough points time decreased significantly with an increase in volumetric flow. The observed trend can be attributed to the mere fact that an increase in volumetric flow rate resulted in an increase in the Reynolds number, subsequently increasing the degree of turbulence and mixing which then result in shorter breakthrough points time as elucidated by Lin *et al.* (2017). Similar trends were observed in Figure 73d and Figure 7.3e for PFOS and PFOA breakthrough curves with varying volumetric flow rate with PFOS recording relatively high breakthrough points time as compared to PFOA. This suggests that CCNT hydrogel beads demonstrated higher affinity towards PFOS than it did with PFOA. The findings of the present study on the effect of volumetric flow rate on the breakthrough curves is congruent to the other studies that are reported in literature (Darweesh and Ahmed 2017; Lin *et al.* 2017; He *et al.* 2022). Therefore, it is evident that low feed flow rates are advisable for the treatment of antibiotics and PFAAs in order to achieve relatively high volumes of treated column effluent. However, it is worth noting that low feed flow rates may result in prolonged operating times, subsequently increasing the operating cost, and risking of rendering the system expensive.

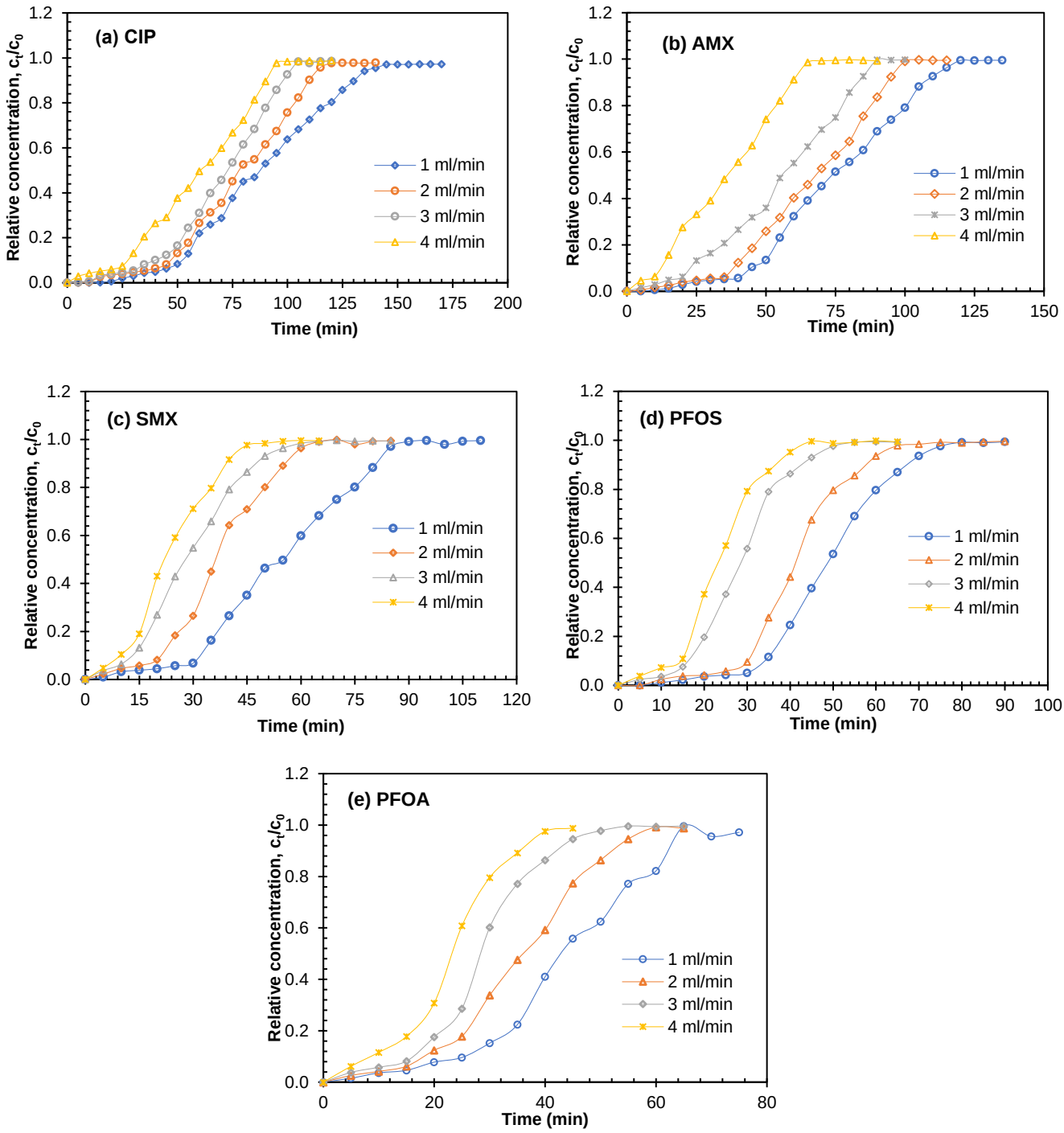

Figure 7.43: **(a)** CIP, **(b)** AMX, **(c)** SMX, **(d)** PFOS and **(e)** PFOA breakthrough curves with varying volumetric flowrate

7.4.2. The effect of initial concentration on the breakthrough curves

Herein, the effect of initial adsorbate concentration was investigated for a concentration range of 15 $mg.L^{-1}$, 20 $mg.L^{-1}$ and 25 $mg.L^{-1}$ for the model antibiotics. On the other hand, the effect of initial concentration was investigated for a range of 5 $mg.L^{-1}$, 10 $mg.L^{-1}$ and 15 $mg.L^{-1}$ for PFOA and PFOS.

Experimental studies were conducted for a fixed column bed height of 35 cm and a volumetric feed flow rate of 1 ml.min^{-1}. Figure 7.4 depicts the findings of the present study.

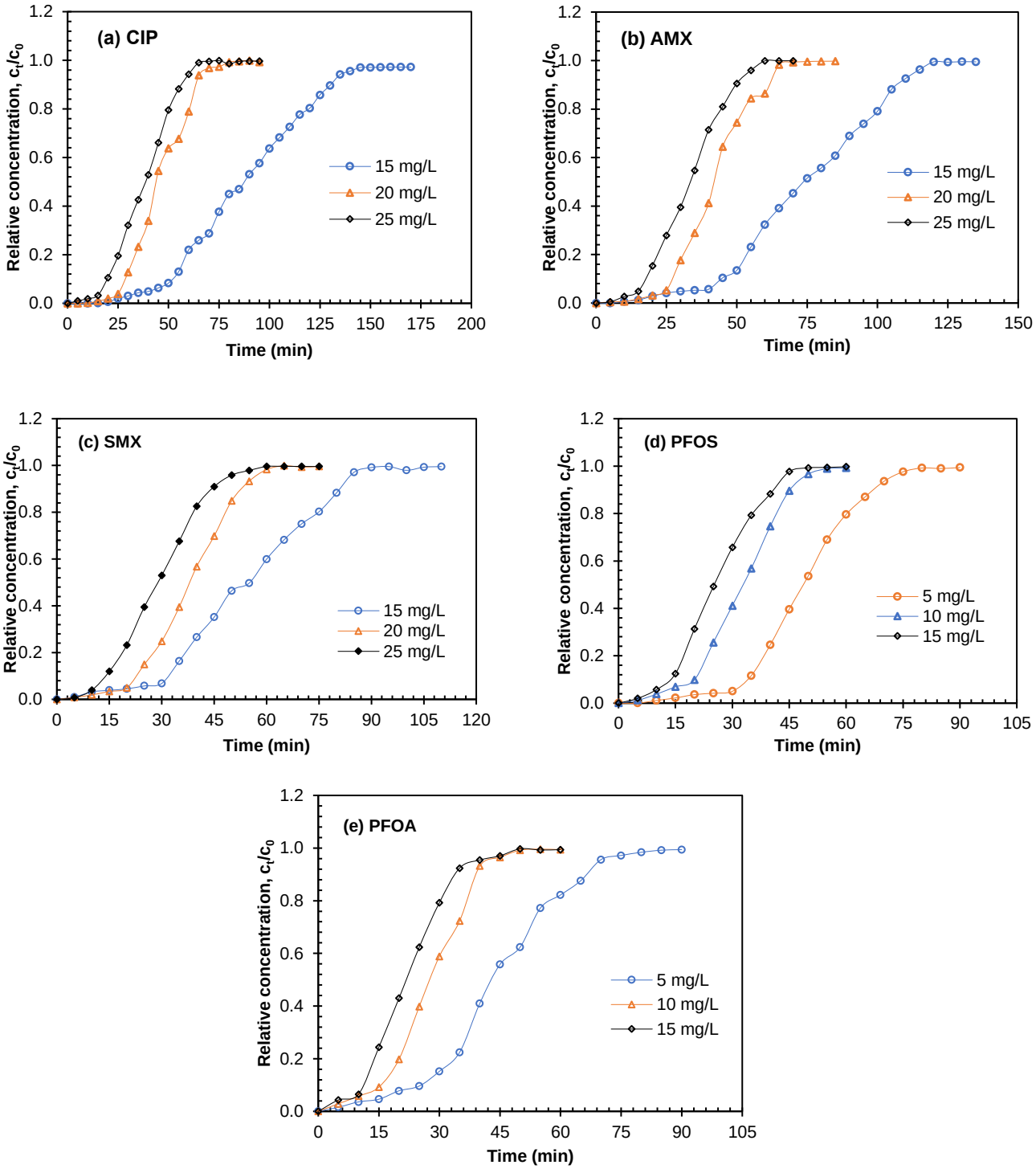

Figure 7.44: **(a)** CIP, **(b)** AMX, **(c)** SMX, **(d)** PFOS and **(e)** PFOA breakthrough curves with varying initial concentration.

It can be inferred from Figure 7.4a to Figure 7.4e that an increase in the initial adsorbate concentration tends to move the breakthrough curves towards the origin. The observed trend is evident that the mass transfer driving force in the liquid film was enhanced by the increase in adsorbate initial concentration resulting in a decrease in breakpoint times. It is worth noting that for CIP (Figure 7.4a), AMX (Figure 7.4b) and SMX (Figure 7.4c), the breakthrough curves demonstrated steeper slopes for an initial concentration of 20 $mg.L^{-1}$ and 25 $mg.L^{-1}$ which is evident that indeed the mass transfer driving force was enhanced with an increase in concentration. A similar trend in the breakthrough curves was observed for PFOS (Figure 7.4d) and PFOA (Figure 7.4e) at an initial concentration of 10 $mg.L^{-1}$ and 15 $mg.L^{-1}$. Moreover, the observed trend of the breakthrough curves with increasing adsorbate initial concentration can be ascribed to the acceleration of the adsorption rate with increasing concentration subsequently leading to early saturation of the column bed as elucidated by Darweesh and Ahmed (2017).

7.4.3. The effect of column fixed-bed height on the breakthrough curve

The effect of fixed-bed column height on the model antibiotics and PFAS breakthrough curves were investigated at a fixed-bed height of 15 cm, 25 cm, and 35 cm. CIP, AMX and SMX concentration was maintained at 15 $mg.L^{-1}$ with PFOS and PFOA concentration kept as 5 $mg.L^{-1}$. The volumetric flow rate was maintained at 1 $ml.min^{-1}$ for all systems investigated. It is apparent from Figure 7.5 that the breakthrough points time increased with an increase in column bed height. The results obtained suggest that indeed relatively high fixed-bed heights correspond to an increase in active sites on the adsorbent surface available for the uptake of the model adsorbate (i.e., CIP, AMX, SMX, PFOS and PFOA). Furthermore, it can be seen from Figure 7.5 that the breakthrough curves shape changed from being a steep concave to flat concave as the column bed increased from 15 cm to 35 cm leading to a relatively large mass transfer zone in the liquid film. The broadened mass transfer zone with an increase in bed height suggest that the total surface area of the adsorbent was accessible to the adsorbate molecules, thus enhancing the uptake of CIP (Figure 7.5a), AMX (Figure 7.5b), SMX (Figure 7.5c), PFOS (Figure 7.5d) and PFOA (Figure 7.5e). It is worth noting that Liao *et al.* (2013) reported low uptake of tetracycline on bamboo charcoal with an increase in column bed height. This was due to tetracycline molecules not being able to access all the surface area of the bamboo charcoal. Therefore, the findings of the present study suggest that CCNT hydrogel beads have a relatively high void fraction allowing adsorbate molecules to access all active sites available for adsorption, thus potentiating CCNT hydrogel beads to be an effective adsorbent.

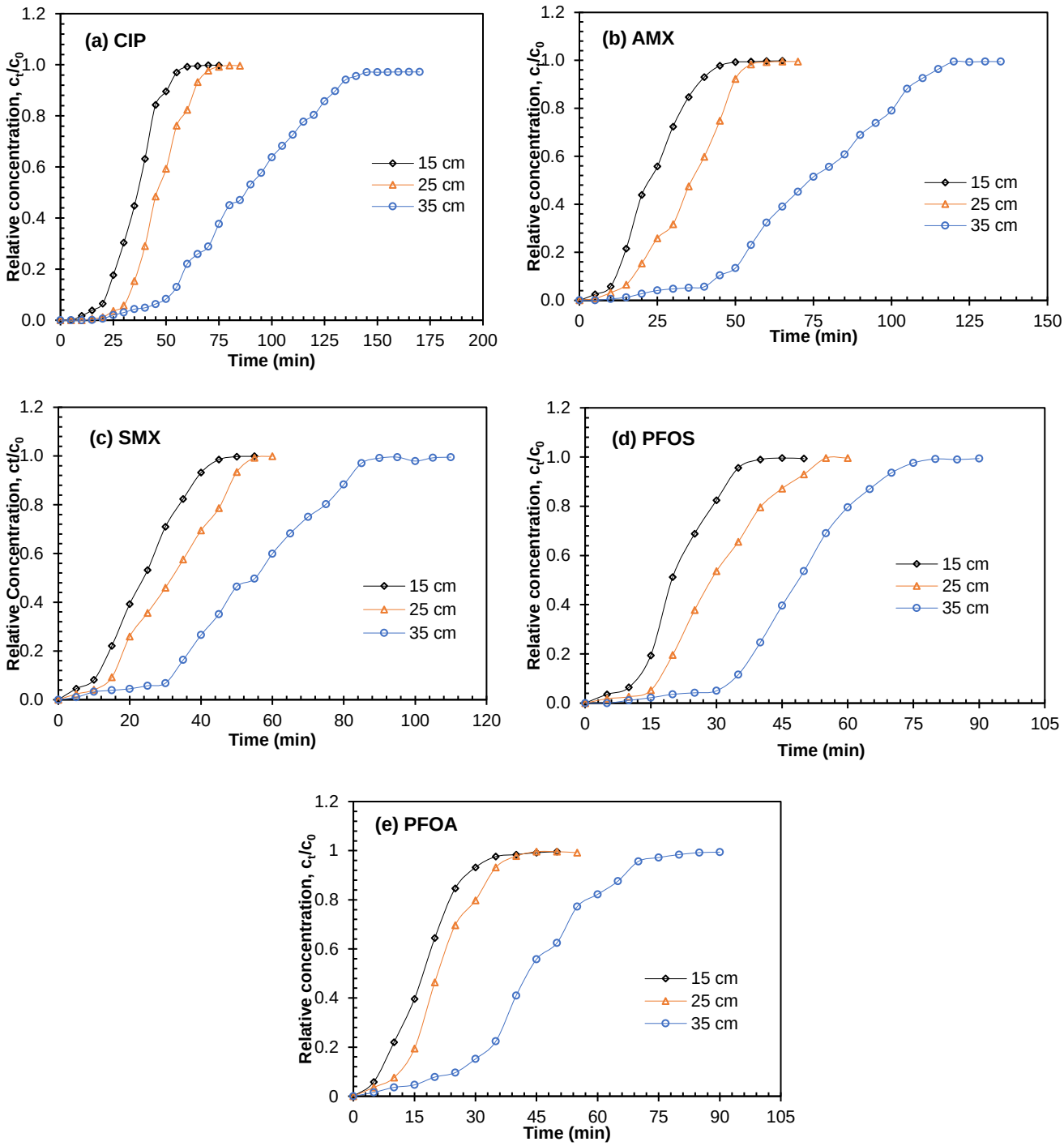

Figure 7.45: **(a)** CIP, **(b)** AMX, **(c)** SMX, **(d)** PFOS and **(e)** PFOA breakthrough curves with varying column bed height.

7.4.4. Adsorption column breakthrough curves modelling

The successful design and operation of a typical fixed-bed adsorption column requires adequate prediction of the breakthrough curve for the effluent (Darweesh and Ahmed 2017). Herein, breakthrough curves experimental data for the uptake of AMX, CIP, SMX, PFOA and PFOS were fitted

in the Thomas, log-Gompertz and Bohart-Adams models aimed at investigating the dynamic behavior of the fixed-bed adsorption system. Breakthrough curve experimental data for at a volumetric flowrate of 1 ml.min^{-1}, fixed-bed height of 35 cm as well as adsorbate concentration of 15 mg.L^{-1} for AMX, CIP and SMX and 5 mg.L^{-1} for PFOA and PFOS were subjected to nonlinear regression analysis. From the results presented in Table 7.1, it can be inferred that the Thomas model recorded the highest values of R^2 for AMX (R^2 = 0.9976), CIP (R^2 = 0.9965), SMX (R^2 = 9950), PFOA (R^2 = 0.9975) and PFOS (R^2 = 0.9991) when compared to the log-Gompertz and Bohart-Adams breakthrough curve models. The findings of the present study suggest that experimental data were well fitted by the Thomas model. The goodness of fit of the Thomas model was further confirmed by the relatively high values of the adj. R^2 of greater than 0.99 for all model contaminants. The difference of less than 0.2 between the R^2 and adj. R^2 values for the Thomas model (Table 7.1) suggest that the predicted R^2 values are in reasonable agreement with the adjusted R^2 values obtained. Furthermore, chi-test square, χ^2 values of less than 0.01 and SSE values of less than 0.017 were recorded by the Thomas model cementing that the breakthrough curves experimental data were well fitted by the Thomas model. The small difference between experimental and model predicted breakpoint times, t_b suggest that the Thomas model can be used to navigate the design space with minimal error as depicted in Figure 7.6a to Figure 7.6e.

Table 7.31: Thomas, log-Gompertz, and Bohart-Adams breakthrough curves model parameters for the uptake of AMX, CIP, SMX, PFOA and PFOS on CCNT hydrogel beads fixed-bead.

Model	**Model parameters**	**AMX**	**CIP**	**SMX**	**PFOA**	**PFOS**
Thomas	k_T (cm^3.mg^{-1}.min^{-1})	0.7656	0.6986	0.5571	0.6275	0.7289
	q_0 (mg.g^{-1})	7.914	8.176	10.05	9.755	11.00
	R^2	0.9976	0.9965	0.9950	0.9975	0.9991
	Adj. R^2	0.9973	0.9961	0.9942	0.9969	0.9989
	χ^2	0.0021	0.010	0.001	2.9E-04	0.001
	SSE	0.0230	0.018	0.017	0.0074	0.003
	t_{bexp} (min)	32	40	22	15.63	30
	t_{bcalc} (min)	29.96	30.7	18.05	17.15	26.01
Log-Gompertz	k_{G1}	14.45	13.92	12.52	13.80	17.83
	k_{G2} (min^{-1})	3.477	3.236	3.280	3.782	4.722
	R^2	0.9916	0.9856	0.9808	0.9868	0.9932
	Adj. R^2	0.9909	0.9847	0.9788	0.9851	0.9923
	χ^2	0.0485	0.037	0.046	0.049	0.041
	SSE	0.081	0.073	0.067	0.039	0.022
	t_{bexp} (min)	32	40	22	15.63	30
	t_{bcalc} (min)	46.22	52.24	32.03	28.10	34.25
Bohart-Adams	k_{AB} (cm^3.mg^{-1}.min^{-1})	0.5478	0.4807	0.4839	0.4125	0.4498
	N_0 (mg.cm^{-3})	0.1036	0.1069	0.0992	0.1158	0.1214

Table 7.1: Continues

	R^2	0.9556	0.8618	0.8531	0.8397	0.8473
	Adj. R^2	0.9498	0.8480	0.8376	0.8053	0.8146
Bohart-	χ^2	0.048	0.046	0.041	0.043	0.061
Adams	SSE	0.429	0.703	0.510	0.471	0.487
	t_{bexp} (min)	32	40	22	15.63	30
	t_{bcalc}	---	---	---	---	---

Furthermore, the log-Gompertz model recorded relatively high R^2 values of greater than 0.98 and 0.83, respectively, with a difference of less than 0.2 between adj. R^2 and R^2 values. However, the significant difference between the experimental and model predicted breakpoint times explicitly indicate that the breakthrough curves experimental data was not adequately fitted by the log-Gompertz model. The results obtained suggest that the breakthrough curves data reported for the present work cannot be defined by an asymmetric function which defines the log-Gompertz model. Similarly, the simplified Bohart-Adams model did not fit the breakthrough curves experimental data which is evident from the relatively high SSE values of more than 0.4 and low adj. R^2 values. The findings of the present work can be ascribed to the mere fact that the Bohart-Adams model is characterized as an exponential function (Wang et al. 2023), resulting in a poor fit of the experimental data which did not exhibit an exponential function as depicted in Figure 7.6. The Bohart-Adams model is based on the surface reaction theory such that it interprets data on the basis that the equilibrium state is not instantaneous, and the adsorption rate is proportional to both the residual capacity of the adsorbent and the concentration of the adsorbate. As such the model Bohart-Adams model is widely used to describe only the initial stage of the breakthrough curve thus disqualifying it as a suitable model to give a full description of the entire breakthrough curve. Hence, the poor fit of the Bohart-Adams model suggests that surface diffusion was not the rate-limiting step for the adsorption process under investigation. The findings of the present work are congruent to the work reported by Darweesh and Ahmed (2017) on the breakthrough curves for the uptake of norfloxacin on granular activated carbon.

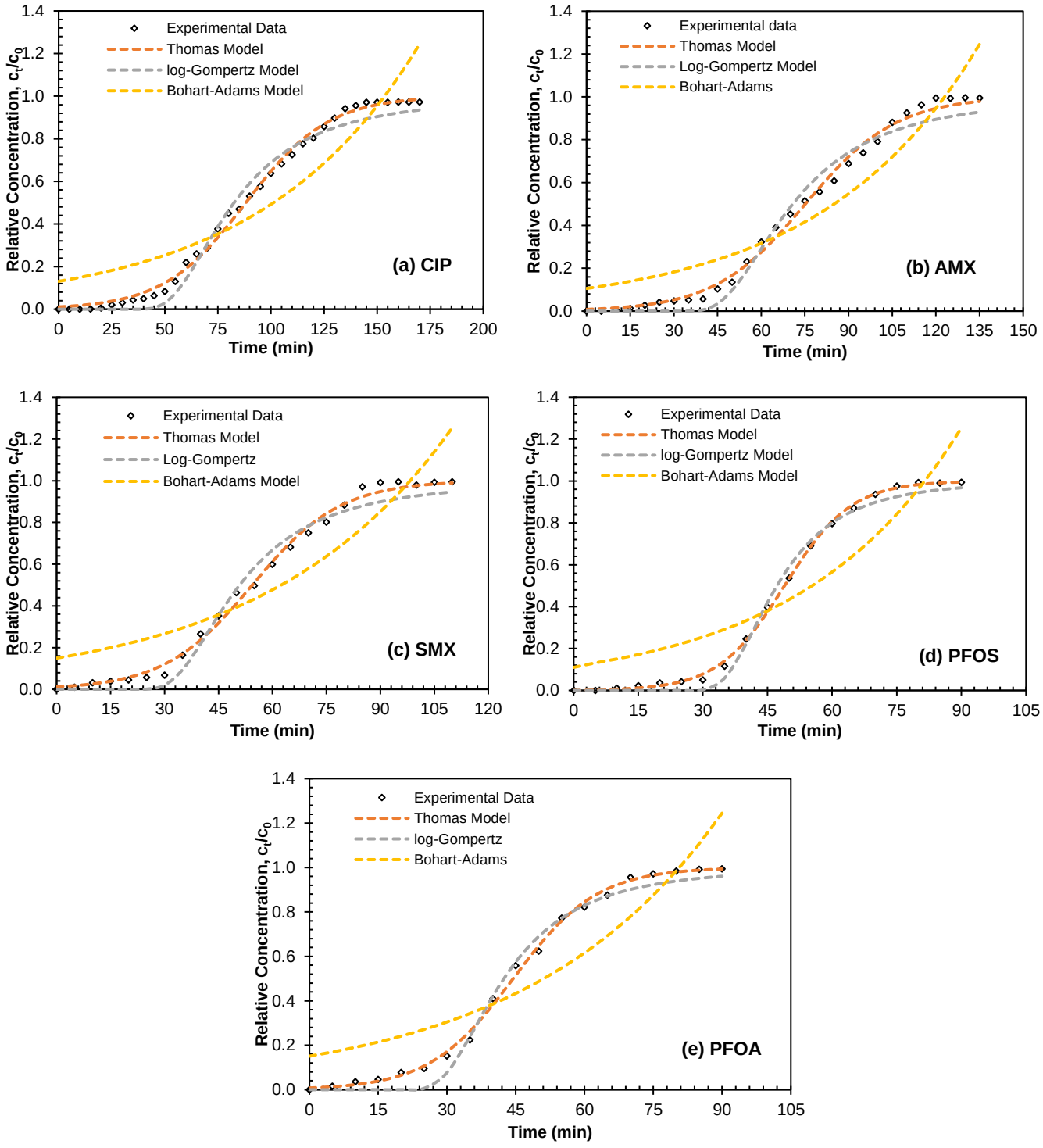

Figure 7.46: Experimental and predicted breakthrough curves for **(a)** CIP, **(b)** AMX, **(c)** SMX, **(d)** PFOS and **(e)** PFOA

7.4.5. Conclusions

The effect of operating parameters i.e., initial adsorbate concentration, bed height, and volumetric flow rate on the breakthrough curves for the sorption of AMX, CIP, SMX, PFOA and PFOS on CCNT

hydrogel beads were investigated. Based on the findings of the current study, it is apparent that the breakthrough point time decreases with an increase in adsorbate initial concentration and operating volumetric flowrate. The opposite was observed with the fixed-bed height. It can be concluded that the decrease in the breakthrough point time with an increase in initial concentration and volumetric flowrate is ascribed to the subsequent decrease in the mass transfer area forcing the breakthrough curves to become more stepper and closer to the origin. Breakthrough experimental data were well fitted in the Thomas model suggesting that the breakthrough curves for the current work can be described by a symmetric function.

References

Chu, K. H. and Hashim, M. A. 2023. Removal of antibiotics through fixed bed adsorption: Comparison of different breakthrough curve models. *Journal of Water Process Engineering*, 56: 104512.

Cuerda-Correa, E. M., Alexandre-Franco, M. F. and Fernández-González, C. 2019. Advanced oxidation processes for the removal of antibiotics from water. An overview. *Water*, 12 (1): 102.

Darweesh, T. M. and Ahmed, M. J. 2017. Adsorption of ciprofloxacin and norfloxacin from aqueous solution onto granular activated carbon in fixed bed column. *Ecotoxicology and environmental safety*, 138: 139-145.

Fan, Y., Zheng, C. and Hou, H. 2019. Preparation of granular activated carbon and its mechanism in the removal of isoniazid, sulfamethoxazole, thiamphenicol, and doxycycline from aqueous solution. *Environmental Engineering Science*, 36 (9): 1027-1040.

Geankoplis, C. J., Hersel, A. A. and Lepek, D. H. 2018. *Transport Processes and Separation Process Principles*. Prentice Hall Press.

Gong, Y., Wang, L., Liu, J., Tang, J. and Zhao, D. 2016. Removal of aqueous perfluorooctanoic acid (PFOA) using starch-stabilized magnetite nanoparticles. *Science of the Total Environment*, 562: 191-200.

He, C., Yang, Y., Hou, Y.-J., Luan, T. and Deng, J. 2022. Chitosan-coated fluoro-functionalized covalent organic framework as adsorbent for efficient removal of per-and polyfluoroalkyl substances from water. *Separation and Purification Technology*, 294: 121195.

Khumalo, S. M., Bakare, B. F. and Rathilal, S. 2022. The occurrence and bioremediation of emerging polyfluorinated compounds in water bodies: a mini review. *Applied Sciences*, 12 (23): 12196.

Khumalo, S. M., Bakare, B. F. and Rathilal, S. 2024. Single and multicomponent adsorption of amoxicillin, ciprofloxacin, and sulfamethoxazole on chitosan-carbon nanotubes hydrogel beads from aqueous solutions: Kinetics, isotherms, and thermodynamic parameters. *Journal of Hazardous Materials Advances*, 13: 100404.

Khumalo, S. M., Lasich, M., Bakare, B. F. and Rathilal, S. 2022. Sorption of perfluorinated and pharmaceutical compounds in plastics: a molecular simulation study. *Water*, 14 (12): 1951.

Khumalo, S. M., Makhathini, T. P., Bwapwa, J. K., Bakare, B. F. and Rathilal, S. 2023. The Occurrence and Fate of Antibiotics and Nonsteroidal Anti-Inflammatory Drugs in Water Treatment Processes: A Review. *Journal of Hazardous Materials Advances*: 100330.

Klein, E. Y., Van Boeckel, T. P., Martinez, E. M., Pant, S., Gandra, S., Levin, S. A., Goossens, H. and Laxminarayan, R. 2018. Global increase and geographic convergence in antibiotic consumption between 2000 and 2015. *Proceedings of the National Academy of Sciences*, 115 (15): E3463-E3470.

Koch, N., Islam, N. F., Sonowal, S., Prasad, R. and Sarma, H. 2021. Environmental antibiotics and resistance genes as emerging contaminants: methods of detection and bioremediation. *Current research in microbial sciences*, 2: 100027.

Lan, L., Kong, X., Sun, H., Li, C. and Liu, D. 2019. High removal efficiency of antibiotic resistance genes in swine wastewater via nanofiltration and reverse osmosis processes. *Journal of environmental management*, 231: 439-445.

Liao, P., Zhan, Z., Dai, J., Wu, X., Zhang, W., Wang, K. and Yuan, S. 2013. Adsorption of tetracycline and chloramphenicol in aqueous solutions by bamboo charcoal: a batch and fixed-bed column study. *Chemical engineering journal*, 228: 496-505.

Lin, X., Huang, Q., Qi, G., Shi, S., Xiong, L., Huang, C., Chen, X., Li, H. and Chen, X. 2017. Estimation of fixed-bed column parameters and mathematical modeling of breakthrough behaviors for adsorption of levulinic acid from aqueous solution using SY-01 resin. *Separation and Purification Technology*, 174: 222-231.

Long, L., Hu, X., Yan, J., Zeng, Y., Zhang, J. and Xue, Y. 2019. Novel chitosan–ethylene glycol hydrogel for the removal of aqueous perfluorooctanoic acid. *Journal of Environmental Sciences*, 84: 21-28.

Parvin, S., Hara-Yamamura, H., Kanai, Y., Yamasaki, A., Adachi, T., Sorn, S., Honda, R. and Yamamura, H. 2023. Important properties of anion exchange resins for efficient removal of PFOS and PFOA from groundwater. *Chemosphere*, 341: 139983.

Tran, N. H., Reinhard, M. and Gin, K. Y.-H. 2018. Occurrence and fate of emerging contaminants in municipal wastewater treatment plants from different geographical regions-a review. *Water Research*, 133: 182-207.

Wang, J. and Zhuan, R. 2020. Degradation of antibiotics by advanced oxidation processes: An overview. *Science of the Total Environment*, 701: 135023.

Wang, T., Pan, X., Ben, W., Wang, J., Hou, P. and Qiang, Z. 2017. Adsorptive removal of antibiotics from water using magnetic ion exchange resin. *Journal of Environmental Sciences*, 52: 111-117.

Wang, Y., Wang, C., Huang, X., Zhang, Q., Wang, T. and Guo, X. 2023. Guideline for modeling solid-liquid adsorption: Kinetics, isotherm, fixed bed, and thermodynamics. *Chemosphere*: 140736.

Xu, B., Liu, S., Zhou, J. L., Zheng, C., Weifeng, J., Chen, B., Zhang, T. and Qiu, W. 2021. PFAS and their substitutes in groundwater: Occurrence, transformation and remediation. *Journal of Hazardous Materials*, 412: 125159.

Yaqubi, O., Tai, M. H., Mitra, D., Gerente, C., Neoh, K. G., Wang, C.-H. and Andres, Y. 2021. Adsorptive removal of tetracycline and amoxicillin from aqueous solution by leached carbon black waste and chitosan-carbon composite beads. *Journal of Environmental Chemical Engineering*, 9 (1): 104988.

Zhang, D., Zhang, W. and Liang, Y. 2019. Adsorption of perfluoroalkyl and polyfluoroalkyl substances (PFASs) from aqueous solution-A review. *Science of the Total Environment*, 694: 133606.

CHAPTER EIGHT: MOLECULAR SIMULATION

SORPTION OF PERFLUORINATED AND PHARMACEUTICAL COMPOUNDS IN PLASTICS: A MOLECULAR SIMULATION STUDY

8.1. Abstract

The aim of this chapter is to investigate the effect of temperature and degree of polymerisation on the thermodynamic interaction of perfluorinated compounds (PFCs) into plastics. The occurrence of contaminants of emerging concern such as pharmaceutical drugs, PFCs, microplastics (MPs), etc., in sources of drinking water have posed significant health risks to aquatic life and humans in recent years. These organic pollutants can interact with MPs and pose much higher health risks; consequently, MPs become a transport vector and thus alter their migration as well as occurrence in the environment. The purpose of this chapter is to examine the adsorption mechanism of perfluorooctanoic acid (PFOA), perfluorooctane sulfonic acid (PFOS), and sulfamethazine (SMT)—relative to water—on polyethylene (PE) and polypropylene (PP) using an extended Flory–Huggins approach. The results suggest that in an aqueous environment, both PFOA and PFOS may be taken up preferentially by PP and PE, although less strongly by PE. The degree of polymerisation of PE and PP did not significantly influence the observed behaviour. In terms of sorption affinity, the observed affinity was PFOA>PFOS>SMT which was consistence for both PE and PP.

8.2. Introduction

Microplastics (MPs), pharmaceutical compounds and perfluorinated compounds (PFCs) such as perfluorooctanoic acid (PFOA) and perfluorooctane sulfonic acid (PFOS) are persistent organic pollutants of emerging concerned (Hassan *et al.* 2020; Al Harraq and Bharti 2021). The occurrence of the aforementioned compounds poses potential toxicity to biotic and abiotic ecosystem (Yaqoob *et al.* 2020). Due to the environmental concerns instigated by water pollution as a result of rapid population growth and industrialisation which has a direct impact on wastewater composition which is now characterised by contaminants of emerging concern (PFCs, pharmaceuticals, MPs, heavy metal ions, etc.,) which have eluded conventional wastewater treatment processes (Chen *et al.* 2011; Armah *et al.* 2021). This is attributed to the fact that conventional wastewater treatment processes are designed to treat wastewater streams characterised with organic pollutants such as chemical oxygen demand, total dissolved solids, biological nutrients e.g., phosphates and nitrates, etc., and they have demonstrated to be ineffective to handle the current wastewater volumes (Ahmed *et al.* 2020; Armah *et al.* 2021; Khumalo *et al.* 2022).

PFCs which constitutes of the carbon-fluorine bond (C-F) characterised by strong polarity and strength, which is attributed by the strong electro negativity of fluorine not only in halogens but in all elements in the periodic table (Espana, Mallavarapu and Naidu 2015; Hassan *et al.* 2020). Due to the aforementioned properties, PFCs have cemented their application in a variety of products and industries. Moreover, these PFCs are resistant to degradation by heat and acid (QIU, FUJII and TANAKA 2007; Arvaniti and Stasinakis 2015; Espana, Mallavarapu and Naidu 2015; Lenka, Kah and Padhye 2021). PFCs are widely used for surface treatment of textiles due to their repulsion behaviour in both water and oil (Espana, Mallavarapu and Naidu 2015), used as a formulation agent of aqueous film forming foams commonly used for combating hydrocarbon fires (Espana, Mallavarapu and Naidu 2015; Ahmed *et al.* 2020), used as food packing paper and in leather treatment (Arvaniti and Stasinakis 2015; Lenka, Kah and Padhye 2021), polymer emulsifier and insecticides (Kissa 2001). PFCs are characterised as a class of emerging persistent organic pollutants that consist of a fully fluorinated hydrophobic alkyl chain attached to a hydrophilic chain end group as depicted in Figure 8.1. (Arvaniti and Stasinakis 2015; Lenka, Kah and Padhye 2021). The occurrence of PFCs in surface water i.e., rivers, ponds and lakes is attributed to the discharge of untreated industrial effluent, leakage from the soil as well as surface deposition (Ahmed *et al.* 2020). Due to long term exposure to PFCs, several studies (QIU, FUJII and TANAKA 2007; Crone *et al.* 2019; Ahmed *et al.* 2020) have reported that some PFCs particularly PFOAs and PFOSs, have been detected in human tissue and blood serum. Crone *et al.* (2019) and EPA (2016) have reported the human health complications associated with exposure to PFOAs and PFOSs which include high cholesterol, increased liver enzymes, testicular and kidney cancer, poor vaccination response, thyroid disorders, pregnancy-induced hypertension and preeclampsia, immune suppression as well as reduced fertility.

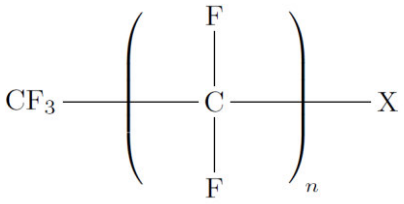

Figure 8.47: General structure of PFCs.

Pharmaceuticals such as sulfamethazine (SMT) characterised as an active drug compound classified as an antibiotic has been detected in the environment (Mulla *et al.* 2021). This may be attributed to the application of SMT for a wide range of antibacterial activity, high therapeutic effectiveness and low costs (Acosta-Rangel *et al.* 2019; Mulla *et al.* 2021). Apart from the usefulness of SMT, its occurrence in the environment poses a serious health-risk to the aquatic ecosystem, flora, fauna and humans, as reported in previous studies (Houtman 2010; Xu *et al.* 2020; Mulla *et al.* 2021). On the other hand, the occurrence of plastic residues in surface water is an emerging environmental problem which is

attributed to the unsustainable disposal of plastic residues which ultimately reaches and persists in the aquatic environment (Llorca *et al.* 2018; Richardson and Ternes 2018; Wu *et al.* 2019). According to Wu *et al.* (2019), these plastic residues can undergo processes of degradation, embrittlement and fragmentation when they are subjected to certain conditions such as solar radiation, wave slap, temperature change as well as biological effects. Upon their degradation, once the size of these synthetic polymers is less than 5 mm without any lower limit, they are called microplastics (Li, Liu and Chen 2018; Wu *et al.* 2019). The hazardous effects of MPs is not limited to their ability to release hazardous organic monomers (Wang *et al.* 2020), but also to their ability to interact with other pollutants (Wu *et al.* 2019) thus posing a high health risk to aquatic life. Note that, MPs with or without pollutants can be ingested by aquatic life thus resulting in bioaccumulation which can consistently adversely affect numerous organs since they are characterised as endocrine disrupting compounds (Ramhøj *et al.* 2018; Wu *et al.* 2019).

Hitherto, researchers are exploring new avenues aimed at designing effective water and wastewater treatment processes aimed at combating the bioaccumulation of emerging contaminants on the environment. Solid-liquid adsorption has drawn so much attention for many researchers as a promising technology to combat the occurrence of pollutants in the environment (Rashid *et al.* 2021; Rathi and Kumar 2021). The purpose of this paper is to study the adsorption mechanisms of PFCs and SMT by investigating the thermodynamic interaction of PFOA, PFOS and SMT in polyethylene (PE) and polypropylene (PP) through phase equilibrium and mixing using the extended Flory-Huggins approach in Material Studio. To the best of our knowledge, there are no reported studies on investigating the effect of temperature and polymerization on the thermodynamic interaction of the aforementioned compounds with PE and PP using the extended Flory-Huggins approach. The findings of the current study will contribute to the design of solid-liquid adsorption wastewater treatment processes aimed at eradicating the occurrence of the model contaminants thus, improving the water quality. Note that, PE and PP are the most frequently detected types of MPs in the aquatic environment (Li, Zhang and Zhang 2018).

8.3. Materials and Methods

The simplest thermodynamic theory to describe mixing and phase separation is the Flory-Huggins approach (Flory 1953), which describes the free energy of mixing (ΔG) in binary systems as follows:

$$\Delta G / (RT) = (\varphi_b / n_b) \ln \varphi_b + (\varphi_s / n_s) \ln \varphi_s + \chi_{bs} \varphi_b \varphi_s \quad (8.1)$$

Wherein φ_i is the volume fraction of component i, n_i is the degree of polymerization of component i, χ_{bs} is the binary interaction parameter, and T and R are the temperature and universal gas constant,

respectively. The subscripts *b* and *s* refer to the role of the component in question in the mixture, namely whether it is the base (*b*) or the screen (*s*). The mixing energy E_{mix} is used to determine the interaction parameter χ_{bs}:

$$\chi_{bs} = E_{mix} / (RT) \tag{8.2}$$

The conventional Flory-Huggins model employs a lattice description for each component. In the case of a lattice with the coordination number set to *Z*, the mixing energy is then a function of the binding energy E_{ij} between each component pair *ij*:

$$E_{mix} = 0.5\ Z\ (E_{bs} + E_{sb} - E_{bb} - E_{ss}) \tag{8.3}$$

The Flory-Huggins approach was extended by incorporating techniques from molecular simulations, specifically by considering the binding energies as averages over an ensemble of molecular configurations (Blanco 1991; Fan *et al.* 1992) as implemented in version 2020 of the computer program Materials Studio (Biovia 2020). Firstly, the interaction parameter's temperature dependence is described explicitly by generating a large number of pair configurations and calculating the associated binding energies, followed by averaging results via the Boltzmann factor and determining the resulting temperature-dependent interaction parameter. Secondly, an off-lattice structure is considered by which the coordination number *Z* is computed explicitly for each of the possible configurations using atomistic molecular simulations. Use of a temperature-dependent interaction parameter χ in the Flory-Huggins expression yields the free energy for all compositions and temperatures, following which the phase diagram can be determined by computing the critical point, binodal, and spinodal curves.

The binding energies given in equation 8.3 were calculated by sampling from energetically favourable configurations by way of the volume constraint method (Blanco 1991), wherein molecules are combined in order for their van der Waals surfaces to get in contact with each other. Depending on the roles of the pair of molecules under consideration, the binding energy is yielded for each of the binding energy combinations E_{bs}, E_{sb}, E_{bb}, and E_{ss}. Note that E_{bs} and E_{sb} are equivalent, and so there are three binding energy pairs that are actually computed. To calculate the binding energy, two molecular structures representing the condensed state are generated, and if a molecule possesses significant flexibility, then a set of conformations is generated which is presentative of the condensed state. A single seed molecule is first introduced into the system following which a packing molecule is positioned such that its centre of mass is located at the same position as the original seed molecule. Next, the packing molecule's rotation is altered randomly, and it is then translated along a randomly selected direction until its van der Waals surface ceases to overlap but remains in contact with the initial seed molecule. The pairwise interaction energy of the resulting configuration is stored, and a histogram

(with a bin width of 8×10^{-2} kJ/mol) of the resulting distribution of the binding energy is derived from 10^7 energy samples. The average weighted binding energy $\langle E_{ij}\rangle_T$ at a specified temperature T is computed as the weighted average of a distribution function using the Boltzmann factor $\exp(-E_{ij}/RT)$:

$$\langle E_{ij}\rangle_T = \int \mathrm{d}E\ E\ P_{ij}(E) \exp(-E/RT) \,/\, [\int \mathrm{d}E\ P_{ij}(E) \exp(-E/RT)] \tag{8.4}$$

The coordination number Z describes the number of molecules of one component that can be packed around a solitary molecule of the other species in the pair under consideration. A single molecule of component i surrounded by Z_{ij} molecules of component j together constitute a cluster of a single seed molecule of i with Z_{ij} packing molecules. The four different combinations of clusters that are considered (using the aforementioned base-screen terminology) are as follows: Z_{bb} (in which the base species plays the role of both seed and packing molecules), Z_{bs} (for which the base species is the seed, and the screen molecules are the packing), Z_{sb} (the converse of Z_{bs}), and Z_{ss} (wherein the screen species is both the seed and the packing). To determine the coordination number, the approach used to estimate the binding energy was extended (neglecting the energy calculation itself). First, a single seed molecule was introduced, following which a packing molecule was added such that its centre of mass was overlaid onto the centre of mass of the initial seed molecule. The packing molecule was then rotated a random amount, following which it was translated in a random direction until its van der Waals surface no longer overlapped with the seed molecule. Subsequent packing molecules are added in a similar fashion, although with overlapping being avoided for the newly added packing molecule with respect to the cluster thus far (i.e., the seed + packing molecules already in the system). Furthermore, any newly introduced packing molecule must be in contact with the seed molecule; if they are not, their introduction into the system is rejected and another attempt is made to add a packing molecule. These steps are repeated for 20 iterations per cluster type and 10^5 samples per cluster to determine the average coordination number.

Once the weighted average binding energies $\langle E_{ij}\rangle_T$ and average coordination numbers Z_{ij} are computed, the mixing energy was calculated via:

$$E_{mix} = 0.5\ (Z_{bs}\langle E_{bs}\rangle_T + Z_{sb}\langle E_{sb}\rangle_T - Z_{bb}\langle E_{bb}\rangle_T - Z_{ss}\langle E_{ss}\rangle_T) \tag{8.5}$$

The binary interaction parameter χ_{bs} is then readily computed as E_{mix}/RT for subsequent use within Flory-Huggins theory as outlined previously. Once the free energy isotherms are known, the phase diagram can be computed. The implementation of the extended Flory-Huggins approach employed in this study included a search for temperature ranges for which phase separation occurs, which may be noted as a limitation of the study. At the critical point (where the two phases become indistinguishable), both the second and third derivatives of the free energy with respect to composition disappear. The

coexistence region is bounded by the binodal curve, which indicates the conditions at which two distinct separate phases may coexist; in the case of the systems under consideration in the study, this implies the existence of a PFC-in-polymer phase in conjunction with a polymer-in-PFC phase. In practice, the concentration of the polymer in the polymer-in-PFC phase is so low as to be negligible, as the polymers are largely not dissolved into the PFC whereas the PFC is absorbed into the polymeric matrix. The binodal curve connects the distant points on either side of the critical point, at which the first derivative of the free energy is equal to the ratio of the free energy difference with respect to the composition difference:

$$(\partial \Delta G / \partial x)_{x1} = (\partial \Delta G / \partial x)_{x2} = [\Delta G(x_2) - \Delta G(x_1)] / (x_2 - x_1) \quad (8.6)$$

where x_i is the binodal composition of phase i. The locations within the coexistence region where the second derivatives of the free energy with respect to the compositions are zero (i.e., inflection points) yields the spinodal curve which describes the point at which phase separation occurs.

The approach of describing sorption in polymers by way of phase equilibrium and mixing is analogous to previous work on water absorption in polyethylene (Johansson *et al.* 2007; Erdtman *et al.* 2016) and polyterafluoroethylene (Lasich, Johansson and Ramjugernath 2013).

8.4. Results and Discussion

Commercial plastics are characterised by synthetic polymers derived from fossil-based sources, such as PE and PP, amongst others (Torres *et al.* 2021), where PP and PE being the most detected synthetic polymers in the environment. The findings of the current study on the interaction between MPs and the model contaminants of emerging concern are interpreted with reference to three main sorption mechanisms, i.e., pore-filling, hydrophobic interaction, and van der Waals forces (Umar *et al.* 2021; Yaqoob *et al.* 2021).

Figure 8.2 to Figure 8.4 show results for the sorption of all studied chemical contaminants on PE and PP. The results are presented in terms of temperature variation for different degrees of polymerisation for each polymer investigated. The standard deviation derived from three independent computations is estimated at about 0.05%, which is too small to display on the diagrams. It is apparent that there is strong correlation between temperature and the degree of sorption whilst the degree of polymerization has a limited effect, at least in terms of molar composition. The pore-filling sorption mechanism as characterised by Wang *et al.* (2020) involves the process of contaminants entering the polymer pores and remaining trapped inside the nano-scale pores because of the many pores of different sizes that exist in polymers. This sorption mechanism is highly temperature dependent. Note that when heat energy is applied to a polymer molecular chain, it allows for the polymer to expand. At the glass transition

temperature, which is the temperature at which 30 – 50 carbon chains start to move (Shrivastava 2018), the amorphous region dissociates from a rigid state to a rubbery state. Thus, increasing the free volume, which is basically the gap between molecular chains, for the sorption of contaminants. While not directly accounted for in this work's methodology, the observed results may be attributed to PE and PP being rubbery plastics as indicated in previous works (Guo *et al.* 2012; Wang *et al.* 2020).

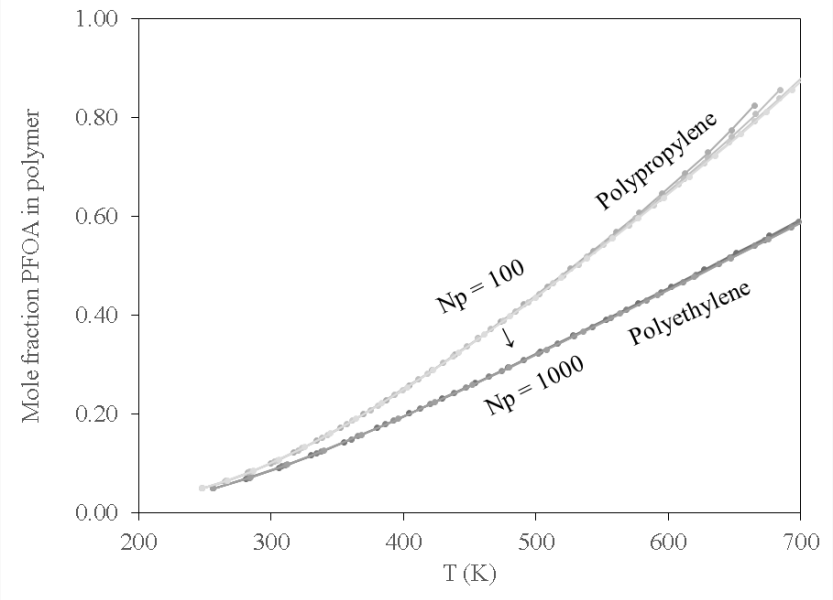

Figure 8.48: Effect of temperature on PFOA content of PP and PE with respect to the degree of polymerization (Np).

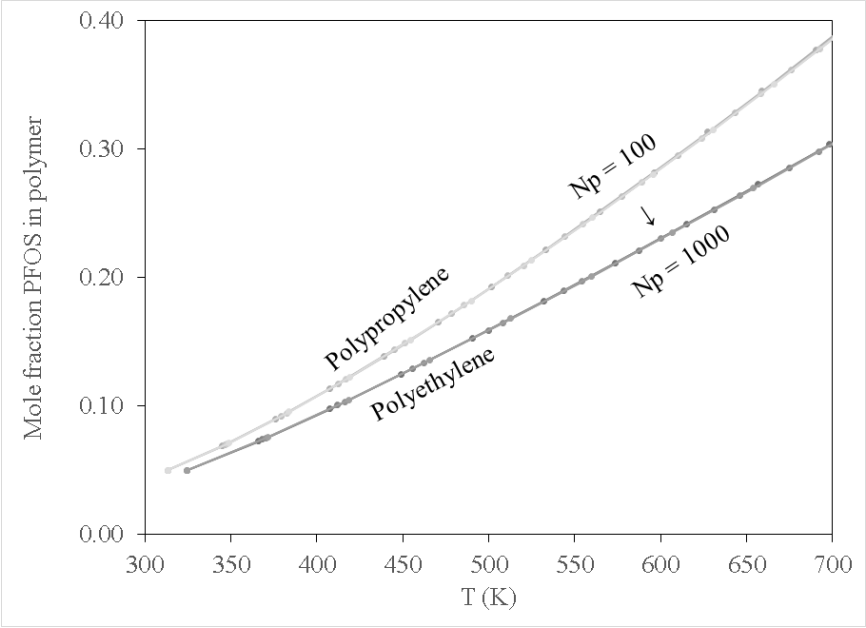

Figure 8.49: Effect of temperature on PFOS content of PP and PE with respect to the degree of polymerization (Np).

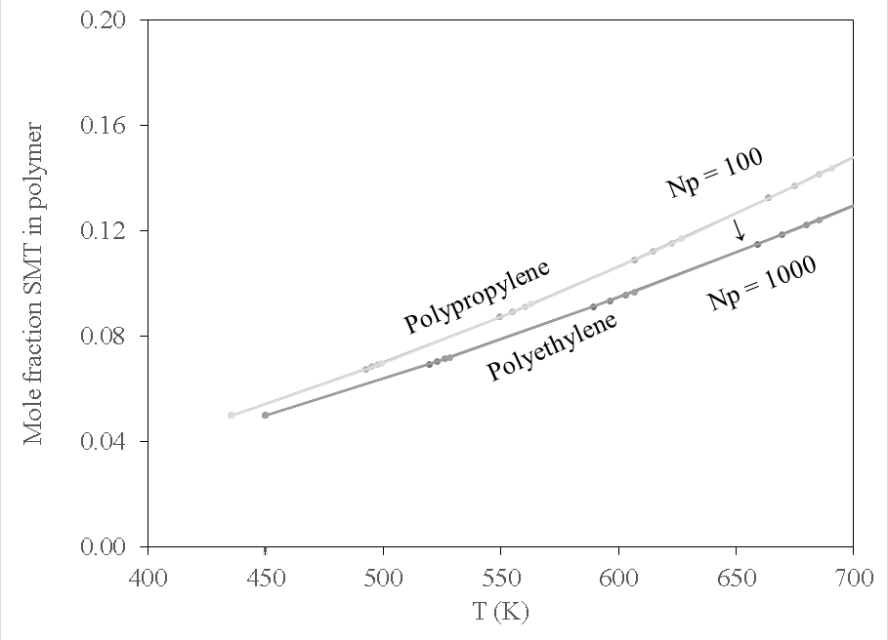

Figure 8.50: Effect of temperature on SMT content of PP and PE with respect to the degree of polymerization (Np).

PP recorded higher contaminant sorption at lower temperatures when compared to PE for all contaminant species. This is attributed to the difference in molecular weight between PP (-CH_2-CH_2-CH_2-)$_n$ and PE (-CH_2-CH_2-)$_n$; according to Young and Lovell (2011), there is a strong correlation in the increase in polymer molecular weight and the total fractional free volume of a polymer, consequently favouring the pore-filling sorption mechanism of contaminants. While not explicitly accounted for in the computations in this study, considering the effect of polymer chain length on the glass transition temperature can be instructive. Note that the glass transition temperature increases with increase in polymer molecular weight, yet the findings of the current study indicate that sorption of PFOA, PFOS and SMT onto PP occurred at a lower temperature compared to PE. This can be attributed to PE having higher crystallinity as compared to PP, thus requiring more thermal energy to expand the PE polymer, consequently increasing its free volume allowing for pore-filling sorption to occur at relatively high temperatures compared to PP. The observed results suggest that this effect or an analogous one may be implicitly produced in the course of the computations employed in this study.

The sorption of PFOS and PFOA on PP and PE at low temperature conditions of 300 K as depicted in Figure 8.2 and Figure 8.3 may be attributed to van der Waals force interaction. This is a relatively weak force characterising the attraction of intermolecular forces between MP molecules (i.e., PP and PE) and organic contaminant molecules thus allowing them to adhere to each other as reported by Wang *et al.* (2020) and Agboola and Benson (2021). Based on previous works (Wang, Shih and Li 2015; Wang *et al.* 2020; Agboola and Benson 2021), it is apparent that the sorption of aliphatic as well as aromatic organic contaminants into aliphatic MPs can also be interpreted by van der Waals force interactions.

Moreover, Xu *et al.* (2018) reported a linear relationship for the sorption of sulfamethoxazole on PE. However, it was reported that under the pH conditions in which the study was conducted, both sulfamethoxazole and PE, MPs recorded negative charges, hence the sorption mechanism could not be explained by hydrophobic or electrostatic interaction. For the current study, based on the findings presented in Figure 8.4, it is apparent that there was significant sorption of SMT at temperature conditions of 450 K and above on both PE and PP. The sorption mechanism of SMT on PE and PP may be attributed to pore-filling. It is imperative to note that SMT sorption on PE and PP is highly temperature dependant which may be attributed to the molecular structure of SMT ($C_{12}H_{14}N_4O_2S$), hence an increase in temperature allows for the motion of molecules for MPs consequently increasing the free volume to allow for the sorption of SMT.

Figure 8.2 shows that PFOA demonstrated high sorption affinity towards PP and PE when compared to PFOS (see Figure 8.3). This may be attributed to the difference in physicochemical properties of the two compounds PFOA is characterised as a non-polar compound whereas PFOS exhibits some polarity because of the sulfonate group. Note that C-C as well as C-H bonds in hydrocarbons are characterised as non-polar molecules, hence PE and PP are non-polar polymers. Due to the non-polarity of PE and PP, PFOA demonstrated high sorption affinity towards PE and PP by the polar-polar interaction as compared to PFOS which exhibited some degree of polarity.

In addition to examining sorption for pure contaminant species, it is instructive to include the results for water since the conditions of interest for PFOA, PFOS and SMT are aqueous environments. These results are presented in Figure 8.5. Direct comparisons between water and the contaminant species at a fixed polymerization of Np = 100 are shown in Figure 8.6 and Figure 8.7 for PE and PP, respectively. In this context, it is apparent that both PE and PP are likely to not be useful to remove SMT in aqueous conditions, since water displays higher affinity for sorption in both polymer species than SMT. Both PFOS and PFOA exhibit stronger affinity for uptake in PE and PP than water. This is not entirely explained by the polarity of PFOS and PFOA with respect to water, since (within the framework of the COMPASS force field) the respective magnitudes of the dipole moments are 3.06, 1.95, and 2.30 Debye, respectively (note that the magnitude of the dipole moment of SMT is 3.85 Debye). As organic molecules, PFOS and PFOA do of course possess carbon chains, which would interact with polymer chains even if the molecules as a whole are significantly polar. Hence, the interactions between the contaminant molecules and polymers (especially when considered within an aqueous environment) require a more nuanced assessment. In terms of the temperature effects, at ambient conditions (i.e., around 298 K), it is apparent that only PFOA has higher sorption in both PE and PP than water. Whereas higher temperatures are necessary to induce preferential uptake of PFOS in aqueous environments (above 390 K for PP, and over 450 K for PE), which shows that these MPs may be vectors for transporting PFOA into the environment in general whilst special conditions are required for environmental transmission of PFOS in this manner. It is then also unlikely that PE and PP are vectors

for the transportation of SMT into aqueous environments. This implies that both PE and PP are transport vectors for PFOA as well as posing a risk for bioaccumulation in marine animals via ingestion of MPs, causing negative health effects as reported by Wu *et al.* (2019) and Ramhøj *et al.* (2018).

In addition to demonstrating that PE and PP are transport vectors for PFOA, this work suggests that these materials may be useful to remove said compounds from aqueous environments, when employed in a controlled scenario such as water treatment. Due to the propensity for PFOA uptake in both PE and PP, it is conceivable that polymer pellets could be used to remove this compound from wastewater to prevent bioaccumulation in the environment. As for SMT and PFOS, alternative removal techniques may be necessary, since PE and PP may only offer targeted removal of PFOA. Expanding on the work of this study may yield additional useful observations which suggest other common materials to remove SMT and PFOS from wastewater and may assist in the design of new water treatment processes to remove these pharmaceutical compounds from the environment.

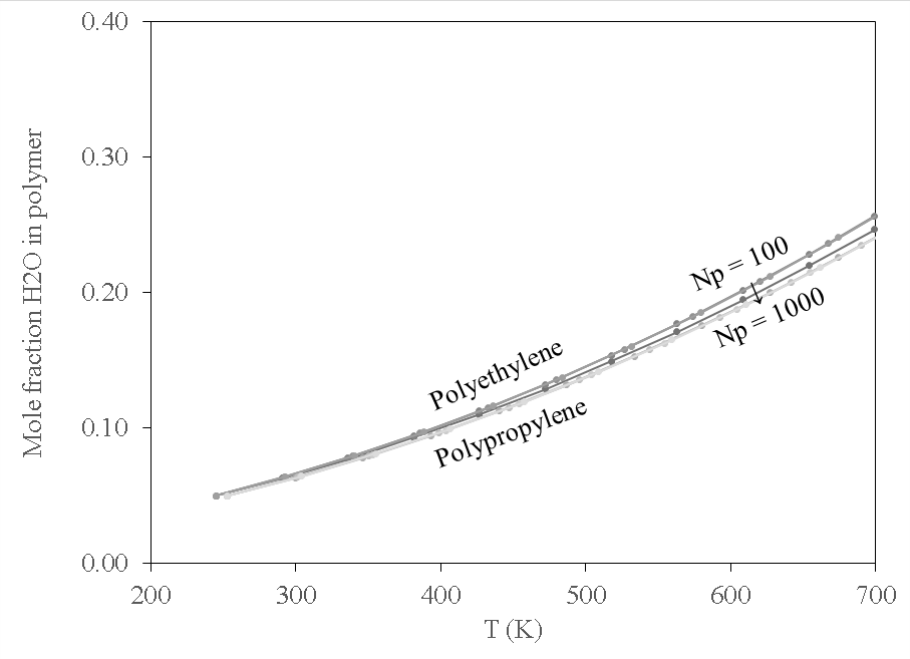

Figure 8.51: Effect of temperature on water (H_2O) content of PP and PE with respect to the degree of polymerisation (Np).

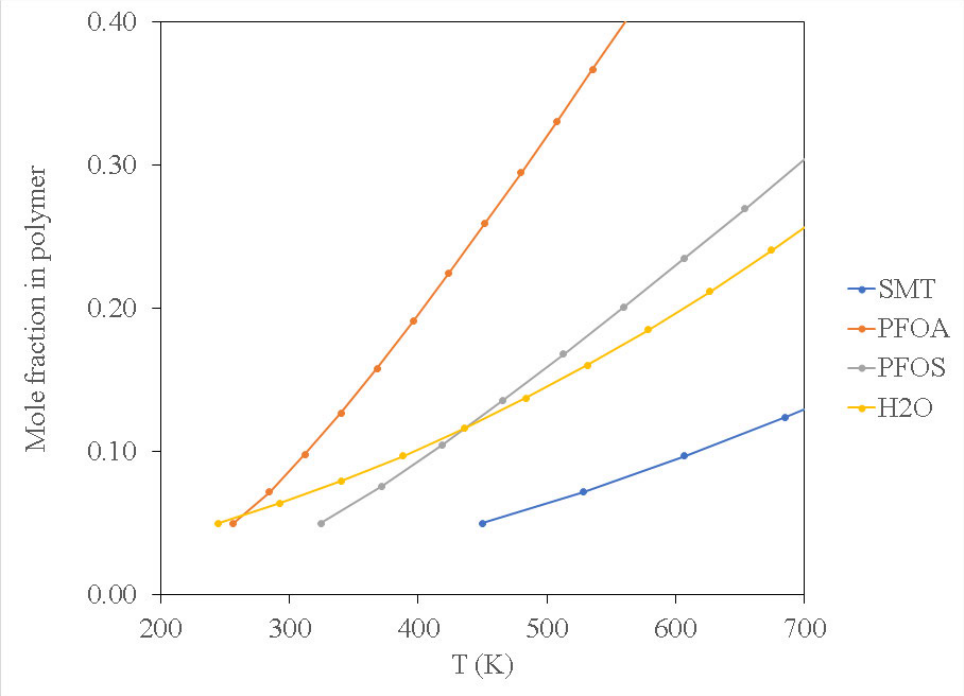

Figure 8.52: Effect of temperature on sorption in PE with respect to a fixed value of Np = 1000.

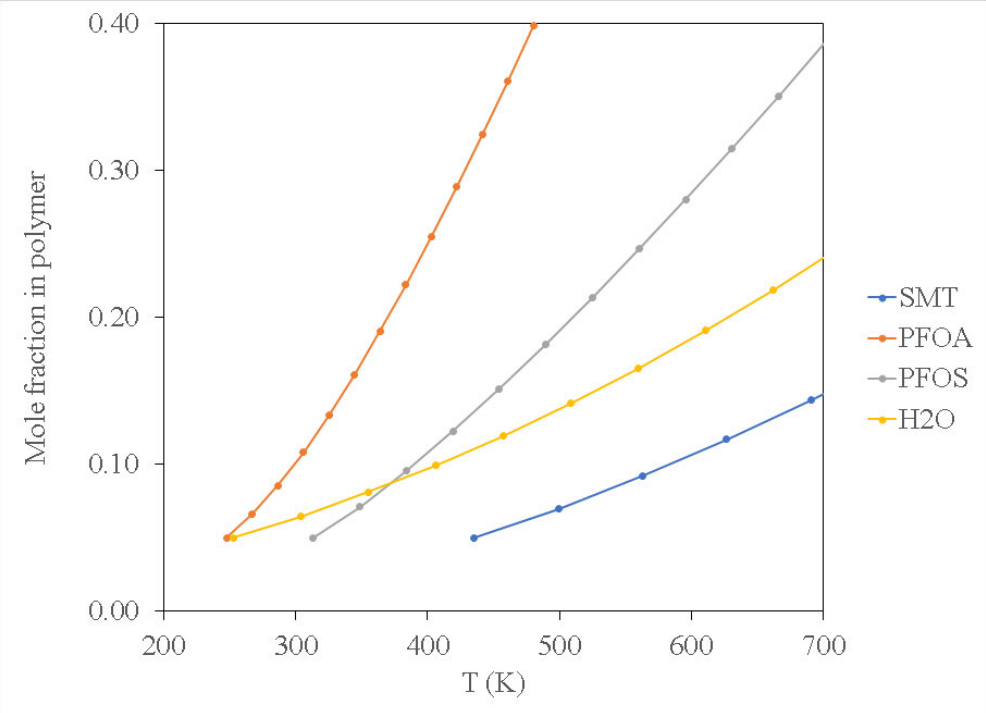

Figure 8.53: Effect of temperature on sorption in PP with respect to a fixed value of Np = 1000.

It is worth noting that at the time this study was conducted, they were no studies reported on investigating the sorption behaviour of SMT, PFOA and PFOS relative to water, PE and PP using the

extended Flory-Huggins approach. Nor are there reported studies on the effect of degree of polymerisation and temperature variation on the sorption behaviour of the above-mentioned model contaminants relative to water and polymer. However, there are reported studies focusing on solid-liquid sorption of perfluorinated compounds in aqueous environment. Lee *et al.* (2019) investigated the sorption of PFOA, perfluoro-n-pentanoic acid (PFPeA), perfluorohexane sulfonate (PFHxS), perfluorohexanoic acid (PFHxA), and perfluorononaoic acid (PFNA) in aqueous environment relative to activated carbon. Lee and co-workers reported that 90% removal of the aforementioned model PFCs was achieved. Meng *et al.* (2019) evaluated the sorption efficiency of magnetic activated carbon on the removal of PFOS, PFOA, PFHxS and perfluorobutane sulfonate (PFBS) in aqueous solution and the observed affinity was PFOS>PFOA>PFHxS>PFBS with adsorption equilibriums of 1.63, 0.90, 0.33 and 0.21 mmol/g, respectively. The findings observed by Meng *et al.* (2019) when compared to the current study, suggests that activated carbon has a higher affinity towards PFOS compared to PE and PP. Such a sorption pattern can be attributed on the fact that activated carbon have a higher affinity towards organic compounds that are more hydrophobic and less polar (Yin and Shang 2020).

8.5. Conclusions and Future Perspectives

An extended Flory-Huggins approach was used to model sorption of SMT, PFOA and PFOS on PE and PP. Previous work (Johansson *et al.* 2007; Lasich, Johansson and Ramjugernath 2013; Erdtman *et al.* 2016) using Gibbs ensemble Monte Carlo simulations modelled sorption in polymers by considering phase equilibria between polymers and fluid systems, analogous to the current work undertaken along different methodological lines. For the sake of reference within the context of aqueous environments, sorption of water in both polymers was also considered. Both temperature and the degree of polymerization were considered, and it was found that on a molar basis the latter did not play a significant role in the uptake of SMT, PFOA, PFOS or water, whereas temperature effects were significant. While not explicitly accounted for in this work, the results were evocative of a pore-filling mechanism.

Based on the findings of the current study, it is apparent that at ambient conditions only the sorption of PFOA on both PE and PP was favoured in aqueous environments, while higher temperatures could induce uptake of PFOS into both polymers. This implies that PE and PP are not only transport vectors for PFOA into the environment at large, but also poses a risk for ingestion by marine or aquatic animals resulting in bioaccumulation of PFOA, causing serious negative health effects as reported by Wu *et al.* (2019) and Ramhøj *et al.* (2018). Sorption of SMT into both polymers was not preferential compared to water at any conditions investigated in this study, suggesting that PE and PP are probably not significant vectors for transportation of SMT into aquatic or marine environments.

To date, adequate studies have been published on the occurrence and concentration levels of PFCs and pharmaceuticals in water receiving bodies with the application of liquid-solid adsorption as a promising technique. However, the is no information available on the interaction of PFCs, pharmaceuticals with polymers i.e., MPs in aqueous environments since these contaminants coexist. Note that the occurrence and bioaccumulation of polymers by aquatic life in the form of MPs have become a global phenomenon. Therefore, it is imperative to understand the interaction mechanisms of MPs with the aforementioned contaminants in order to develop effective tools aimed at detecting and eradicating these emerging contaminants in water bodies. Information on the thermodynamic interaction of PFCs and pharmaceuticals relative to MPs will give an insight at understanding the potential of MPs serving as a transport vector for organic contaminants.

It is appreciated that several studies have been conducted aimed at removing PFCs and pharmaceuticals from aqueous streams using both biological and liquid-solid adsorption separation. However, further studies are needed to investigate the application of polymers as remediation technology for PFCs and pharmaceuticals using raw wastewater aimed at investigating the effect of other organic pollutants on polymer affinity towards PFCs and pharmaceuticals. Moreover, the current study does not account for pH variation and the occurrence of co-pollutants in polymer structures on polymer affinity towards PFCs and pharmaceuticals.

References

Acosta-Rangel, A., Sánchez-Polo, M., Rozalen, M., Rivera-Utrilla, J., Polo, A. and Mota, A. 2019. Comparative study of the oxidative degradation of different 4-aminobenzene sulfonamides in aqueous solution by sulfite activation in the presence of Fe (0), Fe (II), Fe (III) Or Fe (VI). *Water*, 11 (11): 2332.

Agboola, O. D. and Benson, N. U. 2021. Physisorption and chemisorption mechanisms influencing micro (nano) plastics-organic chemical contaminants interactions: a review. *Frontiers in Environmental Science*: 167.

Ahmed, M. B., Alam, M. M., Zhou, J. L., Xu, B., Johir, M. A. H., Karmakar, A. K., Rahman, M. S., Hossen, J., Hasan, A. K. and Moni, M. A. 2020. Advanced treatment technologies efficacies and mechanism of per-and poly-fluoroalkyl substances removal from water. *Process Safety and Environmental Protection*, 136: 1-14.

Al Harraq, A. and Bharti, B. 2021. Microplastics through the Lens of Colloid Science. *ACS Environmental Au*, 2 (1): 3-10.

Armah, E. K., Chetty, M., Adedeji, J. A., Kukwa, D. T., Mutsvene, B., Shabangu, K. P. and Bakare, B. F. 2021. Emerging Trends in Wastewater Treatment Technologies: The Current Perspective. *Promising Techniques for Wastewater Treatment and Water Quality Assessment*, 1: 71.

Arvaniti, O. S. and Stasinakis, A. S. 2015. Review on the occurrence, fate and removal of perfluorinated compounds during wastewater treatment. *Science of the Total Environment*, 524: 81-92.

Biovia, D. S. 2020. Dassault Systèmes; San Diego: 2020. *Discovery Studio*,

Blanco, M. 1991. Molecular silverware. I. General solutions to excluded volume constrained problems. *Journal of computational chemistry*, 12 (2): 237-247.

Chen, X., Xia, X., Wang, X., Qiao, J. and Chen, H. 2011. A comparative study on sorption of perfluorooctane sulfonate (PFOS) by chars, ash and carbon nanotubes. *Chemosphere*, 83 (10): 1313-1319.

Crone, B. C., Speth, T. F., Wahman, D. G., Smith, S. J., Abulikemu, G., Kleiner, E. J. and Pressman, J. G. 2019. Occurrence of per-and polyfluoroalkyl substances (PFAS) in source water and their treatment in drinking water. *Critical reviews in environmental science and technology*, 49 (24): 2359-2396.

EPA, U. 2016. Drinking water health advisory for perfluorooctane sulfonate (PFOS). *Office of Water (4304T), Health and Ecological Criteria Division EPA*,

Erdtman, E., Bohlén, M., Ahlström, P., Gkourmpis, T., Berlin, M., Andersson, T. and Bolton, K. 2016. A molecular-level computational study of the diffusion and solubility of water and oxygen in

carbonaceous polyethylene nanocomposites. *Journal of Polymer Science Part B: Polymer Physics*, 54 (5): 589-602.

Espana, V. A. A., Mallavarapu, M. and Naidu, R. 2015. Treatment technologies for aqueous perfluorooctanesulfonate (PFOS) and perfluorooctanoate (PFOA): A critical review with an emphasis on field testing. *Environmental Technology & Innovation*, 4: 168-181.

Fan, C. F., Olafson, B. D., Blanco, M. and Hsu, S. L. 1992. Application of molecular simulation to derive phase diagrams of binary mixtures. *Macromolecules*, 25 (14): 3667-3676.

Flory, P. J. 1953. *Principles of polymer chemistry*. Cornell university press.

Guo, X., Wang, X., Zhou, X., Kong, X., Tao, S. and Xing, B. 2012. Sorption of four hydrophobic organic compounds by three chemically distinct polymers: role of chemical and physical composition. *Environmental science & technology*, 46 (13): 7252-7259.

Hassan, M., Liu, Y., Naidu, R., Du, J. and Qi, F. 2020. Adsorption of Perfluorooctane sulfonate (PFOS) onto metal oxides modified biochar. *Environmental Technology & Innovation*, 19: 100816.

Houtman, C. J. 2010. Emerging contaminants in surface waters and their relevance for the production of drinking water in Europe. *Journal of Integrative Environmental Sciences*, 7 (4): 271-295.

Johansson, E., Bolton, K., Theodorou, D. N. and Ahlström, P. 2007. Monte Carlo simulations of equilibrium solubilities and structure of water in n-alkanes and polyethylene. *The Journal of chemical physics*, 126 (22): 224902.

Khumalo, S. M., Bakare, B. F., Rathilal, S. and Tetteh, E. K. 2022. Characterization of South African Brewery Wastewater: Oxidation-Reduction Potential Variation. *Water*, 14 (10): 1604.

Kissa, E. 2001. *Fluorinated surfactants and repellents*. CRC Press.

Lasich, M., Johansson, E. L. and Ramjugernath, D. 2013. Monte Carlo simulations of water solubility and structures in poly (difluoromethylene). *Molecular Simulation*, 39 (5): 367-384.

Lee, S.-h., Cho, Y.-j., Lee, M. and Lee, B.-D. 2019. Detection and treatment methods for perfluorinated compounds in wastewater treatment plants. *Applied Sciences*, 9 (12): 2500.

Lenka, S. P., Kah, M. and Padhye, L. P. 2021. A review of the occurrence, transformation, and removal of poly-and perfluoroalkyl substances (PFAS) in wastewater treatment plants. *Water research*, 199: 117187.

Li, J., Liu, H. and Chen, J. P. 2018. Microplastics in freshwater systems: A review on occurrence, environmental effects, and methods for microplastics detection. *Water research*, 137: 362-374.

Li, J., Zhang, K. and Zhang, H. 2018. Adsorption of antibiotics on microplastics. *Environmental Pollution*, 237: 460-467.

Llorca, M., Schirinzi, G., Martínez, M., Barceló, D. and Farré, M. 2018. Adsorption of perfluoroalkyl substances on microplastics under environmental conditions. *Environmental pollution*, 235: 680-691.

Meng, P., Fang, X., Maimaiti, A., Yu, G. and Deng, S. 2019. Efficient removal of perfluorinated compounds from water using a regenerable magnetic activated carbon. *Chemosphere*, 224: 187-194.

Mulla, S. I., Bagewadi, Z. K., Faniband, B., Bilal, M., Chae, J.-C., Bankole, P. O., Saratale, G. D., Bhargava, R. N. and Gurumurthy, D. M. 2021. Various strategies applied for the removal of emerging micropollutant sulfamethazine: a systematic review. *Environmental Science and Pollution Research*: 1-15.

Qiu, Y., Fujii, S. and Tanaka, S. 2007. Removal of perfluorochemicals from wastewater by granular activated carbon adsorption. *Environmental Engineering Research*, 44: 185-193.

Ramhøj, L., Hass, U., Boberg, J., Scholze, M., Christiansen, S., Nielsen, F. and Axelstad, M. 2018. Perfluorohexane sulfonate (PFHxS) and a mixture of endocrine disrupters reduce thyroxine levels and cause antiandrogenic effects in rats. *Toxicological Sciences*, 163 (2): 579-591.

Rashid, R., Shafiq, I., Akhter, P., Iqbal, M. J. and Hussain, M. 2021. A state-of-the-art review on wastewater treatment techniques: the effectiveness of adsorption method. *Environmental Science and Pollution Research*, 28 (8): 9050-9066.

Rathi, B. S. and Kumar, P. S. 2021. Application of adsorption process for effective removal of emerging contaminants from water and wastewater. *Environmental Pollution*, 280: 116995.

Richardson, S. D. and Ternes, T. A. 2018. Water analysis: emerging contaminants and current issues. *Anal. Chem*, 90 (1): 398-428.

Shrivastava, A. 2018. *Introduction to plastics engineering*. William Andrew.

Torres, F. G., Dioses-Salinas, D. C., Pizarro-Ortega, C. I. and De-la-Torre, G. E. 2021. Sorption of chemical contaminants on degradable and non-degradable microplastics: Recent progress and research trends. *Science of the Total Environment*, 757: 143875.

Umar, K., Yaqoob, A. A., Ibrahim, M. N. M., Parveen, T. and Safian, M. T.-u. 2021. Environmental applications of smart polymer composites. In: *Smart Polymer Nanocomposites*. Elsevier, 295-312.

Wang, F., Shih, K. M. and Li, X. Y. 2015. The partition behavior of perfluorooctanesulfonate (PFOS) and perfluorooctanesulfonamide (FOSA) on microplastics. *Chemosphere*, 119: 841-847.

Wang, F., Zhang, M., Sha, W., Wang, Y., Hao, H., Dou, Y. and Li, Y. 2020. Sorption behavior and mechanisms of organic contaminants to nano and microplastics. *Molecules*, 25 (8): 1827.

Wu, P., Cai, Z., Jin, H. and Tang, Y. 2019. Adsorption mechanisms of five bisphenol analogues on PVC microplastics. *Science of the Total Environment*, 650: 671-678.

Xu, B., Liu, F., Brookes, P. C. and Xu, J. 2018. The sorption kinetics and isotherms of sulfamethoxazole with polyethylene microplastics. *Marine pollution bulletin*, 131: 191-196.

Xu, T., Young, A., Narula, J., Sayler, G. and Ripp, S. 2020. High-throughput analysis of endocrine-disrupting compounds using blyes and blyas bioluminescent yeast bioassays. In: *Bioluminescent Imaging*. Springer, 29-41.

Yaqoob, A. A., Ahmad, H., Parveen, T., Ahmad, A., Oves, M., Ismail, I. M., Qari, H. A., Umar, K. and Mohamad Ibrahim, M. N. 2020. Recent advances in metal decorated nanomaterials and their various biological applications: a review. *Frontiers in chemistry*, 8: 341.

Yaqoob, A. A., Safian, M. T.-u., Rashid, M., Parveen, T., Umar, K. and Ibrahim, M. N. M. 2021. Introduction of smart polymer nanocomposites. In: *Smart Polymer Nanocomposites*. Elsevier, 1-25.

Yin, R. and Shang, C. 2020. Removal of micropollutants in drinking water using UV-LED/chlorine advanced oxidation process followed by activated carbon adsorption. *Water Research*, 185: 116297.

Young, R. J. and Lovell, P. A. 2011. *Introduction to polymers*. CRC press.

CHAPTER NINE: CONCLUSIONS AND RECOMMENDATIONS

9.1. Overview

The primary aim of the present study was to investigate the treatment efficiency of chitosan-carbon nanotube hydrogel beads composite for the removal of amoxicillin, ciprofloxacin, sulfamethoxazole, PFOA and PFOS from aqueous solutions. Therefore, this chapter presents the conclusions and recommendations made on the basis of the findings presented in Chapters Four to Eight. In achieving the aim of the research study, the following objectives were defined:

i. Evaluating the performance of synthesised chitosan-carbon nanotube hydrogel beads on the removal of amoxicillin, ciprofloxacin, sulfamethoxazole, PFOA and PFOS from aqueous solutions through batch studies.
ii. Study adsorption kinetics, isotherms, thermodynamic parameters as well as the effect of solution pH, adsorbent dose, contact time as well as initial adsorbate concentration on the removal of the model antibiotics and PFAAs.
iii. Perform fixed-bed adsorption column studies to investigate the effect of operating parameters such as volumetric flow rate, initial adsorbate concentration and fixed-bed height on the adsorption breakthrough curves.
iv. Investigate the sorption of antibiotics and PFAAs relative to water on micro-plastics as a carrier in water bodies by employing the extended Flory-Huggin's approach in Material Studio.

9.2. Summary of thesis findings

Papers I and II presented as Chapters Two and Three in this thesis, explicitly demonstrated that the current WWTPs, particularly in the African region, are not capable of eradicating antibiotics and PFAAs from wastewater streams. On the other hand, solid-liquid adsorption has demonstrated to be an effective technology in eradicating these emerging contaminants of environmental concern due to its simplicity and cost effectiveness. However, there is still a need to explore the use of natural adsorbents and chitosan composites have demonstrated to be effective in eradicating antibiotics and PFAAs despite being a resurfacing bio-adsorbent in water treatment. The reviewed literature in this current study suggests that there is a research gap in elucidating the uptake mechanisms of antibiotics and PFAAs on chitosan-carbon nanotube composites through the study of adsorption kinetics, isotherms, and thermodynamic parameters for an effective system design.

Paper III presented as Chapter Four, systematically examined the findings of the present study based on objectives i and ii. It can be inferred from the findings presented in Chapter Four that chitosan-carbon

nanotube hydrogel beads demonstrated high affinity towards amoxicillin, ciprofloxacin, and sulfamethoxazole. It can also be inferred from the findings presented in Chapter Four that the solution pH plays a vital role in the protonation and/or deprotonation of the adsorbent surface charge as well as the speciation of the model contaminants. Furthermore, it can be concluded from the adsorption kinetics studies that the uptake of amoxicillin, ciprofloxacin, and sulfamethoxazole on chitosan-carbon nanotube hydrogel beads is limited by multiple processes. In elucidating the multicomponent adsorption behaviour of the model antibiotics on chitosan-carbon nanotubes hydrogel beads, the findings of the present study in Chapter Four explicitly indicate that the system exhibited both antagonistic and synergistic effects. On the other hand, results on thermodynamic studies presented in Chapter Four indicated that the uptake of amoxicillin, ciprofloxacin, and sulfamethoxazole on chitosan-carbon nanotubes hydrogel beads can be described by both physical and chemical adsorption processes. Furthermore, when examining the findings of the present work presented in Chapter Five which is based on paper IV it can be concluded that the existence of competing ions did not facilitate the uptake of the model antibiotics on chitosan-carbon nanotube hydrogel beads due to the formation of aggregates with increasing NaCl and HA concentration. Therefore, it can be concluded that the existence of sodium chloride and humic acid in wastewater streams can hamper the uptake of antibiotics during treatment.

Furthermore, when examining the findings of the present work presented in Chapter Six which is based on paper V, it can be concluded that the synthesised chitosan-carbon nanotube hydrogel beads demonstrated high affinity towards PFOS and PFOA with the adsorption equilibrium being reached after 48 hours of contact time. Interestingly, results from the CCD in RSM suggest that the uptake of PFOS and PFOA on chitosan-carbon nanotubes hydrogel beads is strongly influenced by the initial adsorbate concentration when compared to the influence of solution pH. These findings were cemented by the adsorption kinetics results which demonstrated that PFOS and PFOA experimental data was well fitted by the nonlinear PFO kinetic model confirming that the uptake of PFOA and PFOS on chitosan-carbon nanotube hydrogel beads solely depends on the concentration of the model adsorbate. On the other hand, single adsorption isotherm data was well fitted by the Freundlich isotherm model indicating that the uptake of PFOA and PFOS on chitosan-carbon nanotube hydrogel beads was not restricted to the monolayer adsorption process. Therefore, it can be concluded that the adsorption heat and affinities were not uniformly distributed on the heterogeneous surface of the model adsorbent. Moreover, from the binary adsorption results presented in Chapter Six, it can be concluded that both PFOA and PFOS demonstrated antagonistic effects on the uptake of either PFOA or PFOS in PFOA+PFOS solution. Interestingly, it can be concluded that the presence of sodium chloride facilitated the uptake of PFOA and PFOS in solution thus exhibiting synergistic effects. Based on the thermodynamic studies, it can be concluded that the uptake mechanism of either PFOA and PFOS on chitosan-carbon nanotubes, cannot be explicitly explained by the chemical nor physical adsorption mechanism, however, it is described by a physiochemical adsorption process.

Chapter Seven which is based on paper VI, present the findings of the effect of volumetric flow rate, adsorbate initial concentration (i.e., AMX, CIP, SMX, PFOA and PFOS) and fixed-bed height on the breakthrough curves. Based on the results obtained, it can be concluded that the breakthrough points time decreased with an increase in adsorbate initial concentration and operating volumetric. On the other hand, an increase in the bed height resulted in an increase on the breakthrough point time. Therefore, it can be concluded that an increase in bed-height results in an increase in the number of adsorption active sites, thus enhancing the uptake of the model adsorbates. Moreover, based on the breakthrough curves modelling results, it is apparent that all experimental data was well fitted by the Thomas model. Therefore, it can be concluded that the breakthrough curves for the current study can be described by a symmetric function. It is worth noting that, based on the findings of the present work in Chapter Seven, the question raised in objective iii was successfully addressed.

The work presented in Chapter Eight endeavours to answer the question raised in objective iv. Herein, temperature and the degree of polymerisation were considered, and it was found that on a molar basis the latter did not play a significant role in the uptake of SMT, PFOA, PFOS or water, whereas temperature effects were significant. Therefore, it can be concluded that the uptake of SMT, PFOA and PFOS on both PE and PP were limited by the pore-filling mechanism. Moreover, from the results presented in Chapter Eight it can be concluded that the extended Flory-Huggins approach was able to model the sorption of SMT, PFOA and PFOS on PE and PP. The results obtained strongly suggest that PP and PE are not only transport vectors for PFOA and PFOS into the environment at large, but also poses a risk for ingestion by marine or aquatic organisms resulting in their bioaccumulation, which might cause serious negative health effects. On the other hand, the sorption of SMT into both PE and PP was not preferential compared to water at any conditions investigated in this study. Therefore, it can be concluded that PE and PP are not significant vectors for the transportation of SMT into aquatic or marine environments.

9.2.1. Concluding remarks

It is worth noting that the present study ought to answer two fundamental questions raised in Chapter 1.

i. Would chitosan-carbon nanotubes composites, therefore, feasibly be used as an adsorbent for the removal of antibiotics and PFAAs?
ii. Can artificial intelligence through the application of Material Studio as a simulation tool be effectively used in studying the interaction between antibiotics and PFAAs with microplastics relative to water as co-existing contaminants?

As such based on the findings of the study, it can be concluded that chitosan-carbon nanotubes composites have the potential to be applied as adsorbents for the removal of antibiotics and PFAAs

from aqueous solutions. Furthermore, the simulation results obtained suggest that Monte Carlo simulations in Material Studio can be used as an effective tool to effectively in studying the interaction between antibiotics and PFAAs with microplastics relative to water as co-existing contaminants. Therefore, the findings of the present work have successfully addressed the research questions for the current study.

9.3. Recommendations and future perspectives

During the time in which this study was conducted, there was no existing wastewater treatment plant that was using chitosan-based composites for the treatment of wastewater at least in the context of South Africa. As such, this technology (i.e., adsorbent) is yet to be tested for its practical application given the human and aquatic life health risk that is posed by the occurrence of antibiotics and PFAAs in water bodies. Moreover, the study presents the first case of investigating the interaction between antibiotics and PFAAs with microplastics using the extended Flory-Huggins approach in Monte Carlo simulation. As such the following recommendations are made for future perspectives:

i. Despite the positive results demonstrated by chitosan-carbon nanotubes hydrogel beads on the uptake of antibiotics and PFAAs, there is still a need for research studies to investigate the effect of temperature on the mechanical strength of the adsorbent aimed at optimising the operating temperature.
ii. With chitosan composites being a resurfacing technology in water treatment, there is a need to conduct studies on techno-economic analysis aimed at comparing the current adsorbent with conventional adsorbents such as activated carbon since they have demonstrated to be effective in eradicating contaminants of emerging concern such as antibiotics.
iii. It is worth noting that the present study was conducted based on synthetic aqueous solutions due to stringent access to pharmaceutical wastewater streams as a result of resurfacing viruses such as COVID-19, it is recommended that the synthesised adsorbent be tested using raw wastewater.
iv. The Monte Carlo simulation results suggest that PFOA and PFOS can be adsorbed into PP and PE, hence, more work needs to be done on the application of PP and PE for the uptake of PFOA and PFOS from aqueous solutions.